Continuum-Based Numerical Simulation of Static and High-Strain Dynamic Pile Load Testing Adopting Advanced Soil Models

Mehdi Aghayarzadeh

A thesis in fulfilment of the requirement for the award of the degree

DOCTOR OF PHILOSOPHY

School of Civil and Environmental Engineering

Faculty of Engineering and Information Technology

Feb 2019

Certificate of Original Authorship

I, **Mehdi Aghayarzadeh**, declare that this thesis, submitted in fulfilment of the requirements for the award of Doctor of Philosophy, in the School of Civil and Environmental Engineering, Faculty of Engineering and Information Technology at the University of Technology Sydney.

This thesis is wholly my own work unless otherwise referenced or acknowledged. In addition, I certify that all information sources and literature used are indicated in the thesis. This document has not been submitted for qualifications at any other academic institution. This Research is supported by the Australian Geovernment Research Training Program.

Production Note:
Signature: Signature removed prior to publication.

Date: 28 Feb 2019

Acknowledgment

I wish to express sincere gratitude to my principal supervisor Associate Professor Hadi Khabbaz and my co-supervisor Associate Professor Behzad Fatahi for their invaluable guidance and support over the course of this research.

I would also like to thank UTS Graduate Research School and the Faculty of Engineering and Information Technology for high-quality support and several generous travel grants.

Part of the required data for numerical simulations and verification was provided by Arup Australia Pty Ltd and I would like to thank Mr Sergei Terzaghi for his support. My appreciation is extended to Dr Kazem Fakharian, Mr Hossein Ahmadi, Dr Garland Likins, and Dr Harry Far for many valuable technical discussions. My special gratitude goes to my friends Dr Mohsen Ranjbar, Dr Farzad Moghadam, Dr Abbas Vahedian, Dr Behnam Vakhshouri, Dr Amin Noushini and my other colleagues at the UTS Geotechnical Research Group for fostering an enjoyable working environment.

Finally, I greatly thank my parents and my siblings for their unconditional love and support.

List of Research Papers

Accepted Research Articles:

- Aghayarzadeh, M., Khabbaz, H., Fatahi, B. & Terzaghi, S. 2018, 'Continuum Based Numerical Simulation of Dynamic Pile Load Testing for Tubular Steel', **International Journal of Geomechanics**; accepted in May 2019.

Peer Reviewed Conference Papers:

- Aghayarzadeh, M., Khabbaz, H., 2019, 'Numerical Simulation of Concrete Pile Groups' Response Bored in Cemented Sand Deposit under Axial Static Load Testing', **7th International Symposium on Deformation Characteristics of Geomaterials**, Glasgow, UK.
- Aghayarzadeh, M., Khabbaz, H., Fatahi, B. 2018, 'Evaluation of Bored Piles Behaviour in Saturated Loose and Dense Sand during the Static Load Testing', paper presented at the **5th GeoChina International Conference**, Hangzhou, China, pp 75-89. *
- Aghayarzadeh, M., Khabbaz, H., Fatahi, B. 2018, 'Numerical Analysis of Concrete Piles Driving in Saturated Dense and Loose Sand Deposits', **9th European Conference on Numerical Methods in Geotechnical Engineering**, Porto, Portugal, pp 1031-1038.
- Aghayarzadeh, M., Khabbaz, H., Fatahi, B. 2018, 'Evaluation of Reaction Piles Effect on Test Piles in Static Load Testing Using 3-D Numerical Analysis', **10th International Conference on Stress Wave Theory and Testing Methods for Deep Foundations**, San Diego, USA, pp 68-80.
- Aghayarzadeh, M., Khabbaz, H. & Fatahi, B. & Terzaghi, S. 2017, 'Continuum Numerical Modelling of Dynamic Load Test for Steel Pipe Piles', **International Conference on Advancement of Pile Technology and Pile Case Histories**, Bali, Indonesia, pp (F4) 4-9.

* The paper presented in 5th Geo-China International Conference was nominated as a selected and high quality paper for consideration in International Journal of Geomechanics (ASCE).

CONTENTS

ACKNOWLEDEMENT iii

LIST OF RESEARCH PAPERS iv

CONTENTS v

LIST OF FIGURES ix

LIST OF TABLES xvi

NOTATIONS xvii

ABSTRACT xxiii

CHAPTER 1 INTRODUCTION **1**

1.1 BACKGROUND AND PROBLEM STATEMENT 1

1.2 SCOPE AND OBJECTIVES 5

1.3 THESIS OUTLINE 6

CHAPTER 2 LITERATURE REVIEW **9**

2.1 PILE LOAD TESTING OVERVIEW 10

2.2 CLASSIFICATION OF PILES 12

2.3 STATIC PILE LOAD TESTING 20

2.3.1 Static Pile Load Testing Procedure *23*

2.3.2 Interpretation of Test Results *24*

2.4 DYNAMIC PILE LOAD TESTING 26

2.4.1 Proportionality Concept *29*

2.4.2 CAPWAP Background *30*

2.4.3 CAPWAP Model *36*

2.5 CONSTITUTIVE SOIL MODELS 39

2.5.1 Mohr-Coulomb Model (MC Model) *39*

2.5.2 Hardening Soil Model (HS Model) *42*

2.5.3 Hardening Soil with Small Strain Stiffness Model (HS-Small Model) *43*

2.5.4 Hypoplastic with Intergranular Strain Model (HP-IGS Model) *45*

2.6 Remarkable Studies on Pile Load Testing 48

2.6.1 Static Pile Load Testing: Numerical and Experimental Studies *48*

2.6.2 Dynamic pile load testing: numerical, experimental and analytical studies *55*

2.7 Gap and Limitations in Current Literature 68

CHAPTER 3 STATIC PILE LOAD TESTING: NUMERICAL SIMULATION OF SINGLE PILE AND PILES GROUP BEHAVIOURS 70

3.1 Synopsis 70

3.2 Introduction 71

3.3 Numerical Simulation Procedure 73

3.4 Single Bored Pile into Dense and Loose Sand Deposits 75

3.4.1 Overview *75*

3.4.2 Results and Discussion *77*

3.5 Interaction of Reaction Piles on Test Pile 83

3.5.1 Overview *83*

3.5.2 Results and Discussion *87*

3.6 Concrete pile Groups Response Bored in Cemented Sand Deposit 99

3.6.1 Overview *99*

3.6.2 Results and Discussion *105*

3.7 Summary 114

CHAPTER 4 CASE METHOD AND ONE-DIMENSIONAL WAVE PROPAGATION INDUCED BY DYNAMIC PILE LOAD TESTING: THEORY, CONCEPT, AND APPLICATION IN A REAL CASE PROJECT 116

4.1 Synopsis 116

4.2 Introduction 117

4.3 Background 118

4.3.1 Total and Static Soil Resistance *119*

4.3.2 CASE Damping Factor *126*

4.3.3 Pile Driving Stresses *128*

4.3.4 Hammer/Driving System *128*

4.3.5 Total and Static Shaft Resistance *129*

4.4 Case Study 131

4.5 Summary 139

CHAPTER 5 DYNAMIC PILE LOAD TESTING: NUMERICAL SIMULATION, INTERPRETATION OF THE RESULTS, AND ASSESSMENT OF GROUND VIBRATION INDUCED BY DYNAMIC TEST 142

5.1 Synopsis 142

5.2 Introduction 144

5.3 Numerical Simulation Procedure 149

5.4 Concrete Pile Driving in Saturated Dense and Loose Sand Deposits 151

5.4.1 Overview *151*

5.4.2 Results and Discussion *152*

5.5 One-dimensional Wave Propagation in Finite Element Program 166

5.5.1 Overview *166*

5.6 Open-Ended Steel Pipe Pile Driven in Dense Sand Deposit 167

5.6.1 Overview *167*

5.6.2 Results and Discussion *170*

5.7 Open-Ended Steel Pipe Pile Driven in Multilayer Soil 176

5.7.1 Overview *176*

5.7.2 Results and Discussion *183*

5.7.3 Impact of Interface and Stiffness Degradation Parameters *196*

5.8 Ground Vibration Induced by Dynamic Pile Load Testing 200

5.8.1 Overview *200*

5.8.2 Allowable Ground Vibration *205*

5.8.3 Results and Discussion *210*

5.9 Summary 215

CHAPTER 6 CONCLUSIONS AND RECOMMENDATIONS FOR FUTURE RESEARCH 217

6.1 SUMMARY 217

6.2 CONCLUSIONS 219

6.2.1 Static Pile Load Testing: Numerical Simulation of Single Pile and Piles Group Behaviour 219

6.2.2 CASE Method: Theory, Concept and Application in a Real Case Project 221

6.2.3 Dynamic Pile Load Testing: Numerical Simulation, Interpretation of the Results, and Assessment of Ground Vibration Induced by Dynamic Testing 221

6.3 RECOMMENDATIONS FOR FUTURE RESEARCH 223

REFERENCES 226

APPENDICES 243

LIST OF FIGURES

FIGURE 1.1 APPLICATION OF ADVANCED SOIL MODELS IN ACCURATE PREDICTION OF SOIL BEHAVIOUR DURING STATIC AND DYNAMIC PILE LOAD TESTING 4

FIGURE 2.1 CLASSIFICATION OF PILES BASED ON VARIOUS FACTORS 12

FIGURE 2.2 CAST-IN-PLACE CONCRETE PILES (GARY PUNTMAN 2018) 13

FIGURE 2.3 DRIVEN STEEL PIPE PILES AND THE MEASUREMENT OF SOIL PLUG LENGTH (AFTER FATTAH & AL-SOUDANI 2016) 15

FIGURE 2.4 DRIVING SHOE, WHICH IS WELDED AT THE PILE TOE (ESC GROUP 2018) 16

FIGURE 2.5 CLOSED-ENDED STEEL PIPE PILE (PILE BUCK 2018) 16

FIGURE 2.6 DIFFERENT STAGES OF SOIL PLUGGING: (A) UNPLUGGED (B) PARTIALLY PLUGGED AND (C) FULLY PLUGGED. X ILLUSTRATES THE PENETRATION DISTANCE OF THE PILE (AFTER KARLOWSKIS 2014) 18

FIGURE 2.7 DIAGRAM OF COMPRESSION LOAD TEST SETUP USING KENTLEDGE SYSTEM (DUTCH INTERNATIONAL 2017) 22

FIGURE 2.8 SCHEMATIC OF HYDRAULIC JACK ACTING AGAINST ANCHORED REACTION FRAME (AFTER ASTM INTERNATIONAL 2013) 22

FIGURE 2.9 TYPICAL LOAD-DISPLACEMENT CURVE AND THE OFFSET LIMIT METHOD 25

FIGURE 2.10 (A) TYPICAL DYNAMIC PILE TEST SET-UP (B) DYNAMIC LOAD TESTING (APPLELIANLIAN 2013) 28

FIGURE 2.11 FREE BODY DIAGRAM OF A SMALL SEGMENT OF A PILE (AFTER GARNIER 2001) 31

FIGURE 2.12 (A) REAL PILE AND DRIVING ACCESSORIES (B) SMITH PILE AND SOIL MODEL (C) CAPWAP MODEL (D) SMITH SOIL MODEL (AFTER NG 2011) 33

FIGURE 2.13 STRESS STRAIN (LOAD –DEFORMATION) DIAGRAM OF THE SOIL RESISTANCE AT A PILE POINT (AFTER NG 2011) 34

FIGURE 2.14 SIGNAL MATCHING ANALYSIS ALGORITHM IN CAPWAP (AFTER ROBINSON AND RAUSCHE 2000) 38

FIGURE 2.15 TYPICAL OUTPUT OF CAPWAP MEASURED FORCE OR VELOCITY RESPONSE WITH TIME (A) RESULTS OF SIGNAL MATCHING ANALYSIS (MEASURED VERSUS COMPUTED FORCE) AND (B) FORCE AND VELOCITY TRACES RECORDED BY PDA MEASURED VERSUS TIME 39

FIGURE 2.16 BASIC PRINCIPLE OF MC MODEL (AFTER WEHNERT & VERMEER 2004) 41

FIGURE 2.17 HYPERBOLIC STRESS-STRAIN RELATION IN PRIMARY LOADING FOR A STANDARD DRAINED TRIAXIAL TEST (AFTER BRINKGREVE, KUMARSWAMY & SWOLFS 2017) 44

FIGURE 2.18 PROCESS OF INSTALLATION OF CFA PILES (NATURALZEMIN 2019) 49
FIGURE 2.19 COMPARISON OF CALCULATED AND MEASURED LOAD-SETTLEMENT CURVES (AFTER HOĽKO & STACHO 2014) 50
FIGURE 2.20 COMPARISON OF CALCULATED AND MEASURED LOAD DISTRIBUTION CURVES OVER THE PILE LENGTH (AFTER HOĽKO & STACHO 2014) 50
FIGURE 2.21 NUMERICALLY ESTABLISHED LOAD-SETTLEMENT CURVES FOR THE SINGLE AND PILE GROUPS (AFTER COMODROMOS, ANAGNOSTOPOULOS & GEORGIADIS 2003) 51
FIGURE 2.22 MAINTAINED LOAD TESTS ON SQUARE AND CIRCULAR CELL FOUNDATIONS (AFTER YETGINER, WHITE & BOLTON 2006) 53
FIGURE 2.23 COMPARISON OF SINGLE PILE LOAD-DISPLACEMENT AND RATZ BACK-ANALYSIS (AFTER YETGINER, WHITE & BOLTON 2006) 54
FIGURE 2.24 DISTRIBUTION OF CAPWAP TO SLT RATIOS FOR 226 PILES (AFTER LIKINS & RAUSCHE 2004) 56
FIGURE 2.25 MODES OF WAVE PROPAGATION IN THE PILE-PLUG SYSTEM (AFTER PAIKOWSKY & CHERNAUSKAUS 2008) 59
FIGURE 2.26 APPARENT SOIL MODEL PROPOSED BY LEE ET AL. (1988) 63
FIGURE 2.27 A TYPICAL DISCRETISATION USED IN FEM (AFTER NATH 1990) 65
FIGURE 2.28 COMPARISON OF (A) PILE RESISTANCE AND (B) DRIVING STRESS BETWEEN WAVE EQUATION AND FINITE ELEMENT METHODS (AFTER NATH 1990) 66
FIGURE 3.1 SIMULATED DRAINED TRIAXIAL TEST SAND APPLYING MOHR-COULOMB AND HARDENING SOIL MODELS FOR (A) DENSE SAND AND (B) LOOSE SAND 77
FIGURE 3.2 FINITE ELEMENT MODEL OF THE PILE AND THE ADJACENT GROUND WITH THE CORRESPONDING GENERATED MESH 78
FIGURE 3.3 MESH SIZE DEPENDENCY OF FINITE ELEMENT MODELS WITH (A) MC, (B) HS AND (C) HP CONSTITUTIVE MODELS 79
FIGURE 3.4 COMPARISON OF OBTAINED LOAD-DISPLACEMENT CURVES USING DIFFERENT SOIL MODELS IN (A) DENSE AND (B) LOOSE SAND SOILS 81
FIGURE 3.5 INFLUENCE OF (A) CRITICAL STATE FRICTION ANGLE AND (B) GRANULAR HARDNESS ON LOAD-DISPLACEMENT CURVE OF CONCRETE BORED PILE IN SATURATED SAND 84
FIGURE 3.6 INFLUENCE OF (A) SENSITIVITY OF GRANULAR SKELETON TO CHANGE OF PRESSURE (B) CRITICAL VOID RATIO AT ZERO PRESSURE ON LOAD-DISPLACEMENT CURVE OF CONCRETE BORED PILE IN SATURATED SAND 85

FIGURE 3.7 INFLUENCE OF (A) MAXIMUM VOID RATIO AT ZERO PRESSURE (B) EXPONENT DESCRIBES THE TRANSITION BETWEEN PEAK AND CRITICAL STRESS ON LOAD-DISPLACEMENT CURVE OF CONCRETE BORED PILE IN SATURATED SAND..... 86

FIGURE 3.8 INFLUENCE OF THE EXPONENT REPRESENTING THE CHANGE OF STIFFNESS AT CURRENT DENSITY ON LOAD-DISPLACEMENT CURVE OF CONCRETE BORED PILE IN SATURATED SAND..... 87

FIGURE 3.9 PILE LOAD TESTING – NORMALISED INTERGRANULAR STRAIN TENSOR FOR (A) DENSE SAND AND (B) LOOSE SAND 88

FIGURE 3.10 COMPARISON OF LOAD-DISPLACEMENT CURVE OF REAL STATIC LOAD TEST WITH SIMULATED TEST USING MOHR-COULOMB AND HARDENING SOIL MODELS..... 90

FIGURE 3.11 INTERPRETATION OF LOAD-SETTLEMENT CURVE USING DAVISSON METHOD 90

FIGURE 3.12 THREE-DIMENSIONAL FINITE ELEMENT MODEL USED IN SIMULATION: (A) PLAN VIEW (B) THREE-DIMENSIONAL VIEW 93

FIGURE 3.13 PLAN VIEW OF A SIMULATED STATIC LOAD TEST WITH (A) TWO REACTION PILES AND (B) FOUR REACTION PILES 94

FIGURE 3.14 COMPARISON OF INTERACTION OF TWO AND FOUR REACTION PILES WITH THE TEST PILE ($D_{TEST\ PILE} = D_{REACTION\ PILE}$ AND $L_{TEST\ PILE} = L_{REACTION\ PILE}$)..... 94

FIGURE 3.15 COMPARISON OF LOAD-DISPLACEMENT CURVE OF TEST PILE IN DIFFERENT DISTANCES OF REACTION PILES ($D_{TEST\ PILE} = D_{REACTION\ PILE}$ AND $L_{TEST\ PILE} = L_{REACTION\ PILE}$)..... 95

FIGURE 3.16 EFFECT OF REACTION PILE LENGTH ON THE TEST PILE WITH A LENGTH OF 9.5 M ($D_{TEST\ PILE} = D_{REACTION\ PILE}$)..... 96

FIGURE 3.17 EFFECT OF REACTION PILE DIAMETER ON TEST PILE WITH A DIAMETER OF 1.3 M ($L_{TEST\ PILE} = L_{REACTION\ PILE}$)..... 97

FIGURE 3.18 EFFECT OF DIFFERENT REACTION PILES (A) CONCRETE PILE, (B) STEEL PIPE PILE WITH FULLY UNPLUGGED BEHAVIOUR AND (C) STEEL PIPE PILE WITH PARTIALLY PLUGGED BEHAVIOUR ON TEST PILE WITH A DIAMETER OF 1.3 M ($L_{TEST\ PILE} = L_{REACTION\ PILE}$) 98

FIGURE 3.19 EFFECT OF STEEL PIPE PILE AS THE REACTION PILE ON THE TEST PILE 98

FIGURE 3.20 SUMMARY OF SOIL CONDITION AND CAP DIMENSION..... 101

FIGURE 3.21 PLAN VIEW OF (A) GROUP A AND (B) GROUP B (AFTER ISMAEL 2001)..... 103

FIGURE 3.22 FINITE ELEMENT MODEL OF PILE GROUP AND ADJACENT SOIL 104

FIGURE 3.23 PILE GROUP LAYOUT FOR DIFFERENT ANALYSES 105

FIGURE 3.24 (A) MEASURED AND PREDICTED LOAD-DISPLACEMENT CURVES FOR GROUP A (B) GROUP B 106

FIGURE 3.25 COMPARISON OF MEASURED AND PREDICTED AXIAL LOAD DISTRIBUTION ALONG THE CENTRAL PILE IN GROUP A 110

FIGURE 3.26 PREDICTED AND AVERAGED LOAD – DISPLACEMENT OF PILE GROUP B VERSUS THE SINGLE PILE 110

FIGURE 3.27 GROUP SETTLEMENT RATIO VERSUS PILE GROUP SETTLEMENT 111

FIGURE 3.28 TOP (T_i) AND BASE (B_i) LOAD IN CENTRAL PILE IN PILE GROUP 112

FIGURE 3.29 RATIO OF THE INDIVIDUAL PILE LOAD TO THE AVERAGE INDIVIDUAL LOAD 113

FIGURE 3.30 INDIVIDUAL PILE LOAD-DISPLACEMENT CURVE FOR PILE GROUP B..... 113

FIGURE 4.1 FREE PILE TOP FORCE AND VELOCITY UNDER ACTION OF SUDDENLY APPLIED CONSTANT FORCE (AFTER RAUSCHE, GOBLE & LIKINS 1985) 120

FIGURE 4.2 FREE PILE TOP VELOCITY UNDER ACTION OF SOIL RESISTING FORCE..... 123

FIGURE 4.3 INDUCED AND REFLECTED WAVES DUE TO THE HAMMER IMPACT OVER THE PILE HEAD..... 130

FIGURE 4.4 (A) STRATIGRAPHY OF SITE AT THE LOCATION OF PILE ISU5 (B) CROSS SECTION OF THE STEEL H-PILE (AFTER NG ET AL. 2011)..... 133

FIGURE 4.5 SIGNALS MEASURED AT (A) END OF DRIVING (B) SIXTH RESTRIKE TEST (AFTER NG ET AL. 2011) 134

FIGURE 4.6 COMPARISON OF TOTAL SOIL RESISTANCE (RTL) BETWEEN PDA AND THE MATLAB CODE..... 135

FIGURE 4.7COMPARISON OF MAXIMUM STATIC SOIL RESISTANCE (RMX) BETWEEN PDA AND THE DEVELOPED CODE USING MATLAB 136

FIGURE 4.8 COMPARISON OF MAXIMUM COMPRESSIVE STRESS (CSX) BETWEEN PDA AND THE MATLAB CODE 136

FIGURE 4.9 COMPARISON OF MAXIMUM ENERGY TRANSFERRED TO THE PILE (EMX) BETWEEN PDA AND THE MATLAB CODE 137

FIGURE 4.10 THE EFFECT OF CASE DAMPING FACTOR ON THE MAXIMUM STATIC SOIL RESISTANCE IN BOTH CONDITIONS END OF DRIVING (EOD) AND BEGINNING OF RESTRIKE (BOR) 137

FIGURE 4.11 INCREASING OF MAXIMUM STATIC SOIL RESISTANCE (RMX) WITH TIME USING DIFFERENT CASE DAMPING FACTOR..... 138

FIGURE 4.12 THE AMOUNT OF MAXIMUM STATIC SOIL RESISTANCE (RMX) RELATIVE CHANGES WHEN CASE DAMPING FACTOR CHANGES FROM 0.7 TO 1 138

FIGURE 5.1 FINITE ELEMENT MODEL OF THE PILE, APPLIED HARMONIC LOAD AND THE ADJACENT GROUND WITH THE CORRESPONDING GENERATED MESH AND POINTS A, B, C AND D AND THEIR CORRESPONDING RADIUSES r_A=1M, r_B=3M, r_C=6M AND r_D=9M..... 153

FIGURE 5.2 VARIATION OF SHEAR STRESS IN SOIL AT DIFFERENT DISTANCES FROM PILE SHAFT, (A) DENSE SAND, AND (B) LOOSE SAND (HARDENING SOIL MODEL) 154
FIGURE 5.3 PILE HEAD DISPLACEMENT (A) DENSE SAND AND (B) LOOSE SAND 156
FIGURE 5.4 IMPEDANCE × VELOCITY VARIATION WITH TIME, RECORDED AT THE GAUGE LOCATION FOR (A) DENSE SAND, AND (B) LOOSE SAND 158
FIGURE 5.5 VELOCITY × IMPEDANCE AND FORCE TRACES, RECORDED AT THE GAUGE LOCATION USING HARDENING SOIL MODEL FOR DENSE SAND BY APPLYING HARMONIC LOADING WITH A FREQUENCY OF 50 HZ 159
FIGURE 5.6 APPLIED HARMONIC LOAD WITH A FREQUENCY OF 250 HZ 159
FIGURE 5.7 VELOCITY × IMPEDANCE AND FORCE TRACES, RECORDED AT THE GAUGE LOCATION USING HARDENING SOIL MODEL FOR DENSE SAND BY APPLYING A HARMONIC LOAD WITH A FREQUENCY OF 250 HZ 160
FIGURE 5.8 INFLUENCE OF HYPOPLASTIC MODEL PARAMETERS ON THE MEASURED PILE HEAD DISPLACEMENT DURING THE PILE DRIVING IN DENSE SAND (A) CRITICAL FRICTION ANGLE, AND (B) GRANULAR HARDNESS 163
FIGURE 5.9 INFLUENCE OF INTERGRANULAR STRAIN PARAMETERS DEFINED IN HYPOPLASTIC MODEL ON THE MEASURED PILE HEAD DISPLACEMENT DURING THE PILE DRIVING IN DENSE SAND (A) βr AND (B) χ 164
FIGURE 5.10 CONCRETE PILE DRIVING – NORMALISED INTERGRANULAR STRAIN TENSOR FOR (A) DENSE SAND, AND (B) LOOSE SAND 165
FIGURE 5.11 ROD WITH TWO DIFFERENT TIP CONDITIONS (A) FIXED-END (B) ELASTIC SUPPORT AND (C) THE APPLIED HARMONIC LOAD (AFTERMASOULEH & FAKHARIAN 2008) 168
FIGURE 5.12 (A) COMPARISON OF NUMERICAL RESULTS REPORTED BY MASOULEH AND FAKHARIAN (2008) USING FLAC 2D WITH PLAXIS 2D PREDICTIONS CONDUCTED IN THIS STUDY: (A) FIXED-END ROD AND (B) ROD ON ELASTIC SUPPORT (E = 10 MPA) 169
FIGURE 5.13 CONE PENETROMETER RESULTS FOR THE SITE AT SHENTON PARK (AFTER BYRNE 1995) 171
FIGURE 5.14 FINITE ELEMENT MODEL OF THE PILE AND THE ADJACENT GROUND WITH THE CORRESPONDING GENERATED MESH 172
FIGURE 5.15 MEASURED FORCE WITH TIME AND NUMERICAL PREDICTIONS, (A) THE EFFECT OF DIFFERENT PARAMETERS ON SIGNAL MATCHING AND (B) THE BEST MATCH OBTAINED 174
FIGURE 5.16 COMPUTED DISPLACEMENT AT THE PILE HEAD 175
FIGURE 5.17 MAXIMUM COMPRESSIVE (A) AND TENSILE STRESSES (B) DISTRIBUTION ALONG THE PILE SHAFT 175

FIGURE 5.18 COMPARISON OF MEASURED AND PREDICTED PILE LOAD-DISPLACEMENT VARIATION DURING STATIC LOAD TESTING 176
FIGURE 5.19 (A) CONSTRAINED MODULUS OBTAINED THROUGH CPT, CPTU AND SDMT TESTS (B) SOIL STRATIGRAPHY AT THE LOCATION OF PILE 11B IN TERMS OF SOIL TYPE, AND (C) SOIL STRATIGRAPHY AT THE LOCATION OF PILE 11B IN TERMS OF SOIL ORIGIN 180
FIGURE 5.20 SHEAR MODULUS OBTAINED FROM SDMT TESTS 181
FIGURE 5.21 STRESS-STRAIN GRAPHS OBTAINED FROM TRIAXIAL TESTS CONDUCTED ON SAMPLES TAKEN FROM DIFFERENT DEPTHS 182
FIGURE 5.22 STIFFNESS DEGRADATION CURVE OBTAINED FOR DIFFERENT SOIL LAYERS 183
FIGURE 5.23 (A) SCHEMATIC DIAGRAM OF THE SIMULATED MODEL, AND (B) GEOMETRY OF THE PILE ALONE 185
FIGURE 5.24 AN AXISYMMETRIC FINITE ELEMENT MODEL OF THE PILE AND ADJACENT GROUND WITH THE CORRESPONDING GENERATED MESH 186
FIGURE 5.25 FORCE (F) AND VELOCITY TIMES IMPEDANCE (ZV) TRACES MEASURED BY PDA 187
FIGURE 5.26 COMPARISON OF (A) REAL PILE, (B) CAPWAP, AND (C) SIMULATED PILE IN NUMERICAL MODELLING 188
FIGURE 5.27 COMPARISON OF MEASURED AND PREDICTED VELOCITIES 189
FIGURE 5.28 COMPARISON OF MEASURED AND PREDICTED DISPLACEMENTS 189
FIGURE 5.29 PILE RESISTANCE TRACES: (A) TOTAL RESISTANCE, AND (B) STATIC RESISTANCE 190
FIGURE 5.30 CORRELATION OF PREDICTED AND MEASURED DATA (A) DOWNWARD, AND (B) UPWARD TRAVELLING WAVES 193
FIGURE 5.31 PREDICTED AND MEASURED APPLIED ENERGIES VERSUS TIME 194
FIGURE 5.32 COMPARISON OF LOAD-SETTLEMENT CURVE OBTAINED BY CAPWAP AND THE FINITE ELEMENT PROGRAM ... 195
FIGURE 5.33 INFLUENCE OF THE PILE-SOIL STRENGTH AND DEFORMATION PROPERTIES ON THE PILE HEAD VELOCITY 197
FIGURE 5.34 INFLUENCE OF THE PILE-SOIL STRENGTH AND DEFORMATION PROPERTIES ON THE MAXIMUM STATIC PILE RESISTANCE (RMX) 198
FIGURE 5.35 NEW STIFFNESS DEGRADATION CURVE FOR SILTY SAND LAYER BY CHANGING THE REFERENCE SHEAR STRAIN ... 199
FIGURE 5.36 COMPARISON OF MEASURED AND PREDICTED DISPLACEMENTS BETWEEN CAPWAP AND THE CONTINUUM NUMERICAL MODEL BY ASSIGNING THE REFERENCE SHEAR STRAIN EQUAL TO $10 - 4$ TO ALL SOIL LAYERS 199
FIGURE 5.37 WAVES GENERATED FROM PILE DRIVING AND DYNAMIC LOAD TESTING OPERATIONS (AFTER DUNGCA ET AL. 2016) 203

FIGURE 5.38 MEASURING GROUND VIBRATION USING SEISMOGRAPH..... 204

FIGURE 5.39 GROUND VIBRATIONS INDUCED BY DYNAMIC LOAD TESTING, (A) THREE DIFFERENT BOREHOLES DEFINED IN THE MODEL, (B) THREE-DIMENSIONAL SIMULATED MODEL, AND (C) PLAN VIEW AND THE LOCATIONS OF VIBRATION MEASUREMENT 206

FIGURE 5.40 THE VARIATIONS OF VERTICAL PARTICLE VELOCITIES IN DIFFERENT DISTANCES FROM SOURCE OF VIBRATION... 212

FIGURE 5.41 THE VARIATIONS OF PARTICLE VELOCITIES IN DIFFERENT DISTANCES IN THREE DIFFERENT ORTHOGONAL DIRECTION, (A) 5M, (B) 10 M, (C) 20 M, (D) 30 M AND (E) 40 M..... 213

FIGURE 5.42 THE VARIATIONS OF PEAK VERTICAL PARTICLE VELOCITIES IN DIFFERENT DISTANCES FROM THE SOURCE OF VIBRATION..... 214

FIGURE 5.43 RESPONSE OF THE BUILDING AND INHABITANTS IN A VICINITY OF PILE DRIVING SITE..... 214

LIST OF TABLES

TABLE 2.1 SUMMARY OF SUGGESTED DYNAMIC SOIL PARAMETERS (AFTER NG & SRITHARAN 2013) 36

TABLE 2.2 REQUIRED PARAMETERS FOR MOHR-COULOMB MODEL (AFTER BRINKGREVE, KUMARSWAMY & SWOLFS 2017) 41

TABLE 2.3 REQUIRED PARAMETERS FOR HARDENING SOIL MODEL (AFTER BRINKGREVE, KUMARSWAMY & SWOLFS 2017) . 45

TABLE 2.4 REQUIRED PARAMETERS OF GRANULAR MATERIAL FOR HYPOPLASTIC MODEL (AFTER DUNG 2009) 47

TABLE 2.5 DEFINED PARAMETERS IN INTERGRANULAR STRAIN CONCEPT (AFTER DUNG 2009)..... 48

TABLE 3.1 BASKARP SAND PROPERTIES (AFTER DUNG 2009)..... 76

TABLE 3.2 MOHR-COULOMB MODEL PROPERTIES FOR BASKARP SAND 76

TABLE 3.3 INTERFACE PARAMETERS OF DIFFERENT SOIL MODELS DEFINED IN NUMERICAL MODELLING 78

TABLE 3.4 ADOPTED SOIL PARAMETERS IN THE NUMERICAL MODELLING (AFTER WEHNERT & VERMEER 2004)..... 89

TABLE 3.5 ULTIMATE CAPACITY OF THE TEST PILE USING DAVISSON METHOD 91

TABLE 4.1 SUMMARY OF CASE DAMPING FACTORS (AFTER HANNIGAN ET AL. 1998) 127

TABLE 4.2 SCHEDULE OF RESTRIKE TESTS BASED ON THE ELAPSED TIME AFTER END OF DRIVING (AFTER NG ET AL. 2011) ... 134

TABLE 5.1 PROPERTIES OF THE CIRCULAR ROD USED IN THE MODEL 166

TABLE 5.2 PROPERTIES OF DENSE SAND IN SHENTON PARK..... 171

TABLE 5.3 HARDENING SOIL WITH SMALL STRAIN STIFFNESS MODEL SOIL PROPERTIES..... 184

TABLE 5.4 COMPARISON OF SHAFT RESISTANCE BETWEEN DIFFERENT METHODS 191

TABLE 5.5 COMPARISON OF PILE RESISTANCE OBTAINED BY CAPWAP AND PLAXIS 192

TABLE 5.6 CAPABILITY OF CORRELATION OF DYNAMIC AND STATIC BEHAVIOUR OF PILE IN THE NUMERICAL MODEL 194

TABLE 5.7 DISPLACEMENT OF PILE HEAD AND TOE DUE TO THE SLS LOADING 196

TABLE 5.8 TYPICAL RANGE OF STRUCTURAL RESPONSES TO THE PILE DRIVING (AFTER BRITISH STANDARD 1990)..... 208

TABLE 5.9 TRANSIENT VIBRATIONS GUIDE VALUES FOR COSMETIC DAMAGE (AFTER BRITISH STANDARD 1993) 209

TABLE 5.10 GUIDELINES VALUES FOR TRANSIENT VIBRATION ON STRUCTURES (AFTER GERMAN STANDARD 1999)..... 209

NOTATIONS

Latin Letters

A	Cross section of pile
c	Wave propagation speed
c	Soil cohesion
D	Pile diameter
D_r	Relative density
e_{c0}	Critical void ratio at zero pressure
e_{d0}	Minimum void ratio at zero pressure
e_{i0}	Maximum void ratio at zero pressure
E	Elastic modulus
E_{50}	Secant elastic modulus for a mobilization of 50% of the maximum shear strength
E_{50}^{ref}	Secant stiffness in standard drained triaxial test
E_M	Menard modulus
E_{oed}^{ref}	Tangent stiffness for primary oedometer loading
E_{ur}^{ref}	Unloading / reloading stiffness
F	Force measured at the gauge location
F_c	Correction factor
$F_m(t^*)$	Measured force at any time at the gauge location
$F_T(t)$	Force measured at the pile head
h_s	Granular hardness
J	Damping factor

J_c	CASE damping factor
k_0^{nc}	k_0 for normal consolidation
L	Length of pile
L_c	Length of stress wave
M	The total mass of a pile
m	Power for stress level dependency of stiffness
m	Maximum steps
m_R	Stiffness increase for a 180 degree reversal
m_T	Stiffness increase for a 90 degree change of strain path direction
n	Sensitivity of granular skeleton to change of pressure
n	Number of sub-steps
P_s	The mean particle pressure
P^{ref}	Reference stress for stiffness
Q_{ave}	Average individual pile head load
q	Soil quake
R	Radius of elastic range
R_d	Dynamic soil resistance
R_{int}	Interface strength reduction factor
R_f	Failure ratio
R_s	Group settlement ratio
R_s	Static soil resistance
R_{toe}	Static toe resistance

S	Settlement without the influence of reaction piles
S_m	Settlement considering the influence of reaction piles
t_{max}	The time of impact
t^*	Time corresponding to measured force and velocity (any time)
t_1	Impact time (time corresponding to first peak in force and velocity traces)
t_2	Time corresponding to wave reflection from pile toe
v	Velocity measured at the gauge location
v_b	Velocity of the pile toe
$v_m(t^*)$	Measured velocity at the gauge location
$v_R(t)$	The particle velocities of the generated waves due to the resistance
$v_T(t)$	Velocity at the pile head
$v_T^d(t)$	Pile top velocity due to the downward travelling wave caused by soil resistance
$v_T^u(t)$	Pile top velocity due to the upward travelling wave caused by soil resistance
W_D	Downward travelling wave
W_U	Upward travelling wave
Z	Pile impedance

Greek Letters

α	Exponent describes the transition between peak and critical stress
α	Influence of mass in the damping
β	Exponent represents the change of stiffness at current density
β	Influence of stiffness in the damping
β_R	Material constant
$\gamma_{0.7}$	Threshold shear strain
Δt	Duration of dynamic loading
δt	Time step used in dynamic calculations
σ_c	Compressive stress
σ_T	Tensile stress
υ_{ur}	Poisson ratio for unloading-reloading
ϕ_c	Critical state friction angle
χ	Material constant represents stiffness degradation

Acronyms

BOR	Beginning of restrike
CAPWAP	CAse Pile Wave Analyses Program
CL	Centre line
CSX	Maximum compressive stress

DSX	Maximum displacement of pile
EMX	Maximum transferred energy at gauge location
EOD	End of driving
HP	Hypoplastic
HS	Hardening Soil
HS-Small	Hardening Soil with Small Strain Stiffness
IGS	Intergranular Strain
LE	Linear elastic
MC	Mohr-Coulomb
PDA	Pile driving analyser
PPV	Peak particle velocity
RMX	Maximum static soil resistance
RTL	Maximum total resistance
RX0	Maximum static soil resistance with CASE damping factor zero
SDMT	Seismic dilatometer test
SET	Permanent displacement of pile
SFR	Static shaft resistance

SFT	Total shaft resistance
TC	Temporary compression
WEAP	Wave equation analysis program

ABSTRACT

Piles are generally used to carry structural loads when the soil at the ground surface is low in strength or the loads are substantial. It is very common to conduct pile load testing to assess whether the piles will behave as predicted in the design stage. Static load testing (SLT) is considered to be the benchmark for assessing the performance of piles since it is known the most fundamental way of pile load testing. However, this kind of test is time consuming and expensive, and in cases such as offshore operations, SLT is generally not possible for many cases. In spite of this, powerful computer programs for pile testing simulation have been revolutionised and are available. Of these different methods, the dynamic load testing (DLT) method for assessing the static bearing capacity of piles is of major interest and importance. A dynamic pile test is based on the signal matching technique in which the pile-soil system is modelled using the CAse Pile Wave Analyses Program (CAPWAP). This program tries to calculate the tip and side resistance of embedded piles and produces a force versus time signal which matches the measured data. The signal matching analysis uses a one-dimensional wave equation analysis of piles based on the Smith model to differentiate between toe and shaft resistance, to ascertain the distribution of frictional resistance along the pile shaft to determine the tensile and compressive stresses during pile driving. However, this technique uses a mass–spring–dashpot system to model the soil media surrounding and below the toe which imposes some restrictions such as being user-dependant process and using constant uncommon soil parameters such as quake along the pile length, regardless of soil strata, which can be layered or uniform. Furthermore, using CAPWAP to analyse pile driving interrupts the continuity of different stages of pile modelling from simulating pile driving, quality control, and investigating settlement. GRLWEAP or CAPWAP generally should be used

with a second software package such as PLAXIS in order to investigate any subsequent settlement or interaction.

In order to overcome the aforementioned limitations and assess pile behaviour during load testing in more detail, so-called continuum numerical models using the finite element program PLAXIS are established. In these numerical models, wave propagation, the static and dynamic response of piles during load testing for solid concrete piles and open-ended tubular steel piles are evaluated. In fact, the numerical simulations in this study are a remarkable improvement compared to the previous numerical studies because when simulating pile load testing, different soil models such as the Mohr-Coulomb, hardening soil, hardening soil with small strain stiffness and hypoplastic with intergranular strain are utilised to carry out a more rigorous deformation analysis.

To investigate the capability of the numerical model, the dynamic and static responses of a driven steel pipe pile monitored as part of a highway bridge construction project in New South Wales, Australia is simulated and numerically analysed using the finite element method. During these dynamic and static load testing simulations, a hardening soil model with small strain stiffness is used to obtain the best correlation between the large and small strains, while the pile is under a static load and being driven. The numerical predictions obtained using two-dimensional continuum finite element simulations are then compared with the corresponding predictions obtained from the CASE method and CAPWAP program to evaluate the predictions. Moreover, the total and static soil resistances as well as displacement and velocity traces obtained from numerical model are compared with the existing data acquired from the field measurements. The results indicate that the hardening soil model with small strain stiffness exhibits a reasonable correlation with the field measurements during static and dynamic loading.

Evaluation of static and dynamic pile load testing based on the continuum based finite element model has many advantages for geotechnical engineers dealing with pile design, because an established continuum numerical model can assess pile testing under more realistic conditions. This model can also be used to evaluate the performance of piles under different loading conditions on a single pile or group of piles, and piles built close to existing structures. Furthermore, this method retains the continuity of different stages of modelling from simulating pile driving, quality control, and investigating settlement, while all these analyses are carried out using one appropriate finite element based software.

CHAPTER 1 Introduction

1.1 Background and Problem Statement

The main function of piles, as columnar elements in a foundation, is to transfer the load from the superstructure via weak layers of soil (or water), onto stiff soils or rock (Rajapakse 2016; Randolph 2003; Tomlinson & Woodward 2014). Piles when used to support high-rise buildings subjected to overturning forces from wind may be required to bear uplift loads, while in offshore structures they are subjected to lateral loads from waves. Likewise, on those occasions where piles are used to support bridge piers, retaining walls, and abutments, they can carry a combination of vertical and horizontal loads. Despite the fact that methods for designing piles has advanced considerably over the past few decades, the principal aspect of pile design is still estimating the axial bearing capacity, and this depends mainly on empirical correlations (Alielahi & Adampira 2016; Mijena 2012; Rezazadeh & Eslami 2017).

These days, pile load testing is known as the most decisive method for specifying the pile load capacity and it plays a significant role in the field of deep foundation design. The tests can be conducted by either static and non-static methods, but according to Hertlein & Davis (2007) the key objective of pile load testing is to provide information about the following properties:

- The pile's bearing capacity
- The load-displacement behaviour of a pile

- The performance of a pile during testing
- The integrity of a pile

As discussed by Fleming et al. (2008), pile load tests may be carried out at different stages of construction, including those tests carried out during and after the construction. Different methods of pile testing, based on Handley et al. (2006), are best described by the length of time in which a force is applied to a pile and the strain generated in the pile. Static load testing, where large forces are applied for long periods of time, are used to evaluate the pile load capacity, whereas low energy and low-strain tests that only involve impact from a hammer (a non-destructive test) are used to check a pile's integrity. During the high-strain dynamic load testing the force is applied in shorter period than that of a static load testing, although, it is comparable in magnitude.

To verify the axial capacity and static load–displacement behaviour of piles, static pile load testing has long been regarded as the most valid method, but since it is expensive and takes time, non-static pile load testing are considered to be proper substitutes. With the advent of high powered computers, pile testing has continued to develop in conjunction with a diversity of tests for estimating and measuring pile resistance, as well as a variety of methods for quickly and economically testing their integrity. The cost effectiveness and performance of high-strain dynamic load testing methods compared to static load testing (SLT) methods means that non-static methods can widely be used. Non-static pile load tests are carried out by applying an impact force onto the pile head, which is then the responses of the pile are measured and recorded to determine the results. However, careful consideration is needed when interpreting the dynamic influences in order to determine the static load capacities (Hussein & Goble 2004; Svinkin & Woods 2009).

As Smoltczyk (2003) states, most of the current dynamic test methods are governed by one-dimensional wave propagation theory. As cited by Masouleh & Fakharian (2008), Smith, in 1960, proposed an innovative solution to the one-dimensional wave equation analysis in piles by simulating a pile with a number of masses, which attached together by elastic springs and replacing the soil by a number of springs, sliders and linear viscous dampers. This discretised model does need to estimate some important soil parameters such as damping coefficients and quake, as well as the hammer efficiency which significantly affects the results of the analysis. Rausche (1970) and Rausche, Goble & Likins (1985), based on the Smith model, proposed a signal matching technique and developed CAPWAP program which uses the results of a pile dynamic test to determine pile bearing capacity.

However, since this technique uses a mass–spring–dashpot system to model the surrounding and below the pile toe soil media therefore it indicates some limitations; for instance, during the analysis, soil inertia or the radiation damping effect is automatically omitted, and considering this option for very cohesive or plastic soils causes the program to produce unreasonable results and over-predicts the bearing capacity of the pile. In addition, a real pile is a continuum body with an enormous number of degrees of freedom enclosed by a continuum medium that is soil while, in the mass-spring-dashpot system the boundary conditions differ from a real system and cause deviations in the system response. Hence, developing a so-called continuum based numerical model to overcome some of the restrictions inherent in mass-spring-dashpot system for accurate interpreting the results of dynamic pile load testing is inevitable. In addition, applying the developed numerical model means that design continuity remains by the use of real soil parameters. Therefore, all analyses, including installation and quality control, are carried out using the same software, whereas GRLWEAP (Goble & Rausche 1976) or CAPWAP requires

to employ a second software package such as PLAXIS (Brinkgreve, Kumarswamy & Swolfs 2017) to investigate the subsequent settlement or interaction. In the limited studies available in the literature (Kasali et al. 2006; Pinto, Grazina & Lourenco 2008; Fakharian, Masouleh & Mohammadlou 2014) signal matching analyses have been carried out using the continuum finite element or finite difference methods, where the installation of solid concrete piles is simulated by utilising the elastic – perfectly plastic Mohr-Coulomb soil model. These studies reveal a reasonable match between measurements and predictions after updating the soil parameters through signal matching. According to these studies more rigorous soil models that can simulate the cyclic behaviour of soil from small to large strains, as observed during dynamic and static load testing, are necessary. The procedure of capturing the real soil behaviour, adopting advanced soil models during static and dynamic load testing simulation, is shown in Figure 1.1.

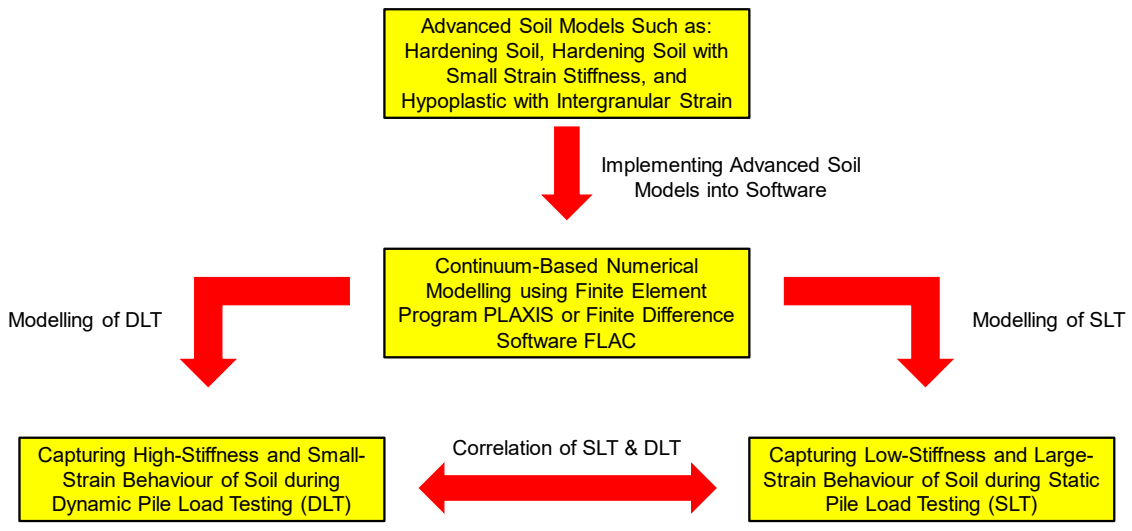

Figure 1.1 Application of advanced soil models in accurate prediction of soil behaviour during static and dynamic pile load testing

1.2 Scope and Objectives

The main objective of this research is to simulate static and dynamic pile load testing using numerical modelling. Since full-scale static load tests are difficult and costly, there is an objective need to predict a single pile or pile group response under static load testing using proper numerical modelling. In addition, the literature review indicates that existing studies into the numerical simulation of dynamic pile load testing are limited, especially those incorporating the steel pipe piles characteristics, using advanced soil models. This study, therefore focuses on the application of advanced soil models for predicting large and small strain behaviour of piles, as observed during static and dynamic load testing. In this research, the numerical approaches are carried out with the following specific research scopes and objectives:

1. To provide an insightful review of the current knowledge of different methods of pile load testing to determine the bearing capacity of piles.
2. To present the results of finite element numerical approach in order to compare the effects of different soil models on load-displacement curves obtained during static load testing a concrete solid pile whose behaviour is evaluated by applying prescribed displacements over its head.
3. To evaluate the interaction of reaction piles on the performance of test pile during the static load testing applying the reaction pile system in terms of recorded pile head displacement to provide appropriate distance needed to avoid the interaction effects.
4. To achieve a reasonable correlation between predicted and measured load-settlement curves obtained during axial static load testing of concrete bored piles group and to assess the behaviour of piles group in more detail to overcome the difficulties and cost of full-scale load tests.

5. To investigate the principals behind the CASE method as an approximate and a direct method used in a pile driving analyser (PDA) to predict the static bearing capacity and performance of a pile being driven and to evaluate the sensitivity of maximum static soil resistance (RMX) to CASE damping factor (J_c) in both consolidated and unconsolidated soil conditions.
6. To evaluate the response of driven open-ended steel pipe piles during dynamic load testing in more realistic conditions than with the discretised model used in CAPWAP or GRLWEAP programs, and to retain continuity to assess the settlement and performance of piles under different loading conditions using one software.
7. To investigate ground vibration induced by dynamic pile load testing at different distances from the source of vibration in terms of peak particle velocity (PPV) as a parameter used to analyse ground vibrations and identify the minimum distance needed to avoid the adverse effects of ground vibrations based on different codes and standards.

1.3 Thesis Outline

The structure of this thesis is as follows:

- Chapter 1 presents the research background, introduces pile load testing and describes the issues that need to be addressed, along with the aims and scope of the present research.

- Chapter 2 delivers a comprehensive review of the literature relevant to methods of pile testing and interpreting the results. Existing analytical, numerical and experimental approaches are examined to assess the behaviour of piles during static and dynamic load testing, and to evaluate those factors affect the results such as

dynamic soil parameters such as quake and damping. The findings of this chapter are summarised, and important gaps in our present knowledge are highlighted.

- Chapter 3 describes a numerical approach to investigate static load testing. In this chapter the behaviour of concrete bored pile during static load testing is evaluated using the common soil model (i.e. Mohr-Coulomb model) and the advanced soil models (e.g. hardening soil and hypoplastic with intergranular strain). Moreover, the interaction of reaction piles on the test piles is evaluated in the case of static load testing conducted with anchored piles, using PLAXIS 3D. Furthermore, different analyses including a combination of non-linear and linear analysis is performed to capture a reasonable correlation with data measured for a bored pile group under static load testing.

- Chapter 4 contains the background of CASE method for dynamic pile load testing analysis. In this chapter, the required equations for estimating the total and static soil resistances are presented. The MATLAB program is used to write a code to analyse pile driving, and the results of a real case dynamic pile load testing are compared with the results generated by the written code.

- Chapter 5 presents the background of dynamic load testing and the methods used to assess the static pile capacity. In this chapter, the dynamic pile load testing of real case projects using Mohr-Coulomb and advanced soil model of HS-Small are simulated in the finite element program PLAXIS 2D, and the ability of advanced soil models to capture large and small strain behaviours, observed in dynamic and static load testing are evaluated. Finally, the ground vibrations generated by hammer blows during a real dynamic pile load testing, using PLAXIS 3D is evaluated to obtain the

peak particle velocity (PPV) as a managed value, in association with vibration risk and as a parameter used to analyse ground vibrations.

- Chapter 6 summarises the thesis and the key findings from this study, and also makes some recommendations for future research.

CHAPTER 2 Literature Review

As a consequence of existing problems in pile load testing, especially interpreting the results of dynamic load testing, this subject is still challenging for many researchers and engineers, despite the number studies carried out to investigate this matter. This chapter presents a review of existing static and dynamic pile load testing mechanisms as well as studies related to these kind of tests, especially experimental and numerical studies.

This chapter has seven main sections, which survey the existing studies and theoretical concepts of pile load testing. Section 2.1 shows how piles were used in ancient structures and the main reason for pile load testing. Section 2.2 reviews different kind of piles based on factors such as the method of installation, the materials used, and the mechanism for transferring load to the adjacent soil. It also comprises general discussion on the advantages and limitations of different types of piles. Section 2.3 discusses traditional and fundamental method of the static load testing (SLT), it also introduces the different approaches used to carry out SLT and how to interpret the load-displacement curve. Section 2.4 presents dynamic load testing (DLT) as a relatively new technique for evaluating the capacity of piles and also discusses how this test was introduced and the background and limitations of CAPWAP software. Section 2.5 explains a number of different constitutive soil models, ranging from basic to advanced soil models such as Mohr-Coulomb (MC), hardening-soil (HS), hardening-soil with small strain stiffness (HS Small) and hypoplastic with intergranular strain (HP-IGS). These soil models can be used to evaluate the behaviour of piles during static and dynamic load testing.

Section 2.6 presents several studies carried out in the field of pile load testing, including a number of field case studies and numerical simulations. In this section, the key challenges of numerical modelling associated with the correlation of static and dynamic test results are discussed. The last section summarises the gap and limitations in the existing literature.

2.1 Pile Load Testing Overview

The piles have been used in construction work for many centuries. Hussein & Goble (2004) point out the ancient Egyptians, Phoenicians, Romans, Greeks, Mesopotamians, Chinese, etc., used piles. According to Hussein & Goble (2004), in the place located between Switzerland and Germany, called "Lake Constance" archaeologists have found remains of wood piles that are evaluated to be between 2000 to 4000 years old. These piles supported the houses of the lake's inhabitants which were built in the lake for safety from attack. The Pons Sublicius is one of the oldest Roman bridges and the building procedure of the bridge supported by piles, across the Rhine River by Julius Caesar's army is well-documented (Hussein & Goble 2004). Piles are still used today as deep foundations to support many types of structures in various geotechnical and geological conditions both inshore and offshore. Because they play a key role in supporting structures, a great deal of effort and cost is involved in their construction. Due to the potentially disastrous consequences of pile-supported structures failure, there remains the constant need to evaluate piles according to the very latest available knowledge.

As Likins (2015) explains, after installation, piles cannot be seen and direct quality control of the finished product is not possible, therefore the process of installing piles must be controlled to obtain the desired end product. In recent decades a number of test

methods has fortunately become available and they are routinely applied to indirectly evaluate the structural integrity and load bearing capacity of piles. According to Likins (2015), the relatively moderate cost of testing compared to the cost of the foundations, carrying out pile testing is justified since it reduces the risk of foundation failure and in many cases reduces the overall cost of the foundations.

According to Huang et al. (2016), Weech (2002), and Fuller & Hoy (1970), the bearing capacity of a single pile or group of piles should be determined based on load testing results for specifying the safe load on piles. The aim of pile load testing is to establish criteria for the design and installation of a pile foundation and to prove the sufficiency of the pile-soil system for a proposed pile design load. In the first category tests are generally routine and they are carried out at the start of the construction at twice the proposed working load. To develop design and installation criteria, tests usually involve more complex programs and the piles are usually tested to failure. Routine pile load testing may be necessary based on a particular building code or general specification, but it is often a decision taken by the foundation engineer. Other objectives of a test program are to produce data to specify the most economical and appropriate pile foundation, the type of pile, highest working load for each pile type, the required length of pile, and the installation techniques required to obtain the desired results.

2.2 Classification of Piles

The primary functions of a pile foundation are to (a) transfer the structural load through the weak layer to one with adequate bearing capacity (b) increase the load bearing capacity of the soil, (c) tolerate lateral loads and function as a guard to prevent damage and shock, and (d) eliminate unpleasant settlement. The type of pile selected for a given footing should be based on a comprehensive study of long-term settlement, cost, stability under lateral and vertical loading, the required installation method, and the pile length needed to mobilise sufficient end bearing and frictional resistance. As Gunaratne (2013), Sitharam (2013) and Grand (1970) explain, piles can be classified based on several different factors, as shown in Figure 2.1:

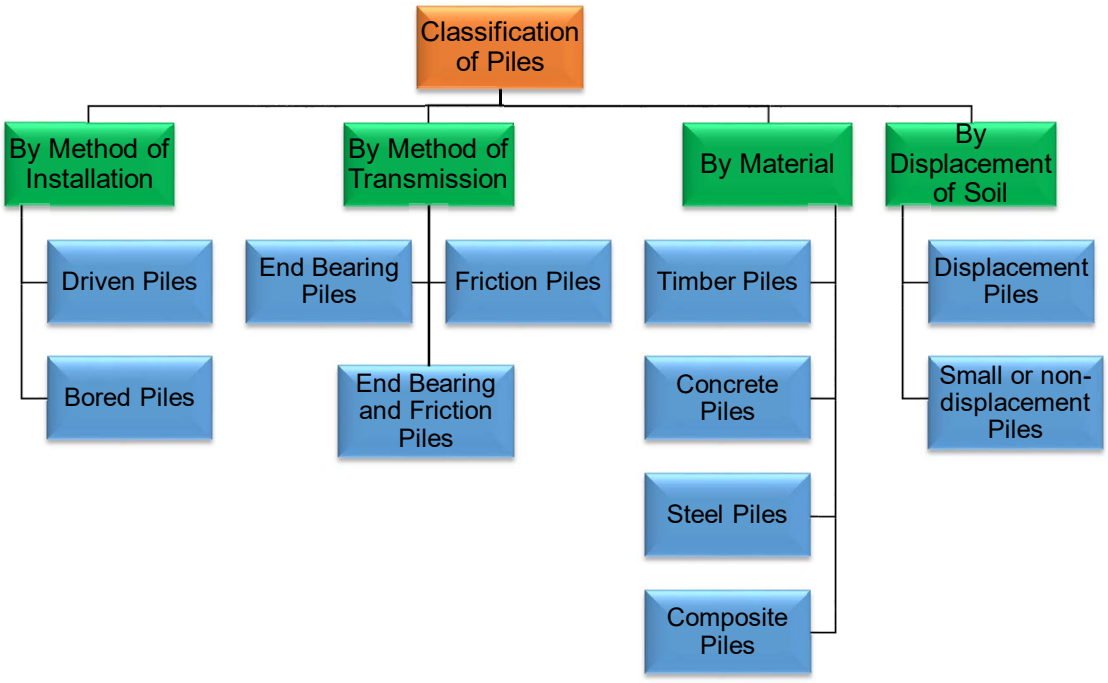

Figure 2.1 Classification of piles based on various factors

2.2.1.1 Based on Pile Material

Of the different pile types, concrete and steel piles are known as the most practical piles and are explained in this summary (Gunaratne 2013, Sitharam 2013, Grand 1970):

Concrete Piles: Concrete piles are either precast or cast in-situ. In general foundation work, cast-in-place piles are more commonly than precast piles. Cast-in-situ piles are constructed by drilling a hole into the ground, positioning the reinforcement, and then filling the hole with freshly prepared concrete. Depending on the conditions of the foundation and the type of concrete pile chosen, the bearing capacity of the pile can be mobilised as either skin friction or end bearing or a combination of the two. The main disadvantages of concrete piles are damage caused by an acidic environment, and abrasion from wave action in offshore foundations. They are widely used due to their relatively high capacity and reasonable cost. The installation process of typical cast-in-place concrete piles is shown in Figures 2.2.

Figure 2.2 Cast-in-place concrete piles (Gary Puntman 2018)

Steel Piles: Steel piles are made from rolled H-sections and pipe sections, they are used to withstand large impact stresses and where fewer disturbances from pile driving is desired. Steel piles are very strong in both compression and tension and are highly resistant to structural damage during driving; they can also be spliced to suit any desired length.

Steel pipe piles are increasingly being used as deep foundations for marine and onshore structures (Fattah & Al-Soudani 2016, Klos & Tejchman 1981, Lee, Salgado & Paik 2003). For instance, in the construction of the then-longest cross-sea bridge in the world, the Hangzhou Bay Bridge in China, more than 5,000 steel pipe piles were used (Yu & Yang 2011). Pipe piles are classified as open-ended and closed-ended; open-ended piles are similar to closed-end piles except there is no cap at the toe of the pile, but their behaviour is completely different. Pipe piles can be extended via obstructions since interferences can be broken or removed through the open-ended piles. They are often used where soil displacement would be unpleasant or where driving vibrations should be minimised. Open-ended pipe piles can be driven to great depths and at the site with sloping bedrock they can also be partially socketed into the rock. Sometimes they are filled with concrete after cleaning out them by water jets and compressed air, but sometimes open-ended steel pipe piles are carrying the load in skin friction and end bearing which indicates the soil in the pile is acting like a plug. Unless the plug generated during driving contributes to the problems, the entire plug is kept without any disturbance. Driven steel pipe piles are shown in Figure 2.3. Ideal conditions for open-ended pipe piles are known as:

- In a case where a soft stratum is followed by a layer of dense soil. In this case, the soil is pulled out from the pile after it has been driven to the required depth and refilled with concrete.
- In a case where a layer of medium dense soil is followed by a dense stratum. In this case, a closed-end pipe pile may not be a suitable choice because driving closed-end pipe piles via medium dense layers of soil may be difficult.

Figure 2.3 Driven steel pipe piles and the measurement of soil plug length (after Fattah & Al-Soudani 2016)

An open-ended pipe can be equipped with a special driving shoe that makes the steel at the toe thicker and it reduces stress and damage at the pile toe (Figure 2.4). The pile tip should be covered with a steel plate if the bearing capacity from the whole pile tip area is needed, in fact, a steel plate is used to cover the bottom of pipe piles to build the closed-end pipe piles (Figure 2.5). In most cases closed-end steel pipe piles are either filled with concrete or protective layer need to be used inside the pile.

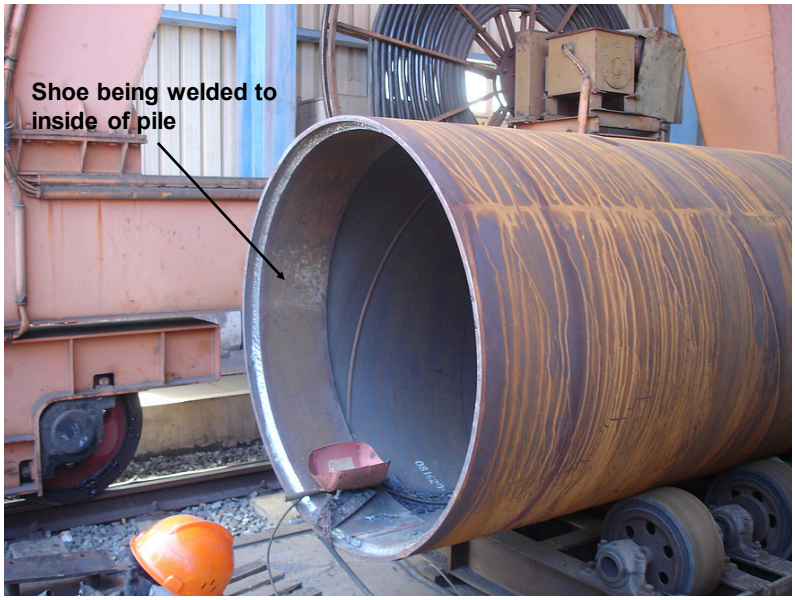

Figure 2.4 Driving shoe, which is welded at the pile toe (ESC Group 2018)

Figure 2.5 Closed-ended steel pipe pile (Pile Buck 2018)

According to field test results (Szechy 1961), the number of blows needed to drive open-ended piles into sand is less than closed-ended piles therefore it is generally accepted that an open-ended pile needs less endeavour to install than a closed-ended pile under the similar soil conditions.

- Plugging Effect

While impact driving open-ended piles through non-cohesive soils such as sand, internal shaft resistance due to the presence of soil inside the pile may be mobilised to stop new soil going inside the pile. This phenomenon, which is referred to as soil plugging, affects the driving specifications of an open-ended pile and changes the pile behaviour to a closed-end full displacement pile. The different stages of soil plugging are illustrated in Figure 2.6. As stated by Karlowskis (2014), when driving begins, soil enters the pile at approximately the same rate as the pile penetrates; this is called the unplugged state, but as the soil continues to move inside the pile, internal shaft resistance is mobilised so slippage is partly prevented and the rate of moving soil inside the pile is inhibited. This stage is referred to as partial plugging because while soil can still enter the pile, it is not at the same rate at which the pile penetrates the soil. Finally, internal shaft resistance increases until more soil cannot enter the pile hence it is considered to be fully plugged.

However, some studies (Smith, To & Wilson 1986 ; Brucy, Meunier & Nauroy 1991) have shown that the mode in which pile being driven is a substantial parameter in driving resistance. The behaviour of pile driven in a plugged mode is the same as a closed-ended pile, and a large-diameter pipe pile that is driven into sand will tend to be driven in unplugged mode (fully coring), while smaller diameter piles will be only partially plugged. Soil plug formation is facilitated by deeper penetration and lower relative densities because the soil plug that forms inside the pile during pile driving affect the driving response and static bearing capacity of open-ended piles.

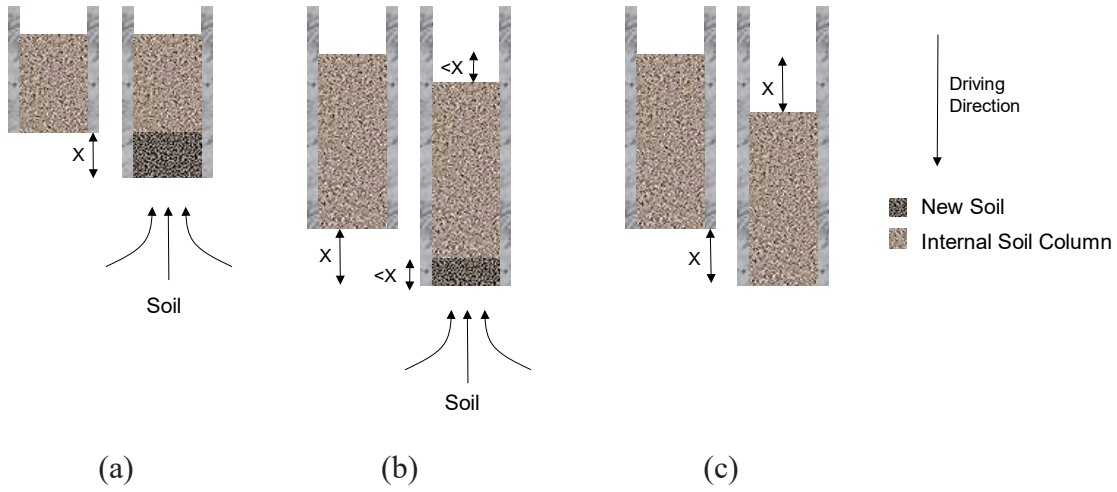

Figure 2.6 Different stages of soil plugging: (a) unplugged (b) partially plugged and (c) fully plugged. X illustrates the penetration distance of the pile (after Karlowskis 2014)

2.2.1.2 Based on load transmission method

End Bearing Piles: End piles or point bearing piles transfer the major part of their load through the toe (base) onto the dense soil layer. In fact, these kinds of piles can transmit the superstructural load through water or weaker soils onto a proper bearing layer by pile tip resistance, while at the same time, a portion of the load can be transferred to the surrounding soil layer via shaft friction (Gunaratne 2013; Sitharam 2013; Grand 1970).

Friction Piles: In these types of piles, the pile resistance is mainly mobilised by skin or shaft friction along the side of the pile (pile shaft). Pure friction piles (floating piles) are usually quite long because the load bearing capacity depends on the shaft area surrounded by soil. When no rock layer or rock-like material exists at a reasonable depth at a site, end bearing piles will be quite long and uneconomical hence the piles are driven via the soft soils to a specified depth. In other words, piles which mobilise most of their load-bearing capacity by shear stress along the shaft of the pile are appropriate where less compressible

stratums are too deep to reach economically (Gunaratne 2013, Sitharam 2013, Grand 1970).

Friction and End Bearing Piles: In most cases the load bearing capacity of piles depends on both end-bearing and shaft friction; for instance, the performance of an open-ended pipe pile can be summarised in two different cases (Gunaratne 2013; Sitharam 2013; Grand 1970):

1) The pile resistance is mainly mobilised via external and internal shaft friction while only a small part of the resistance is mobilised through the toe of the pipe.

2) A part of pile resistance is mobilised via external shaft friction while part of the resistance is mobilised through the soil plug that develops in the end of the pile as well as the toe of the pipe.

2.2.1.3 Based on installation method

Driven or Displacement Piles: With these types of piles, the pile is driven by hammer impact or jack and any variations in the stress state such as the degree of compaction in the surrounding soil or below the toe are complicated to measure, hence making it more sophisticated to predict the axial capacity of the pile. As explained by Swan (2013) the pile driving process can potentially generate large stresses and deformation in the nearby soil, therefore the pre-construction soil properties do not necessarily represent the post-construction properties. This is an important source of ambiguity in pile foundation analysis and design.

Bored or Replacement Piles: With these piles, where casing or drilling mud and proper construction situation are utilised, the initial state of stress is relatively kept without any change in the vicinity of the pile shaft and below the toe.

2.2.1.4 Based on the displacement of soil during installation

Piles may be classified based on the degree of displacement of the soil in which the piles are installed.

Displacement Piles: Examples of these piles are driven solid piles which cause lateral displacement of the soil and consequently pre-construction soil properties may change.

Small or Non-displacement Plies: Piles with rolled steel sections, screw piles, and open-ended hollow section piles displace small amounts of soil during driving hence they are called small-displacement piles. With bored piles, a hole is bored into the soil, and then a pile is constructed by concreting the cased or uncased hole after placing the reinforcement inside the hole; these piles are called non-displacement piles. Bored and cast in-situ or bored precast piles are examples of non-displacement piles.

2.3 Static Pile Load Testing

Static load testing (SLT) involves directly measuring the displacement of a pile head while applying a test load. It is the most principal form of pile load testing and is regarded to be the yardstick of pile performance. This kind of testing is normally conducted in the load range of 10 to 2000 tonnes (Paikowsky 2006). This method is suited for all types of piles regardless of how they are installed, and may therefore be performed on working piles or sacrificial initial piles. The main reason for constructing trial or sacrificial initial

piles is to perform load tests, hence they are commonly loaded to failure. However, testing working piles is limited to demonstrate that a pile will operate properly at the design load or more to confirm that the pile has secure capacity and will remain in service. During an SLT, the applied load and the obtained settlement are measured to trace a load-settlement curve that is then used to specify the pile's nominal resistance.

An SLT may performed for the following load characteristics:

- Vertically in the direction of the pile shaft (in compression or in tension)
- Laterally by applying a load horizontally to the pile head

According to Crowther (1988), the load applied in the SLT method can be either by direct dead weight or hydraulic jacking. With a direct dead weight the load is applied to the test pile by adding incremental weights such as water tanks, timber cribs containing soil, concrete blocks and pig iron. However, applying a load by adding dead weights is now non-existent, but a dead weight is still used as a reaction to hydraulic jacking. With an SLT, a load is sometimes applied by a jack acting against a reaction mass (Kentledge or dead weight) as shown in Figure 2.7, but it is most commonly applied against a reaction beam (Figure 2.8), supported by cable anchors or reaction piles (as the anchorage system) installed into the ground to supply tension resistance. The test load is usually applied incrementally and it is maintained for a determined time period in each increment or until the rate of pile movement is less than a specified value according to the appropriate code.

According to ASTM International (2013), to apply a load with a hydraulic jack which is acting against an restrained reaction frame, a sufficient number of anchor piles or anchoring devices including cable anchors are necessary to provide enough reactive capacity for the test beams.

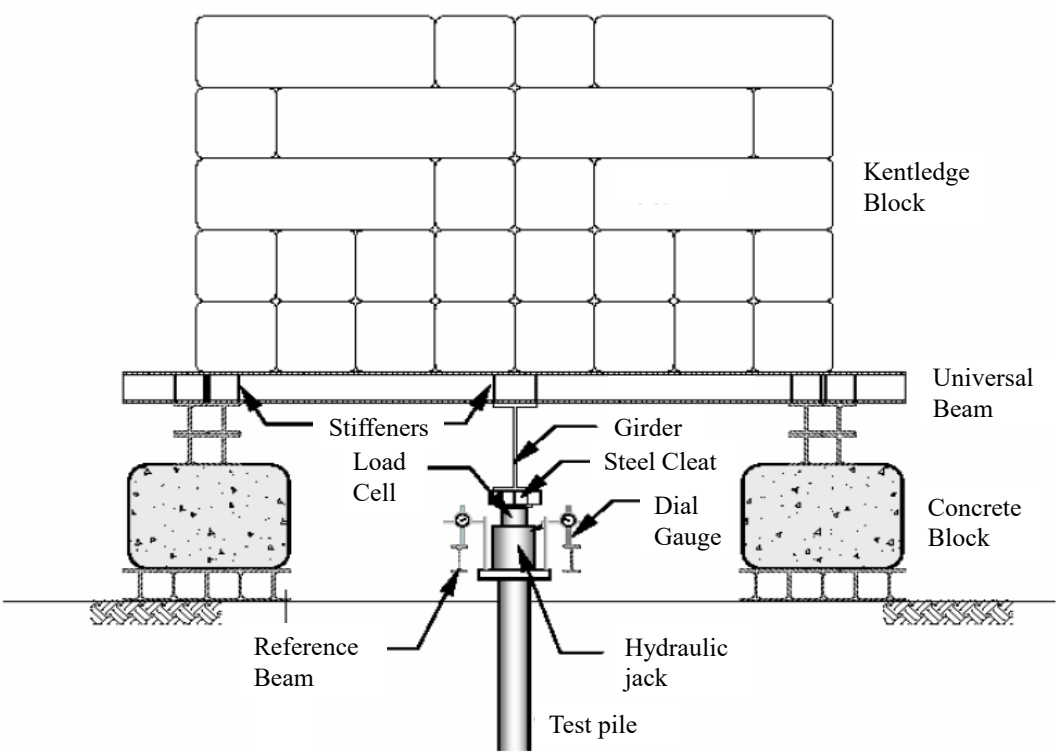

Figure 2.7 Diagram of compression load test setup using kentledge system (Dutch International 2017)

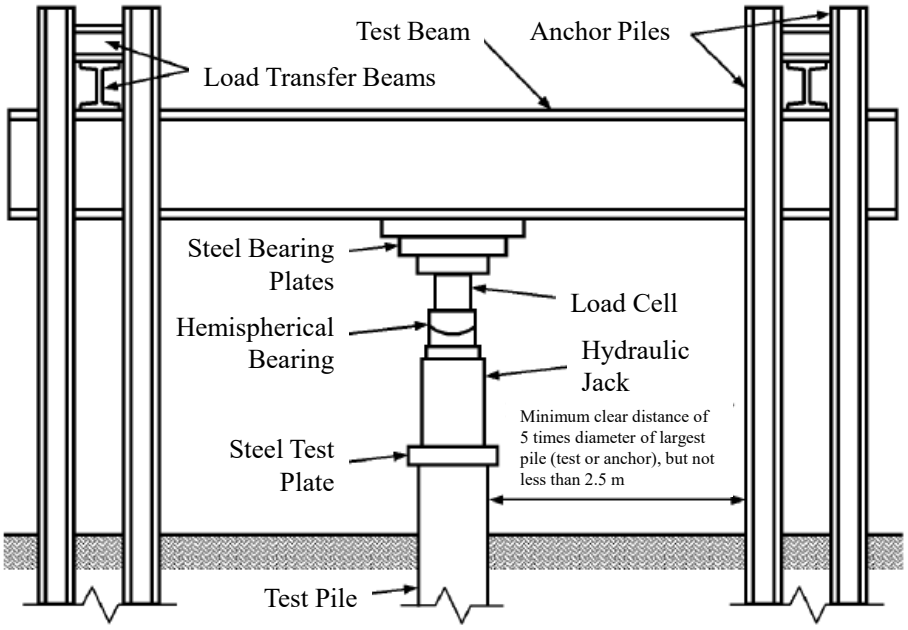

Figure 2.8 Schematic of hydraulic jack acting against anchored reaction frame (after ASTM International 2013)

Moreover, to reduce the effect of anchor piles on the test piles, the distance from the test pile must be greater than or equal to 2.5 m and at least five times of the maximum diameter

of the largest anchor or test pile(s). This clear distance may increase or decrease by the engineer based on various parameters such as the type and depth of reaction, magnitude of loads, and soil conditions.

2.3.1 Static Pile Load Testing Procedure

As explained by Stuckmeyer (2014) and Coduto (2001), static load testing can be categorised as either controlled strain tests or controlled stress tests. In controlled stress tests specified loads are applied to a test pile and then the resulting displacement is measured, whereas controlled strain tests are commonly the reversed. Because controlled stress tests are the most practical method, they are discussed below. One of the most common methods used to determine the nominal resistance of a pile from the load – displacement curve is the Davisson method, which is also presented in this section.

2.3.1.1 Slow Maintain Load Method

The slow maintained load method is regarded to be the conventional and standard loading procedure. According to Fang, Winterkorn & Van Nostrand (1975), in this technique, the load is applied over the test pile in eight equal increments of 25, 50, 75, 100, 125, 150, 175, and 200% of the design resistance.

As pointed out by Fellenius (1990), each increment is sustained until a minimum movement, usually known as the zero movement, is reached. The zero movement is usually described as either 0.254 mm per hour or 0.051 mm per 10 minutes; to meet this criterion each load must be maintained for 1 to 2 hours. The maximum load is equal to 200% or more; hence, it is always kept for 24 hours, which is why a slow maintained load

test can take from 30 to 70 hours to be completed (Fang, Winterkorn & Van Nostrand 1975).

2.3.1.2 Quick Maintain Load Method

As explained by Coduto (2001), Fellenius (1990) and Prakash & Sharma (1990) the quick maintained load test, also known as quick test, is similar to the previous method, but contrary to the slow maintained load test and irrespective of the rate of pile movement, each load increment in this method is kept for a specific time interval before proceeding. For most quick tests, up to 200% of the specified allowable load is still applied, but in most cases the number of loading increments has raised. A typical quick test may include 10% load increments kept from 5 to 15 minutes each. ASTM International (2013) permits intervals as short as 2 minutes between load increments even though intervals of less than 5 minutes may not be practical. A quick test can usually be conducted within 3 to 6 hours, highly depends on the interval each load is kept. Due to the technical, practical and economic advantages of quick tests, their use has increased significantly in practice.

2.3.2 Interpretation of Test Results

Data collected during pile load testing are used to develop the load-settlement curve, which once obtained, is used by the engineer to determine a pile's nominal resistance. Fellenius (1975 & 1980) proposed nine different explanation of pile capacity assessed from load-movement records of a static loading test, which makes it difficult to choose the most appropriate one; in reality the choice depends on previous experience and the definition of failure.

2.3.2.1 The Davisson Offset Limit Load

This method suggested by Davisson (1972) is where the load associated with movement that exceeds the elastic deformation of a pile (without any soil resistance) by a value of 3.8 mm plus a component equal to the diameter of the pile divided by 120, is regarded as the bearing capacity of a pile. It is assumed in this method that the ultimate capacity of a pile is mobilised at a certain small toe movement. The primary aim is to use the test results associated with driven piles, hence while this method can also be applied to bored piles the estimated capacity becomes impractical or conservative. Since the wave equation analysis of driven piles and dynamic testing has increased in popularity, the Davisson method has gained widespread use in phase. To interpret the load-displacement curve using this method, a load-displacement curve should be plotted to an appropriate scale (Figure 2.9). The line OO1 demonstrates the relationship between the load and elastic deflection of an axially loaded pile without any soil resistance, which equals QL/AE. The line CC1 is traced parallel to OO1 at an offset distance OC, where D is in mm and OC equals (3.8+ D/120) in mm. The intersection of CC1 with the load-displacement curve gives the ultimate pile load Q_{ult}.

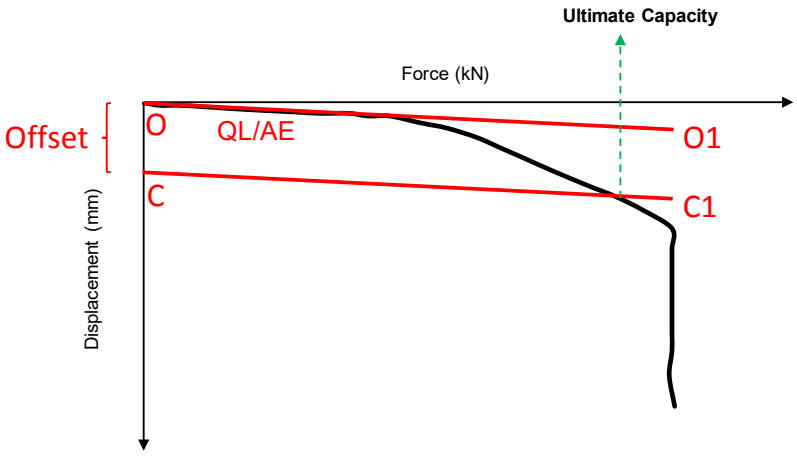

Figure 2.9 Typical load-displacement curve and the offset limit method

2.4 Dynamic Pile Load Testing

Over the last few decades, the advent of powerful computers has resulted in advanced methods for pile testing, whereas previous testing consisted of slow and costly static load testing. Nowadays, there are a variety of tests that can be used to estimate or measure pile resistance, as well as many methods for quickly and economically testing their structural integrity. These methods are best characterised by how long a load is applied to a pile and the internal strain generated during testing, hence tests comprising large forces for long periods of time (e.g. static load tests), will evaluate their load capacity while small energy low-strain tests will evaluate their integrity. Although the force in high-strain dynamic testing is comparable in magnitude to the corresponding force in a static load testing, the load is applied over a very short period of time (e.g. 5 ms to 10 ms). The first research on dynamic pile testing dates back more than 55 years ago at Case Western Reserve University, but then the Ohio Department of Transportation (ODOT) and Federal Highway Administration (FHWA) supported a project beginning in 1964 to enhance this technology. According to Surjadinata (2007) the aim of dynamic pile load testing is to predict the performance of a pile and also measure the pile load and accompanied movements which are not directly made with this kind of test. To carrying out dynamic load testing and determine pile performance, as predicted by resistance mobilised during the test, equipment containing the following components are used:

• Normally two or four sets of strain gauges and accelerometers mounted onto opposite sides of the pile.

• A portable field computer (pile driving analyser) to capture and store the strain and acceleration signals.

During dynamic pile load testing, the impact force is usually provided by a piling hammer. According to Benamar (2000), this impact leads to a stress wave, which travels down the pile and reflects off the toe; therefore any irregularities or discontinuities in the shaft or interaction between the pile and surrounding soil causes the downward travelling wave to be partially or completely reflected and produce upward travelling waves. After capturing the signals, the measured signals of strain and acceleration are transmitted to the field computer and then integrated to produce force and velocity results. To model the transition of upward and downward travelling waves, some relationships are used and then pile performance is predicted. These predictions are made primarily by a pile driving analyser (PDA) and should be acknowledged by the signal matching (or reverse analysis) methods. The PDA is essentially a computer, loaded with special software, which uses a closed-form solution (CASE method) for the pile-soil-hammer system in real time. The main input data of the software are the strains and the accelerations, measured near the pile top. In can be noted that dynamic load testing requires measurements of the force and velocity at the head of the pile over time to determine the extent of head displacement. Due to the effects of dynamic nature of the applied load and wave propagation, induced by the pile driving hammer, the plot of measured force versus measured displacement does not simulate a static load-displacement curve. Hence, in order to calculate the static load-displacement curve, the equivalent static component of the force must be deduced by subtracting the dynamic components from the total load-displacement values. This is why dynamic analytical methods such as the CAse Pile Wave Analysis Program (CAPWAP) and WEAP programs, developed by Goble & Rausche (1980) and Goble & Rausche (1976), are used to interpret the results of dynamic pile load testing and quality control during construction and the installation of piles. An illustration of a typical test set-up and dynamic load testing is shown in Figures 2.10a-b, respectively.

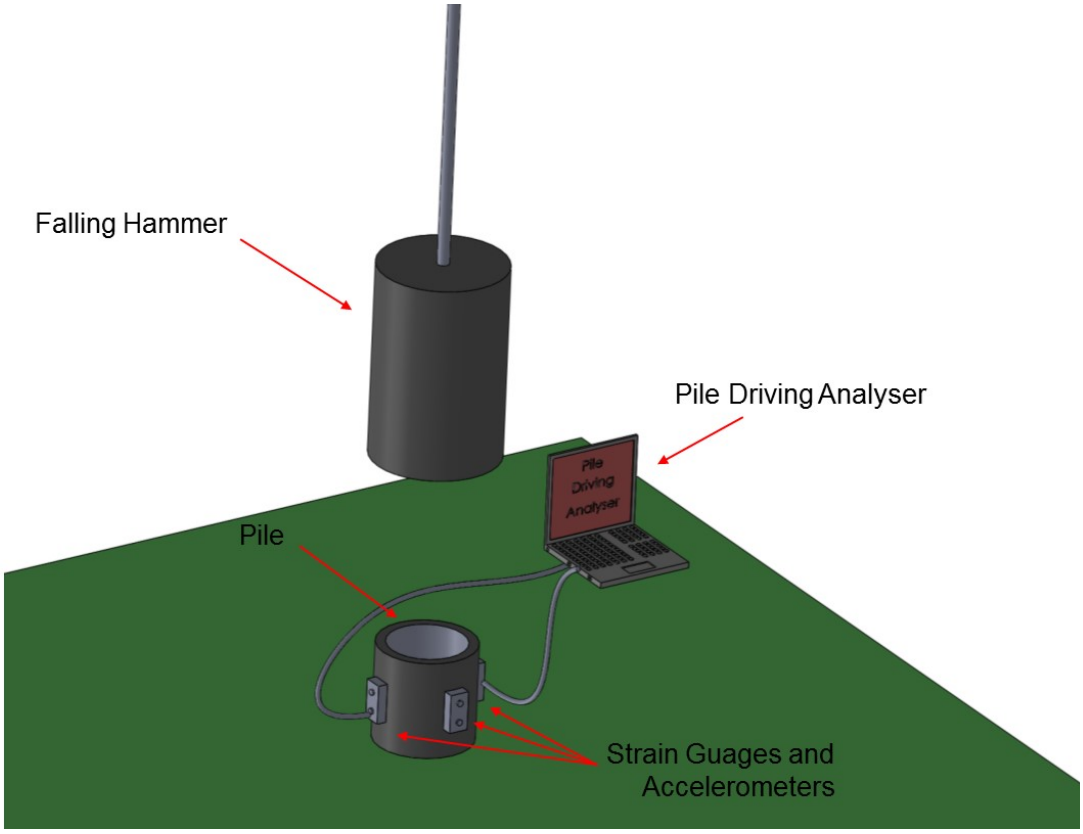

(a)

(b)

Figure 2.10 (a) Typical dynamic pile test set-up (b) Dynamic load testing (Applelianlian 2013)

In order to complete the PDA test, the field data are analysed by an experienced geotechnical engineer using the CAPWAP program. This analytical program models the pile-soil system using different soil and pile properties and then compares the obtained model with the measured force or velocity response of the pile over a set period of time.

2.4.1 Proportionality Concept

When a rapid axial force is applied over a slender rod (or a pile), a stress wave is generated, traveling away from the point where force is applied. As long as the stress waves at the point where measurements are being made travel in only one direction and no reflections arrive at this point, the force on the pile is proportional to the velocity of particle motion. Direction of the wave velocity in a free top and bottom rod remains constant (while after each reflection the sign of stress varies). The proportionality between the two curves (force and velocity) is ruined as soon as the generated waves due to the soil resistance reflect back to the top of the pile. This relationship can be written as (Green & Kightley 2005):

$$v(t) = \frac{c}{EA} F(t) \tag{2.1}$$

where,
v(t) = particle motion velocity at the respected point (downward positive) (m/s)
$F(t)$ = the force at the same point (compression positive) (kN)
c = velocity of the stress wave propagated (m/s)
A = pile (rod) cross-sectional area (m^2)
E = elastic modulus of the pile material (kPa)
$Z = \frac{EA}{c}$ = impedance = proportionality coefficient between force and velocity (kN.s/m)

2.4.2 CAPWAP Background

According to Lowery et al. (1969), Isaacs was a pioneer who incorporated wave action during pile driving to estimate the pile load capacity. Issacs (1931) states that the pile behaviour during driving is governed by the one-dimensional wave equation and does not follow the Newtonian impact supposed by many simplified pile driving formulae. He proposed a solution to the wave equation by assuming that the tip of a pile is fixed without side resistance, but these assumptions proved to be very restrictive so the solution was probably never used in practice.

2.4.2.1 One-dimensional wave equation

Since piles are much longer than their width and diameter, a wave can be considered to be one-dimensional during driving. If a pile with a constant cross sectional area A, comprising a linear elastic material and with an elastic modulus of E is regarded, and if a small segment of the bar/pile is also considered (Figure 2.11), then Newton's second law leads to Equation 2.2 (the equation of motion of an element).

Therefore, by combining Equation 2.2 with the constitutive equation $\sigma=E\varepsilon$ (Hooke's law) and kinematic equation $\varepsilon=\frac{\partial u}{\partial x}$ leads to Equation 2.3 (Garnier 2001):

$$N + \frac{\partial N}{\partial x}\Delta x - N - R = \rho A \Delta x \frac{\partial^2 u}{\partial t^2} \tag{2.2}$$

Regarding N= σ A and σ= E ε:

$$EA\frac{\partial^2 u}{\partial x^2} - \frac{R}{\Delta x} = \rho A \frac{\partial^2 u}{\partial t^2} \tag{2.3}$$

If there is no resistance along the pile shaft, the one-dimensional wave equation can be written as:

$$c^2 \frac{\partial^2 u}{\partial x^2} = \frac{\partial^2 u}{\partial t^2} \tag{2.4}$$

where,
N = internal normal force (kN)
A = cross sectional area (m^2)
u = displacement in axial direction (m)
Δx = small length of pile (m)
t = time (s)
$c = \sqrt{\frac{E}{\rho}}$ = wave speed (m/s)
E = Young's modulus of pile (kPa)
ρ = density of pile (kg/m^3)
ε = strain
R = resitance force (kN)

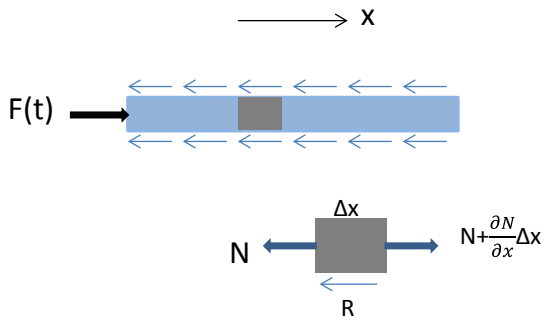

Figure 2.11 Free body diagram of a small segment of a pile (after Garnier 2001)

As explained by Lowery et al. (1969) and Ng (2011), Smith proposed more realistic solutions to the problem of longitudinal impact and the one-dimensional wave equation. Using the 1-D wave equation for the pile-hammer-soil system, Smith (1960) developed a mathematical model (Smith Model) and then used a digital computer for his pile driving analysis. In the Smith model, the pile, hammer and driving accessories are divided into a series of short different sectional weight (W) and springs (K), as illustrated in Figure 2.12. The shaft resistance of the pile is demonstrated by a series of springs along the pile and the tip resistance is accounted for by a single spring at the bottom of the pile (Figure 2.12b). In order to maintain the step by step calculations ahead of the stress wave, the time period during which the force pulse travels along the pile and reflects from the tip to the head, should be divided into smaller intervals. The velocity and the impact of the

hammer generates a displacement in every weight, and when the displacements of two adjacent weights occurs, it produces a compression or tension in the spring between them, and this compression or tension, develops a force in the spring. A net force on each weight is created due to the forces of the two springs and resistance from the ground which either accelerates or decelerates it, this action results in a new velocity and displacement in the next time interval. This procedure is repeated at each time interval for each weight until all the downward velocity is lost. In this method, the hammer ram shown in Figure 2.12a looks like a short, heavy and rigid single weight without any elasticity, whereas the cap block is illustrated by a spring that can only transfer compression but no tension (Figure 2.12b). Moreover, the pile cap is illustrated by a single rigid weight, and in a bid to protect the piles from damage, a cushion represented as a non-tensional spring has been placed under the cap. The real pile and Smith model for pile driving analysis is shown schematically in Figures 2.12a-b, respectively.

Ng (2011) pointed out that Smith adapted the concept whereby soil surrounding and at the bottom of a pile compresses elastically to a displacement called quake (q) (the required displacement to mobilise the soil resistance) and fails plastically with a constant ultimate static soil resistance (R_u) (the load at which the soil spring behaves purely plastically) as shown with a black solid line OABC, as shown in Figure 2.13. The total driving resistance comprises static and dynamic soil resistance where the dynamic component represents soil damping. Smith replaced the soil continuum by viscous soil springs that are characterised by non-standard soil parameters such as the viscous damping coefficient, J and the quake value, q.

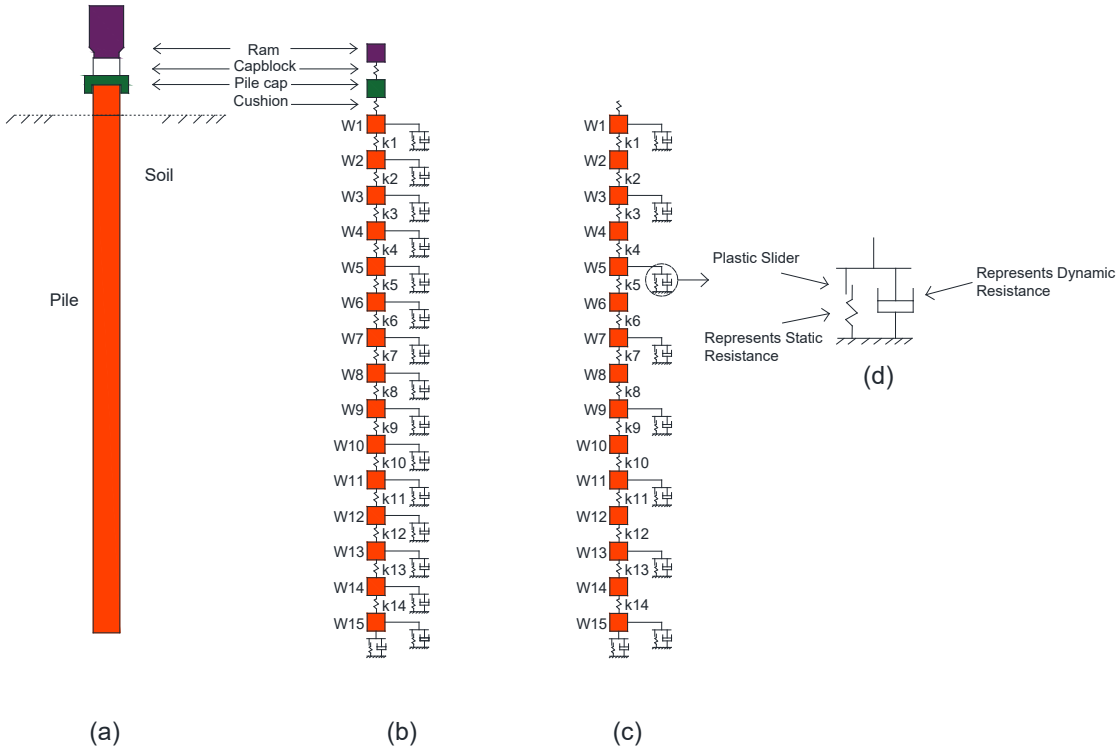

Figure 2.12 (a) real pile and driving accessories (b) Smith pile and soil model (c) CAPWAP model (d) Smith soil model (after Ng 2011)

Smith developed a mathematical equation that considers the static and dynamic soil behaviour, as shown by the dash line OA′BC in Figure 2.13. For instance, at any point x′ (deformed as x) on the line OA′BC the total soil resistance can be found by Ng (2011):

$$R = R_s + R_d = Kx + J_s R_s v_p = R_s(1 + J_s v_p) \tag{2.5}$$

where,
R = total soil resistance (kN)
R_s = static soil resistance (kN)
R_d = dynamic soil resistance (kN)
J_s = Smith's damping constant (s/m)
v_p = velocity of a pile segment (m/s)
K = spring constant for soil model (kN/m)
x = soil deformation (m)

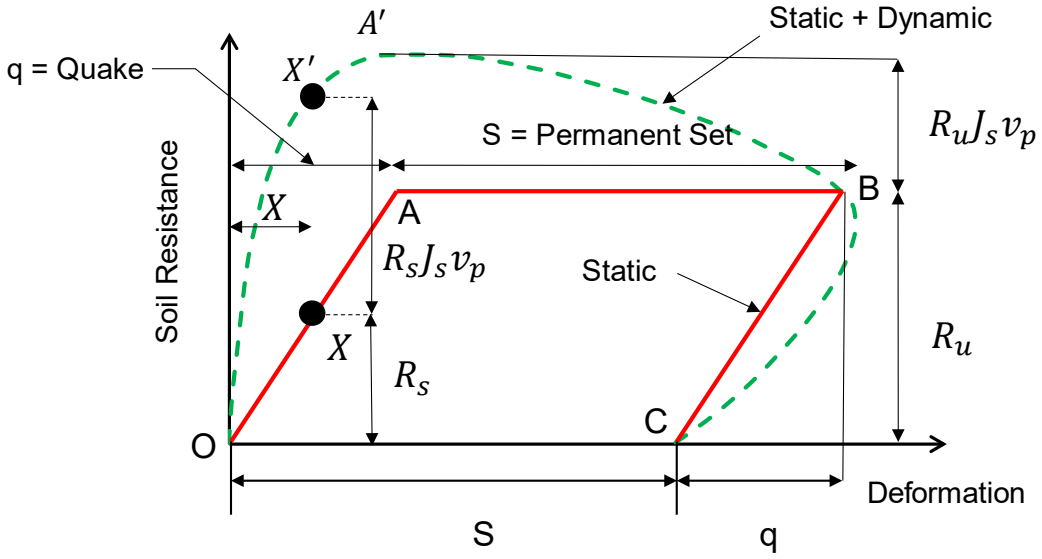

Figure 2.13 Stress strain (Load –Deformation) diagram of the soil resistance at a pile point (after Ng 2011)

2.4.2.2 Ultimate static soil resistance

For the side or friction soil resistance, R_u is the maximum static soil resistance against the side of a given segment of pile by:

$$R_u = f_s \, p \, \Delta L \tag{2.6}$$

where,
f_s = maximum soil adhesion or friction (kPa)
p = perimeter of pile segment (m)
ΔL = length of pile segment (m)
At the toe of the pile R_u is determined by the maximum static bearing strength of the soil, and is found by:

$$R_u = Q_u A_p \tag{2.7}$$

where,
Q_u = bearing capacity of soil (kPa)
A_p= area of pile point (m^2)

2.4.2.3 Quake and damping constants

According to Lowery et al. (1969), determining the elastic deformation of soil (quake) for different conditions is difficult hence the range of quake (q) in both friction and end bearing situations is from 1.27 mm to 3.81 mm and a typical value for average pile driving conditions is 2.54 mm. If the pile tip is overlaid on very soft soil, it is possible for quake to go as high as 5.1 mm or more. Smith (1960) states that the value of soil damping (J) in friction along the shaft is smaller than the pile toe. He recommends that the J value in friction is about $^1/_3$ those at the tip. Ng & Sritharan (2013) study have summarised different recommendations for quake and damping factors according to Table 2.1.

2.4.2.4 Smith's soil model

According to Lee et al. (1988) and Christophe (2014), in a typical pile driving analysis, a pile is considered to be an elastic bar, along which stress waves propagate. In this analysis in order to illustrate the interaction between the soil and the pile, a combination of dashpot, nodal springs, and plastic sliders as proposed by Smith, are used. In this model, spring stiffness and dashpot constants are determined by the empirical quake and damping factors respectively.

These days, more complicated models have been derived to predict the bearing capacity of pile foundations more accurately. However, the analytical solutions required to determine the various parameters for sophisticated models which are not valid in every situation; therefore, it limits the practical implementations of these models. The spring-damper combination in the Smith model consists of one spring with a slider (to describe plastic deformation) parallel to a dashpot (Figure 2.12 d); in this model hysteretic,

radiation or viscous damping are not considered separately, they are summed up by one general damping constant (J). The value of this parameter is obtained empirically and as a result of its extensive use, a large database exists (Table 2.1). In this model, the soil spring behaves elastically as long as the deformation equals q (quake) and after that it yields plastically.

Table 2.1 Summary of suggested dynamic soil parameters (after Ng & Sritharan 2013)

Reference	Damping Factor (J) (s/m)		Quake Value (q) (mm)	
	Shaft (J_S)	Toe (J_T)	Shaft (q_s)	Toe (q_T)
Smith (1960)	0.16	0.49	2.54	2.54
Coyle, Bartoskewitz & Berger (1973)	0.66 for clay 0.16 for sand 0.33 for silt	0.03 for clay 0.49 for sand 0.49 for silt	2.54	2.54
Hannigan et al. (1998)	0.66 for cohesive soils 0.16 for non-cohesive soil	0.49	2.54	D*/120 for dense and hard soil D/60 for soft soil

*D is the pile diameter

2.4.3 CAPWAP Model

As explained by Ng (2011), Ng et al. (2011) and Robinson & Rausche (2000), the Case Pile Wave Analysis Program (CAPWAP) was prepared by Professor Goble and his students in the 1970s, and like Smith's model, CAPWAP includes both pile and soil models and uses PDA data to find two of the three unknowns, the pile velocity and force. The remaining unknown is attributed to the soil media including the distribution of resistance, and the soil damping factors and soil quake. In order to calculate the soil properties, CAPWAP performs an inverse analysis to determine the unknown parameters

of a soil model (Figure 2.14). This inverse analysis is usually called a signal matching analysis. In this type of analysis, the solution must be achieved iteratively, i.e., first assumes unknown soil parameters and then carry out an analysis with one of the measured quantities (force) as a top boundary condition to test these assumed parameters. If the measured and calculated response parameters of the top of the pile (velocity) disagree, the computation is iterated with a revised set of soil model parameters. It is clear that if the most realistic soil models are used, ability to match with the measured quantities would be better. However a very complex soil model parameters may not be uniquely determined by the matching process, which is why the relatively simple Smith soil model (comprising two unknowns damping and quake) has been used successfully for dynamic signal matching. CAPWAP can be used in an interactive mode or in an automatic manner where the automatic procedure using a step by step procedure (also recommended for interactive signal matching), searches for a best match.

A schematic diagram of the CAPWAP model is shown in Figure 2.12c. In this program a pile is modelled with a series of masses, springs, and the soil resistances along and at the tip of the pile are modelled with linear dashpots and elasto-plastic springs. The CAPWAP model is identical to Smith's but it does not comprise the driving systems and the section of pile above the PDA gauges. According to Ng & Sritharan (2013), verifying pile resistance using CAPWAP is carried out by matching the measured pile velocity and force signals collected from a pile driving analyser (PDA) with the computed signals by the one-dimensional soil-pile model presented by Smith.

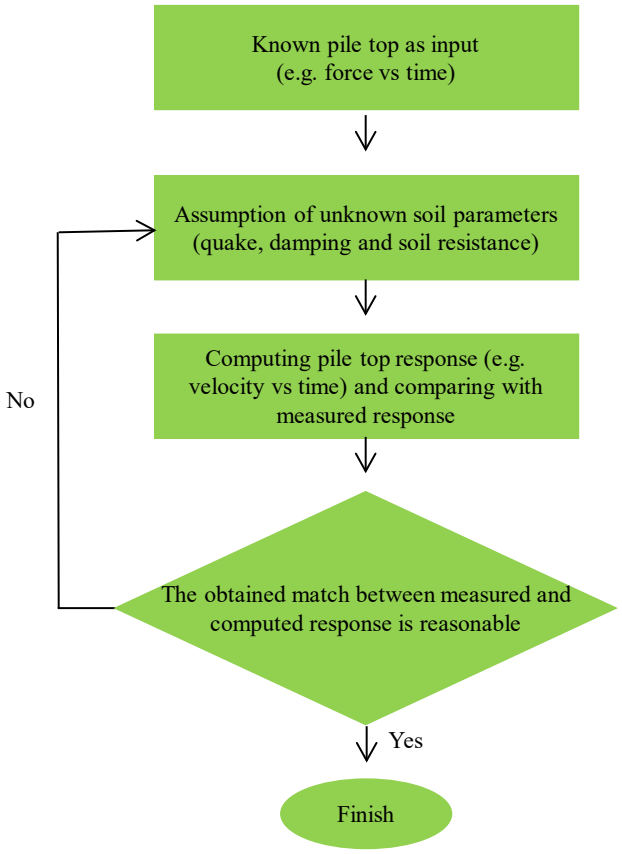

Figure 2.14 Signal matching analysis algorithm in CAPWAP (after Robinson and Rausche 2000)

The precision of verifying pile resistance using CAPWAP based on this model depends on selecting two appropriate dynamic soil parameters, i.e., the damping factor (J) and the quake value, (q). Finally, a match quality (MQ) is used to evaluate the accuracy of signal matching in CAPWAP. The limitations of this routinely used technique is that CAPWAP results are not unique since they are highly affected by the magnitude of the dynamic soil parameters, the shaft, and tip resistances. Hence, for finding the best match these parameters can be modified arbitrarily. Due to the unknown nature of this signal matching technique and since the dynamic soil parameters cannot uniquely be determined based on measurable soil properties; therefore, different dynamic soil parameters are recommended in different literatures (Table 2.1). As explained by Ng (2011) and Ng & Sritharan (2013) the CAPWAP analysis procedure has some limitations including:

- The estimated distribution of soil resistance may not demonstrate the actual soil layers properties and profile.
- Fixed dynamic soil parameters, such as the shaft damping factor and shaft quake in CAPWAP, are assigned for the whole length of embedded pile irrespective of various soil layers.
- The solution generated from the signal matching analysis is non-unique.

A typical output of CAPWAP is shown in Figure 2.15.

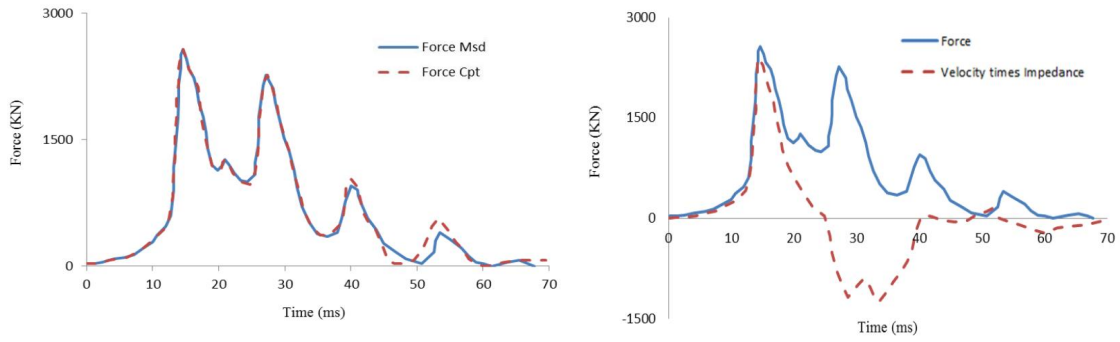

(a) (b)

Figure 2.15 Typical output of CAPWAP measured force or velocity response with time (a) results of signal matching analysis (measured versus computed force) and (b) force and velocity traces recorded by PDA measured versus time

2.5 Constitutive Soil Models

2.5.1 Mohr-Coulomb Model (MC Model)

According to Dung (2009), the Mohr-Coulomb model is a linear elastic perfectly plastic model that can be used as an initial evaluation of soil behaviour. The perfectly plastic part of this model is based on the Mohr-Coulomb failure criterion, whereas the linear elastic part is according to Hooke's law of isotropic elasticity. Plasticity is the development of

irrecoverable strains and in order to assess the possibility of plasticity in a calculation, a yield function (f) of stress and strain is defined in this model (plasticity occurs when f=0). The friction angle, ϕ, and the cohesion, c, are the two well-known plastic model parameters emerging in the yield functions. A constant hexagonal cone in principal stress space is represented by the full MC model yield condition comprises six yield functions. The points inside the yield surface presents the situation in which the behaviour of stress states is totally elastic and all the strains are recoverable.

As explained by Brinkgreve, Kumarswamy & Swolfs (2017) and Wehnert & Vermeer (2004), six plastic potential functions have been specified for this model, as well as the yield functions, and these functions consist of a third plasticity factor called the dilatancy angle ψ. This parameter is needed to model the plastic volumetric strain that develops during plastic shearing. The dilatancy angle for sands is highly the angle of internal friction dependant, whereas clays (irrespective of any overconsolidated layers) are characterised without any dilation ($\psi = 0$). The value of dilation angle for granular soils (sand, gravel) with the friction angle $\phi > 30$ can be estimated as:

$$\psi = \phi - 30^o \tag{2.8}$$

The Mohr-Coulomb model needs five parameters, which can be acquired from primitive tests on soil samples. These parameters are listed in Table 2.2.

It is worth mentioning that according to Brinkgreve, Kumarswamy & Swolfs (2017), the initial slope of the stress-strain curve (tangent modulus) during triaxial testing soil samples is usually expressed as E_0 and the secant modulus at 50% strength is referred to as E_{50}. When loading soils E_{50} is generally used in analyses but for materials with high elastic range it is practical to use E_0. A typical Mohr-Coulomb stress-strain curve obtained from a triaxial test is shown in Figure 2.16.

Table 2.2 Required parameters for Mohr-Coulomb model (after Brinkgreve, Kumarswamy & Swolfs 2017)

Parameter	Unit	Description
E	kN/m^2	Young's modulus
υ	-	Poisson's ratio
c	kN/m^2	cohesion
ϕ	degree	friction angle
ψ	degree	dilatancy angle

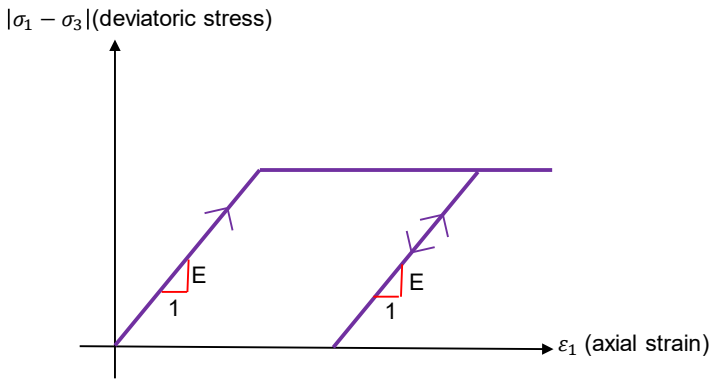

Figure 2.16 Basic principle of MC model (after Wehnert & Vermeer 2004)

As mentioned by Dung (2009), although this model characterises the failure behaviour of soil quite well, it has many restrictions for the behaviour of real soil. Firstly, the Mohr-Coulomb model does not cover stress-dependency and stress-path dependency of stiffness because in this model linear elasticity occurs until failure; secondly, in undrained condition should be careful due to an unrealistic stress path, and hardening or softening rules, which are not included in this model.

2.5.2 Hardening Soil Model (HS Model)

According to Brinkgreve, Kumarswamy & Swolfs (2017) the hardening soil model is a sophisticated model for simulating the behaviour of soft soil and stiff soil, as well as shear hardening and compression hardening. Unlike the Mohr-Coulomb model, this hardening soil model controls the stress level dependency and also instead of a bi-linear curve uses a hyperbolic stress-strain curve. For real soils Young's modulus highly depends on the existing stress level inside the soil, whereas in the Mohr-Coulomb model the user must select a constant value of this stiffness. However, during analysis, the hardening soil model considers the stress-path dependent stiffness. The fundamental idea for formulating the hardening soil model is defined as the hyperbolic relationship of the deviatoric stress, q, and vertical strain ε_1 in initial triaxial loading. This relationship is plotted in Figure 2.17.

As explained by Wehnert and Vermeer (2004), the stress dependency stiffness for the HS model is described by E_{oed} and E_{50} and E_{ur}, where E_{oed} is the oedometer stiffness defined as a tangent stiffness modulus, and the other two stiffness parameters E_{50} and E_{ur} are related to the standard drained triaxial tests. E_{50} and E_{ur} are the elastic modulus for initial loading and unloading and reloading respectively which depend on confining stress. In this model, the failure criterion is met and perfectly plastic yielding happens, as defined by the Mohr-Coulomb model, as soon as deviatoric stress (q) in the standard drained triaxial test reaches to the ultimate deviatoric stress (q_f). This is why some parameters of the hardening soil model, including the cohesion, the friction angle, and the dilation angle, are the same as the Mohr-Coulomb model. The parameters of the hardening soil model are summarised in Table 2.3.

Based on Schanz, Desrues & Vermeer (1997) study, in practice $E_{ur}^{ref} = 3E_{50}^{ref}$ is considered and for engineering practice $E_{oed}^{ref} = E_{50}^{ref}$ can be assumed. As mentioned by Dung (2009), despite the advantages of the memory of pre-consolidation stress and the stress-dependency, the HS model still has some restrictions. First, in this model dilatancy increases infinitely hence it does not consider the softening behaviour induced by dilatancy and de-bonding effect. Second, the HS model does not consider any increase in stiffness at a small strain compared to reduced stiffness at a large strain level. Third, this model has a drawback in the small stress cycles region since in cyclic loading it causes an excessive accumulation of deformation.

2.5.3 Hardening Soil with Small Strain Stiffness Model (HS-Small Model)

As Likitlersuang et al. (2013) and Obrzud (2010) have explained, the hardening soil model with small strain stiffness (HS-Small model) is an advanced version of the hardening soil (HS) model formulated by Benz (2007) to handle the commonly observed phenomenon of large variations in stiffness as the shear strain increases in the small strains and hysteretic nonlinear elastic stress-strain relationships that in the range of small strains are applicable.

These features indicate that the HS-Small model can deliver more precise and reliable approximations of displacement that can be useful for dynamic load testing applications. The initial stiffness modulus is an important parameter that affects the prediction of ground movements and interpretations of field data. In earthquake engineering and soil dynamics, the maximum small strain shear modulus (G_{max}) and the damping ratio are

key fators in soil desription. In the HS-Small model, the shear stiffness for a wide range of shear strains is explained by a stiffness degradation curve.

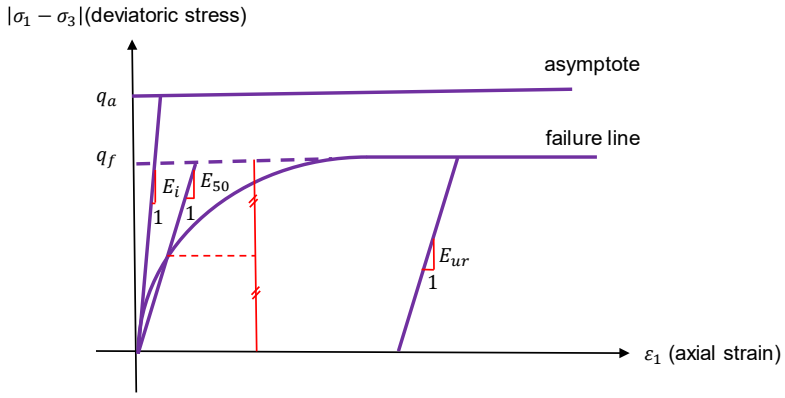

Figure 2.17 Hyperbolic stress-strain relation in primary loading for a standard drained triaxial test (after Brinkgreve, Kumarswamy & Swolfs 2017)

According to Cox & Mayne (2015):

$$G_0 = G_{max} = \rho_T \times V_s^2 \tag{2.9}$$

where ρ_T is the total density of the soil mass and V_s is the shear wave velocity. In-situ seismic testing techniques can be used to determine G_0 for various geomaterials. Common in-situ tests to measure the profile of shear wave velocity (V_s) with depth include suspension logging, downhole surveys, geophysical cross-hole seismic surveys, seismic dilatometer (SDMT), a spectral analysis of surface waves (SASW/MASW), and seismic piezocone penetration tests (SCPTu) (Cox and Mayne 2015). Laboratory tests such as resonant column and bender elements are also available to determine G_0 for soils, but determining V_s through the direct measurements by field tests such as SDMT are in priority because sample disturbance and stress relaxation issues can affect the lab results. Moreover, in the hardening soil model with small strain stiffness (HS-Small), the reference threshold shear strain ($\gamma_{0.7}$) is introduced to define the stiffness degradation

curve and is defined as the level of shear strain at which the secant shear modulus drops to about 70% of G_0.

Table 2.3 Required parameters for Hardening Soil model (after Brinkgreve, Kumarswamy & Swolfs 2017)

Parameter	Unit	Description
c ϕ	the same as Mohr-Coulomb model	
E_{50}^{ref}	kN/m^2	secant stiffness in standard drained triaxial test
E_{oed}^{ref}	kN/m^2	tangent stiffness for primary oedometer loading
E_{ur}^{ref}	kN/m^2	unloading/reloading stiffness
m	-	power for stress-level dependency of stiffness
υ_{ur}	-	Poisson's ratio for unloading-reloading
p^{ref}	kN/m^2	reference stress for stiffness
k_0^{nc}	-	K_0 value for normal consolidation
R_f	-	failure ratio q_f/q_a

2.5.4 Hypoplastic with Intergranular Strain Model (HP-IGS Model)

As explained by Mašın (2010), hypoplasticity is a specific class of incrementally nonlinear constitutive soil models particularly prepared to predict the soils behaviour. For the first time the elementary structure of these hypoplastic models was proposed at the University of Karlsruhe during 1990's. In hypoplasticity, contrary to elasto-plasticity, the models do not take into account the plastic potential surface and the notions of the yield surface, and the strain rate is not divided into elastic and plastic parts. However, they can consider soil main behaviour such as the dependency of the peak strength on soil density,

the dependency of the soil stiffness on the loading direction, and non-linear behaviour in the small and large strain ranges and so on.

Kolymbas (1985) proposed the first version of the hypoplastic constitutive model, to characterise the stress-strain behaviour of granular soils in a rate form. This model is based on the stress rate, presented as a function of the strain rate and the stress tensor and; the void ratio was added later on as an extra state variable by Gudehus (1996). The general figure of the hypoplastic model is:

$$\dot{T} = f(T, e, D) \tag{2.10}$$

where, $\dot{T}$ demonstrates the objective stress rate tensor as a function of the current void ratio, e, and T represents the Couchy granular stress tensor, and D represents the stretching tensor of the granular skeleton. The model offered by Gudehus (1996) was later rectified by Von Wolffersdorff (1996) to assimilate Matsuoka-Nakai critical state stress condition. This model, is now regarded to be the standard hypoplastic model for granular soils; this version has also been used in finite element software.

As explained by Elmi Anaraki (2008), the prominent aspect of this model is its straightforward approach, since it identifies inelastic deformation without using any additional notions such as plastic potential or yield surface. Hypoplastic models can anticipate soil behaviour in the medium to large strain range, but in the small strain range and in cyclic loading they cannot predict the high quasi-elastic soil stiffness. In fact, small deformation caused by cyclic loading and creep are not included, which under stress cycles it leads to an excessive accumulation of deformation. To resolve this problem, Niemunis & Herle (1997), suggested an extension of the hypoplastic equation by taking into account an extra state variable termed intergranular strain (IGS), to determine the direction of the previous loading. This correction, which has been implemented in finite

element software, is often referred as the intergranular strain concept. The hypoplastic model can now be used for clays and organic soils as well as cohesionless materials.

As summarised in Table 2.4, the hypoplastic model has eight parameters for describing the behaviour of granular material over a wide range of stresses and densities. It would be valuable to mention that three characteristic void ratios e_i, e_c and e_d denote the loosest state, the critical state, and the maximum densification respectively. These limiting void ratios approach zero for very high mean skeleton pressure and reach the limit values e_{d0}, e_{c0} and e_{i0} at vanishing mean skeleton pressure. Because they are difficult to test, these limit void ratios are assumed to be e_{min}, e_{max} and approximately 1.2 e_{max}. The intergranular starin concept (small strain behaviour) requires five additional parameters that are pointed out in Table 2.5.

Table 2.4 Required parameters of granular material for Hypoplastic model (after Dung 2009)

Parameter	Unit	Description
φ_c	degree	critical friction angle
e_{d0} , e_{i0} , e_{c0}	-	minimum, maximum and critical void ratio at zero pressure
h_s	kN/m^2	granular hardness
n	-	exponent relates to sensitivity of granular skeleton to change of pressure
α	-	exponent describes the transition between peak and critical stress
β	-	exponent represents the change of stiffness at current density

Table 2.5 Defined parameters in intergranular strain concept (after Dung 2009)

Parameter	Unit	Description
m_T	-	stiffness increase for a 90 degree change of strain path direction
m_R	-	stiffness increase for a 180 degree reversal
R	-	radius of elastic range
β_R	-	material constant controls the rate $\dot{h}$
χ	-	material constant represents stiffness degradation

2.6 Remarkable Studies on Pile Load Testing

This section is a critical review of remarkable studies on static and dynamic pile load testing that include theoretical studies, numerical modelling, and field observations.

2.6.1 Static Pile Load Testing: Numerical and Experimental Studies

Static load tests on single piles and pile groups are considered as the most reliable tools of evaluating the response of piles under design loads. Hoľko & Stacho (2014) performed numerical analyses of a single continuous flight auger (CFA) pile under axial static loads and found the CFA technology to be quick, quiet, and economical pile technology which in appropriate geological situations is an appropriate substitute to common bored piles. Appropriate geological situations for CFA piles comprise clays of a medium-to-firm consistency, limestone, and fine coarse-grained soils. The process for installing of CFA piles is shown in Figure 2.18. In the latter study the analysis includes a comparison of computed and measured load-settlement curves and the load distribution over the length of a pile (Figures 2.19 and 2.20). These numerical analyses were carried out using ANSYS and PLAXIS finite element software; they differ in terms of creating numerical models, modelling pile-soil interface, and adopting constitutive material models. The

analyses in Hol'ko & Stacho (2014) study took the form of parametric studies where the methods used to model the interface and the material models of the soil were compared and analysed. Both types of software could model pile foundations, while the results indicated reasonable correlation with measured data. The load-settlement curve calculated using PLAXIS correlated very well with the static load testing (more than 95% degree of accuracy) while the load-settlement curve calculated using ANSYS software was only an approximation of the measured curve. PLAXIS software considering the influence of pore pressures, the over-consolidation of fine-grained soils, and by assuming that the interface reduction factor (R_{int}) is equal to 0.9 could accurately model soil behaviour and indicated better results than the ANSYS software outputs.

During static load testing it is important to specify the extent to which the reaction system affects the load–settlement curve of the test pile. Although a minimum distance between the reaction system and the test pile is recommended by the codes and standards for pile load testing, there are some numerical studies available in the literature which have assessed the effect of the clear distance between the reaction system and the test pile.

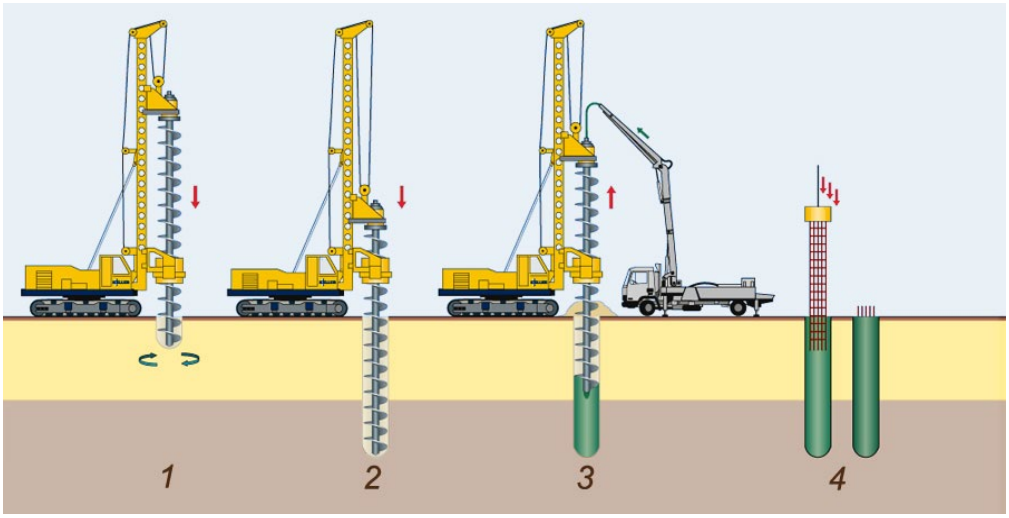

Figure 2.18 Process of installation of CFA piles (Naturalzemin 2019)

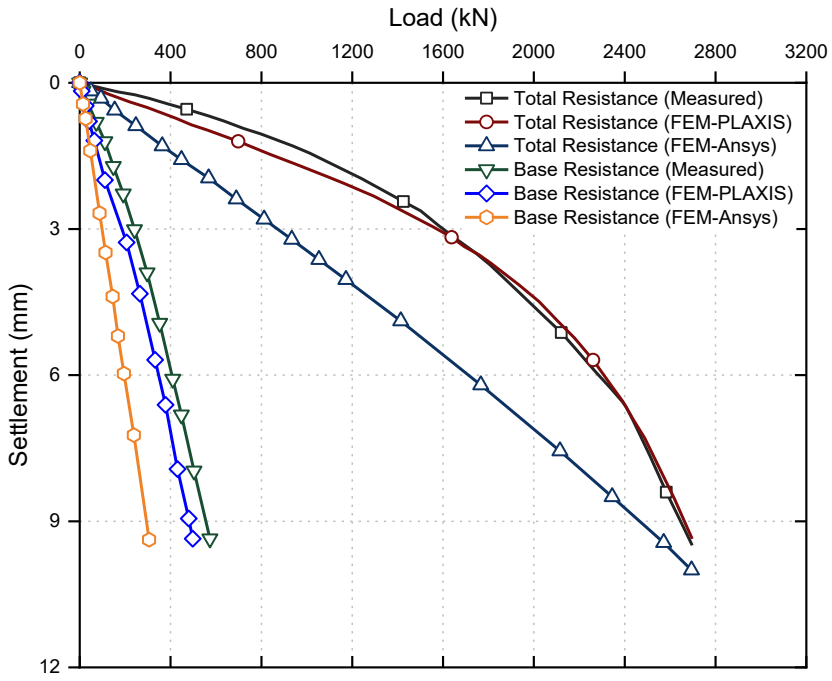

Figure 2.19 Comparison of calculated and measured load-settlement curves (after Hoľko & Stacho 2014)

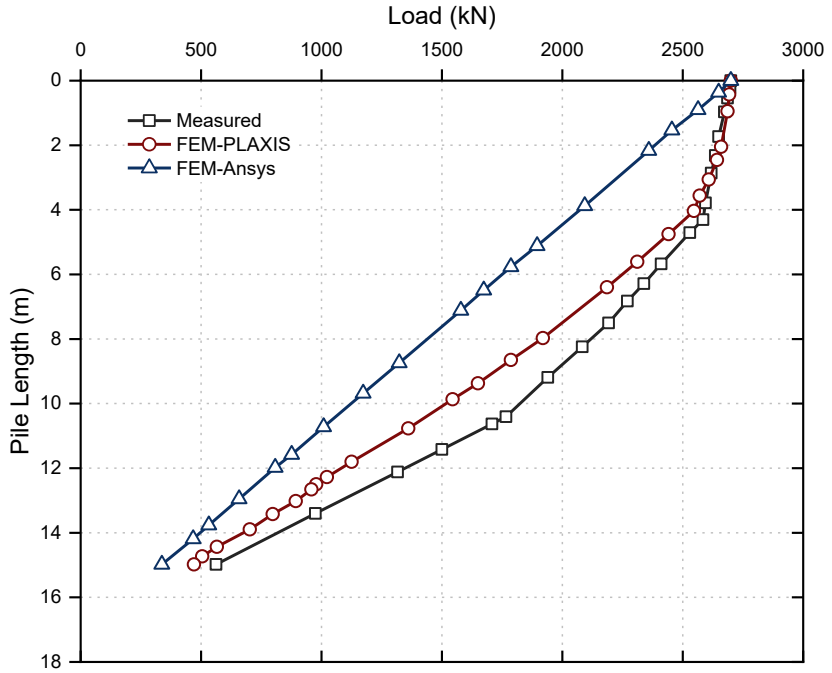

Figure 2.20 Comparison of calculated and measured load distribution curves over the pile length (after Hoľko & Stacho 2014)

Comodromos, Anagnostopoulos & Georgiadis (2003) evaluated the influence that reaction piles have on test pile with regards to the bearing capacity and stiffness of single piles and group of piles, using three-dimensional numerical modelling. To achieve this goal, an inverse analysis of a static pile load test was carried out to determine the response of single pile and to verify the soil properties. A numerical analysis was then performed to develop load-displacement relationships for groups of piles in several different layouts. The results show that interaction between the test pile and the reaction piles influences the load-settlement of the test pile even if the minimum distance of three to four times the diameter of piles is met (Figure 2.21). Moreover, a reduction in settlement of the test pile (due to reaction piles) compared to the single pile (without reaction piles), and a twofold increase in initial stiffness can be observed.

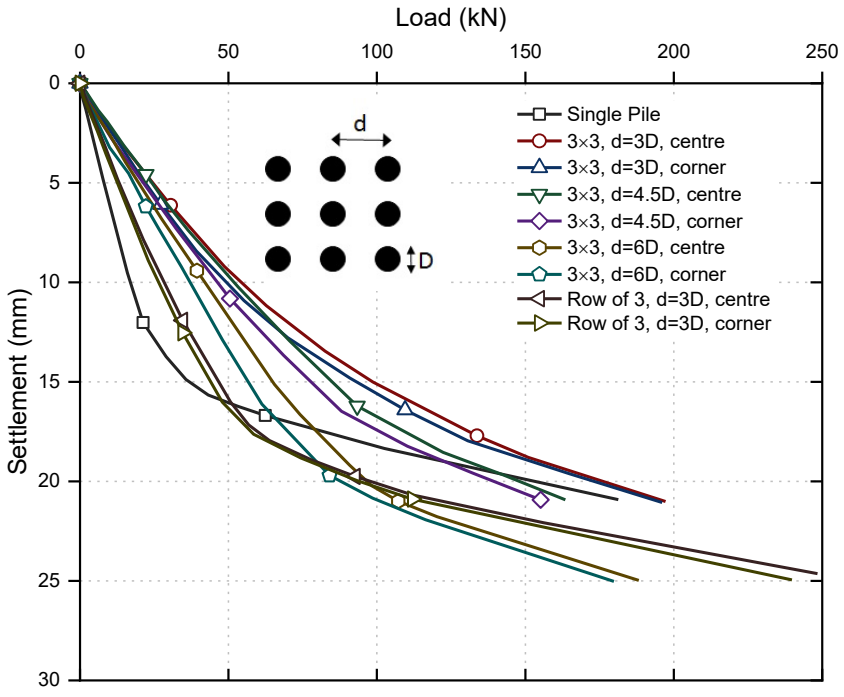

Figure 2.21 Numerically established load-settlement curves for the single and pile groups (after Comodromos, Anagnostopoulos & Georgiadis 2003)

However, during static load testing using sufficient surcharge or the kentledge system, the surcharge must be supported close to the test pile, and consequently these supports affect the stress states and displacement inside the soil near the test pile and also interfere with the pile load–settlement response. Fakharian, Meskar & Mohammadlou (2013) used finite element numerical modelling to assess the influence of pressure generated by surcharge support on load–settlement response of a test pile during static load testing. In the latter study, in order to evaluate an axial compressive static load testing (using kentledge system) under sequential loading, a three-dimensional non-linear finite-element model was developed. The results of a real test were used to verify the numerical model. The obtained results indicate that the pressure induced by surcharge supports had almost no effect on the ultimate capacity of the test pile. It was mainly attributed to the fact that the mobilised skin friction is influenced a little by the surcharge and its influence on toe resistance is negligible. However, the initial stiffness of the test pile may be influenced by generated pressure which is distributed around the pile shaft and this influence increases as the diameter of piles increases. It was shown that the surcharge pressure has a greater effect on piles embedded in frictional soils than cohesive soils. The results show that pile stiffness is 15% to 25% less influenced in a kentledge system compared with those data available in the literature using the reaction pile system.

Yetginer, White & Bolton (2006) back-analysed the axial response of some large-scale pipe piles installed by jacking. In general in jacking method all the piles must be installed close together since some pile jacking machines walk along the pile wall under construction. This geometry is unlike the conventional design guidance, which suggests that a minimum distance is needed between piles to avoid the effect of adverse interaction. In the latter study, static load testing results carried out on jacked piles installed in the distances less than the recommended minimum spacing (typically two or three pile

diameters) were presented. Figure 2.22 illustrates the load-settlement curves associated with different static loads , applied on two groups of 12 piles.

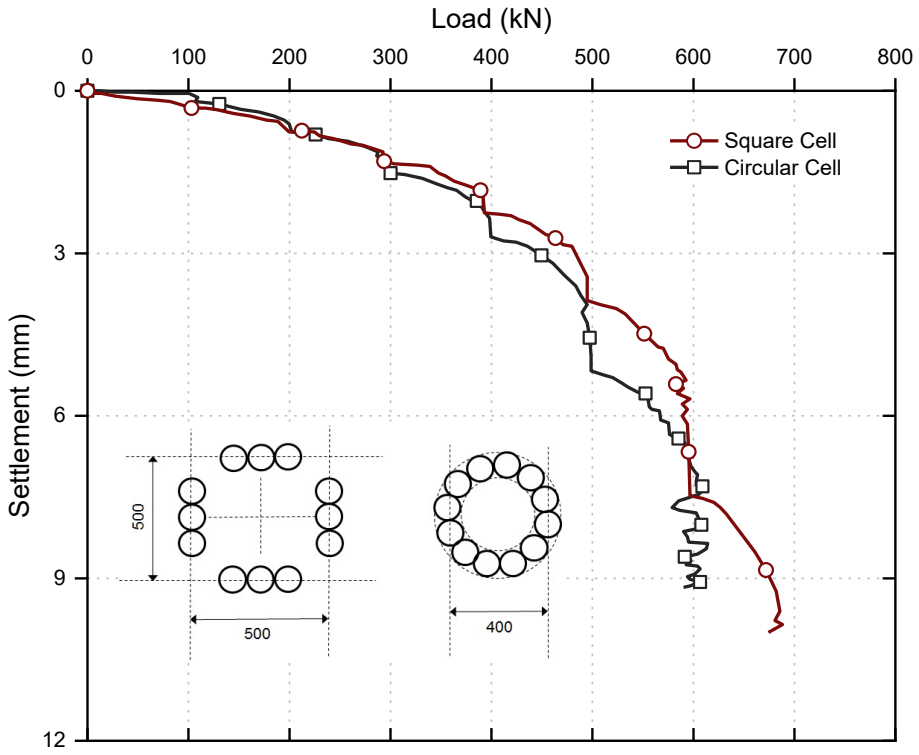

Figure 2.22 Maintained load tests on square and circular cell foundations (after Yetginer, White & Bolton 2006)

In that study the behaviour of jacked piles in sandy soil was back analysed and field tests were carried out to investigate whether in even especial cases where jacked piles are installed in closely spaced groups, traditional design methods can be applied to the respected piles. Very high stiffness behaviour which was observed during the maintained load tests was introduced as the most important characteristic of the results of test. Conducting a back-analysis using a load-transfer approach (RATZ) revealed that this behaviour is caused by the higher stiffness observed at the pile toe due to the pre-loading applied during the final installation stroke, and the existence of a residual base load. In that study, considering the residual base load, a reasonable correlation was observed between the load-transfer analysis (RATZ) and data measured (Figure 2.23). The

obtained response was much stiffer than for the bored or driven piles. While analysing the cell foundations, exactly the same factors which used to back-analyse a single pile were applied and it was revealed that the working settlement of the cell foundations were conservative.

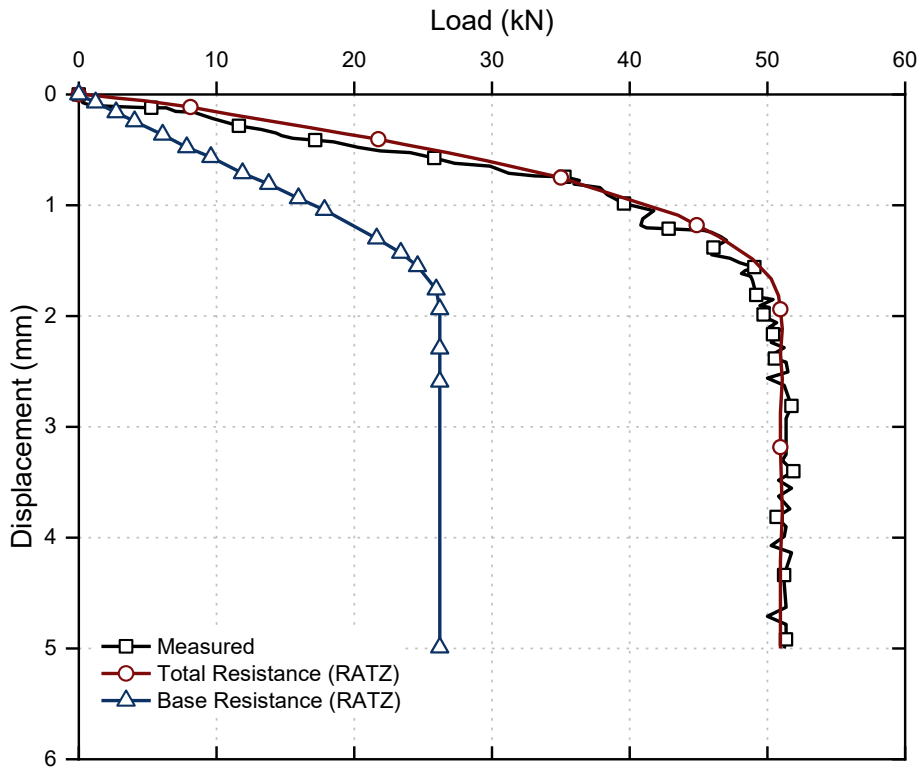

Figure 2.23 Comparison of single pile load-displacement and RATZ back-analysis (after Yetginer, White & Bolton 2006)

In terms of experimental studies, Zhou et al. (2019) study focused on compressive static load testing 40 displacement precast piles including square piles and pipe piles of various lengths. It was calculated that because the layers of soil differed at the driven locations, piles with various lengths would deliver different maximum settlements. The load-settlement curves obtained from concrete piles (the same type) remained relatively parallel during the unloading stages. During the interpretations of solid piles results, the Double Tangent and Chin's methods were used to determine their capacities, and then were compared to the designed ultimate capacity. Since the Double Tangent method is

conservative whereas Chin's method overestimates the pile capacity, this led to introducing the modified Double Tangent and Chin's interpretations.

Dai et al. (2012) study presents the results of real and full-scale static load tests for both single piles and pile groups installed in mixed soil layers of clay and silt in Nanjing, China. The load tests were to determine how the spacing, length, and number of the piles affected the group response, hence in the experiments a parametric study was conducted by changing the number of piles in the group, their spacing, the type of groups, and their lengths. Every pile was 400 mm in diameter, and groups consisting of two, four, and nine piles with lengths of 20 and 24 m were considered. Some piles in the groups and all the single piles were instrumented in order to obtain the load transfer and the load-settlement curves. By back-calculation of measured data obtained from the load tests, the interaction coefficient for each pile in the group was obtained. The results indicate that the interaction coefficient is a function of the size and settlement of the group, and as group settlement increases the interaction coefficient increases.

2.6.2 Dynamic pile load testing: numerical, experimental and analytical studies

Likins & Rausche (2004) pointed out that based on an existing database, there is a reasonable correlation of CAPWAP signal matching results from the dynamic restrike testing with static load testing. In this study, six stress wave conferences (1980 – 2000) were reviewed to gather data and extract correlation cases which included the static load tests and CAPWAP restrike results. Although the databases did show reasonable correlations between CAPWAP and the static load testing methods, in some cases CAPWAP over-predicted or under-predicted the results. For example, dynamic testing of drilled shafts often resulted in a small set per blow and therefore the predicted capacity would be on the conservative side. Figure 2.24 shows the capacity ratios for the CAPWAP

to static load testing (SLT) for different projects collected from the first six stress wave conferences for 226 piles.

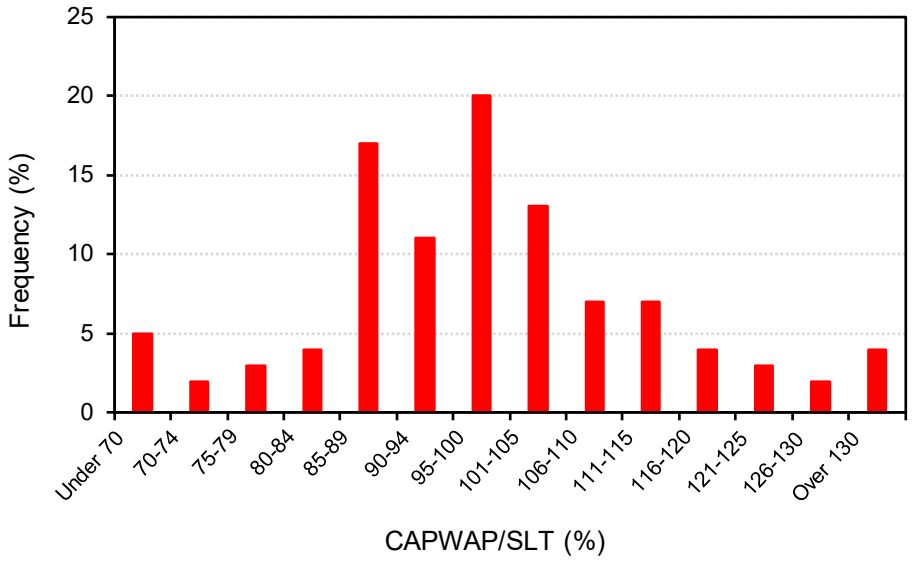

Figure 2.24 Distribution of CAPWAP to SLT ratios for 226 piles (after Likins & Rausche 2004)

As Figure 2.24 shows, there are some situations where the static load testing and CAPWAP analyses yielded different results. Rausche (1990) proposed that CAPWAP may under-predict and over-predict the capacity and the main reasons are classified as follows:

Over-prediction:

- *Soils exhibiting relaxation*: unlike setup, relaxation is defined as decreasing the strength of soil over time. In cases where all the piles are driven into shales, this phenomenon occurs so strength attained immediately after driving decreases over time, which is why a dynamic load testing carried out at the end of driving (EOD) would over-predicts pile resistance.

- *Soils exhibiting creep*: these types of soil initially show capacities which decreases under long term loads and therefore in this case quick load testing may be misleading.

Under-prediction:

- *Sensitive soils*: clays that experience a change in their structure may lose all of their static strength under dynamic loading hence their setup factor may be as high as infinity and their static strength is regained over time.
- *Soils subject to increased pore water pressure*: pore water pressures increase in fine grained soils since they cannot dissipate quickly during pile driving, and even silts and fine sands seem to behave the same way. Increased pore water pressure reduces the effective stresses and the frictional resistance during driving and these pore water pressures decrease overt time depends on permeability and then the soil regains its strength. This effect usually occurs along the pile skin more than at the pile toe.
- *Soil Fatigue*: this effect is similar to losses of strength due to a change in the soil structure or in the effective horizontal stress. It is described for over-consolidated clays whose soil-pile interface becomes smoother and smoother as the number of hammer blows increases.
- *Soil loosening*: this phenomenon occurs in all types of soil. Soil loosening is defined a reduction in horizontal stress and reduced density caused by unavoidable horizontal motions (pile whipping) and by voids created by plugs in open profiles. Most types of soils will firm up around a pile after driving as the soil pressures equalises.

The problems listed above may not be complete and there may be other reasons for inaccurate predictions of capacity by CAPWAP such as liquefaction and strain softening.

Closed-ended and open-ended pipe piles are used widely all over the world. As explained by Paikowsky & Chernauskaus (2008) during the driving an open-ended pipe pile plugging occurs which leads to a complicated interaction between the soil plug and the pile that consequently causes the propagating stress wave to suddenly change. Dynamic analyses of piles are currently based on a one-dimensional wave equation which, while having the ability to consider the inner soil plug indirectly, after the formation of soil plug it is not capable to simulate the physical phenomena accurately. This causes the field observations does not correlate very well with predicted capacity of plugged piles obtained based on analyses. Dynamic conditions of a fully plugged pipe pile differ from closed and open-ended unplugged piles. As mentioned by Paikowsky & Chernauskaus (2008), during pile driving the soil plug is subjected to a propagation of radial shear stress and longitudinal compressive stress and in order to analyse this system the inertia of the soil plug must first be considered even though the plug and pile experience the same displacement. This sophisticated pile-plug behaviour does not correlate very well with the simplified underlying assumption of a one-dimensional wave equation, therefore fully plugged piles cannot be analysed utilising a one-dimensional wave equation.

According to Paikowsky & Chernauskaus (2008) the modes of wave propagation in a soil-plug system shown in Figure 2.25 show how the shear and constrained longitudinal waves propagates in the soil plug, while stress waves in a pile propagate longitudinally. Induced wave due to the hammer impact propagates longitudinally as long as it encounters resistance due to the surrounding soil, which causes the wave to reflect. The longitudinal wave then reaches the soil plug and induces interfacial shear that causes the

shear waves to propagate radially towards the centre of the plug. These shear waves cause within the soil plug to displace vertically and also constrained longitudinal waves to propagate along the soil plug. Because of the higher speed of wave propagation in steel than soil, the induced wave at the pile head may travel down to the pile toe and come back to the pile head, while at the same time the constrained and shear waves propagating in the soil plug may have only moved a part of that distance.

As stated by Paikowsky & Chernauskaus (2008) in driving piles in unplugged mode, the inner and outer shaft resistances can be combined and in this case dynamic pile analysis can be performed appropriately based on the one-dimensional wave equation, which means that a really reasonable correlation of signal matching analyses based on this formulation with the static load testing can be observed. However, in driving piles in fully plugged or partially plugged mode, the internal soil plug-pile interaction disturbs the basic assumptions of the one-dimensional wave equation, hence the results are erroneous even when a reasonable match between the predicted and measured signals are observed.

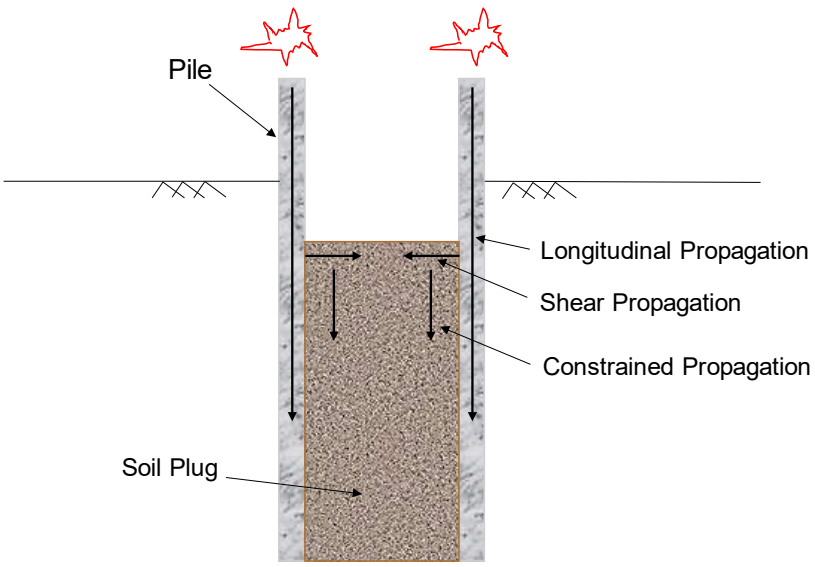

Figure 2.25 Modes of wave propagation in the pile-plug system (after Paikowsky & Chernauskaus 2008)

A more precise formulation of the plug equation of motion has been proposed by Paikowsky & Chernauskaus (2008) to consider the physical phenomenon and longitudinal and shear wave propagation correctly. An analysis based on this formulation indicated a more realistic evaluation of pile resistance compared to the one-dimensional wave equation based methods, even though the similar signal matching was observed.

As explained by Salgado (2008), closed-ended pipe piles during the driving impose larger displacement on the surrounding soil compared to open-ended pipe piles, hence in the same load and soil conditions they have larger ultimate bearing capacity. Piles are often driven into soil with multiple layers of clay, sand, silt, or a mixture of these soils therefore Kim et al. (2009) evaluated the behaviour of closed-ended steel pipe piles driven into multilayered soil profiles. In the latter study, an array of fully instrumented static and dynamic axial load testing were conducted on closed-ended steel pipe piles and then results were presented and interpreted. As explained by Kim et al. (2009), when closed-ended pipe piles are driven into layered soil, developing and dissipating excess pore pressure is much more complex than for single layers of soil. In addition, the toe resistance mobilisation if affected by multiple layers of soil located close to the base of the piles is much more difficult to analyse. The main reason for that study was to evaluate these effects, but in order to carry out the test, the main closed-ended test piles, the closed-ended reaction piles, and the H piles were driven into soil with a mixed profile. Static axial load testing carried out on the main pile and high-strain dynamic testing were carried out on all the other test and reaction piles during initial driving and during restrikes at various times over a 5 month period. The test results obtained by Salgado (2008) indicate that CAPWAP analysis 104 days after pile installation show no increase in the toe resistance while it estimates shaft resistance six times larger than the value obtained at the end of driving condition. Due to the complicated behaviour of axially loaded piles

driven into multi-layered soils, further fully instrumented load testing and detailed site characterisation was recommended to be conducted for a better understanding of the behaviour of piles.

Haque, Abu-Farsakh & Tsai (2016) examined the behaviour of test piles using two setups (with lengths of 44.2 m and 51.8 m) installed within 5D (D denotes the diameter of the pile) spacing. Strain gauges mounted on the piles to measure the setup and the load transfer per layers of individual soil and the 44.2 m long pile was installed two hours after the 51.8 m long pile. Several dynamic and one static load testing were carried out on the test piles to measure the pile setup. In this study the effect that the sequence of installation had on the setup behaviour was evaluated; it was found that both test piles indicated a considerable setup over time. However, the initial shaft resistance of the 44.2 m long pile (installed two hours later) was almost half the shaft resistance of the 51.8 m long pile, but with much higher resistance increase rate due to the sequence in which piles are driven into clayey soils. Driving a 51.8 m long pile caused excess pore water pressure to develop in the surrounding soils which then affected the initial resistance and setup rate of the 44.2 m long pile. Finally, the CAPWAP results were compared with static load testing to obtain the resistance of individual soil layers of soil along the length of piles over time, which shows that clayey soil has a higher setup than sandy-silty layers of soil.

Heritier, Paquet & Stain (1991) examined the accuracy and limitations of full-scale dynamic pile load testing and found that although the predicted pile capacity using the dynamic pile load testing technique for driven piles seems reasonable, when used on bored cast-in-place piles the inaccurate dimensions and properties of the piles influences the accuracy of the predictions. As explained in that study, comprehensive research has been carried out since 1980 by the experimental centre of researchers and the building

and public works (CEBTP) in France, with dynamic tests on bored piles with diameters ranging from 0.2 m to 1.2 m in various soil conditions. That research led to the development of a methodology specifically adapted to bored piles known as SIMBAT with the aim of highlighting the potential errors inherent in dynamic load testing by emphasising the difficulty of obtaining genuine static-dynamic correlations and by comparing the predictions made by the CASE method and the SIMBAT technique in the field of dynamic load testing. According to Heritier, Paquet & Stain (1991), the SIMBAT technique, like CASE method, uses many of the original wave equation theories, but it differs mainly in the conversion of total resistance to static resistance (deducing the dynamic resistance from total resistance). The classical CASE method relates the dynamic to static conversion to the velocity of pile top whereas the SIMBAT method expresses the velocity at which the pile penetrates the soil as a function is used in the relationship between dynamic and static resistance:

$$R_{Static} = R_{total} - f(V_{pen}) \tag{2.11}$$

where, $f(V_{pen})$ is a function of the velocity of pile penetration; the velocity of the pile and the velocity of penetration are quite different. Moreover, the SIMBAT technique does not require a soil damping factor to be assumed.

Alternatively, in terms of proposing a new model for analysing pile driving, Lee et al. (1988) proposed a one-dimensional wave equation model where the pile is represented by discrete elements, and the soil is replaced by a series of springs and dashpots, and unlike to the Smith model it uses conventional soil mechanics parameters. Moreover, through radiation or geometric damping this model regards the dissipation of wave energy to the soil as well as the influence of the increase in soil resistance to failure due to rapid loading. Figure 2.26 illustrates a schematic representation of this model. Lee et al (1988)

stated that the use of a 1-D wave equation based model to analyse pile-driving is largely attributed to Smith (1960), whereas previous analyses were conducted using pile-driving formulae. The parameters used in this model such as soil quake (q) and damping coefficients (J) are non-standard soil mechanics factors that are specified through pile load tests back analysis. To evaluate the capability of the proposed model, two full size instrumented steel pipe piles were evaluated and the pore-water pressures, total stresses, and driving stresses were examined at different levels in the piles. The two piles were 12.6 m long with 457 mm diameter and 19 mm wall thickness; they were similar except that at the toe of one pile, B was closed-ended, while the other pile A, was open-ended. According to the proposed model, the settlement estimated for pile A is 7.2 mm/blow, compared to the field settlement of 7.6 mm/blow, whereas the settlement for pile B is 10.3 mm/blow, compared to the field settlement of 10.2 mm/blow for final penetration. The ability of this new model to estimate settlements is considerable and the stresses predicted by the proposed model correlate well with the measured stresses.

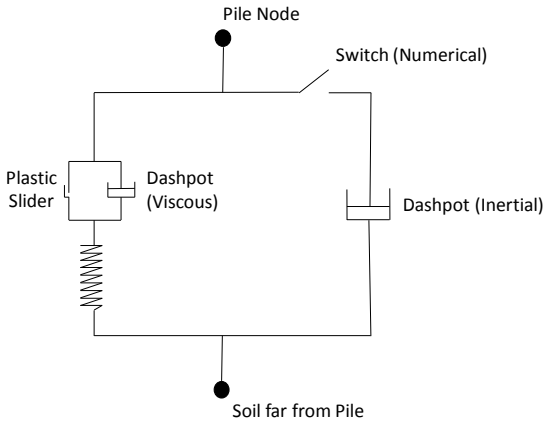

Figure 2.26 Apparent soil model proposed by Lee et al. (1988)

Accordingly, Lee et al. (1988) concluded that their proposed model has several significant advantages compared to the existing Smith (1960) model, such as considering soil

parameters that consists of standard soil mechanics parameters that include the shear modulus, G_s, the soil density, ρ_s, and Poisson's ratio, ν.

As well as theoretical and field studies, some researchers focused on numerical methods for analysing pile driving and dynamic pile load testing problems. Nath (1990) used a continuum method of finite element analysis to predict the performance of a fully embedded steel pipe pile during driving. In that study both the pile and the soil were assigned different properties as two different parts of the same solid continuum. The soil medium behaviour, supposed to be semi-infinite and nonlinear, was considered to be a hyperbolic stress-strain relationship. The problem was analytically solved in the time-domain with the central difference scheme by discretising the pile-soil system with axi-symmetric finite elements. The main purpose of Nath's (1990) study was the comparison of the wave equation method with the continuum method of pile driving analysis in which the pile-soil system is assumed to be an elastic continuum and the soil medium is considered to be semi-infinite. To achieve this aim, the continuum method (finite element method) was used to calculate the permanent settlement and static bearing capacity of a driven pile into a soil medium with non-linear material properties. The settlement and resistance values obtained by the wave equation method were then compared with a corresponding values found by continuum based method. The pile was a uniform steel pipe pile and fully embedded into a semi-infinite soil medium and driven by a falling hammer that impact on the head of the pile via a cap block and cushion. The soil was isotropic layered with nonlinear behaviour.

Figure 2.27 shows the typical discretisation of a pile-soil system and axi-symmetric finite element (FE) analysis of the problem in which the far boundary of the FE model is placed as much as the length of one pile. Referring to Nath (1990), two different criteria were

used to compare the results of the wave equation method and those obtained from the continuum method, including total resistance versus the number of blows (Figure 2.28a) and driving stress in the pile versus the number of blows (Figure 2.28b). Finally, since the continuum method is based on a more realistic conditions compared to the wave equation method, comparing the results with field observations indicated that a continuum analysis would be more accurate than the wave equation method and could therefore be used to analyse the pile driving problem more accurately.

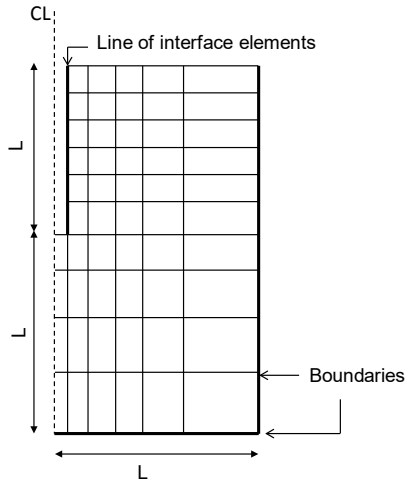

Figure 2.27 A typical discretisation used in FEM (after Nath 1990)

It is well established that the behaviour of pile foundations under dynamic excitation is highly complicated since that involve nonlinearities in material behaviour and a sophisticated interaction between soil and pile. One of the primary objectives of designing a pile foundation under a dynamic load is to set the amplitude of vibration to an allowable value while at resonance, where the foundation experiences large vibration amplitudes; this is why, estimating the resonant frequency of a soil-pile system is a very crucial function.

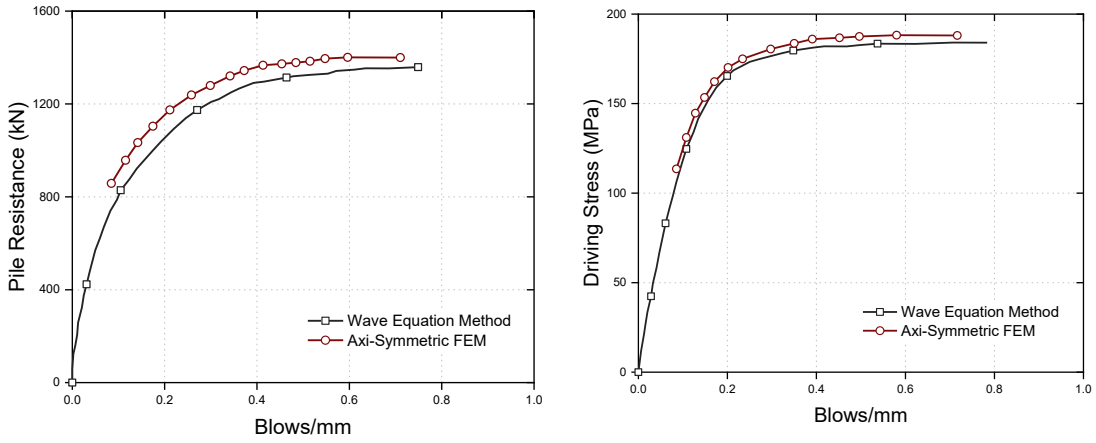

(a) (b)

Figure 2.28 Comparison of (a) pile resistance and (b) driving stress between wave equation and finite element methods (after Nath 1990)

Bhowmik, Baidya & Dasgupta (2016) investigated the nonlinear behaviour of single hollow steel piles under different levels of vertical dynamic load both numerically and experimentally. During their experimental investigation, the average vertical amplitude of a pile-soil system was captured from two vibration pickups; these results indicated that the moment of excitement increases while the resonant amplitude increases but resonant frequency decreases. They concluded that increasing the length of the pile increases the resonant frequency whereas the resonant amplitude decreases. The results of numerical studies (using the finite element model developed in Abaqus software) matched quite well with the experimental results hence it was suggested that the proposed finite element model used to analyse the behaviour of a single pile under a vertical dynamic load could be used with reasonable accuracy.

Manna & Baidya (2009) investigated two full-scale single piles under a vertical static load and a vertical vibratory load, and also predicted the vertical dynamic response of the test piles using the finite element software PLAXIS-2D. Using a numerical simulation, they predicted the changes of resonant amplitude of vertical vibration along the length of

a pile in layered soil. To verify these results a Novak' plane strain model was used to predict the dynamic response of single piles and then the results were compared with the finite element model. The results generated by the model means that most of the pick amplitudes predicted through finite element analysis correlate very well with the experimental peaks, however, Novak's solution could not predict the complicated behaviour of full-scale pile embedded in layered soil. Manna and Baidya (2009) also stated that although the dynamic analysis of full-scale pile in a layered soil medium is a sophisticated problem in practice, an advanced finite element model can still analyse the complicated dynamic pile-soil interaction problem if the layers of soil, the piles and the interfaces are modelled properly.

The effect of installing driven piles has been modelled by Dung (2009), using a standard small strain analysis in the PLAXIS 2D finite element code. In that study, the effect of installation can considered by increasing the volume of the pile cluster, and by using the displacements prescribed at the pile-soil boundary, or volumetric expansion. According to Dung's study, the most important issue in the FEM program is capturing the behaviour of the soil because it changes continuously as piles are installed. Furthermore, since the Mohr-Coulomb model has many limitations with regards to the behaviour of real soil it cannot be used in this case, and although the hardening soil model is an advanced model for soil behaviour simulation, some important features are still not included in this model. Dung (2009) study therefore concludes that the Hypoplastic model is currently the most suitable model for driven piles the void ratio has been introduced as a state variable, and because of the intergranular strain concept.

2.7 Gap and Limitations in Current Literature

After carrying out a comprehensive literature review and studying the background of different techniques and concepts of static and dynamic pile load testing, determining the pile bearing capacity, interpreting the behaviour the test results, and assessing the behaviour of piles under static and dynamic loads is still a challenge for researchers and engineers. According to the studies published previously, numerical modelling is a powerful and economical approach which can be used to predict the response of different kind of piles, including solid and tubular piles under different loading conditions. Numerical simulations can evaluate the behaviour of a single pile and a group of piles under static load testing, hence there is no need for sophisticated instrumentation to achieve accurate results. Moreover, continuum-based numerical simulations provide more realistic conditions than one-dimensional wave equation-based programs, such as CAPWAP and GRLWEAP, and they can assess the behaviour of piles under dynamic loading more appropriately. At the same time they can maintain continuity between design and quality control, and also feasibly execute more rigorous analyses, including settlement, ground vibrations, and interaction analyses.

However, the most challenging part of numerical simulation is adopting a soil model that can capture the non-linear behaviour of soil precisely, by considering the stress-path dependent stiffness, and the dissipation of energy through the natural, hysteretic, and geometric damping features of soil simulation. Therefore, advanced soil models such as hardening soil with small strain stiffness and hypoplastic with intergranular strain during static and dynamic pile load testing can be adopted.

Note that the intention of expressing the potential errors and limitations of static and dynamic load tests is not to discredit them, but to be aware of the potential errors and the measures that can be taken to decrease them.

CHAPTER 3 Static Pile Load Testing: Numerical Simulation of Single Pile and Piles Group Behaviours

3.1 Synopsis

Pile displacement induced by static load testing either using kentledge or reaction pile method can mobilise the soil resistance along the pile shaft and toe. However, the evaluation of ultimate soil capacity in different soil conditions still is a challenging mission. Due to the difficulties and the cost of full-scale load tests, there is an objective to predict the response of single piles and piles group under static load testing, using proper numerical modelling. Realising numerical analyses may provide useful insights, this chapter describes numerical modelling techniques to simulate static load testing and investigate how different soil models including basic to advanced soil models can affect the load-displacement curves, obtained during the simulation. In addition, in this chapter the interaction of reaction piles and test piles during the static pile load testing is evaluated by numerical simulation. The stiffness variation, existing inside the pile group under axial load testing, is assessed by three different analyses including linear elastic, completely non-linear, and a combination of non-linear and linear analyses. All numerical simulations are conducted employing finite element software PLAXIS 2D and 3D to capture large strain and low stiffness behaviour, which is observed during the static load testing and to draw load-displacement curves as the main outputs of pile load testing to assess the ultimate bearing capacity. In numerical simulations, different soil models Mohr-Coulomb, hardening soil and hypoplastic with intergranular strain are assigned to

the soil layers, while elastic model used for the pile element. Where possible, the predicted responses of piles during the numerical simulation are compared to existing measured data based on real experimental tests. Predictions reveal that numerical simulations applying advanced soil model such as hardening soil can capture the actual non-linear behaviour of soils and indicates more accurate results in terms of ultimate pile capacity compared with elasto-plastic soil model when the results are compared with real test data.

3.2 Introduction

According to Yu & Yang (2012), the assessment of foundation materials and the selection of suitable geological conditions to support the pile foundation are known as the most important aspect of pile design. In some conditions comprising cohesive subsoils, the pile shaft contribution is necessary to be considered in minimising the foundations settlement rather than to mobilise load capacity. The proper selection of a pile type for a given foundation depends on a comparative study of cost, durability, stability under vertical and a horizontal loading, long-term settlement and method of pile installation. According to Chapman (1993), static load testing (SLT) often forms an important part of many piling projects and it is crucial for those involved in the design and setup of such tests to have a full understanding of the available testing methods and analytical techniques. Static tests can be performed for variety of reasons, including one or more of the following:

- To acknowledge that the pile performs properly at the working load in terms of settlement and the load bearing capacity

- To determine the ultimate capacity of the pile to correlate with other methods of estimating capacity such as geotechnical computations and dynamic measurements

- To obtain back-calculated soil parameters to be employed in pile design or soil-structure modelling

- To specify single-pile load-settlement behaviour at the design working load to allow piles group settlement to be calculated

An accurate deformation analysis should be conducted using the advanced constitutive models that approximate the stress-strain relationship more precisely than a simple constitutive model (the Mohr-Coulomb model), and consequently the form of displacement fields during pile load testing can be modelled more realistically (Obrzud 2010). As explained by Dung (2009), the most important issue in FEM programs is capturing the soil behaviour, which varies continuously during the pile installation and pile load testing. Hence, it is vital to use a suitable model that can consider and simulate the real soil behaviour. Mohr-Coulomb model is known as a model, which has a number of limitations to embrace the real soil behaviour, while the hardening soil model can be considered as an advanced model to simulate the soil behaviour. The hardening soil (HS) model can reproduce soil deformations more realistically, as the stress-strain relationship is approximated by a non-linear curve. In addition, as the formulation of the HS model combines two hardening mechanisms, it is appropriate for modelling both plastic shear strains (observed in overconsolidated cohesive soils and granular soils), as well as plastic volumetric strains, typically observed in soft soils. In addition, currently the hypoplastic model with intergranular strain concept is known as another advanced soil model, which can predict successfully the non-linear behaviour of soil in the small to large strain range.

In this chapter firstly, using PLAXIS 2D, the behaviour of a single concrete bored pile in terms of the load-displacement curve resulted from static load testing is evaluated. In numerical modelling three constitutive soil models including Mohr-Coulomb, hardening soil and hypoplastic with intergranular Strain inclusion, are used, and the capabilities of each model during the simulation of static load testing are assessed. Then, the accuracy of the elastic-perfectly-plastic Mohr-Coulomb and hardening soil constitutive models are evaluated in predicting the load-displacement curve of a real static load test using PLAXIS 3D and the predictions are compared together. In the next stage, after interpreting the load-displacement curve using Davisson method, the effects of reaction piles on the performance of the test pile are evaluated. Finally, the behaviour of two real case concrete bored piles group in cemented sand are evaluated by three-dimensional finite element program in which a combined non-linear and linear analysis is performed to capture a reasonable correlation with field measurements.

3.3 Numerical Simulation Procedure

The static pile load testing simulations, presented in this chapter, were performed either in axisymmetric finite element program PLAXIS 2D in which 15 node triangular elements were assigned to the model to simulate the soil or in three-dimensional finite element program PLAXIS 3D in which 10 node tetrahedral elements assigned to the model. According to Brinkgreve, Kumarswamy & Swolfs (2017), the 10-noded tetrahedral elements used in three-dimensional model, are in a lower-order than to the 15-noded elements used in two-dimensional model. That is why, sufficient mesh refinement in the three-dimensional model should be considered in order to capture a better gradient along the pile. However, as expected refining the mesh increases the computation time

considerably. All the concrete piles in numerical models were simulated as solid zones with elastic material properties such as Poisson's ratio of 0.2, an elastic modulus of 30 GPa, and a unit weight of 25 $^{kN}/_{m^3}$. All movements of bottom level of the model were prohibited, whereas, lateral movements perpendicular to the lateral external sides were restrained. In addition, lateral boundaries of the numerical model were taken sides far enough from the pile to avoid the boundary effect. The borehole option described in the program was used to define the soil stratigraphy and the ground surface level. Furthermore, interface elements were specified between the pile and the soil to simulate the interaction between the pile and the surrounding soil.

For interface parameters of MC and HS models, the strength reduction factor R_{inter} was regarded as the main interface parameter, which considers the strength reduction of the interface element in the respected soil layer. However, the interface parameters of HP model defined in PLAXIS include the interface oedometer modulus, E_{oed}^{ref}, the interface strength parameters such as cohesion, the friction angle and the dilation angle. Hence, in this model, instead of using a particular strength reduction factor defined in MC and HS models, the interface shear strength is directly introduced in strength parameters. In addition, in HP model, according to a power law formulation two parameters are included in interface parameters to enable stress-dependency of the interface stiffness (Equation 3.1):

$$E_{oed}(\sigma_n') = E_{oed}^{ref}(\frac{\sigma_n'}{UD-P^{ref}})^{UD-Power} \quad (3.1)$$

where UD-P^{ref} is the reference stress level (usually 100 kPa), UD-Power is the rate of the stress dependency of the interface stiffness, and σ_n' is the effective normal stress in the interface stress point.

3.4 Single Bored Pile into Dense and Loose Sand Deposits

3.4.1 Overview

In this section, in order to assess the behaviour of piles during the static load testing, loose and dense Baskarp sand properties were used in numerical modelling. As explained by Elmi Anaraki (2008), Baskarp sand is a uniform sand and the grain size has been classified as angular to sub-angular with D_{50} of nearly 140μm. This sand has a total unit weight of 20 kN/m^3. Hypoplastic model parameters, including intergranular strain parameters and hardening soil model properties for this kind of soil are shown in Table 3.1. As mentioned by Elmi Anaraki (2008) in order to assess the density dependency of the soil behaviour, the initial void ratio varied between loose and dense conditions. Hence, in numerical modelling, incorporating Hypoplastic soil model, the initial void ratio was selected 0.83 ($D_r = 0.26$) and 0.65 ($D_r = 0.73$) for loose and dense conditions, respectively.

It should be noted that all Hypoplastic parameters were found based on the laboratory tests conducted by Elmi Anaraki (2008), while the material properties of the hardening soil model was found by Dung (2009) using the soil tests option defined in PLAXIS 2D, in such a way that using simulating the drained triaxial and oedometer tests, the soil responses obtained from the hypoplastic model are identical to the hardening soil model. Using this method, by correlating the soil responses from the hardening soil and Mohr-

Coulomb models in drained triaxial test (Figure 3.1), Mohr-Coulomb model properties were derived and shown in Table 3.2.

Table 3.1 Baskarp sand properties (after Dung 2009)

Parameters	Hypoplastic model with intergranular strain concept	Hardening Soil model (dense)	Hardening Soil model (loose)
ϕ_c (degree)	30	-	-
h_s (MPa)	4000	-	-
n	0.42	-	-
e_{d0}	0.548	-	-
e_{c0}	0.929	-	-
e_{i0}	1.08	-	-
α	0.12	-	-
β	0.96	-	-
m_T	2	-	-
m_R	5	-	-
R_{max}	0.0001	-	-
β_r	1	-	-
χ	2	-	-
E_{50}^{ref} (MPa)	-	40.5	31
E_{oed}^{ref} (MPa)	-	50	33
E_{ur}^{ref} (MPa)	-	121.5	93
ϕ (degree)	-	37	31.3
ψ (degree)	-	9	2
m	-	0.5	0.5
ν_{ur}	-	0.2	0.2
p^{ref} (kPa)	-	100	100

Table 3.2 Mohr-Coulomb model properties for Baskarp sand

Parameters	Dense	Loose
E_i (kPa)	60000	45000
E_{50} (kPa)	33000	24750
υ	0.35	0.25
ϕ (degree)	37	31.3
ψ (degree)	9	2

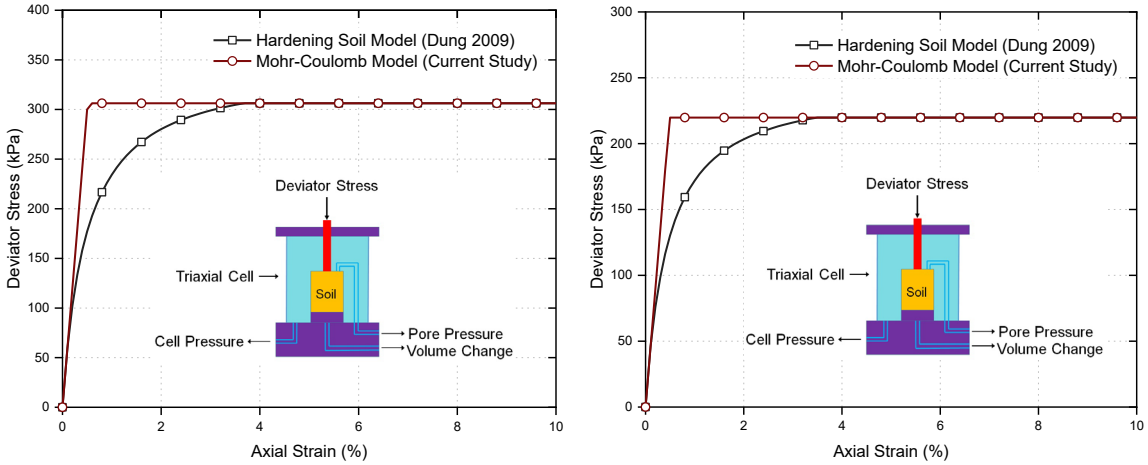

Figure 3.1 Simulated drained triaxial test sand applying Mohr-Coulomb and hardening soil models for (a) dense sand and (b) loose sand

Interface parameters used in numerical modelling for different soil models are introduced in Table 3.3. In the analysis, the length and the diameter of concrete pile were assumed 10 m (penetration depth 9 m) and 0.4 m, respectively. The finite element model of concrete pile is shown in Figure 3.2. The groundwater table was supposed to be at the ground surface and the dense sand and loose sand were assigned to the soil with three different constitutive soil models, as explained earlier.

3.4.2 Results and Discussion

At the first step, the mesh dependency of each constitutive soil model was evaluated by changing the size of mesh from very fine to very coarse in two cases with or without the interface element and the results are shown in Figure 3.3. It should be noted that the load-displacement curves were drawn by applying prescribed displacements of 2, 4, 8, 16, 35 and 50 mm at the top of the pile. As can be seen in Figure 3.3, it is clear that in the case of using interface element between soil and pile, all the models show less sensitivity to the mesh size compared to the cases in which interface element is removed.

Table 3.3 Interface parameters of different soil models defined in numerical modelling

Parameters	Mohr-Coulomb Model	Hardening Soil Model	Hypoplastic Model (Loose Sand)	Hypoplastic Model (Dense Sand)
R_{int}	1	1	-	-
E_{oed}^{ref} (kPa)	-	-	33000	50000
c'_{ref} (kPa)	-	-	0.1	0.1
ϕ' (degree)	-	-	31.3	37
ψ (degree)	-	-	2	9
UD-Power	-	-	0	0
UD-P^{ref} (kPa)	-	-	100	100

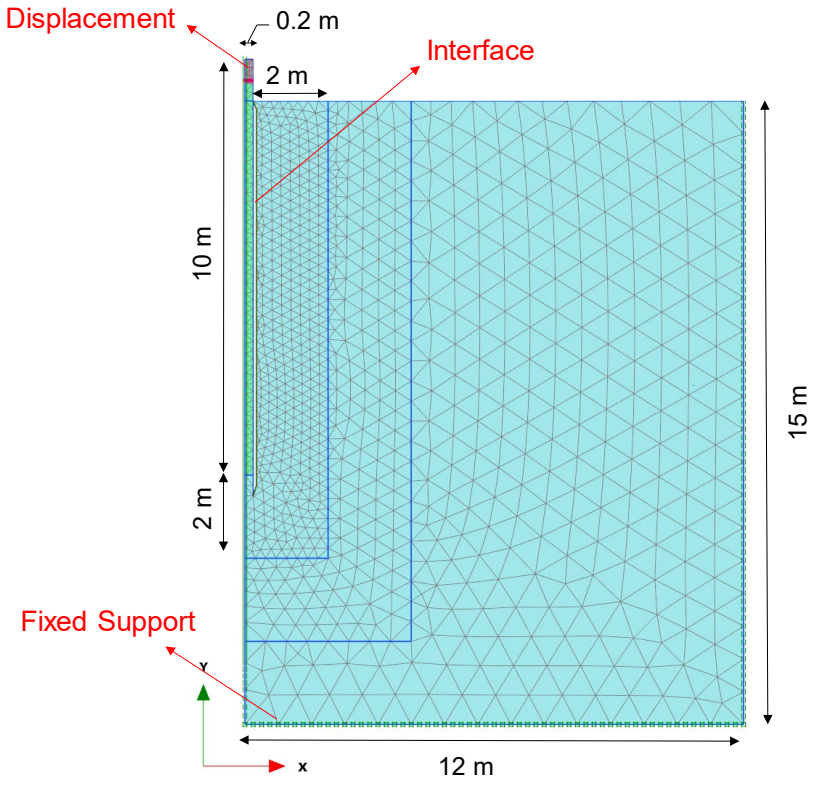

Figure 3.2 Finite element model of the pile and the adjacent ground with the corresponding generated mesh

However, in case of using interface element, both Mohr-Coulomb and hardening soil models showed less sensitivity to element size compared with hypoplastic model. Since in modelling with the Mohr-Coulomb model, the tangent modulus (E_i) was used; hence, the higher load was mobilised compared with two other soil models at the same displacement.

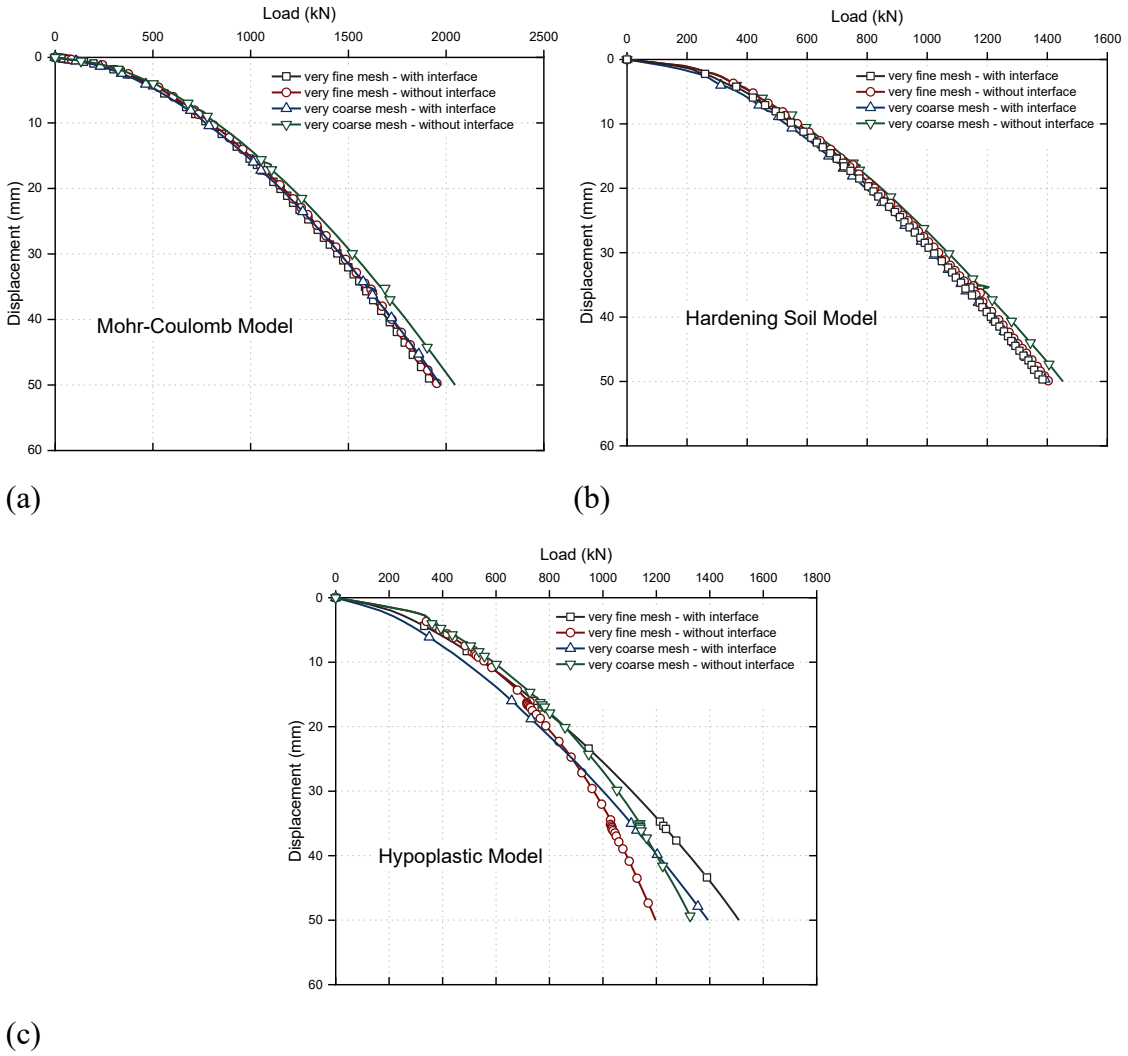

Figure 3.3 Mesh size dependency of finite element models with (a) MC, (b) HS and (c) HP constitutive models

After conducting mesh size sensitivity analysis, in the next step, the load-displacement curves of concrete bored pile were obtained in both saturated dense and loose states in four cases using different constitutive soil models including Mohr-Coulomb, hardening soil, hypoplastic with or without intergranular strain (IGS) incorporating a fine mesh. Load-displacement curves using different soil models are presented in Figure 3.4. It should be mentioned that in this section for modelling with Mohr-coulomb model the secant modulus (E_{50}) was used. As can be seen in Figure 3.4, there is a close correlation between MC, HS and HP models in both dense and loose sand conditions. Because HS

and MC soil models parameters were obtained based on the correlation to each other using the test facility defined in PLAXIS software. If more rigorous experimental tests were carried out on the soil samples, different behaviour of pile in terms of load-displacement curve would be expected. However, by activating the intergranular strain (IGS) concept of the hypoplastic model the load mobilised during static testing is considerably overestimated.

There are different techniques of specifying the ultimate capacity of piles from load-displacement plots, especially in compression. A well-known method takes the ultimate bearing capacity Q_{ult} as the load required to displace the pile 10% of its diameter. Using this method and comparing the bearing capacity of piles in displacement of 40 mm (i.e. 10% of the pile diameter) similar values can be obtained employing different soil models, except when IGS is activated in hypoplastic model. In addition, in order to evaluate the effect of different parameters of hypoplastic model on the load-displacement curve obtained during static load testing of concrete bored pile in dense sand, each parameter in the hypoplastic model was increased 30%, while remaining parameters were kept unchanged. The parametric study's results are shown in Figures 3.5 to 3.8.

Figures 3.5a-b indicate the influence of critical state friction angle (φ_c) and the granular hardness (h_s) on the obtained load-displacement curve. As depicted in Figures 3.5a-b, the critical state friction angle (φ_c) and the granular hardness (h_s) can be determined by measurement of the angle of repose (φ_{rep}) and any proportional compression test such as oedometric test (h_s controls the overall slope of the compression test), respectively. Figures 3.6a-b show the exponent relates to sensitivity of granular skeleton to change of pressure (n) and critical void ratio at zero pressure (e_{c0}).

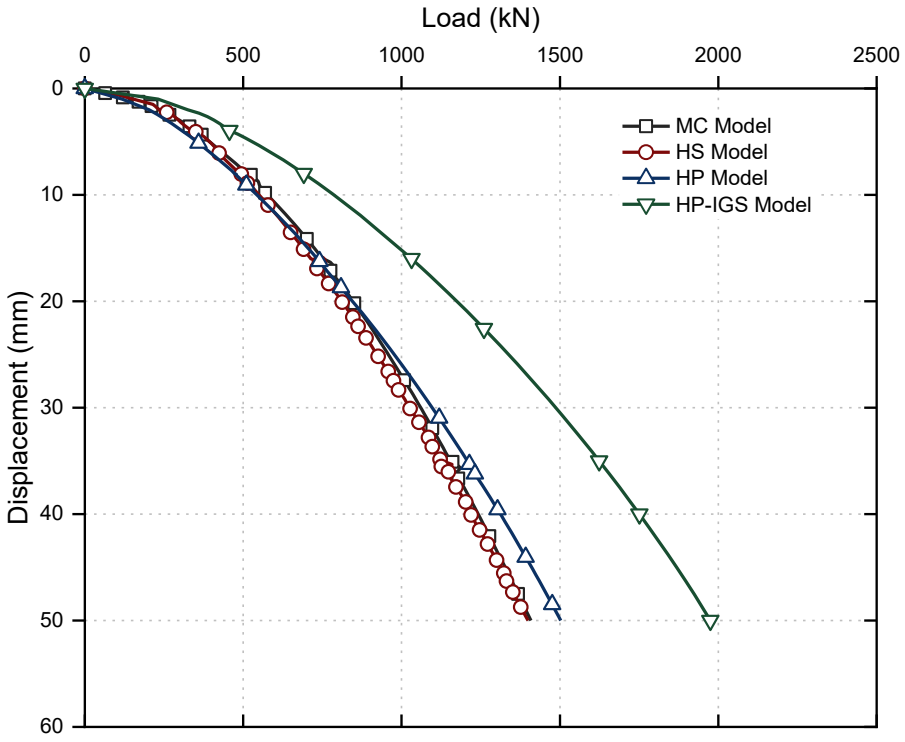

(a)

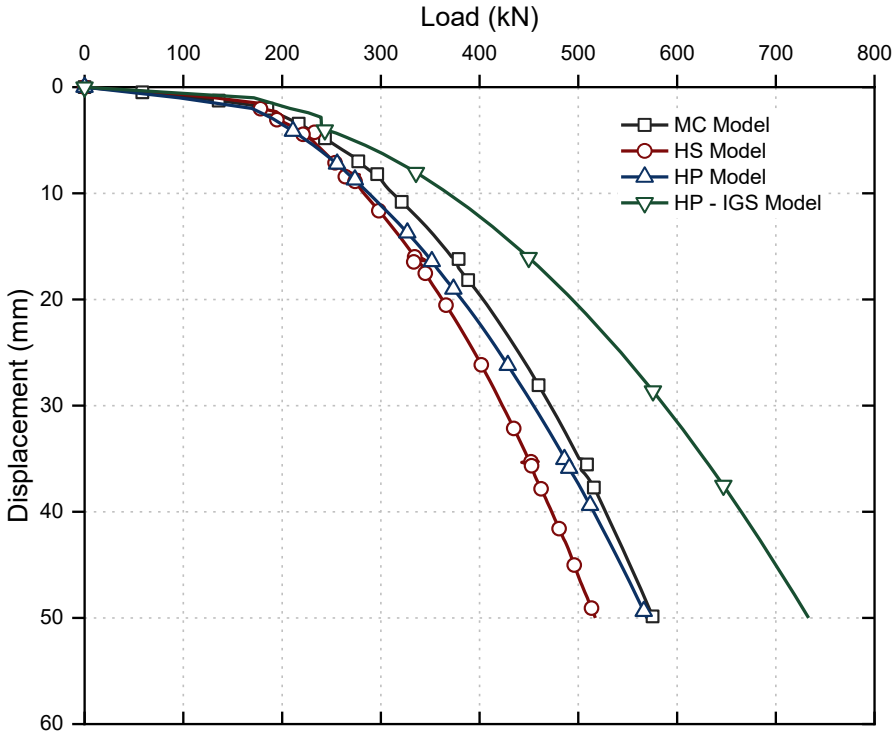

(b)

Figure 3.4 Comparison of obtained load-displacement curves using different soil models in (a) dense and (b) loose sand soils

As shown in Figures 3.6a-b, n controls the curvature of compression curve and can be determined by oedometric test, while e_{c0} defines the position of critical state line in the void ratio (e) vs ratio ($^{p_s}/_{h_s}$) which p_s defines the mean particle pressure. Figures 3.7a-b illustrate the maximum void ratio at zero pressure (e_{i0}) and exponent which describes the transition between peak and critical stress (α). According to Figure 3.7b, parameter α controls the dependency of peak friction angle φ_p. Figure 3.8 shows the influence of exponent value, representing the change of stiffness at current density (β). Similar to parameter α, it is determined using a drained triaxial shear test on the initially dense sample. Referring to Figures 3.5 to 3.8, it is crystal clear that among the evaluated parameters in this study, the granular hardness (h_s) shows the least and the critical friction angle (φ_c) and the exponent relating to the sensitivity of granular skeleton to change of pressure (n) show the most sensitive parameters on the load-displacement curve.

Finally, in order to evaluate the intergranular strain (IGS) concept in modelling of static pile load testing, the test was simulated in both dense and loose sand using hypoplastic (HP) model. The normalised length of the intergranular strain tensors are depicted in Figures 3.9a-b for dense and loose sand, respectively. The normalised length of the intergranular strain tensor changes between 0 and 1 indicating the soil being within the elastic range and representing the situation swept-out of the small-strain memory respectively. The behaviour of soil is governed by the basic hypoplastic model if the normalised length of the intergranular strain being equal to 1. In other words, the normalised length of the intergranular strain tensor indicates in different sections of the modelled geometry how the small-strain stiffness is activated. Figures 3.9a-b show the soil is in the hypoplastic state in the vicinity of the pile and further from the pile, the values of the normalised length of the intergranular strain tensor are very low and at these

places the soil remains elastic. This finding correlates very well with the large strain behaviour of soil around the pile during the static load testing.

3.5 Interaction of Reaction Piles on Test Pile

3.5.1 Overview

In this section, at first the capability of finite element simulation technique for predicting the load-displacement behaviour of a real single pile, a well-monitored real pile load testing, reported by Wehnert & Vermeer (2004), is examined in PLAXIS 3D. Then the effect of interaction of reaction piles on the test pile during the static load testing is evaluated. According to ASTM International (2013), for applying the load by a hydraulic jack in the reaction pile system the test load should be applied to the test pile by a hydraulic jack reacting against the test beam centred over the test pile. In this way, installing an adequate number of anchor piles to supply adequate reactive capacity for the test beam is necessary. In addition, in order to avoid the interaction effect of reaction piles on the test piles, a clear distance, at least five times of the maximum diameter of the largest anchor or test pile, but not less than 2.5 m from the test pile, should be provided. This minimum clear distance may increase or decrease by the engineer based on various parameters such as the soil conditions, type and depth of reaction, and magnitude of loads, if the reaction forces do not significantly affect the test results.

The soil profile used in numerical modelling includes tertiary sediments, which are stiff, overconsolidated clay and the groundwater table is 3.5 m below the surface. The tested pile is a solid concrete pile, which has a diameter of 1.3 m and a length of 9.5 m. The soil and pile properties used in numerical modelling are summarised in Table 3.4.

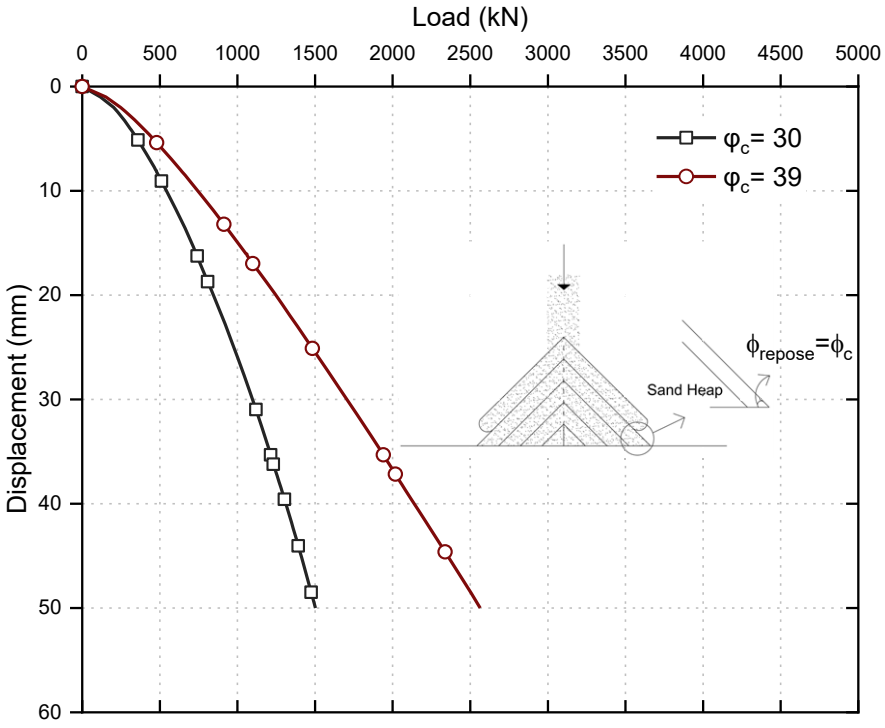

(a)

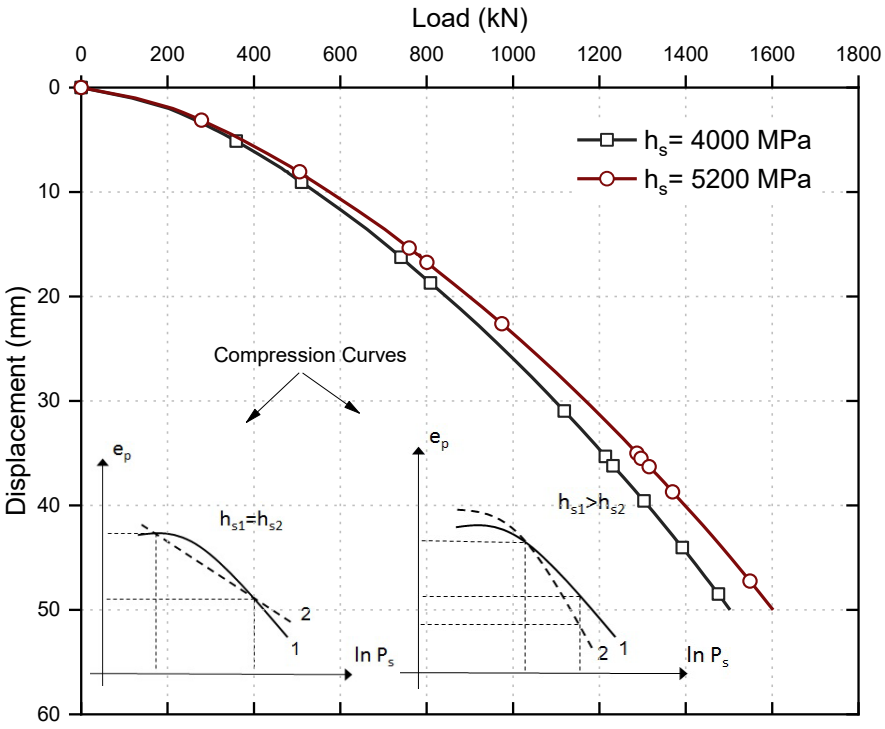

(b)

Figure 3.5 Influence of (a) critical state friction angle and (b) granular hardness on load-displacement curve of concrete bored pile in saturated sand

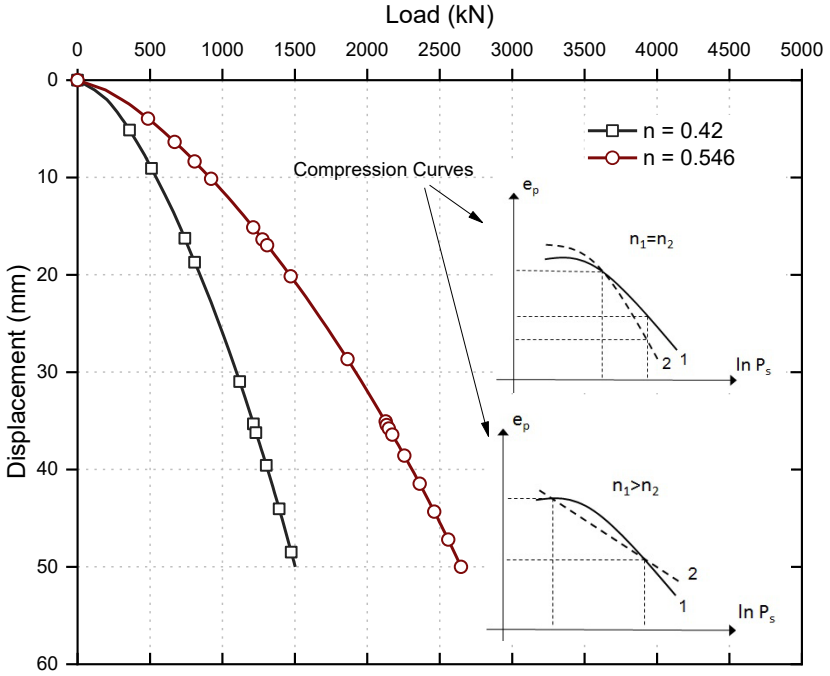

(a)

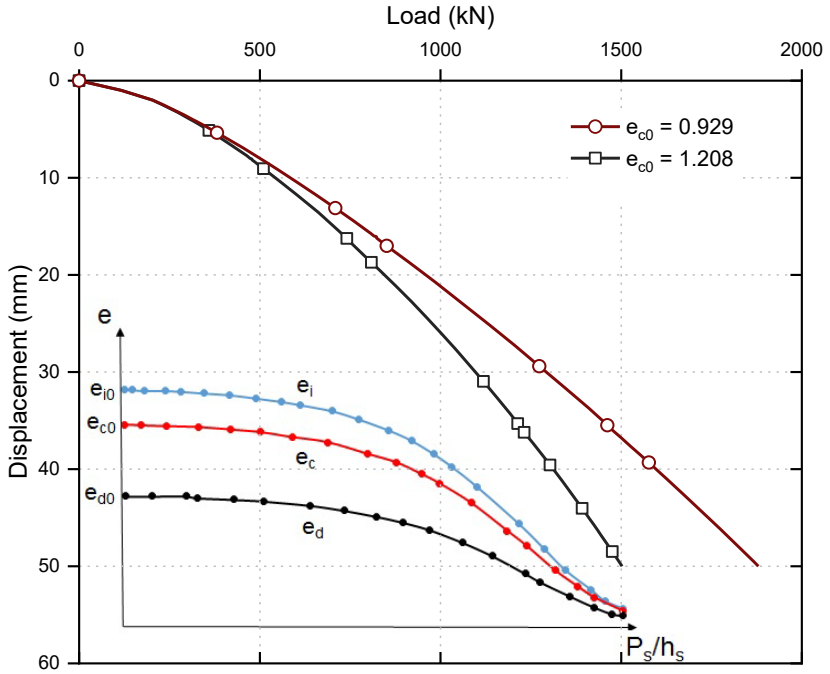

(b)

Figure 3.6 Influence of (a) sensitivity of granular skeleton to change of pressure (b) critical void ratio at zero pressure on load-displacement curve of concrete bored pile in saturated sand

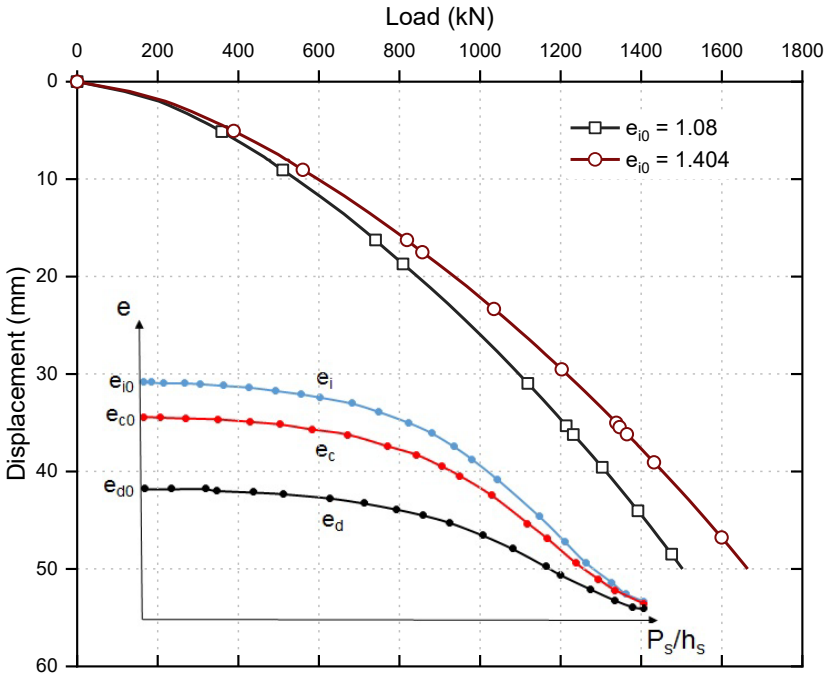

(a)

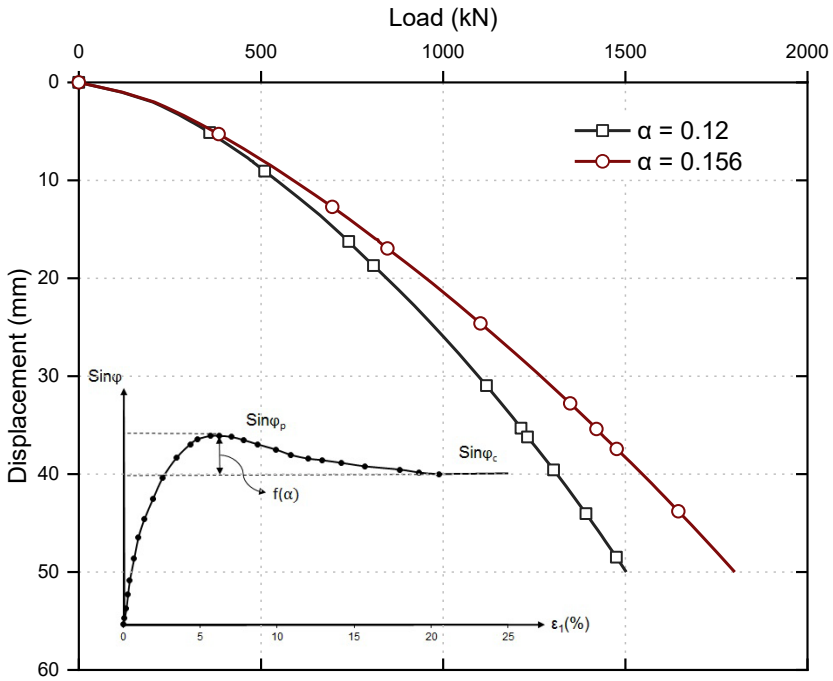

(b)

Figure 3.7 Influence of (a) maximum void ratio at zero pressure (b) exponent describes the transition between peak and critical stress on load-displacement curve of concrete bored pile in saturated sand

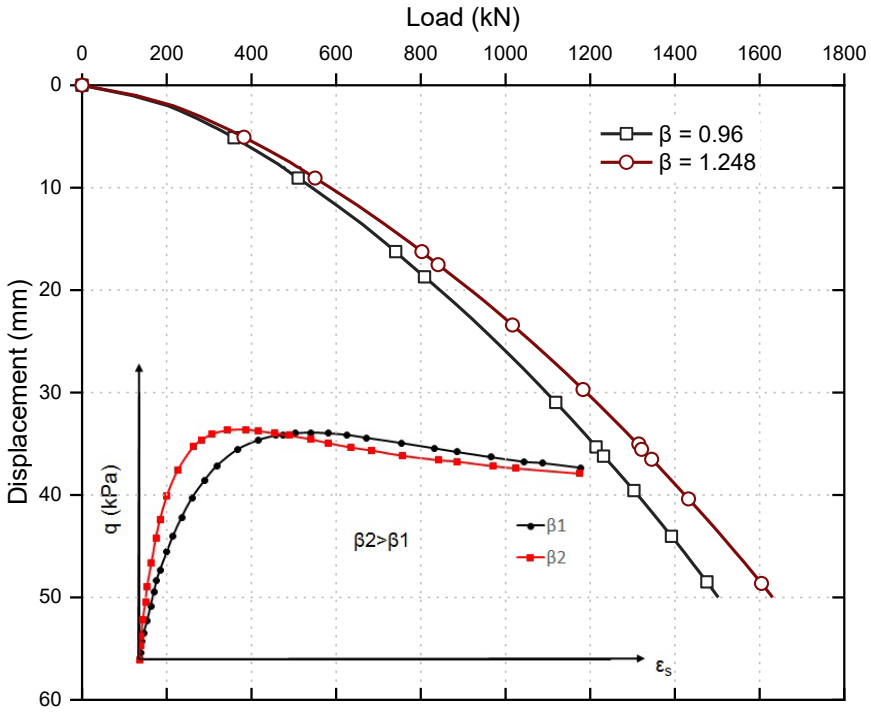

Figure 3.8 Influence of the exponent representing the change of stiffness at current density on load-displacement curve of concrete bored pile in saturated sand

In order to simulate the static load testing, after modelling the pile and soil, prescribed vertical displacements of 2, 4, 8, 16, 30 and 70 mm were applied to the pile head. The load-displacement curves of the pile were predicted for two cases, including linear-elastic-perfectly-plastic Mohr-Coulomb and hardening soil constitutive models. For the sake of simplicity, the strength reduction factor of interface, was assumed to be equal to one.

3.5.2 Results and Discussion

Figure 3.10 compares the load-displacement curves, obtained from the numerical simulation to the measured static load testing results. Figure 3.10 shows a reasonable correlation between the three-dimensional numerical modelling and the field measurements, especially by the advanced hardening soil model compared with Mohr-Coulomb model.

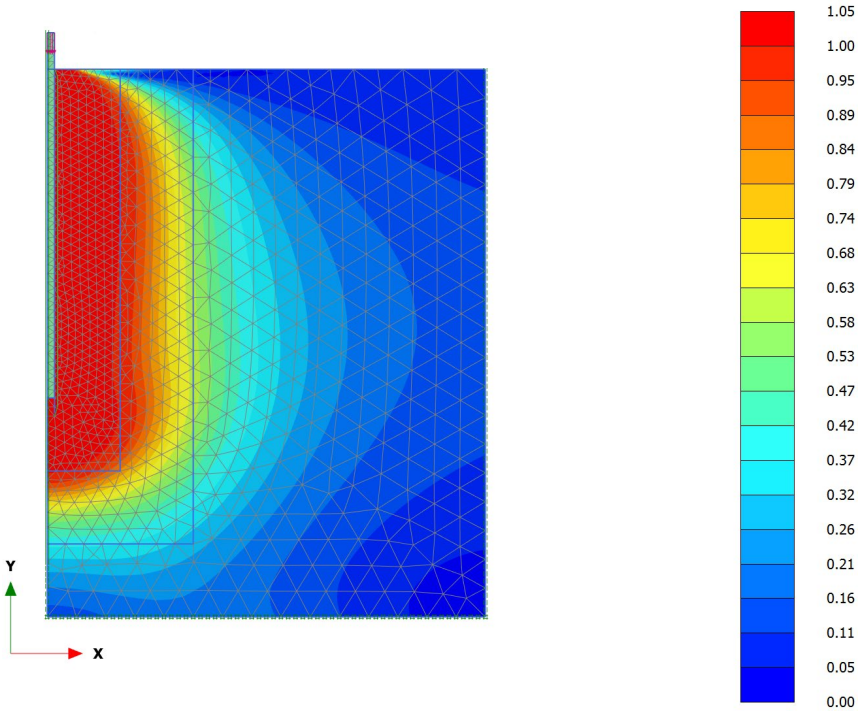

(a)

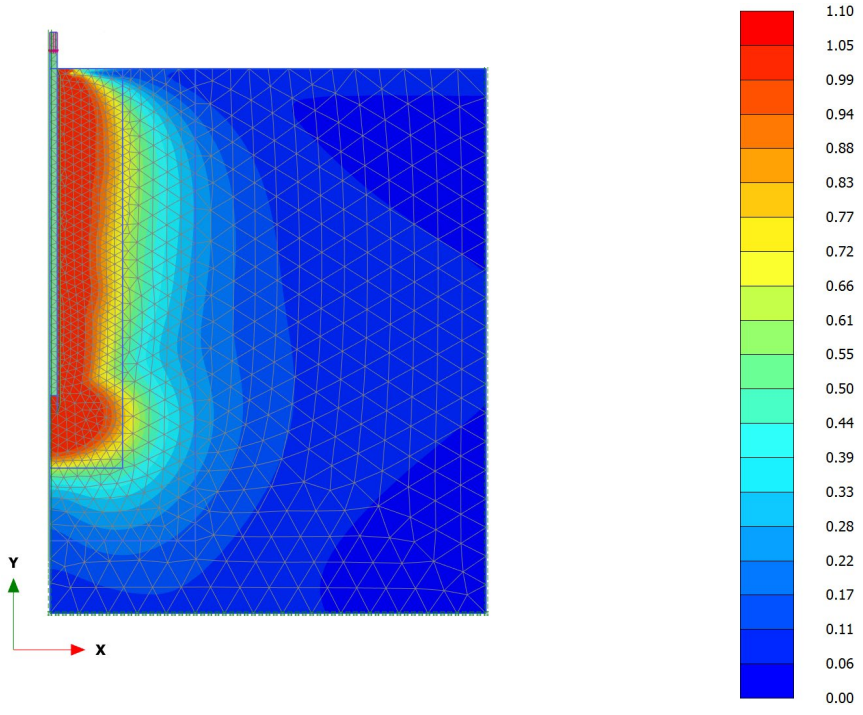

(b)

Figure 3.9 Pile load testing – normalised intergranular strain tensor for (a) dense sand and (b) loose sand

Table 3.4 Adopted soil parameters in the numerical modelling (after Wehnert & Vermeer 2004)

Soil Parameter	Overconsolidated Clay		Concrete Pile (Linear-Elastic Model)
	Mohr-Coulomb Model	Hardening-Soil Model	
E (MPa)	60	-	3.10^4
γ (kN/m^3)	20	20	25
c' (kPa)	20	20	-
φ' (kPa)	22.5	20	-
ν	0.3	-	0.2
E_{50}^{ref} (MPa)	-	45	-
E_{oed}^{ref} (MPa)	-	33	-
E_{ur}^{ref} (MPa)	-	90	-
ν_{ur}	-	0.2	-
R_f	-	0.9	-
m	-	0.5	-
$R_{interface}$	1	1	1

Once the load-displacement curve is established, the engineer can determine the pile's nominal resistance. Using Davisson (1972) approach, explained in Section 2.3.2.1, considering a pile diameter of 1300 mm the offset distance OC would be 14.6 mm (Figure 3.11). Hence, the intersection of CC1 with the load-displacement curve gives the ultimate pile capacity (Q_{ult}), which are summarised in Table 3.5.

The resistances corresponding to the maximum displacement (70 mm) are also summarised in Table 3.5. Although both soil models agree reasonably well with the Davisson capacity, the numerical simulation adopting the hardening soil model predicts the capacity corresponding to the maximum displacement of pile with a greater degree of accuracy compared to Mohr-Coulomb soil model.

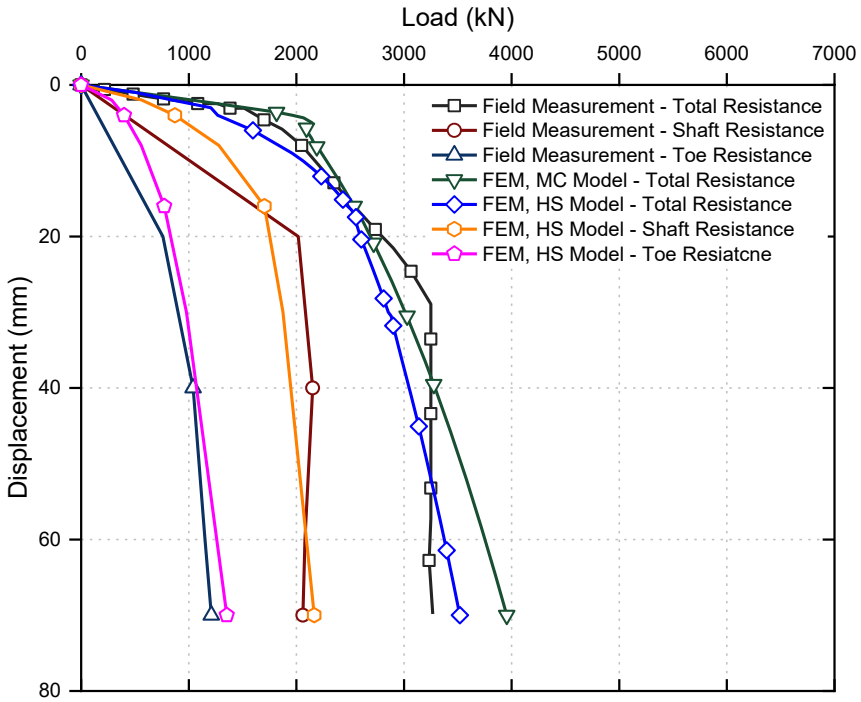

Figure 3.10 Comparison of load-displacement curve of real static load test with simulated test using Mohr-Coulomb and Hardening Soil Models

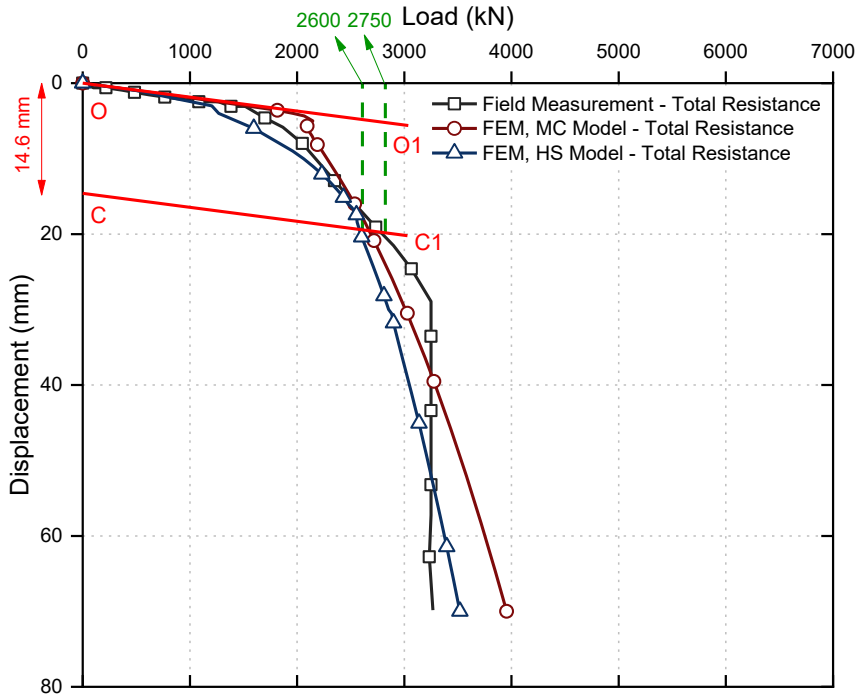

Figure 3.11 Interpretation of load-settlement curve using Davisson method

Table 3.5 Ultimate capacity of the test pile using Davisson method

	Pile Capacity Based on Davisson Method	Pile Capacity Corresponding to the Maximum Displacement
In-situ static load test (kN) (Wehnert & Vermeer 2004)	2750	3270
Current numerical predictions (hardening soil Model) (kN)	2600	3520
Current numerical predictions (Mohr-Coulomb Model) (kN)	2600	3960

In order to assess the effect of reaction piles on settlement of the test pile during the static load testing, the soil-pile system was analysed using a three-dimensional model, employing the hardening soil model with parameters as reported in Table 3.4. The finite element model of the test pile and the reaction piles in three dimensions is shown in Figures 3.12. The plan views of the test pile with two and four reaction piles are shown in Figure 3.13a-b, respectively. During the static load testing when the hydraulic jack applies a compressive force on the test pile, the tensile forces generated by the individual piles are spread in equal portions to the test piles. Herein, the test load was considered as the ultimate bearing capacity of pile (2600 kN), as reported in Table 3.5. Therefore, the reaction pile tensile forces were equal to 1300 kN and 650 kN for the two and four reaction piles systems, respectively.

As explained by Yi (2004), to measure the influence of the reaction system on the settlement of the test pile, a correction factor, F_c, is defined using Equation (3.2):

$$F_c = \frac{s}{s_m} \tag{3.2}$$

where, S represents the settlement, calculated under the ideal test condition (without the influence of the surrounding reaction piles), and S_m is the measured settlement, considering the effect of the reaction piles in the vicinity. Although many parameters related to the soil – pile system can influence the interaction of reaction and test piles, herein only the extent to which the number, length, and diameter of the reaction piles, the type and spacing of reaction piles, such as steel pipe piles with different soil plugging ratio, influencing the results, are studied.

The obtained correction factors (F_c) at different ratios of H/D (H is the centre to centre distance between the test pile and the reaction pile, and D is the diameter of test pile) are depicted in Figure 3.14. It is clear that by increasing the spacing of reaction piles, their effect on the test pile settlement decreases. Moreover, it can be observed that the calculated results correlates reasonably well with ASTM International (2013), which recommends the reaction piles should be at least 6D centre-to-centre spacing (5D clear distance). As can be observed in Figure 3.14, increasing the number of reaction piles has no significant influence on the settlement of test pile, which is about 1.08 for ASTM 6D spacing. The load-displacement curves obtained as the reaction piles move farther away from the test pile (for the case of two reaction piles only) are depicted in Figure 3.15. As the reaction piles move farther away from the test pile, the settlement of the test pile for a given load increases, corresponding to the reduced interaction between piles.

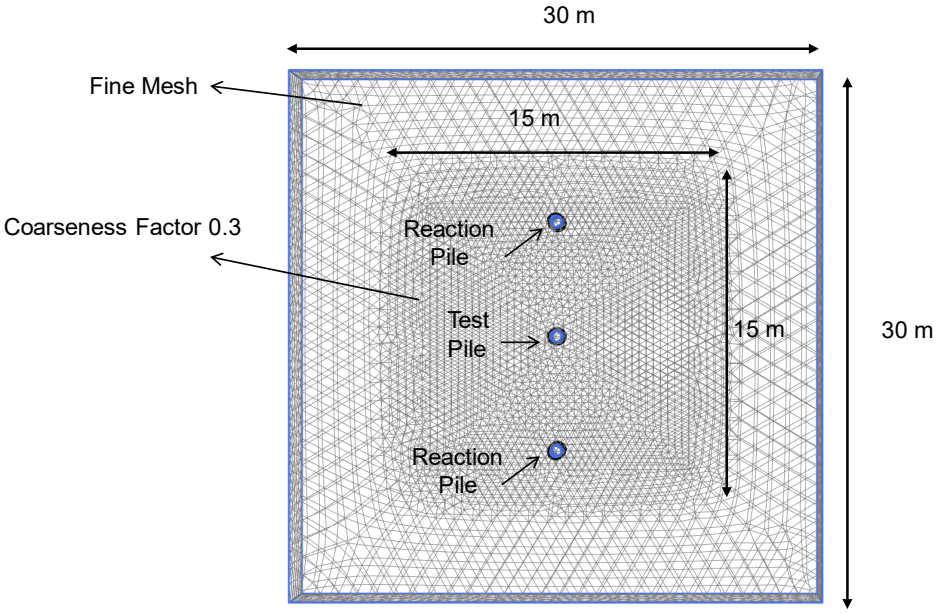

(a)

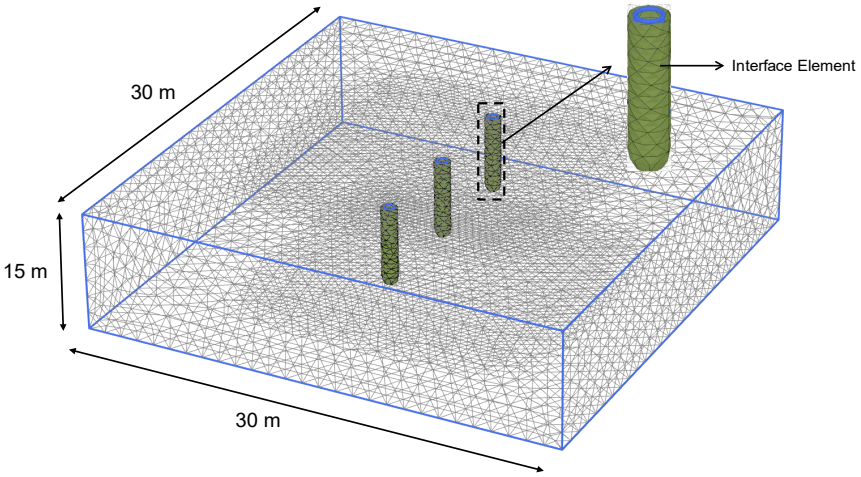

(b)

Figure 3.12 Three-dimensional finite element model used in simulation: (a) plan view (b) three-dimensional view

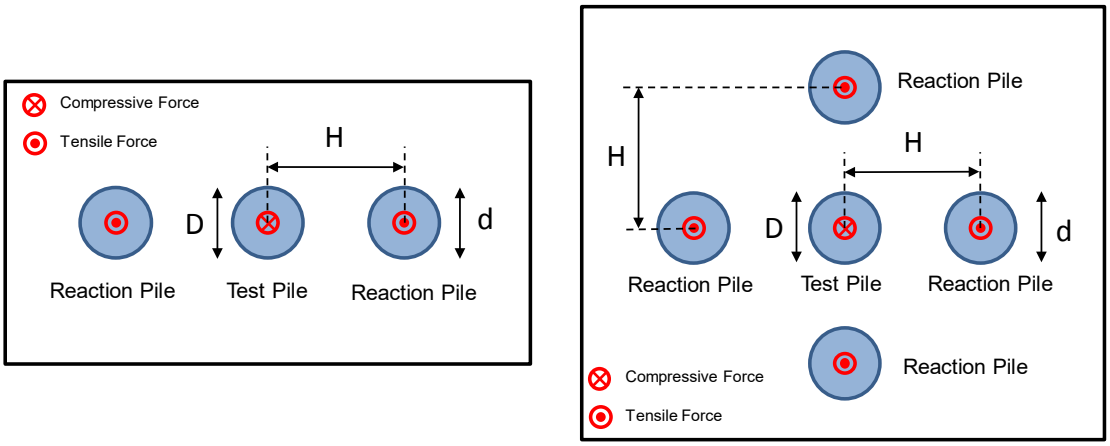

(a) (b)

Figure 3.13 Plan view of a simulated static load test with (a) two reaction piles and (b) four reaction piles

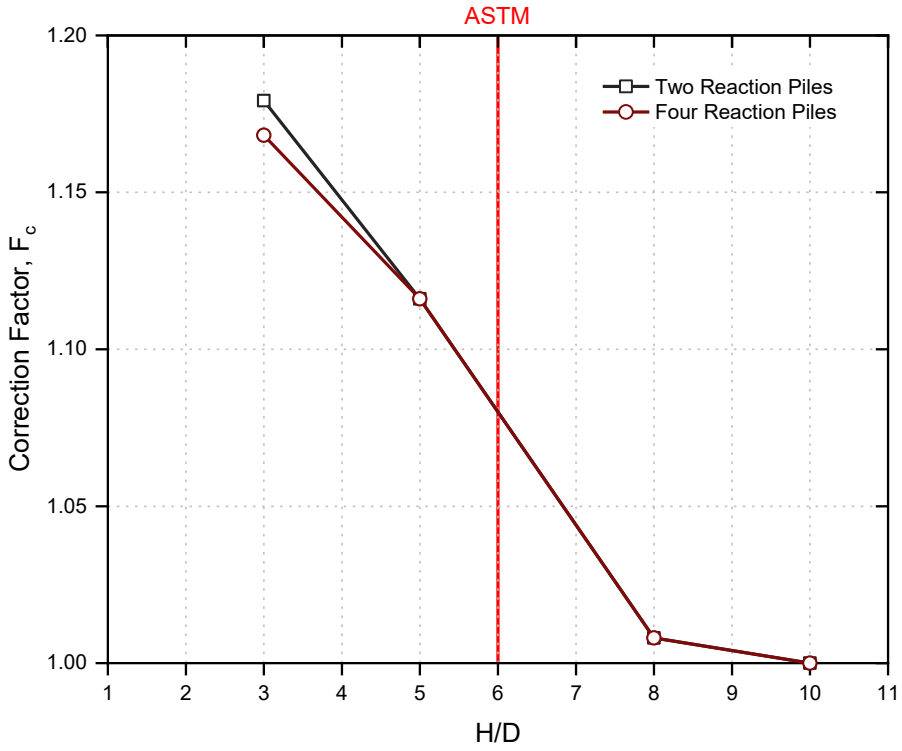

Figure 3.14 Comparison of interaction of two and four reaction piles with the test pile ($D_{test\ pile} = d_{reaction\ pile}$ and $L_{test\ pile} = L_{reaction\ pile}$)

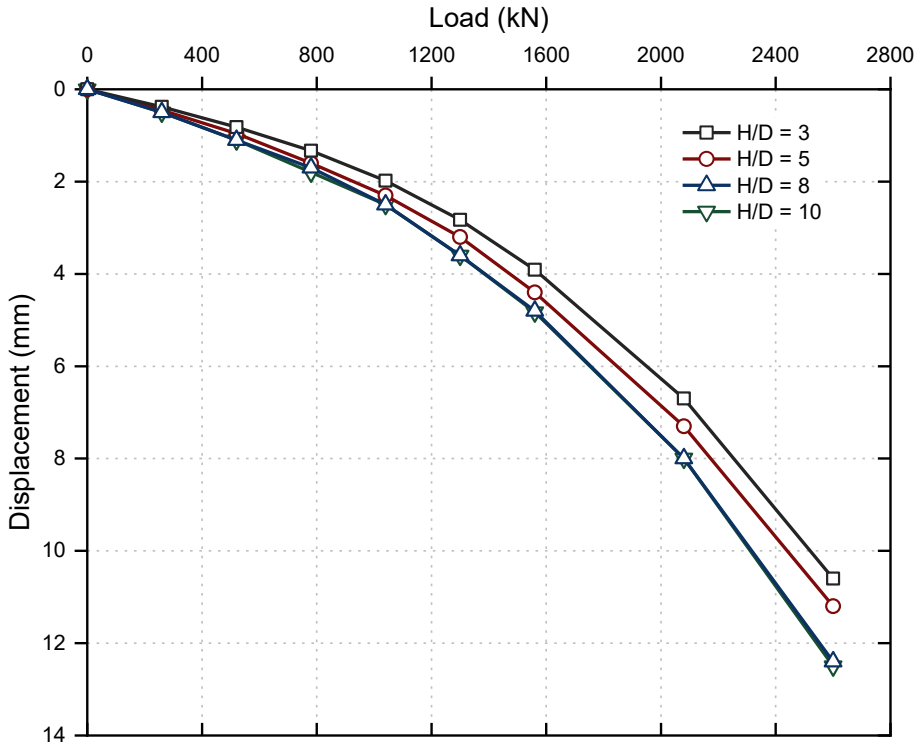

Figure 3.15 Comparison of load-displacement curve of test pile in different distances of reaction piles ($D_{test\ pile}$ = $d_{reaction\ pile}$ and $L_{test\ pile}$ = $L_{reaction\ pile}$)

To evaluate the effect of reaction pile length on the settlement of test pile, various lengths of the reaction piles including 7.5 m, 9.5m, and 11.5 m were tested, while the length of test pile was kept constant at 9.5 m. As can be observed in Figure 3.16, increasing the reaction pile length from 7.5m to 9.5m increases the correction factor (F_c), while further increase in the reaction pile length when the reaction piles are close to the test pile (H/D < 6) contributed to reduction in the interaction effects and therefore F_c. It is worth mentioning that for a given diameter of pile, the extent of interaction between the test pile and the reaction pile very much depends on the deformation of the reaction pile under the applied loads and the soil-pile interaction. Obviously long piles experience less deformation for a give tensile load due to increased shaft friction, while interaction between soil and pile increases. These effects can contribute to the observations, as depicted in Figure 3.16.

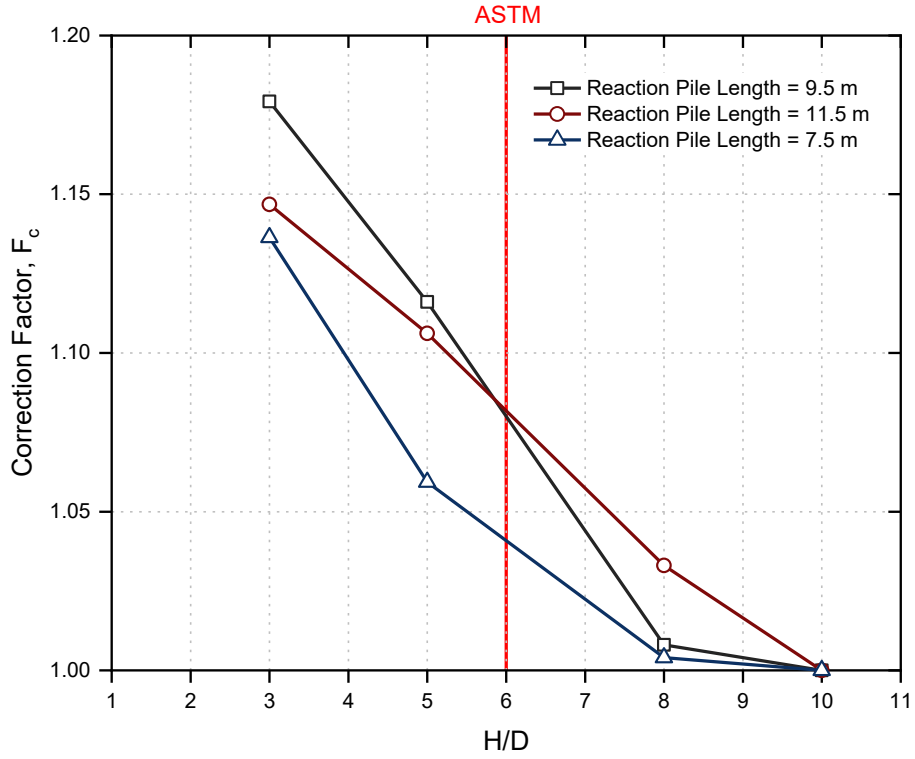

Figure 3.16 Effect of reaction pile length on the test pile with a length of 9.5 m ($D_{test\ pile} = d_{reaction\ pile}$)

To assess the influence of the diameter of the reaction piles (d) on the settlement of the test pile for a given load (i.e. 2600 kN referring to Table 2), the reaction pile diameter is varied from 0.65m to 1.3m. Figure 3.17 indicates that for the model utilised in this study, the effect of reaction pile diameter in the range assessed was insignificant.

To evaluate the effect of reaction piles type on the test pile settlement, the reaction piles were changed to open-ended steel pipe piles while the test pile remained unchanged as the solid concrete pile. For achieving this aim an open ended steel pipe pile with two different conditions, unplugged and partially plugged, were considered as shown in Figure 3.18. In the case of a steel pipe pile with unplugged behaviour, the soil inside the pile was supposed to be at the ground level. For the partially plugged pile, the plugged length inside the pile is assumed to be 2.5 m, as shown in Figure 3.18. Referring to Figure 3.19, it can be inferred that the reaction pile, an open-ended steel pipe pile, exhibits less

interaction with the test pile compared to the solid reaction piles. In addition, the open-ended steel pipe piles with unplugged behaviour indicate less interaction with the test pile in comparison with the partially plugged tubular piles. This is mainly attributed to the higher shaft friction, resulted in lower displacement, as observed in steel pipe piles with unplugged behaviour but not experienced in partially plugged piles.

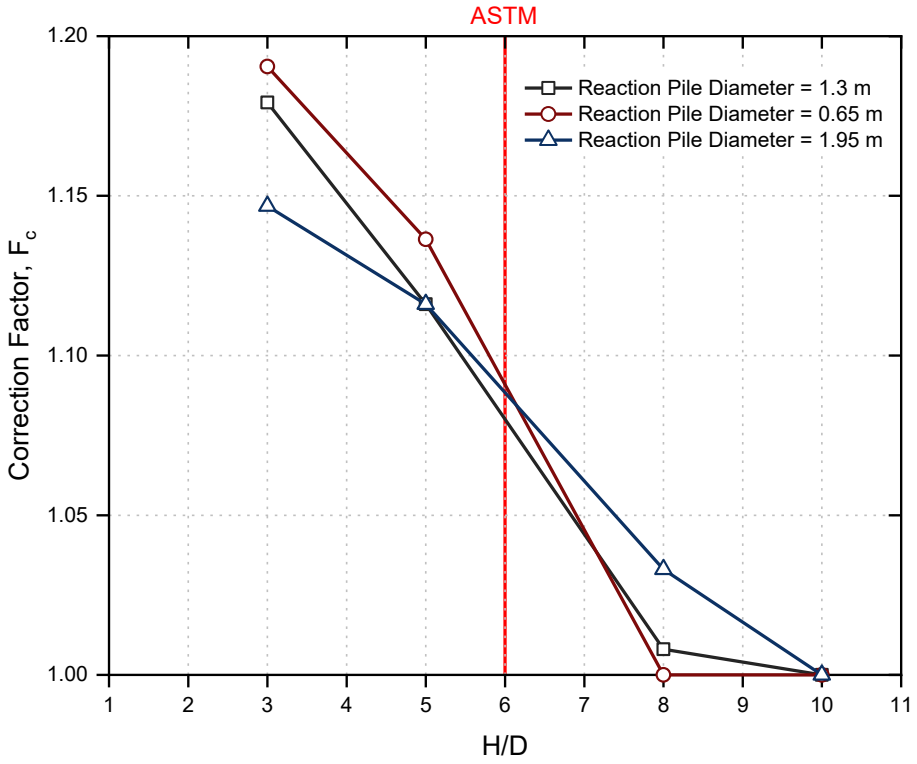

Figure 3.17 Effect of reaction pile diameter on test pile with a diameter of 1.3 m ($L_{test\ pile} = L_{reaction\ pile}$)

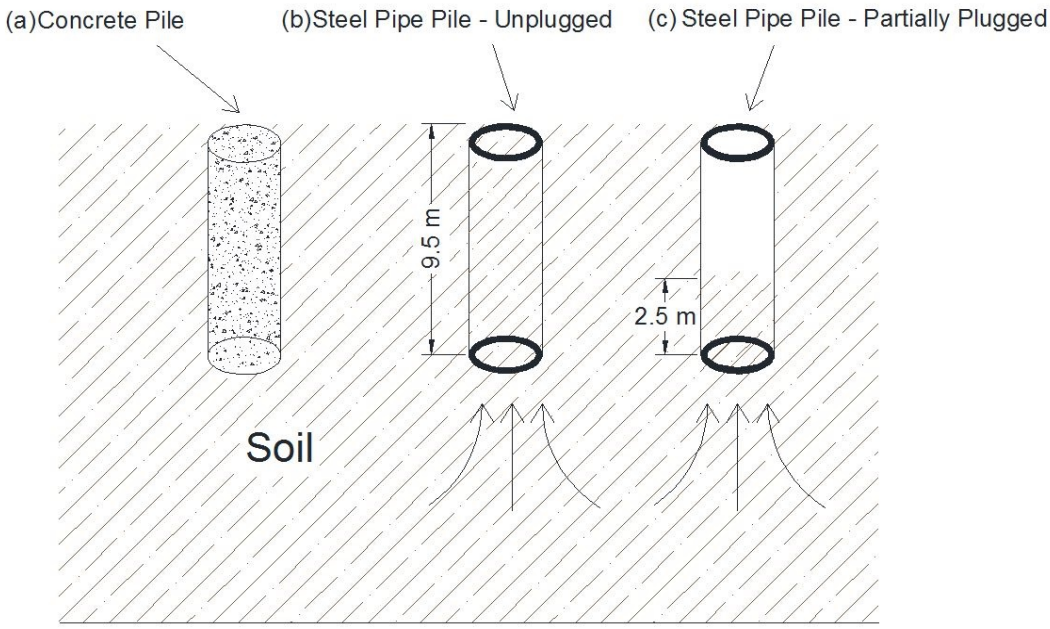

Figure 3.18 Effect of different reaction piles (a) concrete pile, (b) steel pipe pile with fully unplugged behaviour and (c) steel pipe pile with partially plugged behaviour on test pile with a diameter of 1.3 m ($L_{test\ pile} = L_{reaction\ pile}$)

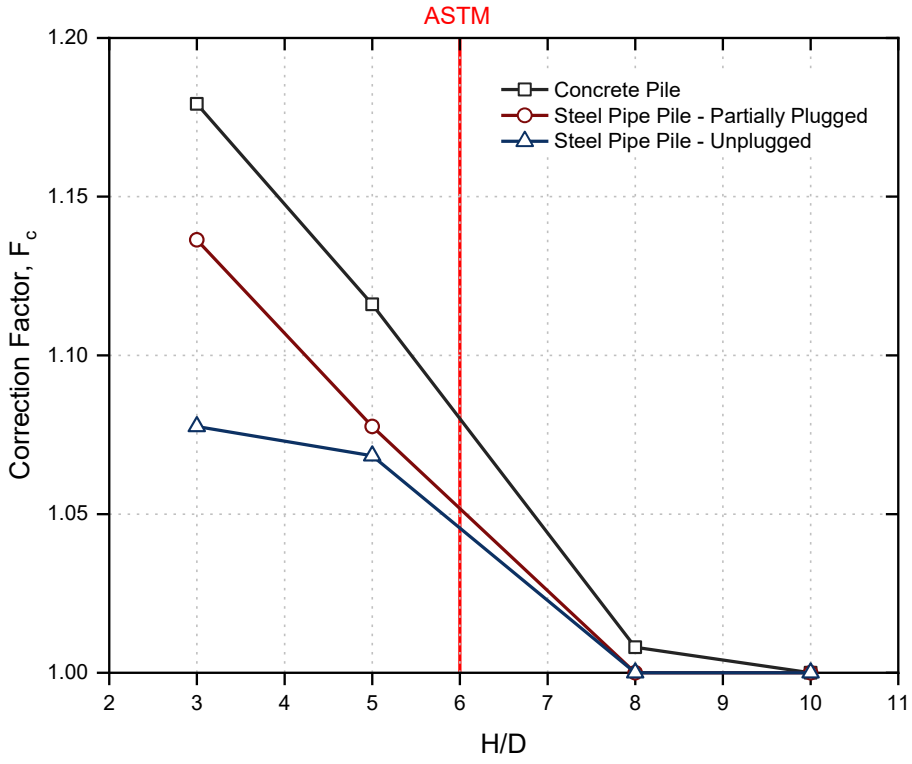

Figure 3.19 Effect of steel pipe pile as the reaction pile on the test pile

3.6 Concrete pile Groups Response Bored in Cemented Sand Deposit

3.6.1 Overview

The behaviour of a single pile under axial loading was evaluated in detail by many researchors (Mayerhof 1976; Vesic 1977; Das 2004). However, the behaviour of pile group is more sophisticated and has not adequately been evaluated or understood (Ismael 2002; Dai et al. 2012). Settlement analyses of pile groups are based on various approaches, including the finite element method and the finite difference method, the boundary element method, and the hybrid load transfer approach. During the last few decades, in spite of some theoretical advances in the analysis of pile group behaviour, the analysis is still based mainly on simplifying the problem or the constitutive behaviour of the soil. Hence, static load testing on group of piles is still known the most reliable tools of evaluating the pile group behaviour under design loads (Dai et al. 2012). Some laboratory and field pile group tests under vertical loads have already been performed and published (Bai et al. 2006; Yetginer, White & Bolton 2006). However, due to the hardness and the cost of full-scale load tests, many small-scale load tests were carried out on the pile groups, irrespective of whether they were carried out in the site or laboratory. Hence, there is an objective need for prediction of the pile group response under static load testing using proper numerical modelling.

In this section, the behaviour of two real case concrete bored pile groups in cemented sand deposit, represented by Ismael (2001), are evaluated using PLAXIS 3D finite element software. During the numerical simulation a combined nonlinear and linear analysis is performed to capture a reasonable correlation with the field measurements. As explained by Ismael (2001), a test site, located in South Surra, Kuwait was selected on flat and cemented sand existing from the ground surface to an extended depth. That

cemented sand is a coastal plain deposit, a non-homogeneous mixture of sand, gravel, silt, clay, and authigenic minerals. At the test site one auger boring was drilled to a depth of 6.5 m and it was found that the soil profile consists of medium dense weakly cemented silty sand layer from the ground surface to a depth of 4.5 m and after that up to the bottom of the borehole there is a very dense silty sand layer with cemented lumps. Groundwater was not observed along the boreholes depth. Some laboratory and in-situ tests were conducted to determine the soil properties of each soil layer. For instance, standard penetration tests (SPTs), dynamic cone penetration tests (CPTs) and pressuremeter tests (PMTs) were performed in the site in the vicinity of the borehole. In addition, the soil strength parameters were determined by drained triaxial compression tests, which show the peak strength parameters c' and φ', 20 kPa and 35° for the upper layer and 0° and 43° for the lower layer, respectively. Figure 3.20 indicates a summary of the soil condition. Detailed information on soil properties, including bulk unit weights, moisture contents, SPT-N values, dynamic CPT results, and pressuremeter modulus can be found Ismael (2001).

In this part, the Menard modulus, E_M, obtained from pressuremeter test, was analysed to acquire a proper elastic modulus to be used in the numerical modelling. According to Fawaz, Hagechehade & Farah (2014), the pressuremeter test was proposed by Louis Menard in 1957, which provides the measurement of stress-strain response of soils and is used to evaluate the expected settlements and the bearing capacity of soil foundations. Using pressuremeter modulus or Menard modulus (E_M) as the elastic modulus of the soil, overestimated footing settlements compared with actual measured settlements. To compensate for this over-prediction of settlements, a correction factor was suggested, which was later designated as the Menard's α factor to predict accurate quasi-elastic

responses of soil masses undergoing loading. In this approach, the pressuremeter modulus (E_M) is empirically related to the elastic modulus of soil (E) as:

$$E = \frac{E_M}{\alpha} \tag{3.3}$$

In which α is termed as the rheological coefficient and has a value between 0 and 1. Generally, this factor for clay is considered to be between 0.55 and 1, while for sand is regarded between 0.25 and 1 (Fawaz, Hagechehade & Farah 2014; Sedran, Failmezger & Drevininkas 2013).

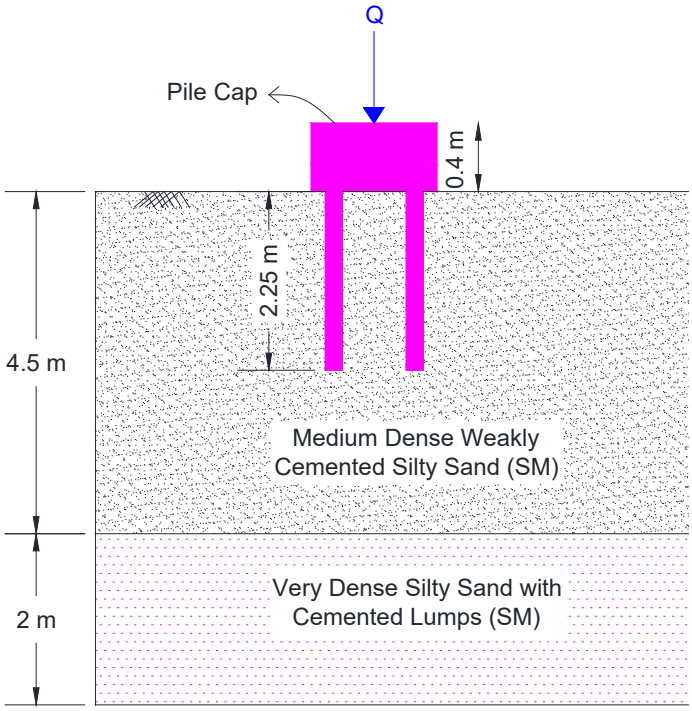

Figure 3.20 Summary of soil condition and cap dimension

Two test pile groups, each comprising five piles with a rigid cap resting on the ground, installed in site and were tested in compression. The piles in “group A” and “group B” were spaced at three and two-pile diameters respectively and the piles in both groups were 0.1 m in diameter and 2.25 m deep. All static load testing were carried out by a reaction beam method in which the reaction piles were installed far enough from the test pile,

minimising the interaction effect of test and the reaction piles. Groups A and B were installed 4 m apart from each other. The piles were installed to a depth of 2.25 m and protruded 0.1 m above the ground surface. Then, a rigid reinforced concrete cap with 0.4 m thickness was poured on the pile groups. Dimensions of pile caps and pile spacing in the groups are shown in Figures 3.21a-b.

The numerical simulation of the pile groups were performed using the finite element PLAXIS 3D software and groups A and B were modelled in two different numerical models with 20 m × 20 m × 6.5 m dimensions. In numerical simulation, the pile cap was modelled using a plate element defined into the program and a linear elastic non-porous and isotropic material model was assigned to the piles and the interface strength reduction factor (R_{int}) was assumed to be equal to 1. Figure 3.22 shows the finite element scheme of the modelled pile group.

In reality, it is well understood that the soil mass stiffness decreases with increasing the strain level. According to Ju (2015) and Gowthaman & Nasvi (2018), for a group of piles, the strain level increases in the vicinity of pile shaft; i.e. where the soil in this thin zone close to the pile shaft is stiffer than between the piles some distance away from the shaft. Hence, to consider this stiffness variation, in simulation of pile group behaviours normally three different types of finite element analyses are performed: (i) a linear elastic analysis (LE) where all soils including the soil adjacent to the pile shaft (Zone A in Figure 3.23) and the soil between the piles (Zone B in Figure 3.23) are supposed to be linear elastic; (ii) a completely nonlinear (CNL) analysis, where both the soil in the vicinity of the pile shaft and the soil between the piles are modelled using the hardening soil (HS) model, and (iii) a combined nonlinear and linear analysis (NL-LE) in which the soil

adjacent to the pile shaft is modelled using the HS model, while the soil in the remaining area is modelled as linear elastic model.

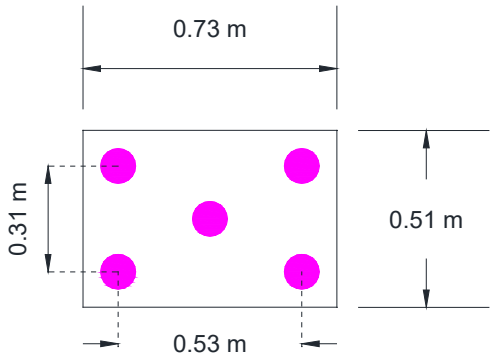

(a)

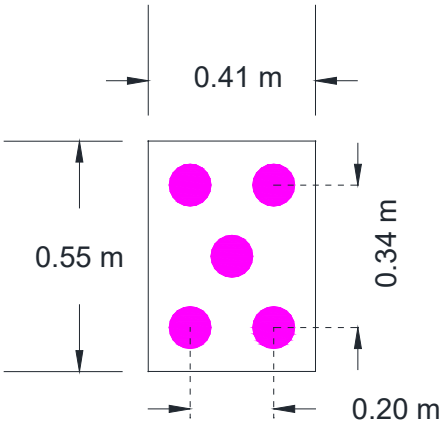

(b)

Figure 3.21 Plan view of (a) Group A and (b) Group B (after Ismael 2001)

In the combined analysis, two different sizes in the adjacent to the pile shaft are selected: a zone extending to a distance (d) which is equal to D/2 from the pile shaft and the other zone extending to a distance (d) which is equal to D/4 (D is the pile diameter). The pile group layout of the combined analysis is shown in Figure 3.23. Model parameters used for linear isotropic elastic model used in cap are the same as concrete piles.

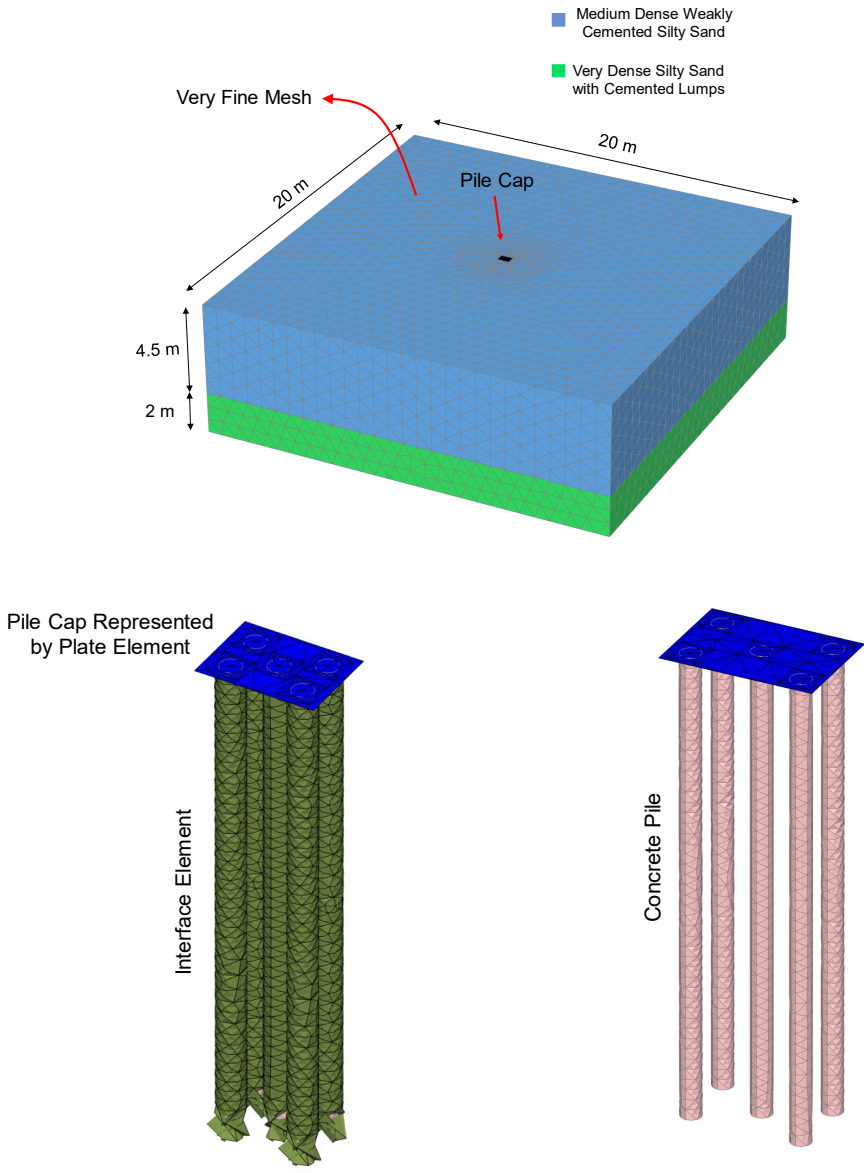

Figure 3.22 Finite element model of pile group and adjacent soil

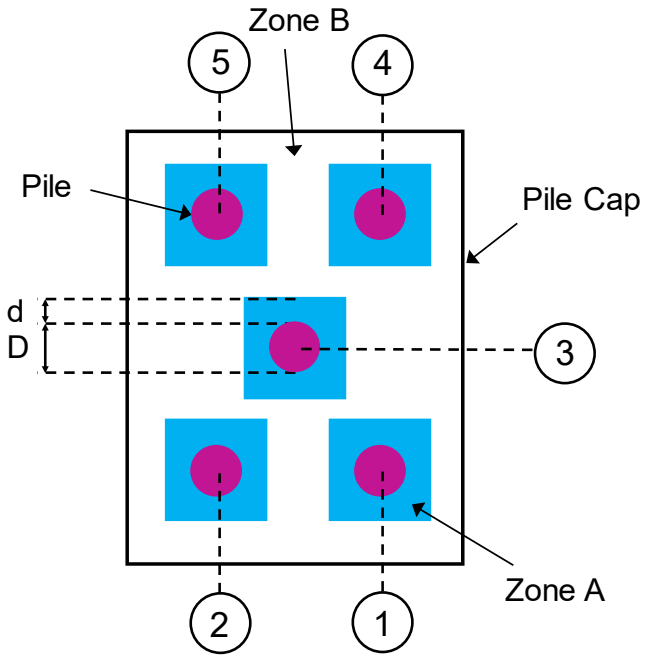

Figure 3.23 Pile group layout for different analyses

3.6.2 Results and Discussion

In numerical simulation procedure, MC model was assigned to the soil around the pile group in all analyses, while LE, HS and LE-HS models were assigned to the soil around the pile shaft and between the piles. The load-settlement curves measured in site for pile groups A and B are shown in Figures 3.24a-b, respectively. In order to predict the load-settlement curve in each pile group, three types of analyses as mentioned earlier (LE, CNL, and NL-LE) were performed.

Referring to Figure 3.24a, the completely non-linear (CNL) analysis (HS model) of pile group A causes an over-prediction of group settlement (or under-estimation of soil stiffness); thus, in the maximum applied load (1078 kN) the numerical analysis indicates a group settlement of 22 mm, which is 38% higher than the measured settlement in site.

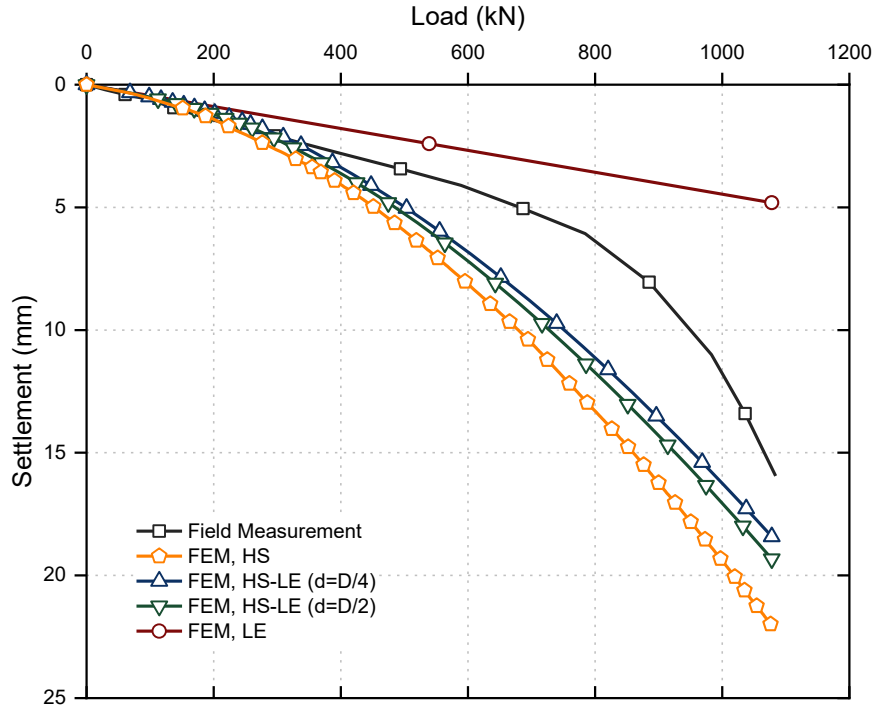

(a)

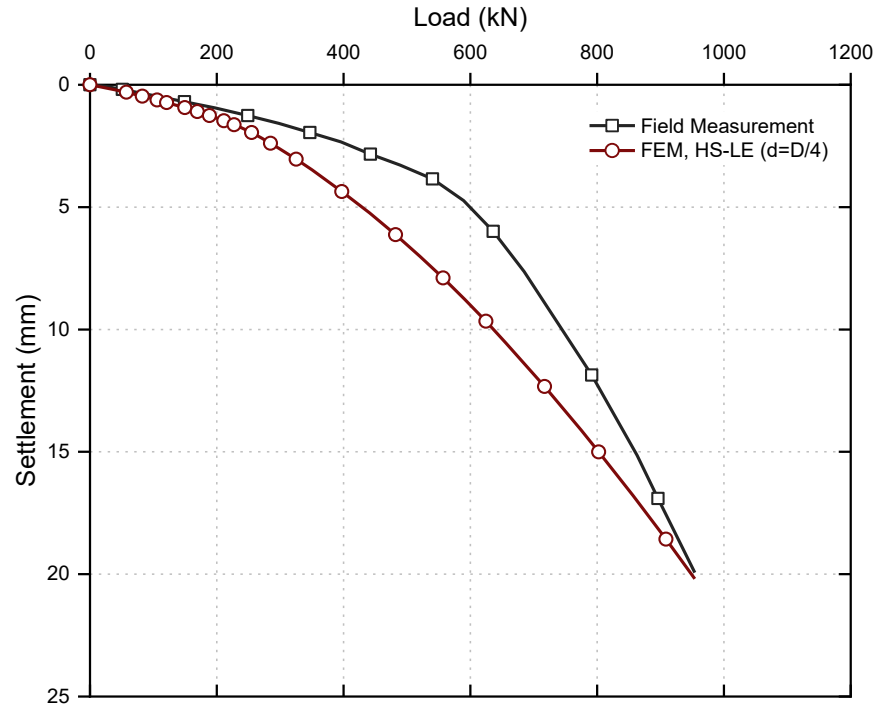

(b)

Figure 3.24 (a) measured and predicted load-displacement curves for Group A (b) Group B

At the same time, the linear elastic (LE) analysis (LE model) under-predicts the group settlement drastically, since this model ignores the soil nonlinearity and influences from the group response. Hence, this analysis is not appropriate when soil nonlinearity affects the interaction. Although HS model is known as a model that can capture the actual nonlinear behaviour of soil compared to MC and LE models, accounting for the stiffness variation that exists inside the pile group a combined analysis (NL-LE) seems necessary to be employed. As mentioned above, in the narrow zone adjacent to the pile shaft stiffness of the soil is less than that in the space between the piles far from the pile skin. Therefore, HS model is assigned to Zone A with two different distances from the pile shaft (d=D/2 and d=D/4), while the remaining soil inside the group area is assigned the LE model. As shown in Figure 3.24a, the combined analysis (HS-LE models) indicates more precise prediction when the thickness of Zone A is assumed to be equal to a half of pile diameter (d=D/2). In this case, the predicted load-settlement curve shows a better correlation with the measured curve and the maximum predicted settlement decreased approximately by 18% compared to the recorded settlement during completely nonlinear analysis. In the next stage, the thickness of Zone A decreased to D/4 and a slight improvement (around 5%) was observed in the load-settlement curve compared to the previous stage (d=D/2). The obtained results proves that by assigning HS model to Zone A (d=D/2) while the remaining area (Zone B) is assigned LE model, it is possible the mechanism of the pile group can be captured properly. However, because by decreasing the Zone A dimensions to D/4 from the pile shaft a better correlation was observed between the measured and the predicted load-settlement curves; hence, this distance was considered as a suitable distance for analysis. Considering this distance, the behaviour of pile group B was evaluated under working load up to 954 kN. From Figure 3.24b, it is crystal clear that the predicted load-settlement, considering Zone A to the distance D/4,

shows a reasonable correlation with the measured curve. Therefore, both curves indicate a settlement of 20 mm at the maximum applied force.

The predicted and the measured axial load distribution along the central pile of group A are compared in Figure 3.25. As shown in Figure 3.25, both curves show the same trend and the axial force along the pile length decreases, which indicates the load transfer from the pile shaft to the soil. It should be noted that both predicted and measured axial force distributions in the respected pile in site were recorded in various depths (0.2, 0.9 and 2.2 m) under the load portion of the central pile from the measured group failure load ($^{902}/_{5} \approx 180\ kN$). As illustrated in Figure 3.25, at the end of the test, the measured pile head load for the central pile in pile group A is 180 kN while the pile base load is 38 kN (corresponding to 20% of pile head load) which proves that the mobilised capacity under the respected loading is mainly due to the skin friction.

Figure 3.27 compares the load-settlement curve for the average load-settlement curves for the pile group B and the single pile. As demonstrated in Figure 3.26, a reasonable correlation between the measured and the predicted averaged load-settlement can be observed. For plotting the average load-settlement curve in the numerical model, the settlement of every single pile in the group was not captured separately because the pile cap was regarded rigid enough, therefore all piles can be supposed to have almost the same settlement. Based on this assumption, the recorded force over each single pile head (due to the working load applied over the group cap) can be averaged and drawn respect to the recorded settlement of the pile group in each load increment (190, 381, 572, 763, 954 kN). Figure 3.26 reveals that both the average measured and predicted curves show a greater settlement than the settlement of single piles under lower loads (initial elastic

range), while at larger loads, this trend is reversed because single piles response the approaches failure at smaller loads.

Since prediction of pile group B behaviour showed a reasonable correlation with the measured data in site, hence in this section the behaviour of group B under axial static load testing is further analysed. Since usually settlement considerations are known as the most dominant aspect of designing pile groups in sand; the group settlement ratio (R_s) will be a very important factor in specifying the settlement of the pile group at the working loads if the settlement of the single pile is known (Ismael 2001; Dai et al. 2012). According to Poulos & Davis (1980), the group settlement ratio (R_s) is characterised as the ratio of a pile group settlement (S_g) to the single pile settlement (S) at the same average load per pile. Figure 3.27 indicates this ratio versus various group settlement levels. It can be observed that at the beginning, the predicted group settlement ratio increases up to 3.4 and then decreases continuously when the settlement increases and reaches to less than 0.5. The overall trend, observed in Figure 3.27, seems reasonable because, as explained in Figure 3.26, at relatively small loads a single pile experiences lower settlement than the average group settlement; however, in higher loads this trend is reversed.

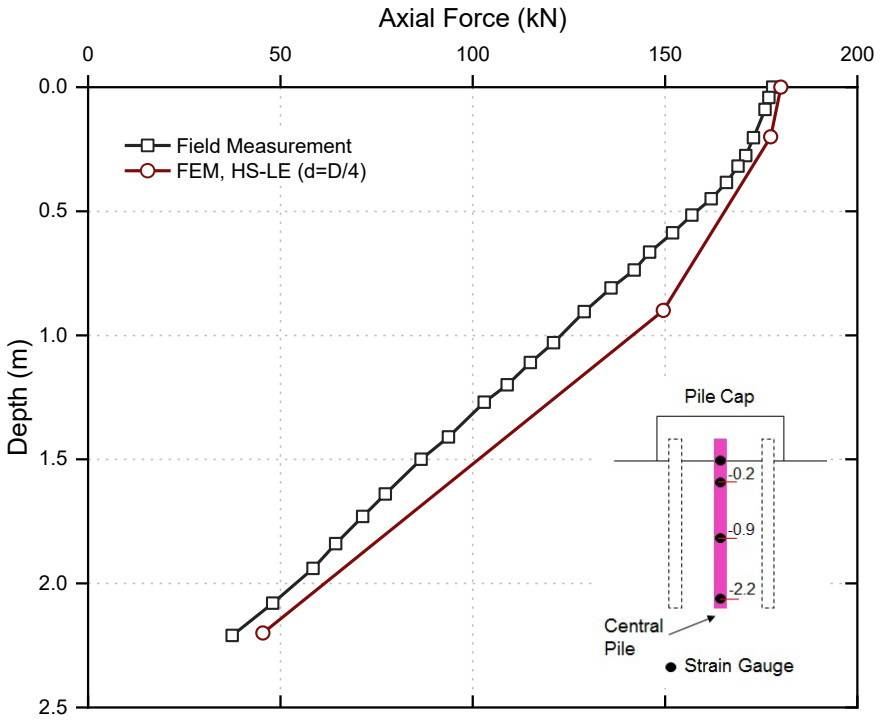

Figure 3.25 Comparison of measured and predicted axial load distribution along the central pile in Group A

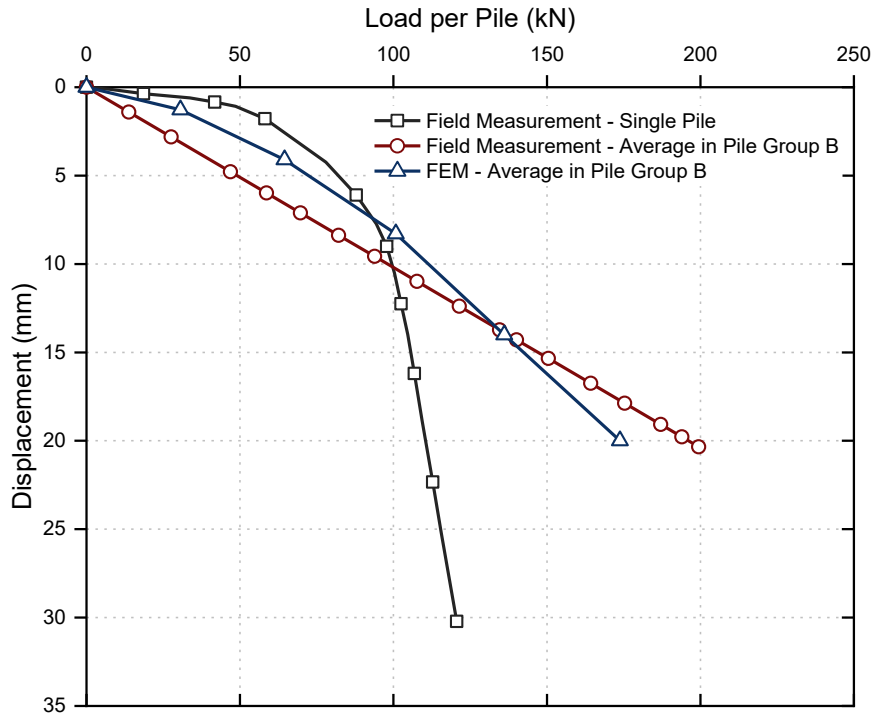

Figure 3.26 Predicted and averaged load – displacement of pile group B versus the single pile

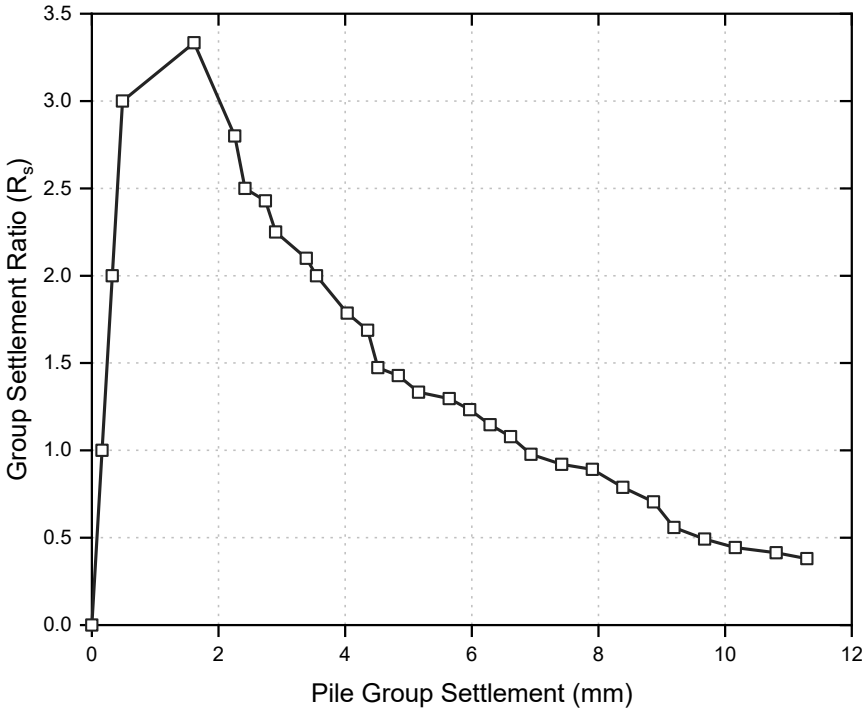

Figure 3.27 Group settlement ratio versus pile group settlement

The pile group layout is displayed in Figure 3.23 in which each pile has a specified number. Pile No. 3 represents the central pile in group B. The variations of top load (T_i) and base load (B_i) (i indicates the pile number) of this pile due to working load applied over the group cap in five different load increments (190, 381, 572, 763, and 954 kN) as shown in Figure 3.28. As can be seen in Figure 3.28, the corner piles (NO. 1, 2, 4 and 5) have larger loads (the pile head and base loads) compared to the central pile (NO. 3). This finding correlates very well with Dai et al. (2012). This result confirms the elasticity concept that if a pile cap is considered flexible, hence the loads applied on all piles are the same, and it is expected that the centre pile to undergo the largest settlement, proving that this pile has the lowest stiffness. However, since the same settlement is considered for all piles; therefore, it is presumed that the centre pile to carry the smallest load as indicated in Figure 3.28. For instance, the pile head force predicted in pile NO. 4 (one of the corner piles) is 18% higher than the central pile, while for the base load, this difference increases to 26%. Figure 3.29 illustrates the ratio of the individual pile head load to the

average individual head load in the group (Q_i/Q_{ave}) versus the average individual head load (Q_{ave}). It is clear that this ratio for piles NO. 2 and No. 4 fluctuates between 1 and 1.2, while for piles NO. 1 and No. 5 are changing around 1. For the central pile (NO. 3) this ratio is less than 1 (around 0.9), which confirms a lower stiffness and a lower load portion of this pile compared with the corner piles. Figure 3.30 depicts each individual pile displacements versus applied loads. Referring to Figure 3.30, it can be inferred that at the same load, pile NO. 3 indicates the largest settlement. On the other hand, at the same settlement, corner piles mobilise higher resistance. For example, based on the $Q_{10\%}$ approach (load corresponding to the displacement equal to the 10% of pile diameter) the bearing capacity of pile NO. 4 (117 kN) is estimated to be 17% higher than the capacity of pile NO. 3 (100 kN).

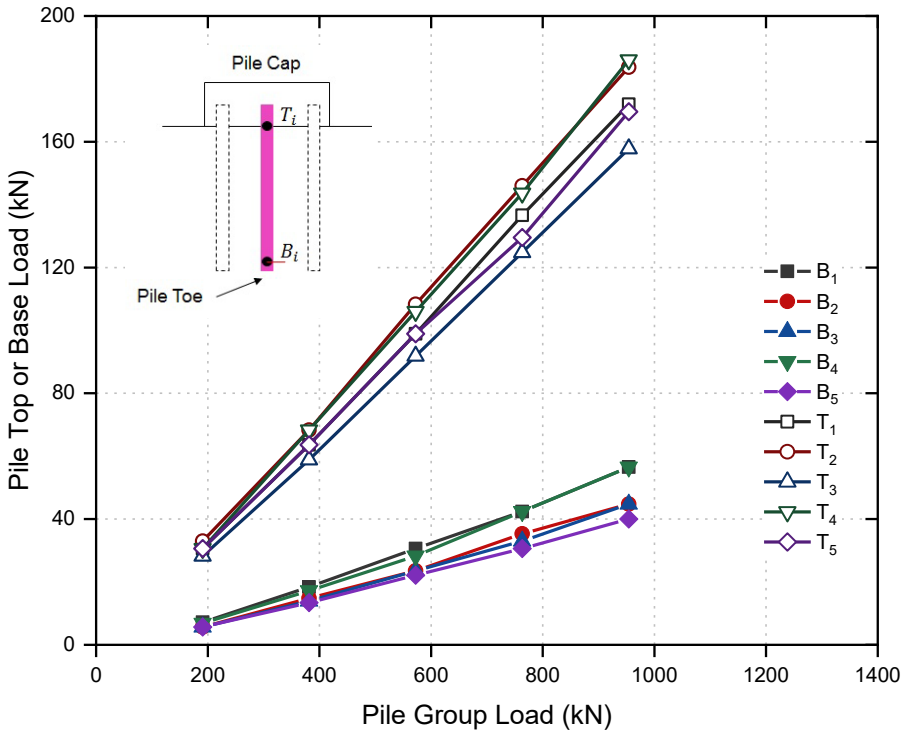

Figure 3.28 Top (T_i) and base (B_i) load in central pile in pile group

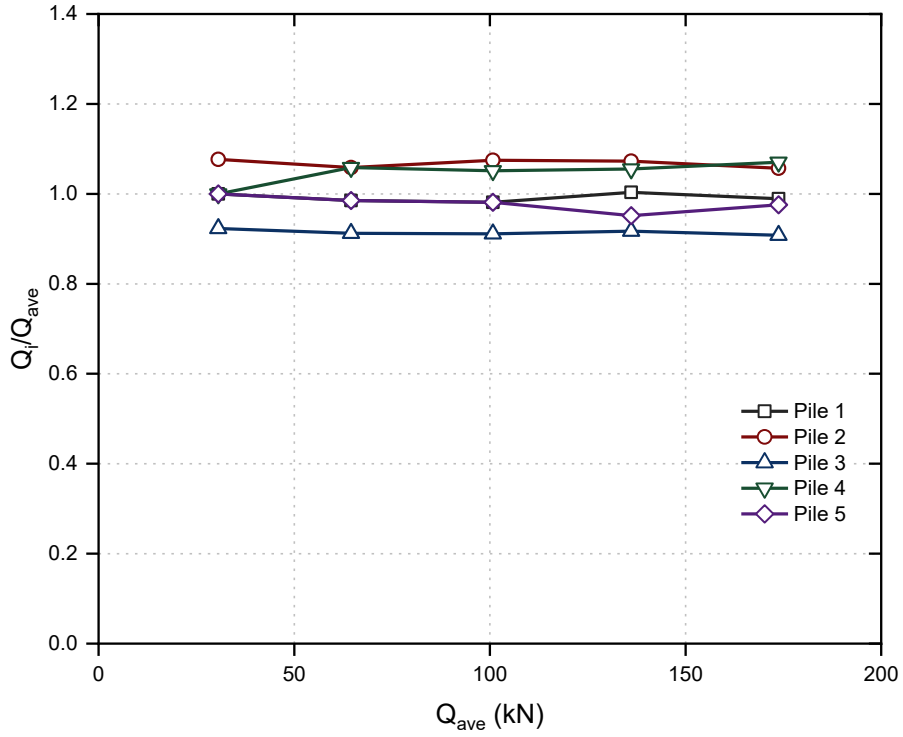

Figure 3.29 Ratio of the individual pile load to the average individual load

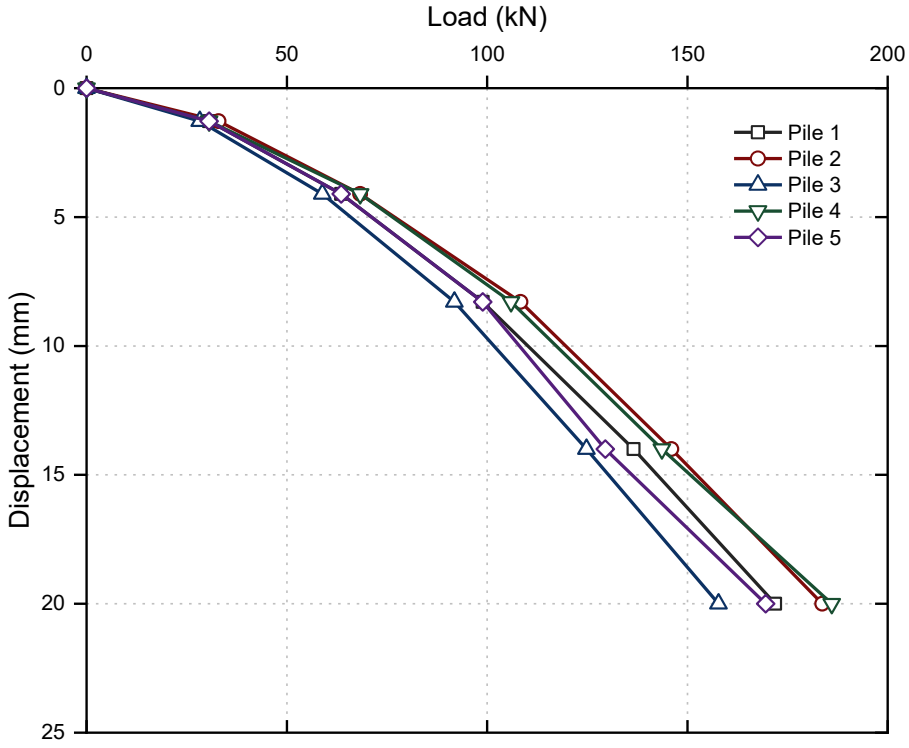

Figure 3.30 Individual pile load-displacement curve for pile group B

3.7 Summary

This chapter describes the principals of numerical modelling of static pile load testing as the most fundamental form of pile load testing and a benchmark for pile performance assessment. During the numerical simulation the influence of the different soil models on the pile performance was evaluated to capture a reasonable correlation with the measured data in the field. For achieving this aim, a variety of different soil models including Mohr-Coulomb, hardening soil, and hypoplastic with incorporating of intergranular strain (IGS) parameters were evaluated to investigate the soil non-linearity observed during the static pile load testing. A comprehensive parametric study was conducted on the hypoplastic soil model parameters to assess how different parameters affect the load-displacement curve obtained during the pile load testing simulation. It was found that among different parameters, the granular hardness (h_s) , the critical friction angle (φ_c) and the exponent relating to the sensitivity of granular skeleton to change of pressure (n) are the most sensitive factors on the load-displacement curve. In addition, it was shown that by activating the intergranular strain concept of the hypoplastic model, the load-displacement curve is considerably overestimated.

Furthermore, the effect of interaction of reaction piles on the test pile during static load testing with anchor piles was evaluated, adopting the hardening soil model during the numerical simulation. This model can properly consider the stress path and its effect on the soil stiffness and behaviour. The numerical modelling predictions provide further evidence for the suitability of ASTM International (2013) recommendations for the minimum distance between the reaction piles and the test piles to avoid the interaction effects. Based on the numerical predictions, it can be concluded that when the reaction piles are positioned 5D clear from the test pile, the interaction effects result in an F_c

correction factor of about 1.08. Finally, the axial behaviour of concrete bored piles under static load testing, using the three-dimensional numerical simulation was examined. From the findings of this section it was concluded that a combined analysis of linear and nonlinear (LE-NL) i.e. a nonlinear narrow zone of soil adjacent to the pile shaft and a linear elastic soil away from this zone, can produce a more reliable prediction of the group pile settlement compared to a completely nonlinear analysis. In addition, during the numerical simulation it was proved that due to the lower stiffness of the central pile, this pile can support a lower load portion compared to the corner piles. Using the conventional definition of the ultimate load capacity, defined as the load corresponding to the settlement of 10% of the pile diameter, the bearing capacity of one of the corner piles estimated 17% higher than the central pile.

CHAPTER 4 CASE Method and One-Dimensional Wave Propagation Induced by Dynamic Pile Load Testing: Theory, Concept, and Application in a Real Case Project

4.1 Synopsis

During the dynamic load testing, two to four strain gauges and accelerometers are mounted in the opposite sides of the pile at a specified location typically one to two pile's diameter below the pile's top. Capturing and processing field data are made with special equipment such as the pile driving analyser (PDA) system, according to the CASE method. The CASE method is a numerical approach, developed from the principals of wave mechanics, used in pile driving analyser to specify the static soil resistance. This chapter describes the principals behind the CASE method and the one-dimensional wave propagation concepts, which are useful in the interpretation and deep understanding of dynamic pile load testing results. In addition, by developing a code in MATLAB software a real case project introduced in the literature is evaluated in terms of four important parameters computed and displayed by the pile driving analyser, including the total soil resistance (RTL), the maximum static soil resistance (RMX), the maximum compressive stress (CSX) and the maximum transferred energy to the pile (EMX). The predicted and computed results are compared to each other in two conditions, namely at the end of driving (EOD) and at the beginning of restrike (BOR). It is observed that by changing the CASE damping factor from 0.7 to 1, the maximum static soil resistance can change

up to 45%. However, as time progresses and dissipation of pore water pressures occurs the sensitivity of predictions to damping decreases.

4.2 Introduction

Driving formulas for over 100 years have been used by foundation engineers to estimate the pile bearing capacity and the required blow counts during driving to obtain capacity. However, those formulas have been criticised for not yielding precise predictions of the actual pile capacity. In addition, they cannot appropriately predict the stresses in piles during driving. However, they are still applied in practice because of their simplicity, particularly for practicing engineers. Furthermore, by increasing pile design loads, conducting static load tests is becoming difficult and costly, hence some dynamic equipment for the capacity prediction are required. Wave analysis has overcome many drawbacks and limitations of dynamic formulas through realistically simulation of pile driving process and the hammer impacts. Accordingly, the results can be used to predict the load capacity of piles. As explained by Christophe (2014), wave analysis can be carried out by different methods including direct or indirect methods. In direct methods, for live on-site analysis during pile driving and dynamic pile load testing, empirical constants are assumed in the calculations to derive the bearing capacity. CASE method is known as the most commonly used direct method, which is utilised in pile driving analyser (PDA) to calculate the pile bearing capacity, compressive and tensile stresses in piles during dynamic pile load testing. However, programs such as CAPWAP, which use indirect methods for determining the pile capacity, are based on Smith (1960) method.

As pointed out by Gravare et al. (1980), research was conducted in 1965 at Case Western Reserve University in Cleveland, Ohio, to develop a method using electronic

measurements captured during pile driving to estimate pile bearing capacity. One of the most commonly used devices is pile driving analyser (PDA) which utilises the strains and accelerations at the top of pile, to predict pile bearing capacity using CASE method. The CASE method is a numerical technique based on wave propagation principals used in the PDA to specify the static pile resistance. This method comprises some assumptions including uniform cross section and linear elastic pile under the axial load which installed in a perfectly plastic soil. In the CASE method, the total soil resistance consisting of the velocity-dependent (dynamic) and the static soil resistance values, is assumed to be concentrated at the pile toe. In this method, there is no distinction between the shaft and the toe resistances.

In this chapter, firstly, the main principals behind CASE method and one-dimensional wave propagation are briefly discussed. Then by developing a code in MATLAB software, this method is evaluated and the results are compared with a real case project introduced in literature. Using the written code the effect of damping factor variation on the maximum predicted static soil resistance is also discussed.

4.3 Background

In this section the main principals which are used in the interpretation of dynamic pile load test results (as explained by Rausche, Goble & Likins 1985, Makredes & Likins 1982, Ng et al. 2011, and Christophe 2014) are summarised and some detailed discussion to clarify these concepts are also presented.

4.3.1 Total and Static Soil Resistance

For a pile under an impact load, the total static and dynamic soil resistance can be written as a function of the time, t^*:

$$R(t^*) = \frac{1}{2}\left[F_m(t^*) + F_m(t^* + \frac{2L}{c})\right] + \frac{EA}{2c}\left[v_m(t^*) - v_m(t^* + \frac{2L}{c})\right] \quad (4.1)$$

Assuming a uniform pile is considered:

$$\frac{EA}{c} = \frac{Mc}{L} \quad (4.2)$$

Then

$$R(t^*) = \frac{1}{2}\left[F_m(t^*) + F_m(t^* + \frac{2L}{c})\right] + \frac{Mc}{2L}\left[v_m(t^*) - v_m(t^* + \frac{2L}{c})\right] \quad (4.3)$$

where,
$F_m(t^*)$ = measured force at the gauge location (kN)
$v_m(t^*)$ = measured velocity at the gauge location (m/s)
t^* = time corresponding to measured force and velocity (any time) (s)
M = the total mass of a pile (kg)
L = length of pile (m)
c = wave propagation speed (m/s)
E= elastic modulus of pile (kPa)
A= cross section of pile (m^2)

It is observed that the resistance computation comprises the average of two forces and accelerations (multiplied by the pile mass) at a time interval of $\frac{2L}{c}$ apart. This formula is simplified to Newton's Second Law as the interval $\frac{2L}{c}$ approaches zero. In fact, Newton's second law is based on the collision of two concentrated rigid masses while in pile driving although the hammer is known as a concentrated mass, the pile is considered as a longitudinally-distributed mass. Hence, during pile driving, the rigid body motion assumption is not reasonable and motion is dominated by stress-wave effects.

Equation (4.1) is inferred based on the principal that the velocity at the pile head, for a free-ended pile with finite length is given:

$$v_T(t) = \frac{c}{EA}[F_T(t) + 2F_T\left(t - \frac{2L}{c}\right) + 2F_T\left(t - \frac{4L}{c}\right) + \cdots] \qquad (\text{for } t \geq \frac{2L}{c}) \qquad (4.4)$$

If a pile with a length of L is completely free (without any resistance), after generating the compressive stress wave at the pile head, the induced wave travels down the pile and will arrive at the pile toe at time $t = \frac{L}{c}$. For a free-ended pile a tensile stress wave with identical magnitude is reflected back toward the pile head. During reflection the velocities in the two waves superimpose, leading to the pile toe velocity to double. Figure 4.1 shows this relationship for a step function applied to the pile head force, F_{Ta}, remaining constant with time.

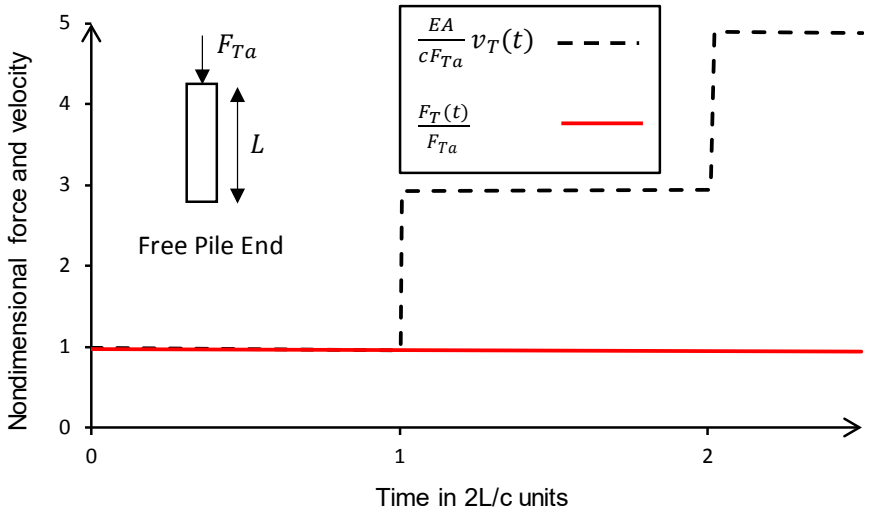

Figure 4.1 Free pile top force and velocity under action of suddenly applied constant force (after Rausche, Goble & Likins 1985)

Resistance forces which act on some intermediate locations along the pile cause a more complicated wave propagation behaviour. For instance, the influence of an upward force applied along a free-ended pile shaft at a location with a distance of x from the pile head is considered. The action of such a force will generate two stress waves in the pile, one compressive wave travelling upward and one tensile wave travelling downward. For reasons of continuity and equilibrium, together with the proportionality requirement

between force and velocity, the forces in each wave must have a magnitude that is one half of the applied force. Each of these waves have the same particle velocities:

$$v_R(t) = \frac{1}{2}\frac{c}{EA}R(t) \tag{4.5}$$

where,
$v_R(t)$ = the particle velocities of each of the generated waves due to the resistance
$R(t)$ = the acting force (resistance force) at a specified location

If it is assumed that acting forces (resistance forces) are applied at n locations, x_i, i=1, 2, …, n (x is distance from the pile head) with magnitude R_i, then:

$$R_i(t) = R_i H(t - \frac{x_i}{c}) \tag{4.6}$$

where, $H(t-a)$ is the Heaviside step function, which is one for $t \geq a$ and zero for $t < a$. If the impact time is considered as the time corresponding to $t = 0$, this resistance law indicates that the resistance forces mobilise only after the induced compressive wave has reached their corresponding locations and that they are constant thereafter.

After generation of upward and downward travelling stress waves induced by $R_i(t)$, the effects of these two waves are felt at the pile head with a delay of x_i/c and $(2L - x_i)/c$ respectively. Therefore, the first influence of the downward travelling wave is felt with the toe reflection due to impact wave at the pile head. For all times, one can write the top velocity due to the upward travelling velocity caused by $R_i(t)$ as:

$$v_T^u(t) = -\frac{c}{EA}R_i\left[H\left(t - \frac{2x_i}{c}\right) + H\left(t - \frac{2x_i+2L}{c}\right) + H\left(t - \frac{2x_i+4L}{c}\right) + \cdots\right] \tag{4.7}$$

$v_T^u(t)$ = pile top velocity due to the upward travelling wave caused by soil resistance. (the upward velocity is assumed to be negative).

Equation (4.7) indicates that if $\frac{2x_i}{c} < t < \frac{2x_i+2L}{c}$, the first Heaveside function will be equal to one, and the upward velocity at the top of the pile will be equal to $-\frac{c}{EA} R_i$. This fact is illustrated in Figure 4.2. Actually, the pile top velocity when either of the two waves (compressive or tensile wave due to soil resistance) arrives and reflects will be twice the magnitude of that in Equation (4.5). It means that when for instance the upward compressive wave reaches to the top of the pile (free head) it reflects as a tensile wave. A compressive wave is defined as a wave in which the movement and velocity directions are the same, while in a tensile wave, the movement and the velocity are in opposite directions. Hence, after reflection of waves at the free head of pile, velocities at top of the pile are superimposed (as shown in Figure 4.2) and the velocity is twice the magnitude in Equation (4.5).

Like the same reason for the upward wave, the pile top velocity can be computed due to the downward travelling portion of the wave:

$$v_T^d(t) = -\frac{c}{EA} R_i \left[H\left(t - \frac{2L}{c}\right) + H\left(t - \frac{4L}{c}\right) + \cdots\right] \quad (4.8)$$

$v_T^d(t) =$ pile top velocity due to the downward travelling wave caused by soil resistance

Finally, the velocity of the pile top can be found by combination of Equations (4.4),(4.7) and (4.8):

$$v_T(t) = \frac{c}{EA}\Big\{F_T(t) + 2\sum_{j=1}^{m} F_T(t - \frac{j2L}{c}) - \sum_{i=1}^{n} R_i[H(t - \frac{2x_i}{c}) + \sum_{j=1}^{m} H(t - \frac{2x_i+j2L}{c}) + \sum_{i=1}^{m} H(t - \frac{j2L}{c})]\Big\} \quad (4.9)$$

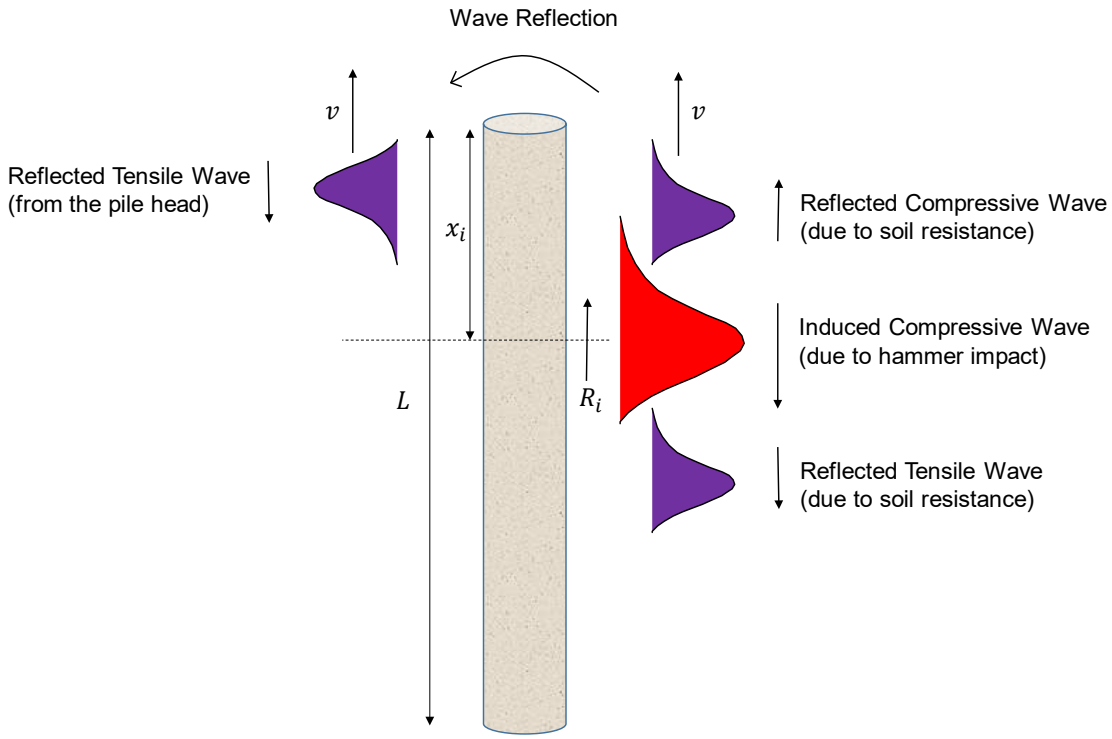

Figure 4.2 Free pile top velocity under action of soil resisting force

where m is the number of completed $^{2L}/_{c}$ time intervals. Considering the measured velocity, $v_M(t)$, at any time, t* in Equation (4.9) and subtracting the measured velocity at a time, $\frac{2L}{c}$, the following equation can be written based on the measured force, $F_m(t)$:

$$\frac{EA}{c}\left[v_m(t^*) - v_m\left(t^* + \frac{2L}{c}\right)\right] = F_m(t^*) + 2\sum_{j=1}^{m} F_m\left(t^* - \frac{j2L}{c}\right) - F_m\left(t^* + \frac{2L}{c}\right) - 2\sum_{j=1}^{m+1} F_m\left(t^* + \frac{2L}{c} - \frac{j2L}{c}\right) - \sum_{i=1}^{n} R_i\left[2m + H\left(t^* - \frac{2x_i+2mL}{c}\right) - 2(m+1) - H(t^* + \frac{2L}{c} - \frac{2x_i+2(m+1)L}{c})\right] \quad (4.10)$$

Since the effects of the Heaviside function terms can be cancelled, hence the expression can be simplified to:

$$\frac{EA}{c}\left[v_m(t^*) - v_m\,(t^* + \frac{2L}{c})\right] = -F_m(t^*) - F_m\left(t^* + \frac{2L}{c}\right) - \sum_{i=1}^{n} R_i\,[2m - 2(m+1)] \quad (4.11)$$

All values of R_i can be combined as:

$$R(t^*) = \sum_{i=1}^{n} R_i \quad (4.12)$$

The total resistance then can be expressed as a function of the time, t^*:

$$R(t^*) = \frac{1}{2}[F_m(t^*) + F_m(t^* + \frac{2L}{c})] + \frac{EA}{2c}\,[v_m(t^*) - v_m(t^* + \frac{2L}{c})] \quad (4.13)$$

The total resistance to penetration (R) can be divided into two parts, including static part, R_s, and dynamic part, R_d. Hence, the total driving resistance is:

$$R = R_s + R_d \quad (4.14)$$

Because the total pile resistance is found from Equation (4.13), after finding R_d, R_s can be specified. Since in the CASE method, all velocity-dependent resistances (dynamic resistance) are considered at the pile toe, hence, the dynamic resistance can be defined as a linear function of the pile toe velocity. Thus:

$$R_d = Jv_b \quad (4.15)$$

where,
v_b = the velocity of pile toe
J = the viscous damping constant (N.s/m)

The pile toe velocity for the pile without any resistance, after the induced stress wave arrives the toe and reflects to the head is:

$$v_b\left(t_{max} + \frac{L}{c}\right) = \frac{c}{EA}F_T(t_{max}) + v_T(t_{max}) = 2v_T(t_{max}) \quad (4.16)$$

where,
t_{max} = the time of impact
$F_T(t_{max})$ = force of the pile top at the time of impact

$v_T(t_{max})$ = velocity of pile top at the time of impact

The effect of the downwards travelling wave induced by resistance forces, R_i, is obtained by twofold the magnitude of Equation (4.5):

$$v_b(t_{max} + \frac{L}{c}) = -\frac{c}{EA} R_i \tag{4.17}$$

Immediately after the hammer blow, the velocity at the top of the pile reaches a relative peak value and then subsides with time. In soft driving, pile top velocity at $\frac{2L}{c}$ after hammer impact increases considerably (due to the tensile reflections from pile tip) and in some occasions it becomes much larger than the pile top velocity at impact time.

The pile toe velocity will reach a relative peak value at time $t = t_{max} + \frac{L}{c}$ and is given by adding Equations (4.16) and (4.17):

$$v_b \left(t_{max} + \frac{L}{c}\right) = v_T(t_{max}) + \frac{c}{EA} [F_T(t_{max}) - \sum_{i=1}^{n} R_i] \tag{4.18}$$

Then the static soil resistance at any time is:

$$R_s = R(t^*) - J[v_T(t^*) + \frac{c}{EA} [F_T(t^*) - \sum_{i=1}^{n} R_i] \tag{4.19}$$

If J is assumed to be equal to $\frac{EA}{c}$ times a damping constant J_c:

$$J = J_c \frac{EA}{c} \tag{4.20}$$

J_c = CASE damping factor (dimensionless)

With substituting Equations (4.20) and (4.12) into Equation (4.19):

$$R_s = R(t^*) - J_c \left[\frac{EA}{c} v_T(t^*) + F_T(t^*) - R(t^*)\right] \tag{4.21}$$

The static resistance derived in Equation (4.21) is dependant of the chosen value of J_c and shaft and toe resistances are not separated. Considering Equation (4.1) with t^* equal to t_{max} gives the maximum static resistance (RMX) as:

$$R_s(t_{max}) = RMX = \frac{1}{2}\left\{(1 - j_c)\left[F_T(t_{max}) + \frac{EA}{c}v_T(t_{max})\right] + (1 + J_c)\left[F_T\left(t_{max} + \frac{2L}{c}\right) - \frac{EA}{c}v_T\left(t_{max} + \frac{2L}{c}\right)\right]\right\} \quad (4.22)$$

If the maximum displacement occurs and the quake value is exceeded, it is generally assumed that the maximum soil resistance is mobilised. However, if the soil resistance is not fully mobilised at the first displacement peak t_{max} , a delay is needed to ensure a sufficient displacement will occur to fully mobilise the soil resistance. In this situation, the identical method as the CASE method with the time interval ($\frac{2L}{c}$) is used but only the start point is altered. In this method, the bearing capacity for a wide range of starting times is calculated and the maximum bearing capacity is iteratively determined: The time t_{max} together with the corresponding reflected wave at $t_{max} + \frac{2L}{c}$ is moved and for different values the bearing capacity is calculated. The obtained maximum resistance is introduced as the result for the calculation method.

4.3.2 CASE Damping Factor

Referring to Equation (4.22), all the parameters on the right hand side can be specified apart from the CASE damping factor J_c (entirely empirical value) that characterises the dynamic soil resistance. Rausche, Goble & Likins (1985) stated that the J_c can be determined by considering the ultimate pile resistance (which specified according to

interpretation of a static load testing) in Equation (4.22). The original J_c values were determined by Goble, Likins & Rausche (1975) from 69 static load testing in which all pile toes were located into five different soil types. The original J_c was correlated with data which indicated at most 20% difference between the results of the static load testing and results predicted by the CASE method. Moreover, the best J_c value (was found based on the correlation study of different soil types) and updated values (were inferred from additional static load test data) are tabulated in Table 4.1.

In very hard driving situation, velocity at the pile toe is negligible and approximately zero, consequently the total resistance is the same as the static resistance and is independent of the value of J_c. On the other hand, in easy driving velocity at the toe is higher and the pile resistance computation highly depends on J_c. Chiesura (1998) stated that a proper value of J_c plays a key role in estimating a realistic static soil resistance, and suggested that both dynamic and static load tests should be conducted to acquire the correct J_c value. Hannigan et al. (1998) suggested that in calculations of the maximum static resistance (Equation 4.22) J_c should be at least 0.40 which it is usually 0.20 higher than the amount used in the standard static resistance obtained from Equation 4.21.

Table 4.1 Summary of CASE damping factors (after Hannigan et al. 1998)

Soil type at pile toe	Original CASE damping factor	Best correlation value	Updated CASE damping factor
Clean Sand	0.05 to 0.2	0.05	0.1 to 0.15
Silty Sand, Sandy Silt	0.15 to 0.3	0.15	0.15 to 0.25
Silt	0.2 to 0.45	0.3	0.25 to 0.4
Silty Clay, Clayey Silt	0.4 to 0.7	0.55	0.4 to 0.7
Clay	0.6 to 1.1	1.1	0.7 or higher

4.3.3 Pile Driving Stresses

In addition to pile resistance prediction, PDA computes both tensile and compressive stresses at the gauge location and checks the stress limits corresponding to the maximum allowable stresses defined based on different pile materials. The compressive and tensile stresses are calculated using Equations (4.23) and (4.24), respectively:

$$\sigma_c = \varepsilon E \tag{4.23}$$

$$\sigma_T = \frac{1}{2}\left[v\left(t_{max} + \frac{2L}{c}\right)Z - F\left(t_{max} + \frac{2L}{c}\right) - v\left(t_{max} + \frac{2(L-x)}{c}\right)Z - F\left(t_{max} + \frac{2(L-x)}{c}\right)\right] \tag{4.24}$$

where,
σ_c = compressive stress (kPa)
σ_T = tensile stress (kPa)
ε = measured strain at gauge location (mm/mm)
E= elastic modulus of pile (kPa)
Z= pile impedance ($\frac{EA}{c}$)
L= pile length (m)
c= pile wave speed (m/s)
x = distance where tensile stress occurs and measured below gauge location (m)

4.3.4 Hammer/Driving System

PDA is also able to examine the hammer energy transferred to a pile to avoid the possibility of pile damage and to enhance the hammer performance efficiency. Hussein et al. (2002) reported that the transferred energy to the pile is highly dependent on hammer ram weight, hammer falling height, and pile and cushion properties. Hannigan et al. (1998) stated that the transferred energy from a hammer can be determined according to Equation (4.25). The maximum energy (EMX) transferred to a pile is determined using Equation (4.26), according to the force and velocity data. The performance of a hammer

is usually assessed in terms of the energy transferred ratio (ETR) (The Hammer Efficiency) given by Equation (4.27).

$$E_p(t) = \int_0^T F(t)v(t)dt \tag{4.25}$$

$E_p(t)$ = Transferred energy to the pile as a function of time t, (kN.m)
T = Maximum time limit corresponding to 0.2048 second, (s) (this time is considered long enough so, thus force and velocity traces subside during this time)

$$EMX = max[\sum_{t=0}^{t=T} F(t)v(t)\Delta t] \tag{4.26}$$

$EMX =$ Maximum transferred energy at gauge location

$$ETR = \frac{EMX}{Manufacturer\ Rated\ Hammer\ Energy} \tag{4.27}$$

4.3.5 Total and Static Shaft Resistance

All different direct methods introduce the total driving resistance obtained during driving as the pile bearing capacity. This resistance comprises the excess pore pressure and dynamic effects due to high-speed displacements. The velocity and force traces during dynamic load testing can be obtained by:

$$F(t) = \varepsilon EA \tag{4.28}$$

$$v(t) = \int_0^t adt \tag{4.29}$$

where ε and a are the strain and the acceleration as measured by the strain gauges and accelerometers, respectively. The soil resistance can be derived by the difference between the respected force without any soil resistance and the actually measured force. In absent of any soil resistance, it can be expected that the similar wave reflects after travelling to the pile tip and back in a time of $\frac{2L}{c}$. The difference between the induced and the reflected

wave is caused by the soil resistance during driving. The impact force applied on the head of a pile by the piling hammer induces internal stress waves that travel downwards and then reflects off the shaft and the stiff toe. At time $t_2 = t_{max} + \frac{2L}{c}$, the waves travelling upwards that reach the top of the pile also include a reflection of the initial impact wave plus a summation of all reflected resistance waves. In general, any discontinuities or irregularities in the shaft or interaction by the pile with the surrounding soil causes the wave travelling downwards (Wave Down) to be partially or completely reflected, and produce waves that travel upwards (Wave Up). This means the forces and velocities in every section of the pile are the summation of downward and upward propagating forces and velocities, respectively (Figure 4.3), by assuming that the superposition principle is valid. Rausche, Goble & Likins (1985) also explained that wave down (W_D) and wave up (W_U) in each section of the pile can be separated by Equations (4.30) and (4.31):

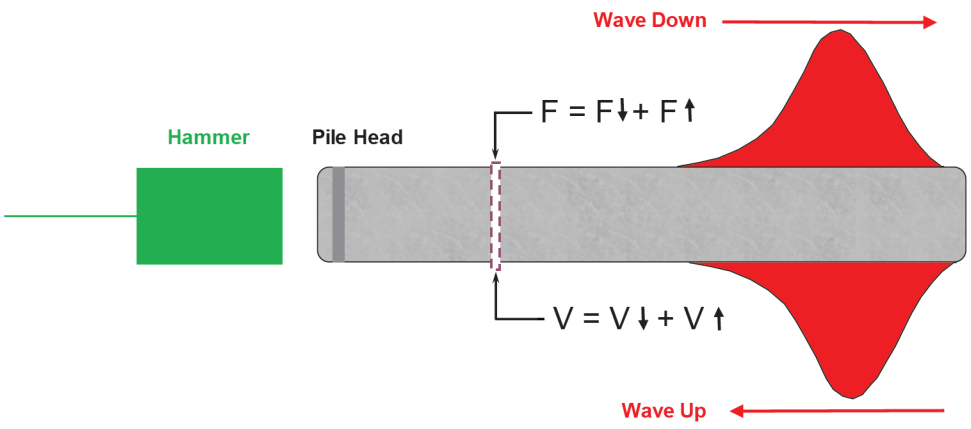

Figure 4.3 Induced and reflected waves due to the hammer impact over the pile head

$$W_D = \frac{1}{2}(F + Zv) \tag{4.30}$$

$$W_U = \frac{1}{2}(F - Zv) \tag{4.31}$$

Furthermore, PDA can estimate the shaft resistance between the impact time and the time corresponding to the reflection of the stress wave from the pile toe ($t < 2L/c$). This resistance is called the total shaft resistance (SFT) (due to dynamic effects) and after a correction for dynamic effects (damping effects), the static shaft resistance (SFR) can be obtained. End bearing resistance is determined by subtracting the SFR from the estimated pile static resistance (assumed as RMX).

$$SFT = 2w_u \tag{4.32}$$

$$SFR = SFT\ (\frac{RMX}{RX0}) \tag{4.33}$$

$$R_{toe} = RMX - SFR \tag{4.33}$$

4.4 Case Study

In this section, four important parameters computed and displayed by the pile driving analyser during a real case dynamic pile load testing, including the total soil resistance (RTL), the maximum static soil resistance (RMX), the maximum compressive stress (CSX) and the maximum transferred energy to the pile (EMX), are compared with a code written by the author. In order to analyse the CASE method and assess the effect of CASE damping factor on the maximum static soil resistance, the existing data for a steel H-pile (ISU5) under a dynamic test as explained by Ng et al. (2011) for both the end of driving (EOD) and beginning of the restrike (BOR) conditions is evaluated. The stratigraphy of soil at pile ISU5, the embedded length of pile, and cross section of the driven pile are shown in Figures 4.4a-b. The hammer used in the field tests was Delmag manufactured open end diesel hammers (Delmag D16-32), and ram weight and equivalent maximum hammer stroke during the test were 1597 kg and 3.5 m respectively.

During the dynamic pile load testing, two strain transducers and accelerometers were mounted on each side of the web at a distance of three times of pile width from pile head. PDA tests were performed according to ASTM International (2010) to examine the pile performance during the test. Force and velocity traces were captured and displayed by the PDA at every hammer blow at both end of driving and beginning of restrikes conditions. Signals measured at the end of driving and the sixth restrike test are shown in Figure 4.5a-b.

The author has written a code using MATLAB software to verify the algorithm and the procedure. The obtained results are compared with the existing data taken from the PDA on site. It is worth mentioning that for solving the respected equations, at first the data related to recorded force and velocity traces were collected in Excel file and then this file was implemented into the MATLAB program. In the written program, the total and the maximum static soil resistance, the maximum compressive stress, and the maximum energy transferred to the pile can be computed and finally the maximum outputs are introduced as the RTL, RMX, CSX, and EMX, respectively (Figures 4.6 to 4.9). Schedule of restrike tests are presented in Table 4.2.

The main purpose of performing the restrike test is to investigate the change in pile resistance because of the dissipation of excess pore pressure generated during pile driving (soil setup). As shown in Figures 4.6 to 4.10, there is reasonable correlation between PDA and MATLAB results and the small difference and inconsistency between the results are attributed to the accuracy of the reading signals from the existing force and velocity traces. In addition, it is observed that over time due to consolidation of soil, the static soil resistance increases, hence during this time RMX increases as much as twice of the EOD condition. The adopted CASE damping constant values for calculating RMX is presented

in Table 4.1. It can be observed that by reducing the grain size, the magnitude of damping increases. The results shown in Figure 4.7 have been obtained based on the CASE damping factor of $J_c = 0.7$, hence by changing the magnitude of CASE damping factor from 0.7 to 1, variation of the maximum static soil resistance have been evaluated in Figure 4.10.

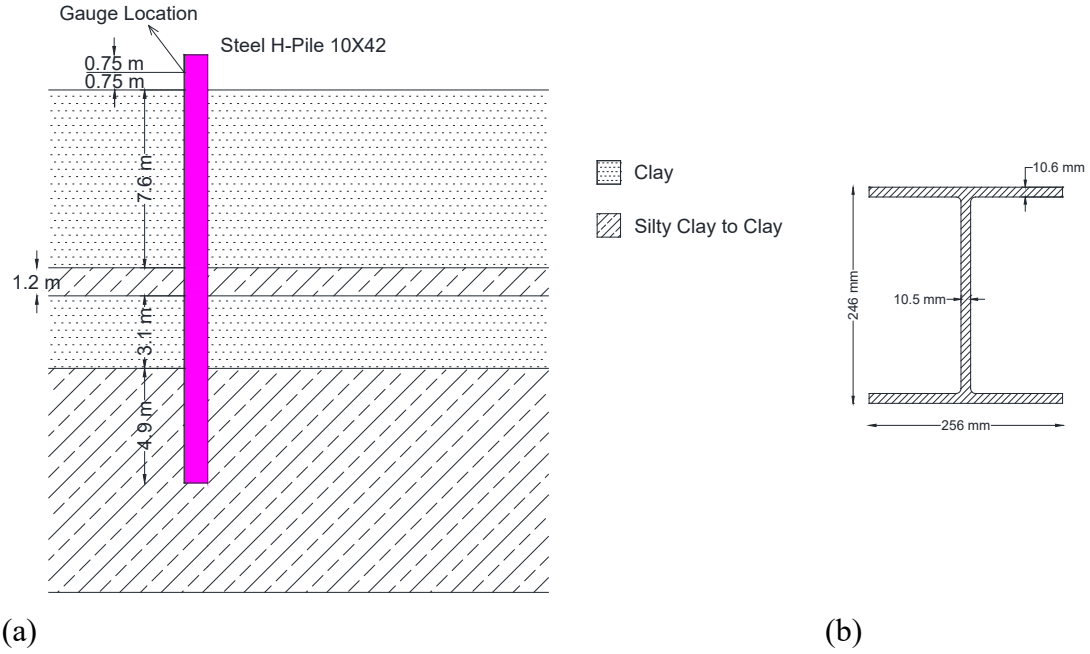

Figure 4.4 (a) stratigraphy of site at the location of pile ISU5 (b) cross section of the steel H-pile (after Ng et al. 2011)

As can be seen in Figure 4.10, with increasing the CASE damping factor consequently dynamic soil resistance increases and the static soil resistance decreases. In addition, between 3rd and 4th restrike tests a considerable gap in the static soil resistance can be observed, indicating that during this time soil has significantly been consolidated. Figure 4.11 shows the increase of the static soil resistance over time and it proves that as time progresses, the soil resistance increases, mostly due to consolidation. Finally, the effects of increasing CASE damping factor on the maximum static soil resistance were assessed

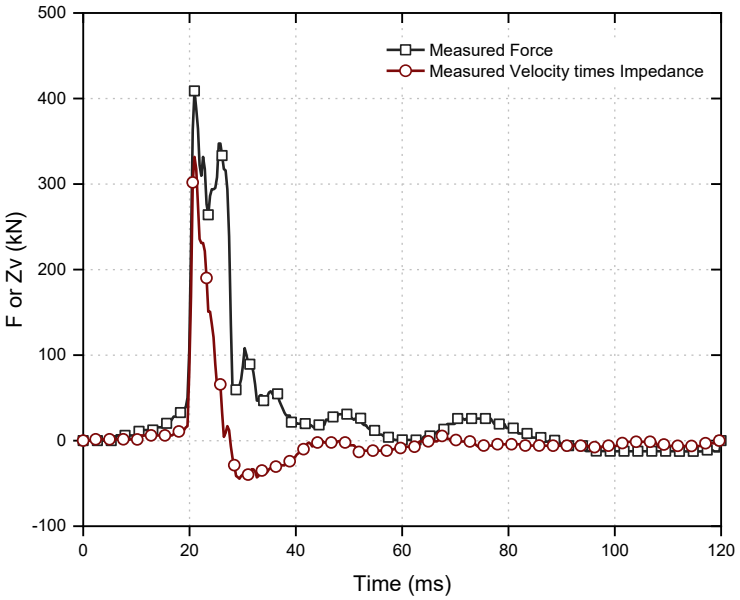

(a)

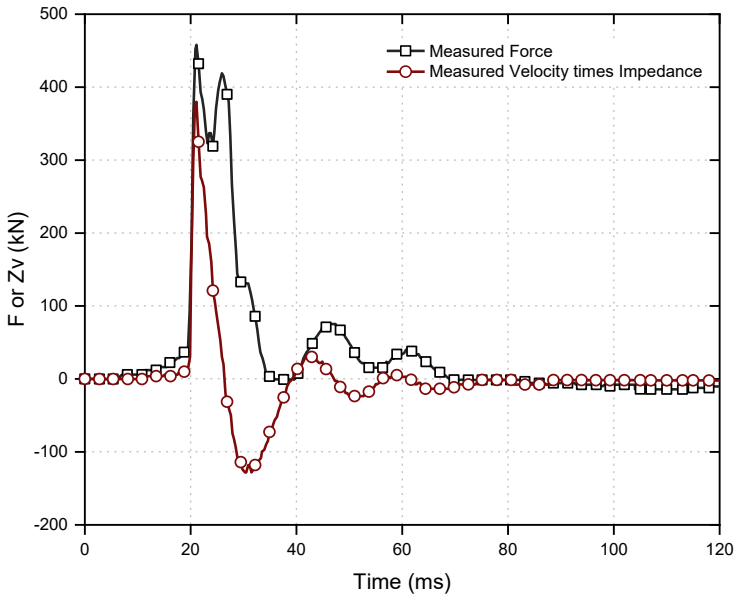

(b)

Figure 4.5 Signals measured at (a) end of driving (b) sixth restrike test (after Ng et al. 2011)

Table 4.2 Schedule of restrike tests based on the elapsed time after end of driving (after Ng et al. 2011)

1st restrike	2nd restrike	3rd restrike	4th restrike	5th restrike	6th restrike
8 minutes	19 minutes	3 hours	22 hours	3 days	8 days

and the results are depicted in Figure 4.12. Referring to this fugure, it can be inferred that by changing CASE damping factor from 0.7 to 1, the maximum static soil resistance changes up to 45%. However, as time moves forward and pore water pressures dissipate, the sensitivity of predictions to damping decreases. In other words, immediately after the driving and in unconsolidated soil conditions, the sensitivity of analysis to the choice of damping factor would be higher than the corresponding values for the consolidated conditions.

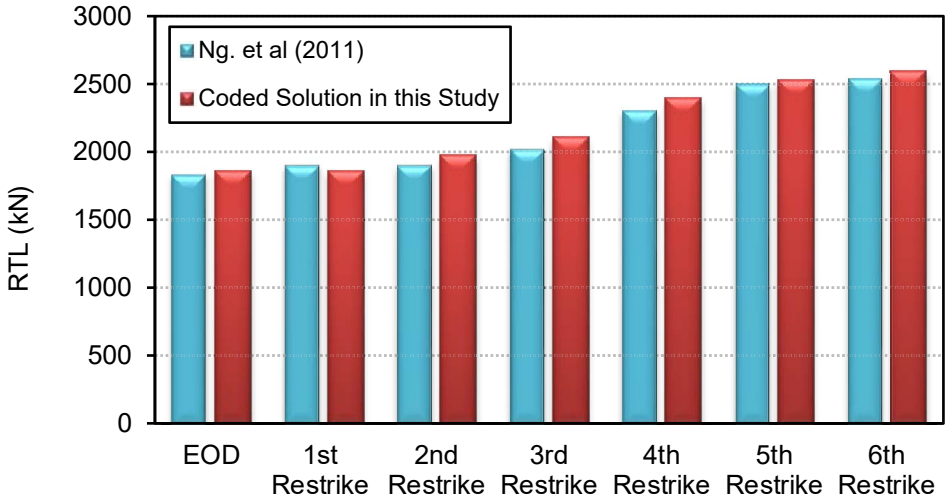

Figure 4.6 Comparison of total soil resistance (RTL) between PDA and the MATLAB code

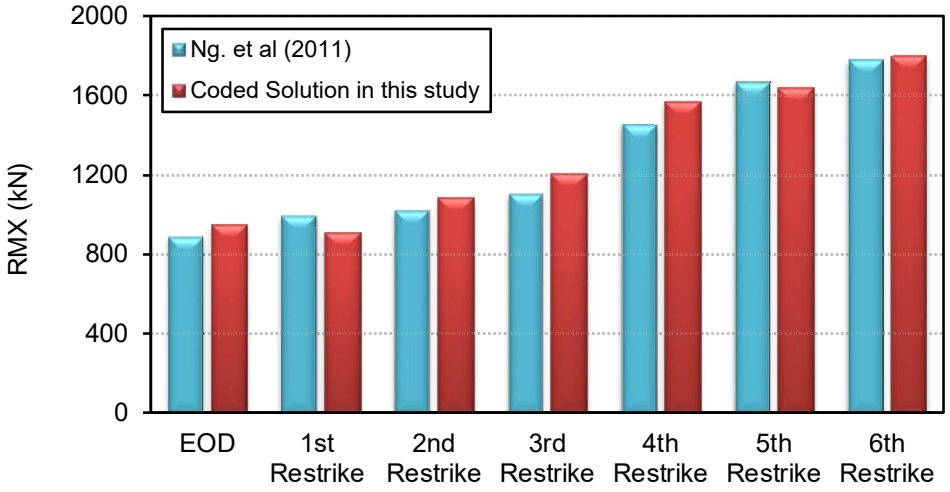

Figure 4.7Comparison of maximum static soil resistance (RMX) between PDA and the developed code using MATLAB

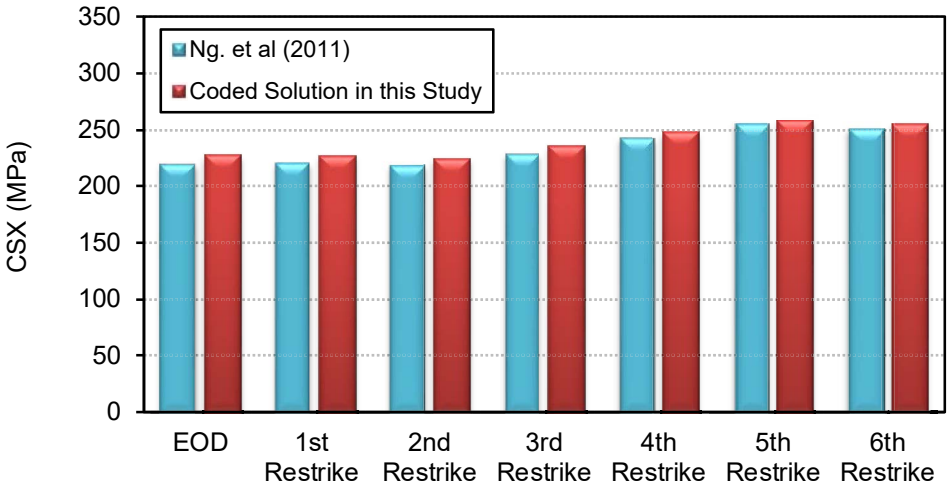

Figure 4.8 Comparison of maximum compressive stress (CSX) between PDA and the MATLAB code

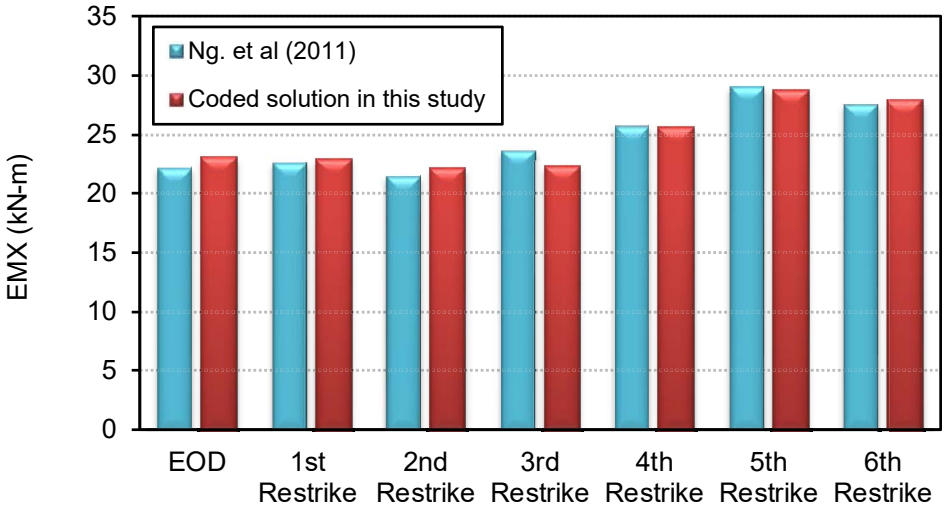

Figure 4.9 Comparison of maximum energy transferred to the pile (EMX) between PDA and the MATLAB code

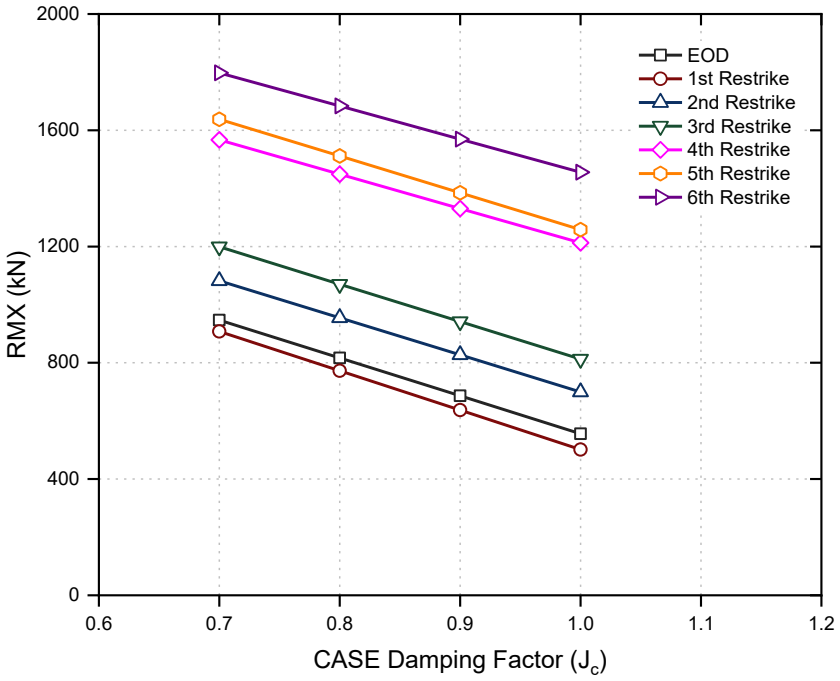

Figure 4.10 The effect of CASE damping factor on the maximum static soil resistance in both conditions end of driving (EOD) and beginning of restrike (BOR)

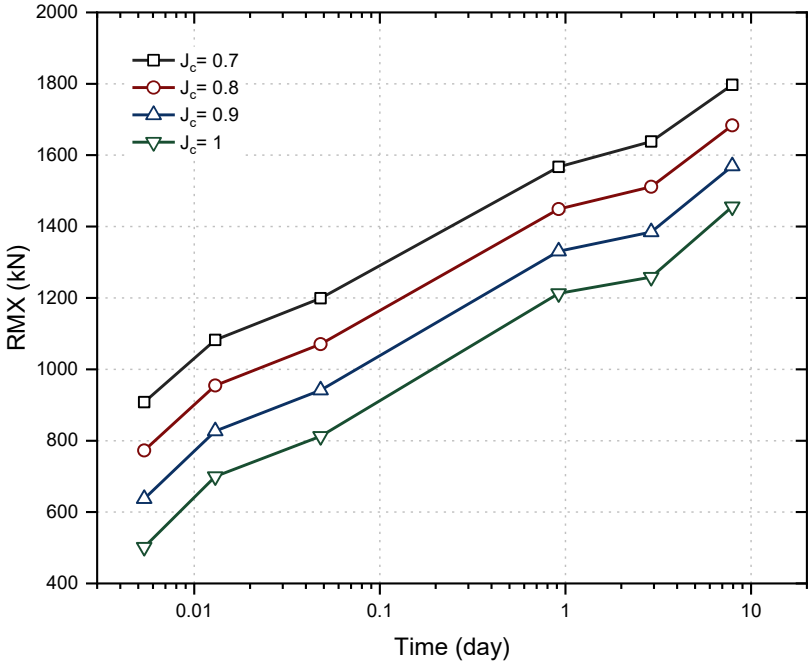

Figure 4.11 Increasing of maximum static soil resistance (RMX) with time using different CASE damping factor

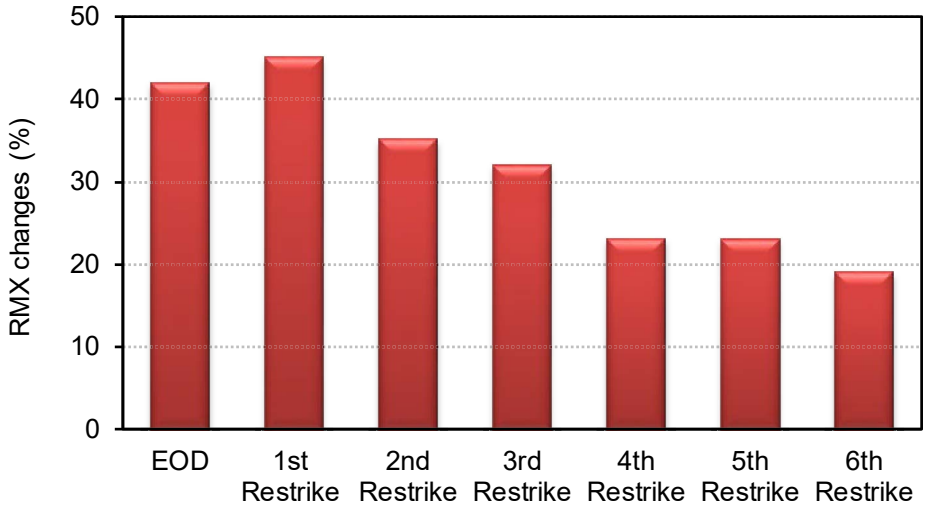

Figure 4.12 The amount of maximum static soil resistance (RMX) relative changes when CASE damping factor changes from 0.7 to 1

4.5 Summary

This chapter has briefly addressed the principals behind the CASE method as a numerical technique, which is used in pile driving analyser for preliminary assessment of pile behaviour during the driving. In addition, the one-dimensional wave propagation concept which is induced due to hammer impact during the dynamic pile load testing has been discussed. The equations presented in CASE method were coded using MATLAB software in order to deep understanding of this method and evaluate the influence of CASE damping factor on the maximum mobilised static resistance of the soil. In the developed code, it was concentrated on four important parameters evaluated during a real case dynamic pile load testing, including the maximum static soil resistance (RMX), the total soil resistance (RTL), the maximum compressive stress (CSX), and the maximum energy transferred to the pile (EMX). Comparing the results indicates a reasonable correlation between PDA and the developed code outputs in both end of driving and beginning of restrike conditions. The slight differences and inconsistencies observed can mainly be attributed to the accuracy of the reading signals from the existing force and the velocity traces.

In the written code, the CASE damping factor changed in a reasonable range for clay and silty clay soils (from 0.7 to 1). The results shows that the maximum static soil resistance changes up to 45%. However, as time elapses and pore water pressures dissipate the sensitivity of predictions to damping decreases. In other words, immediately after the driving and in unconsolidated soil conditions, the sensitivity of analysis to the choice of damping factor would be higher than the corresponding values for the consolidated conditions.

Coded Program for Sixth Restrike Test (CASE damping factor = 1)

```
%% Program (Imperial System Units)

clc
close all
clear

%% Input Data

D=xlsread('Sixth.xlsx');
t=D(:,1);
F=D(:,2);
V=D(:,3);
EP=D(:,4);
L=57.5;          % ft
A=12.4;          % in^2
Step = 0.01;     %
E=30000;         %  kips
c=16.8079;       % ft/s
J=1;             % CASE damping factor

%% Calculations

[FT1c,p_FMax]= max(F);
VT1c=V(p_FMax);
T2=t(p_FMax)+2*L/c;

% -----------  fit F ----------------

[xDataF, yDataF] = prepareCurveData(t,F);
ft1 = 'linearinterp';
Ffit = fit( xDataF, yDataF, ft1, 'Normalize', 'on' );
% -------------
tt=t(1):Step:t(end);
% --------------
Force=Ffit(tt);

% -----------  fit V ----------------

[xDataV, yDataV] = prepareCurveData(t,V);
ft2 = 'linearinterp';
Vfit = fit( xDataV, yDataV, ft2, 'Normalize', 'on' );
Emp=E*A/c;
Velocity=Vfit(tt)./Emp;
FT2c=Ffit(T2);
VT2c=Vfit(T2);
M=t+(2*L/c);
FT1=Ffit(p_FMax);
VT1=Vfit(p_FMax);
FT2=Ffit(T2);
VT2=Vfit(T2);
RTL=0.5*(FT1c+FT2)+0.5*(VT1c-VT2);
RMX=0.5*(((1-J)*(FT1c+VT1c))+((1+J)*(FT2-VT2)));
```

```
RX0=0.5*((FT1c+VT1c)+(FT2-VT2));
WU=0.5*(F-V); %wave up
WD=0.5*(F+V); %wave Down
% -----------  fit WU ----------------

[xDataWU, yDataWU] = prepareCurveData(t,WU);
ft3 = 'linearinterp';
WUfit = fit( xDataWU, yDataWU, ft3, 'Normalize', 'on' );

% -----------  fit WD ----------------

[xDataWD, yDataWD] = prepareCurveData(t,WD);
ft4 = 'linearinterp';
WDfit = fit( xDataWD, yDataWD, ft4, 'Normalize', 'on' );
% --------------
ttt=t(p_FMax):T2;
WaveUP=WUfit(tt);
WUU=2*WUfit(T2);
SFR=WUU*(RMX/RX0);
CSX=max(EP*E);

% -----Integral ------

Work=Force.*Velocity;
Energy=trapz(tt,Work);  % total integral at the end
for I=2:length(tt)
EnergyN(I)=trapz(tt(1:I),Work(1:I));
end
EMX=max(EnergyN);
Displacement=trapz(tt,Velocity);
for I=2:length(tt)
EnergyN(I)=trapz(tt(1:I),Work(1:I));
end

disp('--------------Results-----------------')
disp(['Total Resistance: RTL (kips) = ',num2str(round(RTL,2))])
disp(['Maximum Static Resistance: RMX (kips) = ',num2str(round(RMX,2))])
disp(['Total Static Shaft Resistance: SFR (kips) =
',num2str(round(SFR,2))])
disp(['Maximum Compressive Stress: CSX (ksi) = ',num2str(round(CSX,2))])
disp(['Maximum Energy: EMX (k-ft)  = ',num2str(round(EMX,3))])
disp('-------------------------------------')
```

CHAPTER 5 Dynamic Pile Load Testing: Numerical Simulation, Interpretation of the Results, and Assessment of Ground Vibration Induced by Dynamic Test

5.1 Synopsis

During the last few decades, the advent of high-powered computers has resulted in advanced methods for pile testing, whereas prior to these advances, pile testing consisted of slow and costly static loading tests. Nowadays, there are different tests methods available to predict or measure pile resistance, as well as many methods for quickly and economically testing their structural integrity. Dynamic pile load testing is known as an advanced method for evaluating the bearing capacity of different kinds of piles and their performance during and after the driving. This chapter evaluates and interprets the dynamic pile load testing using continuum based numerical simulation, as a technique besides other methods which are based on discretised pile and soil model such as CAPWAP, adopting different soil models from basic to advanced soil models such as Mohr-Coulomb and hardening soil with small strain stiffness models. The main aim of this chapter is to assess the behaviour of piles during the dynamic pile load testing in more realistic conditions provided by finite element software PLAXIS compared to one-dimensional wave equation based programs such as CAPWAP and GRLWEAP, and evaluate the influences of vibrations induced during the test in the vicinity area. In order to assess the capability of continuum based numerical simulation and the advanced soil

models in prediction of field measurements, dynamic and static response of a real driven open-ended steel pipe pile as part of a highway bridge construction project in New South Wales, Australia, is evaluated. The obtained results indicate that hardening soil with small strain stiffness model by considering the natural damping of soil can appropriately predict the behaviour of pile during the dynamic load testing and shows the best correlation between the large and small strains, occurring while the pile is under static load and being driven. In addition, the established model is used to assess the ground vibration induced during the dynamic test and to obtain the peak particle velocity (PPV) as a managed value in association with the vibration risk and as a parameter used to analyse ground vibrations. The PPV predicted by the numerical simulation is compared to the recommendations and database of a number of standards to introduce the minimum allowable distance in which ground vibrations do not result in damage to adjacent structures or discomfort to nearby inhabitants.

Generally, evaluation of dynamic pile load testing based on the continuum based finite element model has many advantages for geotechnical engineers dealing with pile design. This model can be used to evaluate the performance of piles under different loading conditions, such as combined vertical and lateral loading on a single or a group of piles, and piles near existing structures. Furthermore, this method retains the continuity of different stages of modelling from simulating pile driving, quality control, and investigating settlements, while all these analyses are carried out using one software.

5.2 Introduction

Dynamic testing of piles is a dependable and cost effective method of specifying the load capacity of both driven and bored piles. Dynamic pile testing can be carried out on off-shore and on-shore environments and during initial driving to assess the performance of the hammer, the pile driving stresses, the integrity, and capacity of piles (Morgano, White & Allin 2008). For most constructions including high-rise buildings and bridges, the driving of piles and dynamic pile load testing is inevitable.

Dynamic load testing of piles has been evaluated in many studies. For example as Mhaiskar, Khare & Vaidya (2010) explain, a High Strain Dynamic Pile Test (HSDPT) saves a lot of time and cost, and requires a much smaller space than conventional static load tests. Their study presents the results of nine HSDPTs carried out on 600 mm, 800 mm and 1000 mm diameter socketed piles bored into rock. The load-settlement responses derived from HSDPTs are then compared with those from conventional static load tests. Mhaiskar, Khare & Vaidya (2010) results indicate that the settlement obtained in HSDPT and the static load test agree well up to 150% of the working load. In the study carried out by Wong (2006), the results from static load tests are used as a benchmark and by comparing the predicted pile capacities derived from several computational tools (PDA, CAPWAP, the Hiley formula and the modified Hiley formula) a reliable and practical method for assessing the capacity of piles was recommended. Shooshpasha, Mola-Abasia & Amiri (2013) evaluated the bearing capacity of pipe piles driven into cohesive soils by obtaining information regarding 208 piles driven into four sites with a total area of 1500 m^2.This information is then used to compute and compare the dynamic characteristics related to the bearing capacity of piles in fine grained soils with the corresponding static characteristics. The results indicate that these dynamic approaches can accurately predict

the capacity of piles. Hajduk et al. (2004) refer to a new pier extension for the South Carolina State Ports Authority (SCSPA) at Pier 31C in Georgetown, South Carolina. It is founded on 28 open-ended steel pipe (OEP) piles driven into the underlying limestone and silt. That study provides an overview of the project, discusses the selection, design processes and installation of the steel OEP piles, and also presents the results of the dynamic load testing program carried out to verify the pile design. The study also presents and discusses the time dependent capacity and plugging measurements of piles during installation.

Dynamic analytical techniques such as the CASE Pile Wave Analysis Program (CAPWAP), proposed by Goble & Rausche (1976), are normally used for interpreting the results of dynamic pile load tests and quality control during construction and installation of piles. Similar to Smith (1960) model, the CAPWAP model considers the piles and components of the soil in this analysis. In fact according to Ng & Sritharan (2013), verifying pile resistance using CAPWAP is carried out by an iterative process in which the force of the pile and the velocity signals captured by a pile driving analyser is matched with the simulated signals obtained by the one-dimensional soil–pile model proposed by Smith (1960).

CAPWAP uses the data measured or monitored during pile driving (e.g. through PDA) to predict the required ultimate parameters including the pile resistance. The key parameters requiring signal matching are related to the pile – soil interaction and include the soil resistance distribution as well as soil damping and quake (Rausche et al. 2000; Ng and Sritharan 2013; Bruno and Randolph 1999) . In an inverse analysis, commonly known as signal matching analysis, the optimised solution and back calculated parameters are achieved iteratively. This means the unknown soil parameters are assumed and the

subsequent predictions are compared with the actual field measurements (i.e. the force or velocity measured at the pile head) after analysing the wave propagation, and then the error is calculated. This process continues until the minimum error is achieved, after which the corresponding soil-pile interface parameters are used to obtain the capacity of the pile. However, since these optimised parameters are only related to the soil-pile interface, they cannot be correlated to the actual in-situ soil parameters to make sense of the results or evaluate the validity of the mathematically optimised parameter values.

In reality, accurately predicting the pile resistance using CAPWAP depends mainly on selecting two dynamic soil parameters, i.e., (i) quake (q) measured in mm that defines the maximum elastic deformation of soil indicated by a linear elastic – perfectly plastic spring, and (ii) the damping factor (J) measured in kN.s/m that specifies the viscous damping coefficient indicated by a linear damper. Typically, constant shaft damping factors (Js) and shaft quake (qs) are used in CAPWAP analysis to specify the properties of soil along the shaft regardless of the stratigraphy, even though different types of soil with different characteristics exist along a pile (Ng and Sritharan 2013; Ng et al. 2011; Fellenius and Altaee 2001). Furthermore, since CAPWAP is based on the concept of mass-spring-dashpot, the inertia of the surrounding soil is not automatically considered and the loss of energy attributed to radiation damping is not explicitly considered, whereas uncommon or ostensible parameters at the soil-pile interface such as quake (instead of standard soil properties such as Young's modulus, E, cohesion, c, and the friction angle, φ) are considered (Masouleh and Fakharian 2008; Authier and Fellenius 1980). Hence, developing a so-called continuum based numerical model as a solution to overcome some of the drawbacks of the mass-spring-dashpot system for interpreting the results of pile driving seems valuable. Moreover, employing the developed numerical model, design continuity using real soil parameters remains, and all the analyses,

including installation and quality control are carried out using the same software, otherwise GRLWEAP or CAPWAP should be used with a second software package such as PLAXIS in order to investigate the subsequent settlement or interaction. In limited research studies available in the literature (e.g. Kasali et al. 2006; Pinto, Grazina & Lourenco 2008; Fakharian, Masouleh & Mohammadlou 2014), signal matching analyses have been carried out using the continuum finite element of finite difference methods, where the installation of solid concrete piles is simulated by utilising the elastic – perfectly plastic Mohr-Coulomb soil model. These studies reveal a reasonable match between measurements and predictions after updating the soil parameters through signal matching. A study by Pinto, Grazina & Lourenco (2008) shows that in two-dimensional finite element modelling of dynamic pile testing, material damping could be considered through the plasticity of soil captured in the Mohr-Coulomb yielding criterion, while Rayleigh damping could also consider soil damping in a different manner. These researchers conclude that when simulating dynamic pile driving, a suitable model should be able to consider the dissipation of energy through the natural, hysteretic, and geometric damping features of soil simulation. Because the most commonly used soil models such as linear elastic – perfectly plastic Mohr-Coulomb do not consider the natural damping of soil due to plasticity within the soil body accurately, while hysteretic damping that changes with the level of strain is generally absent. On this basis, more rigorous models that can simulate the cyclic behaviour of soil from small to large strains and wave propagation should be embraced.

As Obrzud (2010) explains, a diversity of soil constitutive models from the Mohr Coulomb to the advanced nonlinear-elasto-plastic cap models such as HS-small strain model are available for numerical simulations. Choosing an appropriate constitutive model depends on factors such as the type of analysis to be carried out, how precise the

predictions would be, and the knowledge of soil properties currently available. Based on the type of analysis, geoengineering computations can be divided into two groups: (a) analyses whose aim is to perform ultimate limit state (ULS) analysis such as bearing capacity and slope or wall stability analyses, and (b) analyses carried out to address serviceability limit state (SLS) issues such as the deformations predicted for deep excavations or tunnelling in urban areas. Generally, for ULS analysis in which deformation predictions are not focused, simple constitutive models, such as linear elastic-perfectly plastic Mohr-Coulomb model, seem to be satisfactory, whereas an accurate deformation analysis requires advanced constitutive models that can approximate the stress-strain relationship more realistically.

One of the challenges facing engineers in deep foundation design and construction is that during the design phase, advanced numerical modelling techniques such as finite element or finite difference techniques (e.g. ABAQUS, PLAXIS, or FLAC software packages) utilise realistic soil constitutive models, but for quality control during installation, different modelling techniques utilise spring - dashpot models (e.g. CAPWAP). This difference in modelling techniques at different phases means that engineers cannot maintain continuity in understanding the real behaviour of the foundation such that they can utilise a unified modelling technique for pile design and evaluation.

In this chapter, at first the dynamic behaviour of a concrete pile under a harmonic load is evaluated adopting different soil models including hypoplastic with intergranular strain concept. Then, dynamic load testing of real small scale and large scale open-ended steel pipe piles are simulated using Mohr-Coulomb and hardening soil with small stiffness (HS-Small) models respectively in finite element software PLAXIS 2D version 2017. Whereas small strain stiffness is well established for analysing small strain dynamics, a

large strain modulus should be used while carrying out static and large strain analysis. Therefore, the aim of this chapter is mainly to establish a continuum numerical model to obtain a reasonable match between measured and predicted results during static and dynamic loading conditions. In addition, the proposed numerical model overcomes the limitations of existing techniques and it can assess pile behaviour in more realistic conditions and indicate how well the continuum based numerical simulation interprets the results of pile driving. The numerical predictions are then compared to the field measurements and the verification exercise is followed. After simulation of dynamic pile load testing, ground vibrations induced by dynamic pile load testing in different distances from the pile is obtained. Finally, the results are compared with the recommendations of different standards, including the Australian and the British standards to identify the minimum distance in order to avoid the adverse effects of ground vibrations on adjacent buildings or nearby occupants.

5.3 Numerical Simulation Procedure

All of the dynamic pile load testing simulations, presented in this chapter, were carried out using the axisymmetric finite element program PLAXIS 2D in which 15 node triangular elements were assigned to the model to simulate the soil. All of the steel pipe piles in axisymmetric models were simulated as solid zones with the thickness of the pipe wall and elastic material properties such as an elastic modulus of 200 GPa, a Poisson's ratio of 0.3 and a unit weight of 78.5 kN/m^3. Viscous boundaries were used in the numerical models to simulate geometric damping and far-field boundaries; a viscous boundary condition was introduced by Lysmer & Kuhlemeyer (1969) to absorb the outgoing wave energy. In this boundary condition, viscous dampers are applied in different directions along the boundary to provide a resisting force in the normal and

tangential directions. Such a boundary is preferred for problems where the dynamic source is inside the mesh, whereas free-field boundary conditions are generally preferable for analysing earthquakes, where a dynamic input is applied along the model boundary (Brinkgreve, Kumarswamy & Swolfs 2017). All the movements at the bottom level of the model were restrained, whereas lateral movements at the lateral external sides were prohibited. The external sides of the numerical model were moved far enough from the pile to avoid any boundary effect, and the borehole option described in the program was used to define the soil stratigraphy and the ground surface level. The number of steps and sub-steps used in dynamic calculation were optimised to acquire more detailed plots and to cover the input signal used in the dynamic loading. As (Brinkgreve, Kumarswamy & Swolfs 2017) denote, the time step (δt) used in dynamic calculations is constant and calculated based on Equation (5.1):

$$\delta t = \frac{\Delta t}{(m.n)} \tag{5.1}$$

where Δt is the duration of dynamic loading, m is the maximum number of steps, and n is the number of sub-steps parameter. The total number of step which is used in the time discretisation is obtained by multiplying the number of sub-steps and maximum step number. In the numerical simulation, interface elements were specified between the pile and the soil to simulate the pile-soil interaction (Cao et al. 2014; Han et al. 2015).

5.4 Concrete Pile Driving in Saturated Dense and Loose Sand Deposits

5.4.1 Overview

In this section, using PLAXIS software and different constitutive soil models including Mohr-Coulomb, hardening soil and hypoplastic with intergranular strain models, the behaviour of concrete piles driven into saturated dense and loose sand deposits under a hammer blow is evaluated. The main objective of this section is to assess the influence of different factors including frequency of loading and hypoplastic soil model parameters on the recorded velocity and pile head displacement as the main outputs measured during a real dynamic pile load testing. It is indicated that using the intergranular strain (IGS) concept, defined in hypoplastic soil model, small strain behaviour of soil around the pile during driving can directly be captured. The results of this section reveals that considering the hypoplastic model, incorporating the intergranular strain concept, can accumulate much less strains than the corresponding predictions excluding the intergranular strain, and hence predict the pile performance during driving more realistically.

The Baskarp sand properties, the characteristics of the numerical model, and bored pile dimensions used in this section are the same as model used in section 3.3.2. In this part, the hammer impact applied over the pile head was simulated as a harmonic signal with an amplitude of 5 MPa, a phase of zero degree and a frequency of 50 Hz similar to what was reported in Brinkgreve, Kumarswamy & Swolfs (2017). According to ASTM International (2010), the strain gauge and the accelerometer during the dynamic load testing should be mounted at least 1.5D (D is pile diameter) below the pile head. Hence, force and velocity traces were recorded at 2D distance below the pile head. An illustration of the finite element model used in analysis is shown in Figure 5.1. As shown in Figure

5.1, half sine load with a dynamic time interval of 0.01 s (i.e. a load frequency of 50 Hz) was applied on the pile head to simulate the hammer load.

5.4.2 Results and Discussion

One of the important advantages of pile driving and pile load testing simulation in finite element and finite difference software is that the radiation or geometric damping is automatically considered in numerical modelling. In fact, the travelling induced wave (due to the hammer impact) along the pile shaft causes a relative sliding between soil and pile, which subsequently a shear wave is generated and propagated radially in the adjacent soil. For evaluating the radiation damping effect, the shear stress variations with time were recorded at a depth of 4 m and at different distances from the pile axis (i.e. 1, 3, 6 and 9 m) in both dense sand and loose sand, while hardening soil model assigned to the soil cluster (Figure 5.2). Figure 5.2 represents a quick subsidence of shear stress wave amplitude with a radial distance away from the pile shaft (e.g. r = 6 m), such that near the external lateral boundaries, it is approximately zero for both dense and loose sand. This finding not only confirms the soil inertia or radiation damping effect in finite element modelling, but also proves that the viscous boundary has been regarded far enough to avoid the wave reflection in the model.

During the pile load testing and pile driving, the pile head displacement is one of the most important factors that should be taken into account. Herein, the pile head displacement using three constitutive soil models are obtained and compared to each other, as illustrated in Figure 5.3. Referring to this figure, it is evident that driving a pile into dense sand induces less displacement compared to loose sand case. All employed constitutive soil models including Mohr-Coulomb (MC), hardening soil (HS) and hypoplastic (HP) with

intergranular strain (IGS) delivered reasonably a similar trend. However, it can be seen that using hypoplastic soil model without activating the intergranular strain generates an increase in the observed displacement of pile head with time. Since the stress wave induced by the hammer impact dissipates, then it is not expected that the displacement to increase significantly. It is crystal clear that HP model with IGS activation yields much less strain compared to the case when the IGS is not applied. Because IGS concept simulates the small strain behaviour, which is dominant during the pile driving.

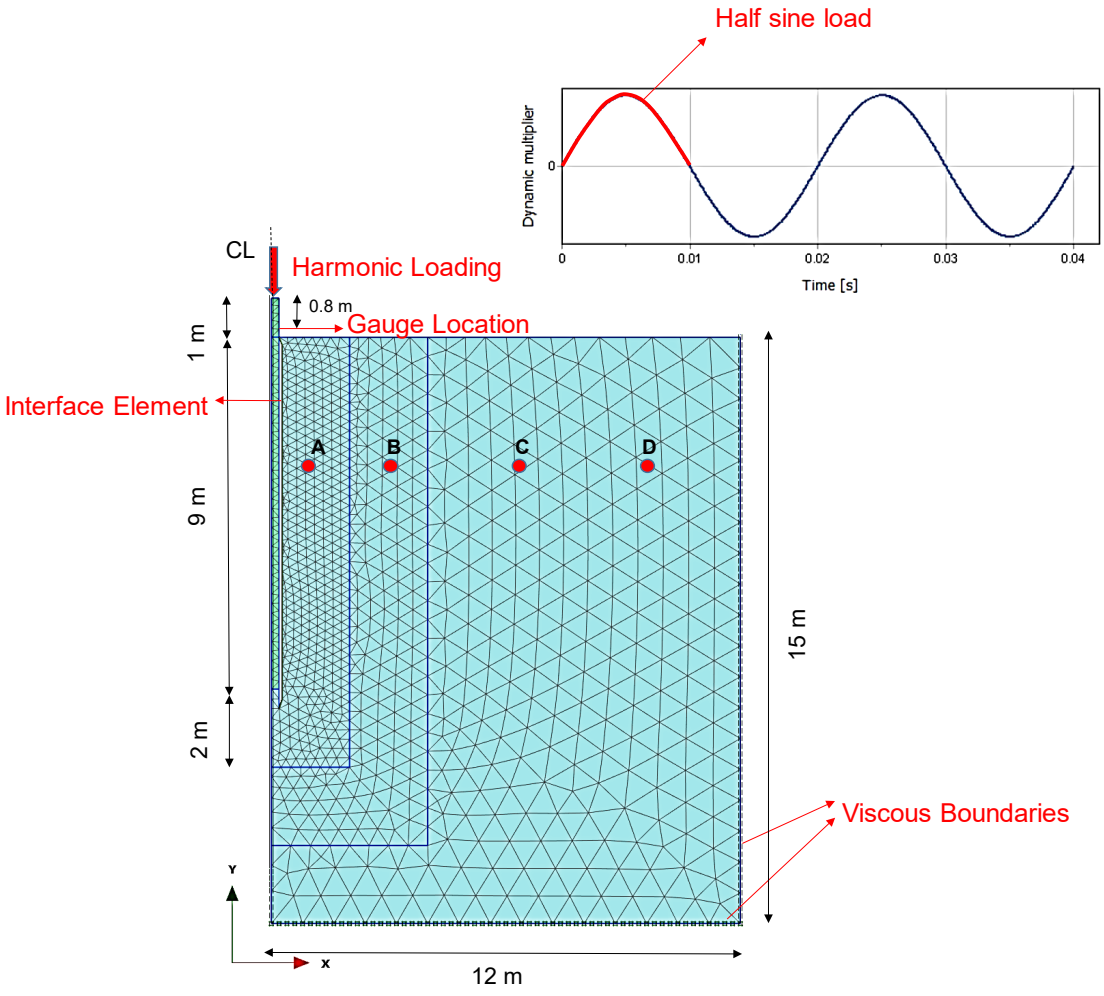

Figure 5.1 Finite element model of the pile, applied harmonic load and the adjacent ground with the corresponding generated mesh and points A, B, C and D and their corresponding radiuses r_A=1m, r_B=3m, r_c=6m and r_D=9m

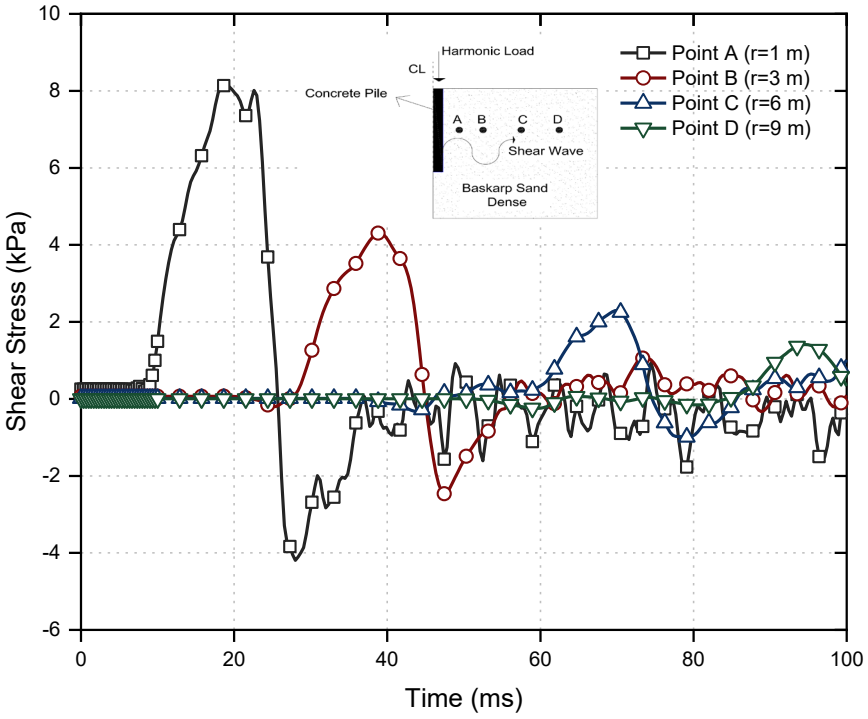

(a)

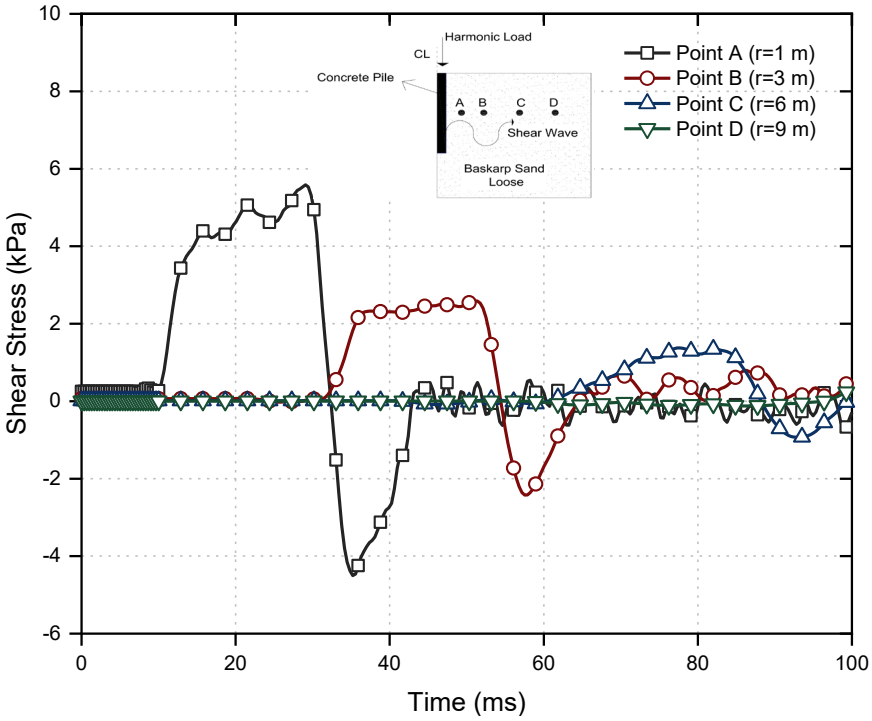

(b)

Figure 5.2 Variation of shear stress in soil at different distances from pile shaft, (a) dense sand, and (b) loose sand (Hardening Soil model)

In fact, the response of a pile during driving consists of loading and rebounding and unloading stages, where the loading stage begins from the time (t_1) corresponding to the first peak in force and velocity traces to $t_2 = t_1 + {}^{2L}/_{c}$, and afterwards is called the unloading stage (Ng 2011; Ng et al. 2013). Considering that the impact time is 10 ms (with a load frequency of 50 Hz) and ${}^{2L}/_{c}$ (L is pile length below the gauge and c is wave speed which is 3600 m/s for concrete piles) is equal to 5 ms, therefore, it is expected that after around 15 ms the unloading stage begins. This finding is in a very good agreement with the observed displacement traces shown in Figures 5.3a-b.

The recorded velocity at the gauge location ($v(t)$) multiplied by the impedance (Z) of the pile is shown in Figure 5.4. As shown in Figure 5.4, velocity traces predicted by different soil models have a reasonable agreement. However, hypoplastic model without considering IGS could not simulate the dissipation of velocity with time. As explained earlier, due to the small strain behaviour, observed during driving, by incorporating the intergranular strain (IGS), a more reasonable response and predictions have been achieved. Force and velocity×impedance traces, recorded at the gauge location, are compared in Figure 5.5. Referring to proportionality concept, it is expected to observe a reasonable correlation between force and velocity×impedance traces particularly before the first peak of both curves. However, as illustrated in Figure 5.5, some discrepancies can be observed. This is mainly attributed to the long stress wave period assumed for the hammer impact, which causes overlapping between the incident and reflected waves within the observation time. For evaluating this wave overlapping effect, the frequency of loading increased from 50 Hz to 250 Hz. As shown in Figure 5.6, and the half sine period or impact time decreased to 0.002 s. The corresponding force and velocity×impedance traces were recorded and shown in Figure 5.7.

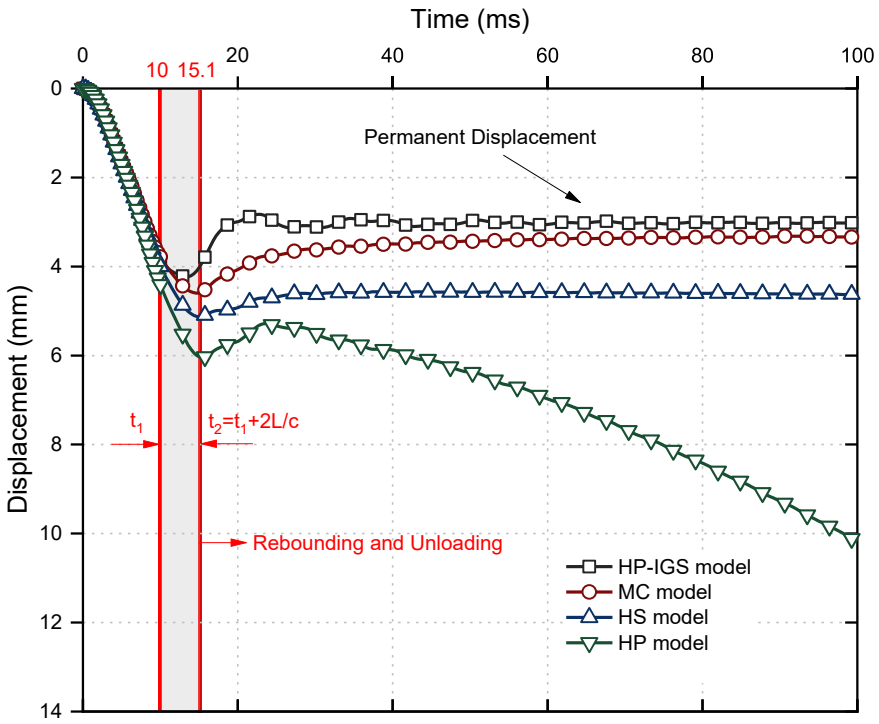

(a)

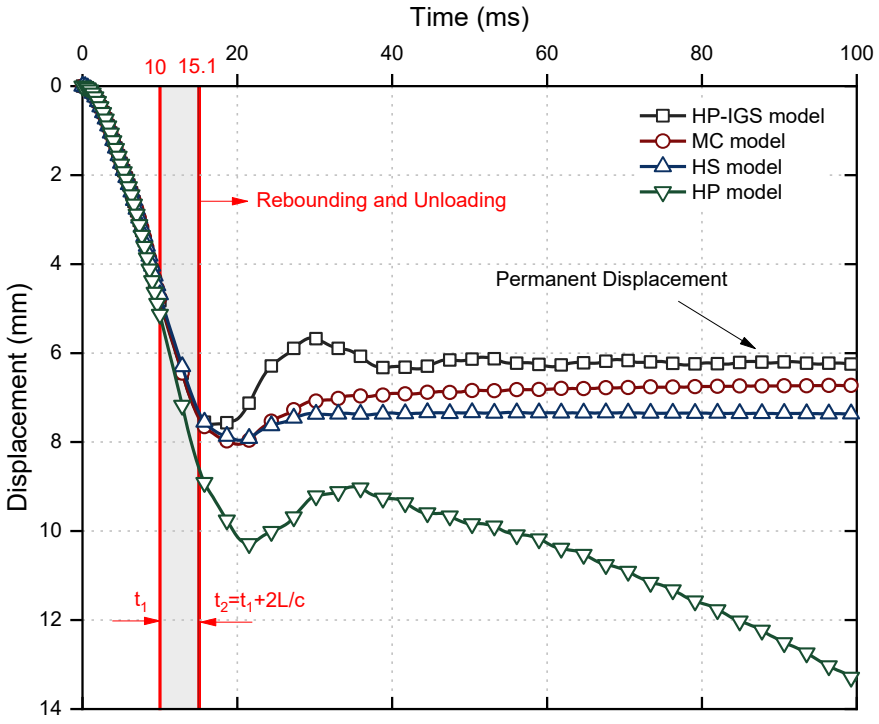

(b)

Figure 5.3 Pile head displacement (a) dense sand and (b) loose sand

Figure 5.7 shows that by increasing the impact load frequency to 250 Hz, the force and velocity traces show reasonable correlations before the first peak (corresponding to t_1) because decreasing the impact time reduces the length of the induced compressive wave. As explained by Lowery et al. (1969), after the hammer impact the induced compressive stress wave travels downward until it reaches the pile toe and depending on soil resistance the induced wave will be reflected back up the pile as the compressive or tensile wave. If the toe is experiencing no resistance from the soil (in very soft driving conditions), the induced compressive wave will be reflected back up the pile as tensile wave which may overlap with the induced downward wave.

However, at very hard driving conditions, the downward induced compressive stress wave will be reflected back up the pile as a compressive stress wave and these two stress waves may overlap. During the driving of short piles (compared to the length of the stress wave) into the soft soils (very soft driving conditions) the reflected tensile stress wave overlaps with the induced downward compressive stress wave, and will cancel each other at the toe and hence little or no wave will be reflected. Moreover, the length of the stress wave induced by ram impact can be calculated by the following equation:

$$L_s = ct_s \tag{5.2}$$

where,
L_s = the length of stress wave (m)
t_s = the time of ram contact (impact time) (s)
c = the velocity of stress wave (m/s) (3600 m/s for concrete piles)

By applying a load with a frequency of 50 Hz (the contact time of hammer and pile is regarded as 0.01 s) the compressive stress wave in a 36 m pile is much longer than the pile, but when the frequency of loading increases to 250 Hz (the contact time of the

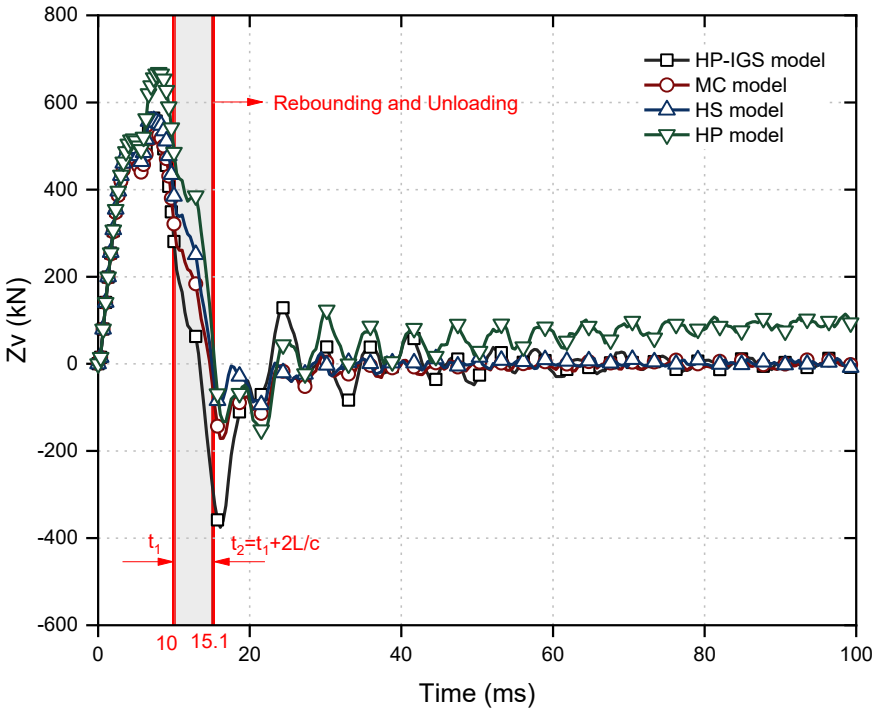

(a)

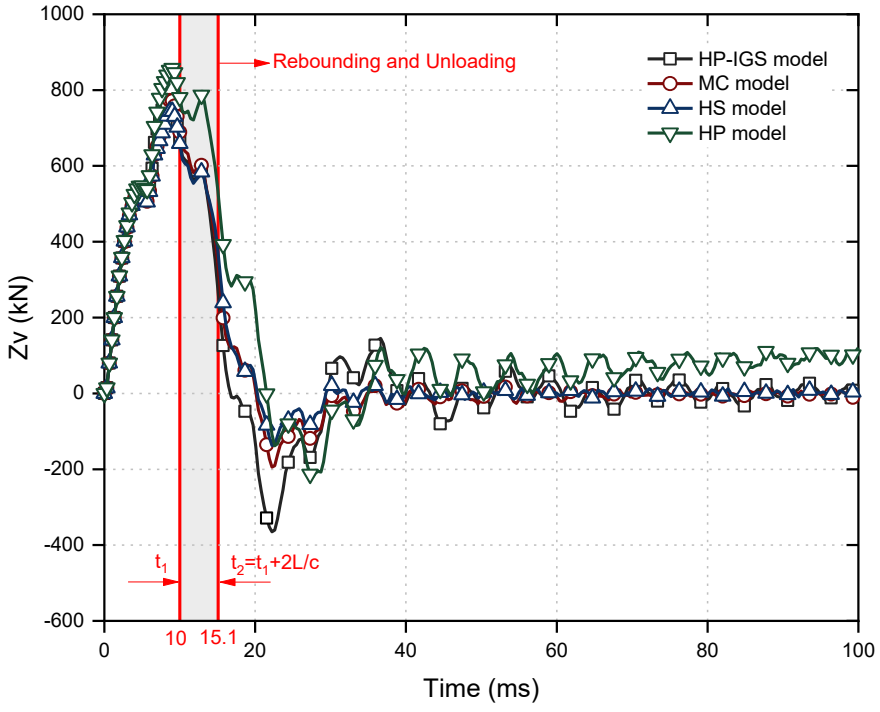

(b)

Figure 5.4 Impedance × Velocity variation with time, recorded at the gauge location for (a) dense sand, and (b) loose sand

hammer and pile decreases to 0.002 s) the corresponding stress wave would be 7.2 m long, which is shorter than the pile.

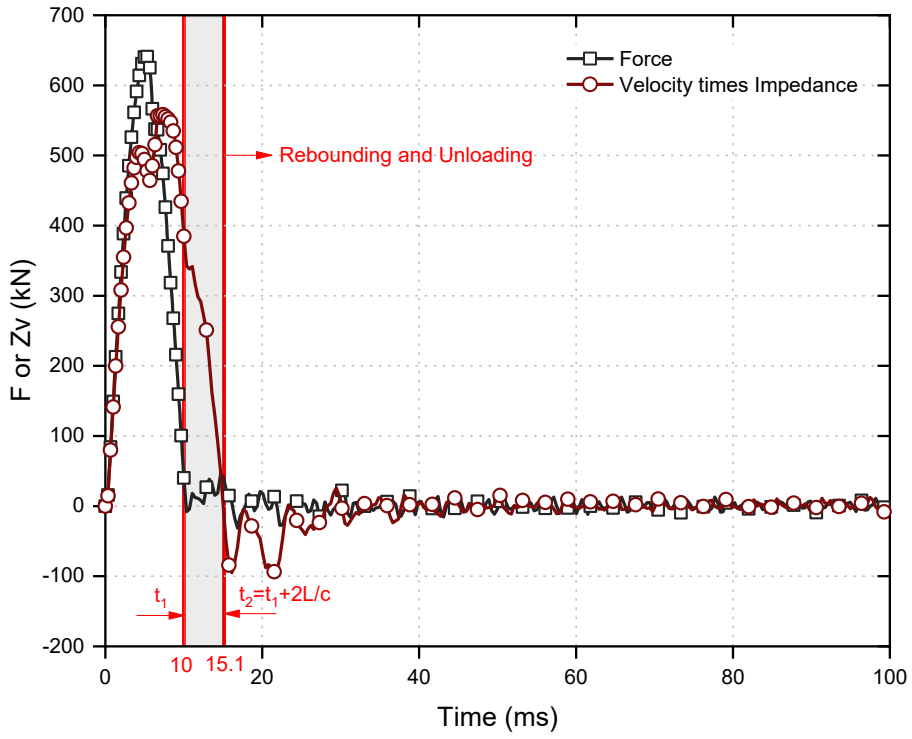

Figure 5.5 Velocity × impedance and force traces, recorded at the gauge location using Hardening Soil model for dense sand by applying harmonic loading with a frequency of 50 Hz

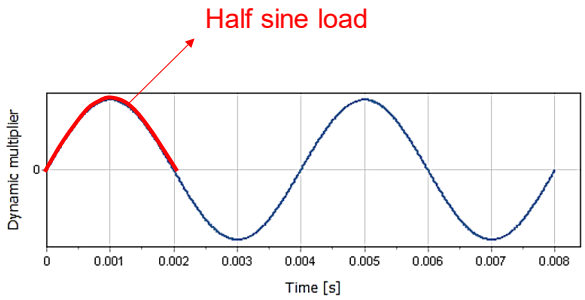

Figure 5.6 Applied harmonic load with a frequency of 250 Hz

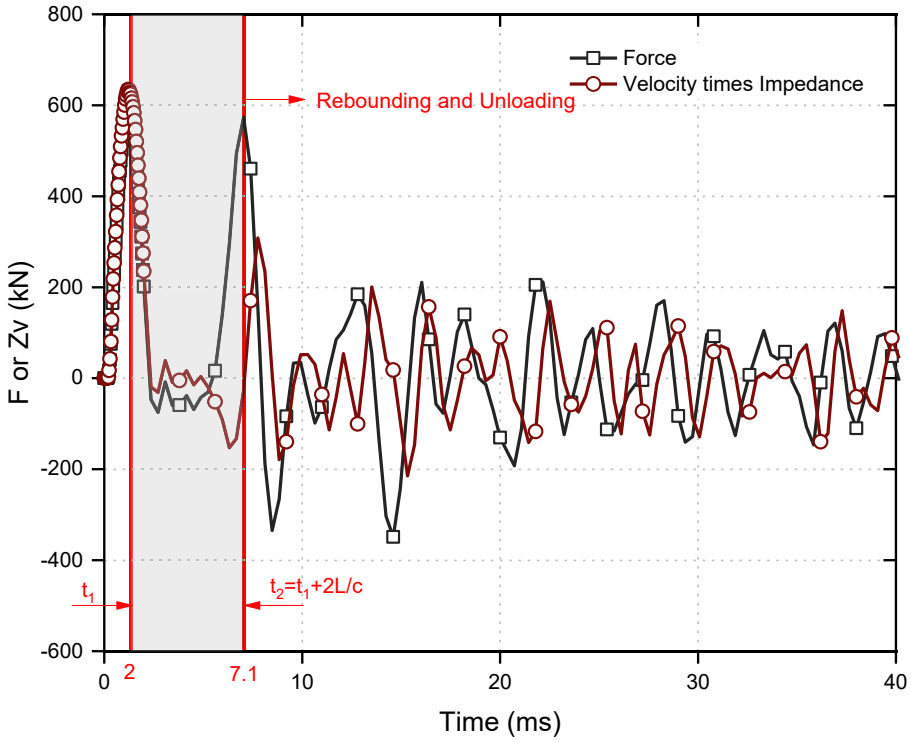

Figure 5.7 Velocity × impedance and force traces, recorded at the gauge location using Hardening Soil model for dense sand by applying a harmonic load with a frequency of 250 Hz

Referring to Figure 5.7, at time t_2 (the time corresponding to travelling down the wave and reflecting from pile toe to the gauge location) the force trace is negative and velocity×impedance is positive, which resembles the reflection of tensile stesss from the pile toe. In reality, the pile tip is driven into a sandy soil layer having a high densification potential during the driving process. According to study conducted by Yang (2006), the influence zone of an axially loaded pile in clean sand and compacted silty sand can extend to 3.5D–5.5D and 1.5D–3D (D is the pile diameter) below the pile toe, respectively. However, in the current study the properties of soil below the toe were not changed and basically assumed to be equal to the initial values of the in-situ conditions. Thus, the pile toe showed a rather low resistance against penetration causing the reflection of tensile stresses.

In addition, the influence of different paramters, defined in the hypoplastic model with the intergranular strain concept on the obtanied pile head displacement during the pile driving is evaluated (considering load frequency 50 Hz). As elaborated in Chapter 3, among the hypoplastic model parameters, the granular hardness (h_s) showed the least impact, whereas the critical friction angle (φ_c) indicated the most significant influence on the load-displacement curve, obtained during the simulation of static load testing. Herein, the effect of these two parameters are evaluated on the recorded pile head displacement during pile driving. To achieve this aim, the critical friction angle increased by 30%, while other hypoplastic factors remained unchanged. As shown in Figure 5.8a, similar to the observed results during static load test, increasing the critical friction angle shows a considerable effect on the recorded displacement. As shown in Figure 5.8a, a suitable way to determine the value of φ_c is measurement of the angle of repose φ_{rep}. Referring to Figure 5.8b, increasing the granular stiffness (h_s) by up to 30% does not show any notable influence on the predicted displacement. In fact, any proportional compression test can thus be used for the determination of h_s; and an oedometric test is known to be the most easiest test to perform. As shown in Figure 5.8b, h_s controls the overall slope of compression curve.

The sensisitivity of the simulated response of the recorded pile head displacement during driving to the varaition of Intergranular Strain paramters are shown in Figures 5.9a-b. In fact both parameters β_r and χ control the shape of stifness degradation curves (Mašín 2015, Niemunis & Herle 1997). Referring to Figure 5.9a-b, it can be inferred that by increasing χ and decreasing β_r the elastic range of stiffness degradation curves increases, and, hence pile head displacement shows more elastic deformation (i.e. shows less permanent displacement).

Finally, the normalized intergranular strain tensors defined in hypoplastic model with IGS concept are depicted in Figures 5.10a-b for dense sand and loose sand at the end of the driving (unloading conditions), respectively. According to Mašın (2010) the normalised length of the intergranular strain tensor changes between 0 and 1, corresponding to the soil being inside the elastic range and swept-out of the small-strain memory, respectively. In other words, the normalised length of the intergranular strain tensor indicates in different parts of the modelled geometry how the small-strain stiffness is activated. The soil behaviour is controlled by the basic hypoplastic model if the normalised length of the intergranular strain being equal to 1. Figures 5.10a-b show that at the end of driving in the vicinity of the pile, the predicted values for normalized length of the intergranular strain tensor are mostly very low and at these locations the soil elements behave elastically and show small strain behaviour. In addition, it is observed that dense sand shows more elastic behaviour compared to loose sand. This clearly indicates the presence of the small strain behaviour of soil around the pile during the propagation and dissipation of the induced wave in the pile.

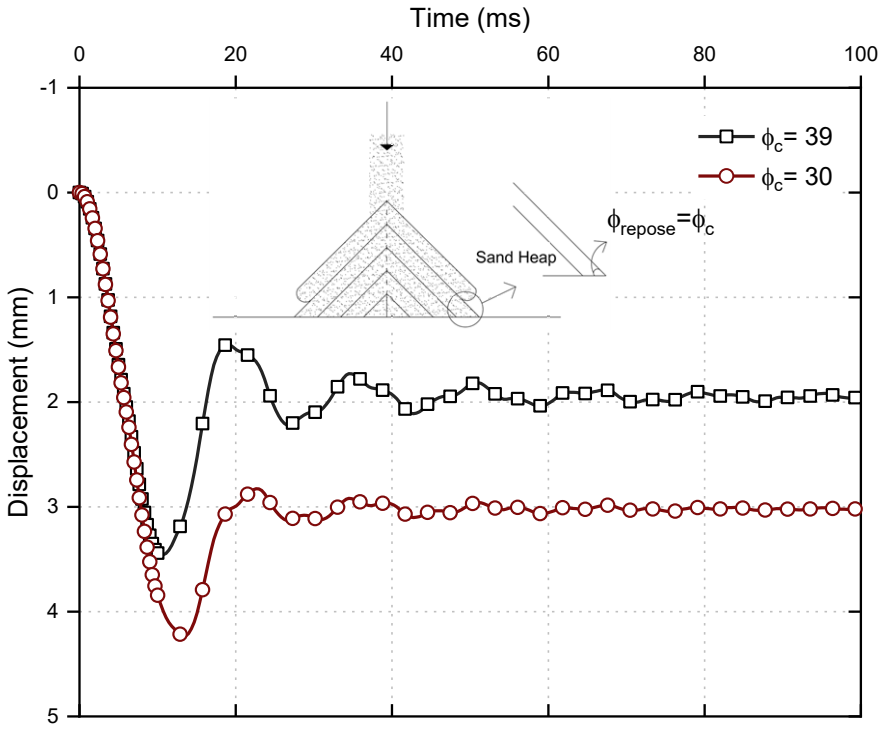

(a)

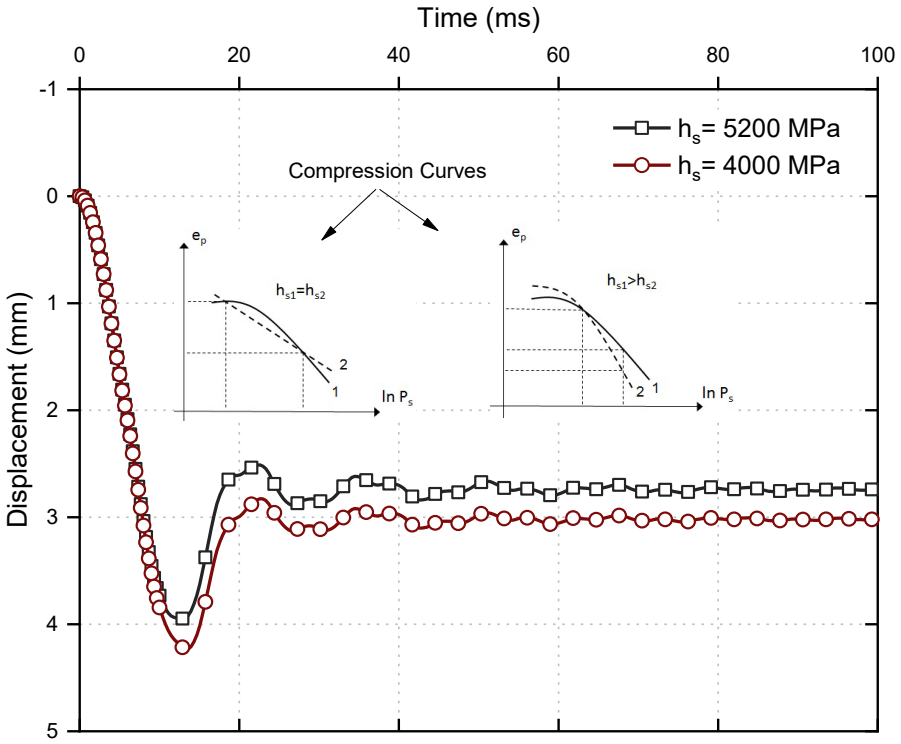

(b)

Figure 5.8 Influence of Hypoplastic model parameters on the measured pile head displacement during the pile driving in dense sand (a) critical friction angle, and (b) granular hardness

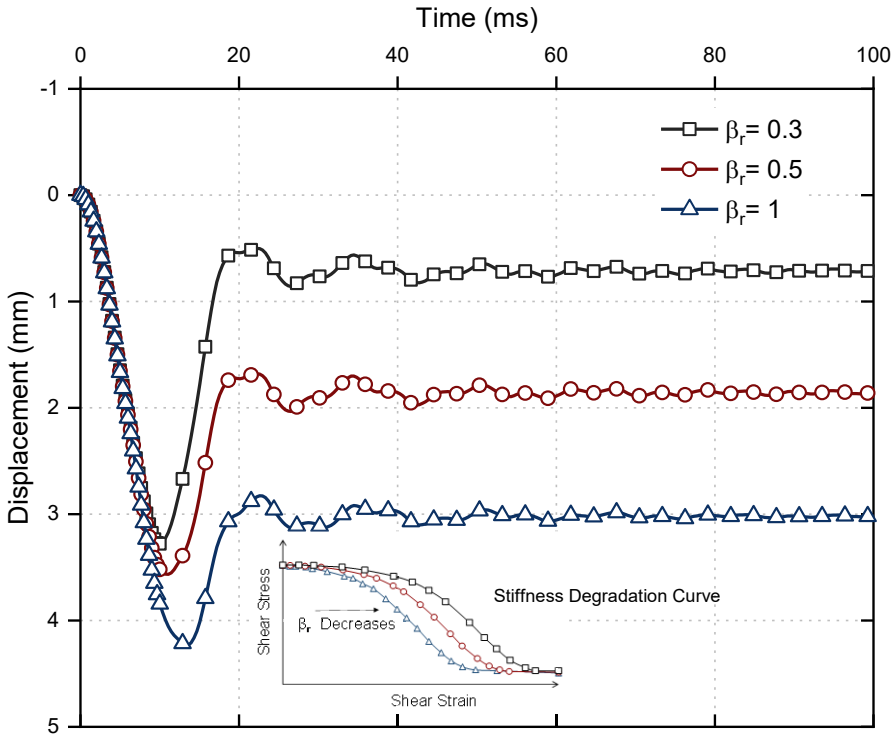

(a)

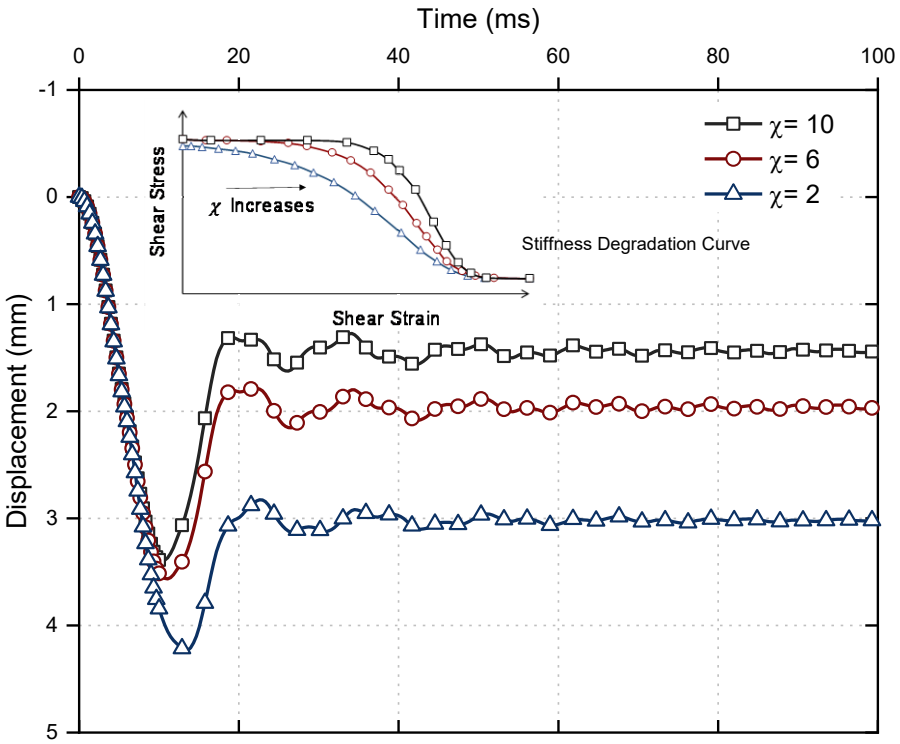

(b)

Figure 5.9 Influence of Intergranular Strain parameters defined in Hypoplastic model on the measured pile head displacement during the pile driving in dense sand (a) β_r and (b) χ

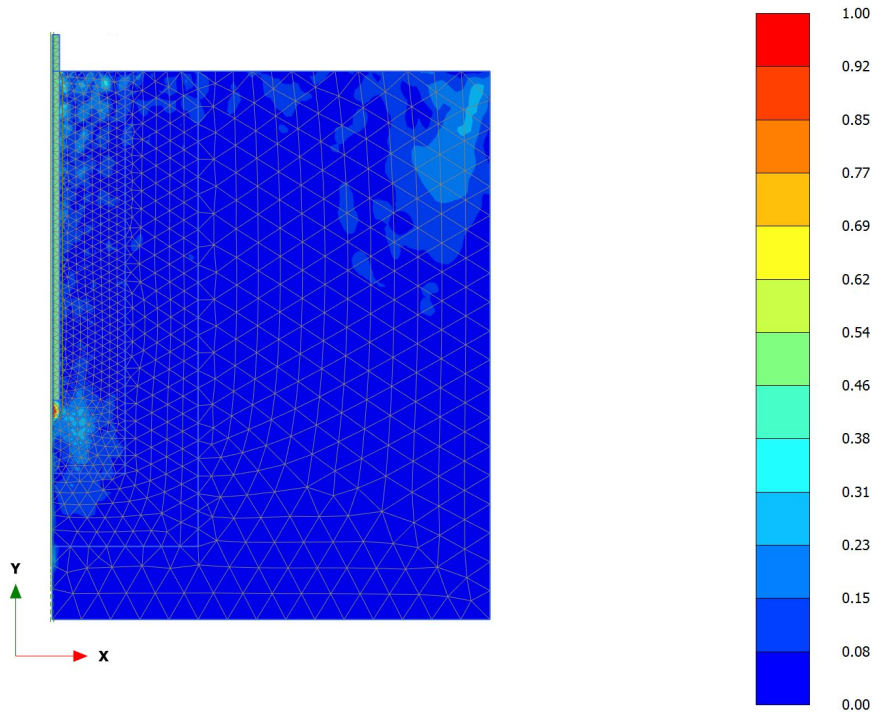

(a)

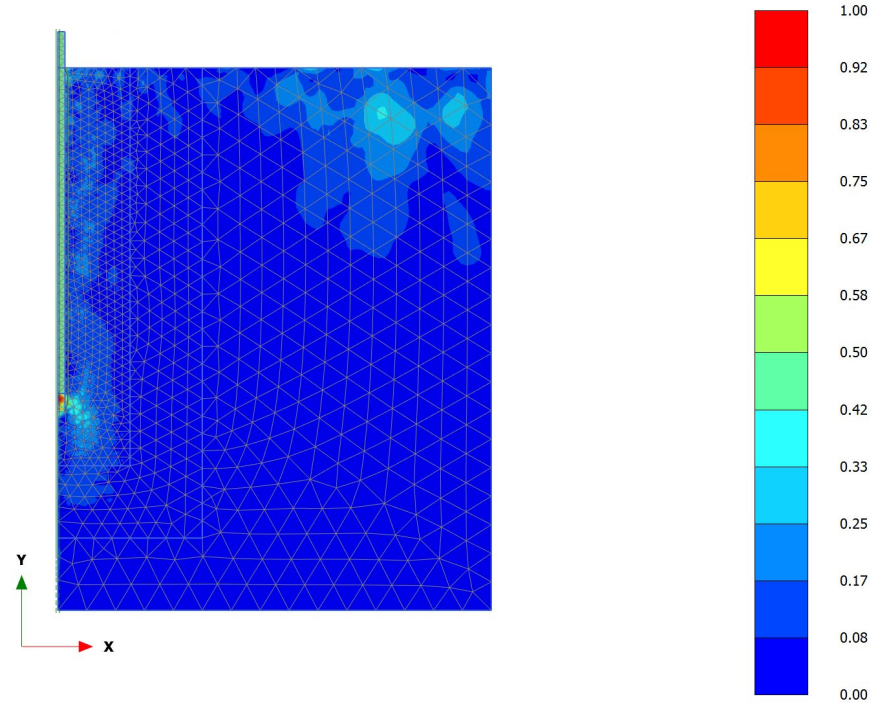

(b)

Figure 5.10 Concrete pile driving – normalised intergranular strain tensor for (a) dense sand, and (b) loose sand

5.5 One-dimensional Wave Propagation in Finite Element Program

5.5.1 Overview

In this section, to verify PLAXIS 2D capabilities in wave propagation modelling, an elastic rod (without any soil resistance) with two different toe conditions: (1) fixed-end pile (2) elastic support at the end, as explained by Masouleh & Fakharian (2008) is simulated. Figure 5.11 shows the schematic configurations of these two rods and the applied harmonic load.

At the first step, the fixed-end rod was simulated in finite element program based on the properties, given in Table 5.1. The hammer impact on the rod head was simulated by a half-sine stress wave with an amplitude of 5 MPa and a frequency of 320 Hz. In order to avoid the overlapping the upward and the reflected downward stress waves at the rod head, velocity was recorded at 5 m below the rod head. In addition, horizontal fixities were assigned to vertical boundaries in simulation of rods in the program.

Table 5.1 Properties of the circular rod used in the model

$L\ (m)$	$D\ (m)$	$E\ (MPa)$	υ	$\gamma\ (kN/m^3)$
20	0.5	25000	0.15	25

Figure 5.12a illustrates the variation of Zv (where Z denotes the impedance and v is the velocity) with time for the case of fixed end rod. Impedance (Z) can be defined as $\frac{EA}{c}$, where E is the pile elastic modulus, c is the longitudinal wave speed travelling though the pile material, A is the pile cross sectional area. Based on one-dimensional wave propagation concept in rods, after the compressive wave reaches to the fixed-end of the rod it will be reflected as a compressive wave, and the direction of the velocity will change to upward. Based on the sign convention (downward is positive) it shows a negative

velocity at the pile head, and after reflection at the free head of the pile the compressive wave is converted to the tensile wave and again the direction of the velocity would be upward. This process is shown in Figure 5.12a. It is evident that PLAXIS software is capable of capturing this process. Referring to Figure 5.12b, when the elastic modulus of the base approaches to a low quantity ($E_s = 10\ MPa$) the behaviour of the rod becomes similar to free end rod. In the free end pile (see Figure 5.12b), the incident compressive wave, which is travelling downward in the pile, is converted to tensile wave after reaching to the base. Therefore, during the circulation process, the direction of the velocity would be downward and positive.

5.6 Open-Ended Steel Pipe Pile Driven in Dense Sand Deposit

5.6.1 Overview

Byrne (1995) conducted a total of 15 field tests at a site in Shenton Park in Perth, Australia, consisting of dynamic and static tests on an open-ended steel pipe pile driven into dense sand was equipped by five different driving shoes. In this section, using continuum numerical modelling, the dynamic and static load testing of an open-ended pipe pile without any driving shoe (Pile BO6), is simulated and the results are discussed. The experimental pile consisted of a steel pipe pile with an external diameter of 51.1 mm, wall thickness of 1.6 mm and an overall length of 2.2 m, which force and velocity traces were capture at 200 mm below the pile head. This pile was driven into the ground using a 4 kg drop weight and pile penetration, plug penetration and the blow counts were measured during installation.

The dense sand in Shenton Park is part of the Spear-wood dune system, and comprises well graded medium to coarse quartz grains with traces of feldspar. The mean particle

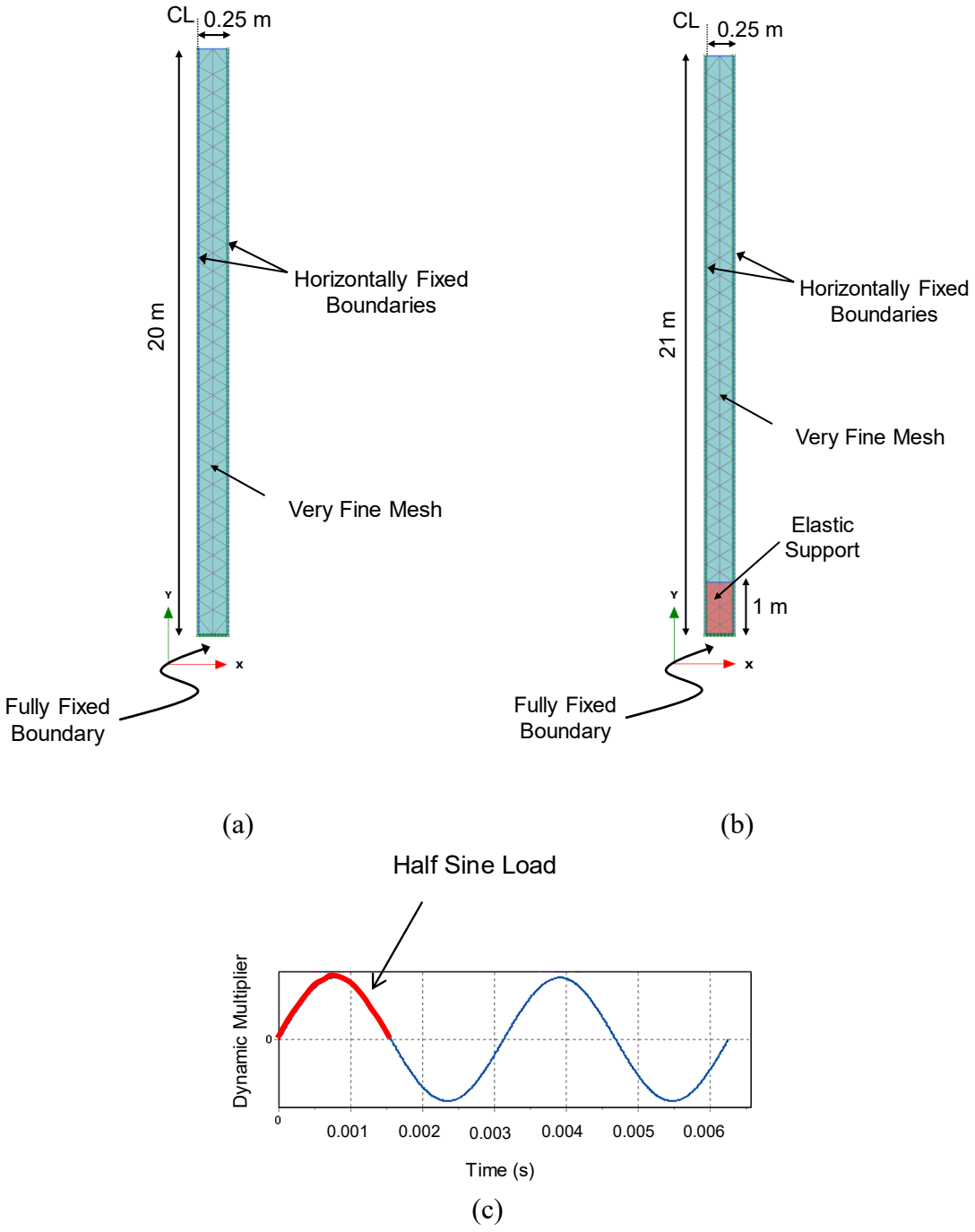

Figure 5.11 Rod with two different tip conditions (a) fixed-end (b) elastic support and (c) the applied harmonic load (afterMasouleh & Fakharian 2008)

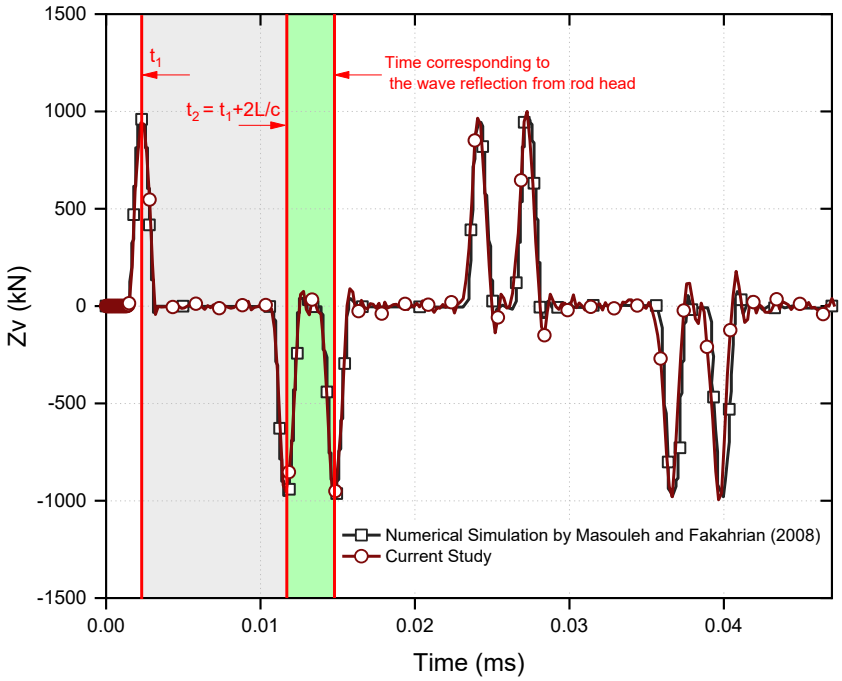

(a)

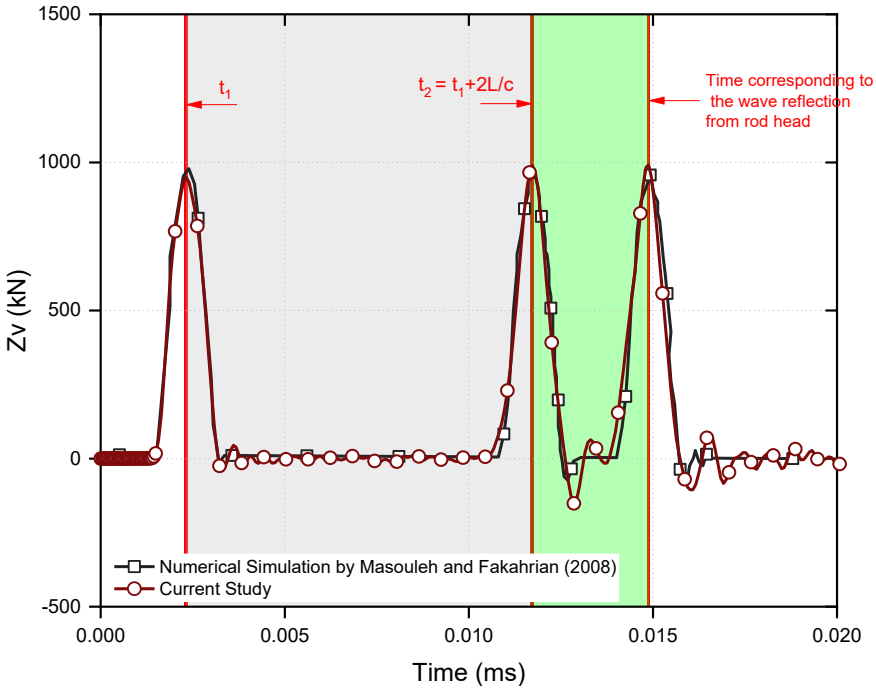

(b)

Figure 5.12 (a) Comparison of numerical results reported by Masouleh and Fakharian (2008) using FLAC 2D with PLAXIS 2D predictions conducted in this study: (a) fixed-end rod and (b) rod on elastic support (E = 10 MPa)

size of soil was $d_{50} = 0.5\,mm$, and the effective particle size range was between 0.15 mm and 1 mm. The pile tests were all conducted in the upper 2 m, which was well above the water table level. Detailed information on the experimental study and site investigation results have been reported and discussed in Byrne (1995), Byrne & Randolph (2003), and Klain (1993). The soil consisted of a dense sand with a cone profile, as shown in Figure 5.13. Based on the CPT results and the recommendations made by Das (2004) and Bowles (1996), soil properties were selected and summarized in Table 5.2.

In this part, using an axisymmetric numerical model built in finite element program, dynamic load testing of Pile BO6 for blow No. 2 at the penetration depth of 1700 mm was simulated. It is worth mentioning that herein only one blow at the end of driving (1700 mm penetration) has been simulated and the whole driving procedure has not been modelled. The simulation of this blow on the pile-soil system was conducted by applying a force trace recorded at the gauge location (referred to the force function) on the pile head. General geometry of the model were taken from the experimental study, and then the pile-soil interface parameters were adjusted to achieve a reasonable comparison between the numerical predictions and the test data. During the numerical simulation, Mohr-Coulomb model was assigned to the soil cluster. Finite element axisymmetric model is depicted in Figure 5.14.

5.6.2 Results and Discussion

Figure 5.15 presents the force (F) and Zv measured by the strain gauges and accelerometers near the pile head, respectively, as well as the Zv computed through numerical analyses using the FE model. Since the difference between F and Zv indicates the magnitude of shaft resistance, these traces are shown together in the figures. The

measured force (F) wave versus time (the force function) was applied as an input loading at the gauge location near the pile head while the soil parameters were defined as reported in Table 5.2. Then Zv values against time at the same location are traced and compared to the measured Zv. After that the interface parameters around the pile shaft were adjusted in an attempt to acquire a better match between the computed and the measured Zv results. The strength reduction factor (R_{int}) is regarded as the main interface parameter, which considers the strength reduction of the interface element in the respected soil layer according to Equations (5.3), (5.4) and (5.5):

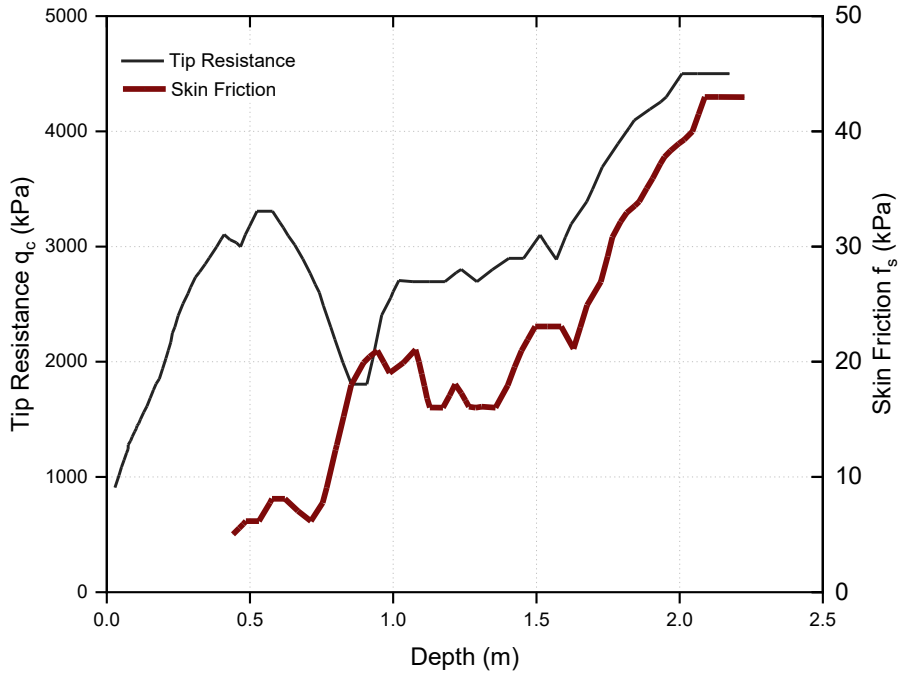

Figure 5.13 Cone penetrometer results for the site at Shenton Park (after Byrne 1995)

Table 5.2 Properties of dense sand in Shenton Park

$\gamma\ (^{kN}/_{m^3})$	$c\ (kPa)$	$E\ (kPa)$	ν	$\phi\ (degree)$	$\psi\ (degree)$
21	0	45000	0.35	40	10

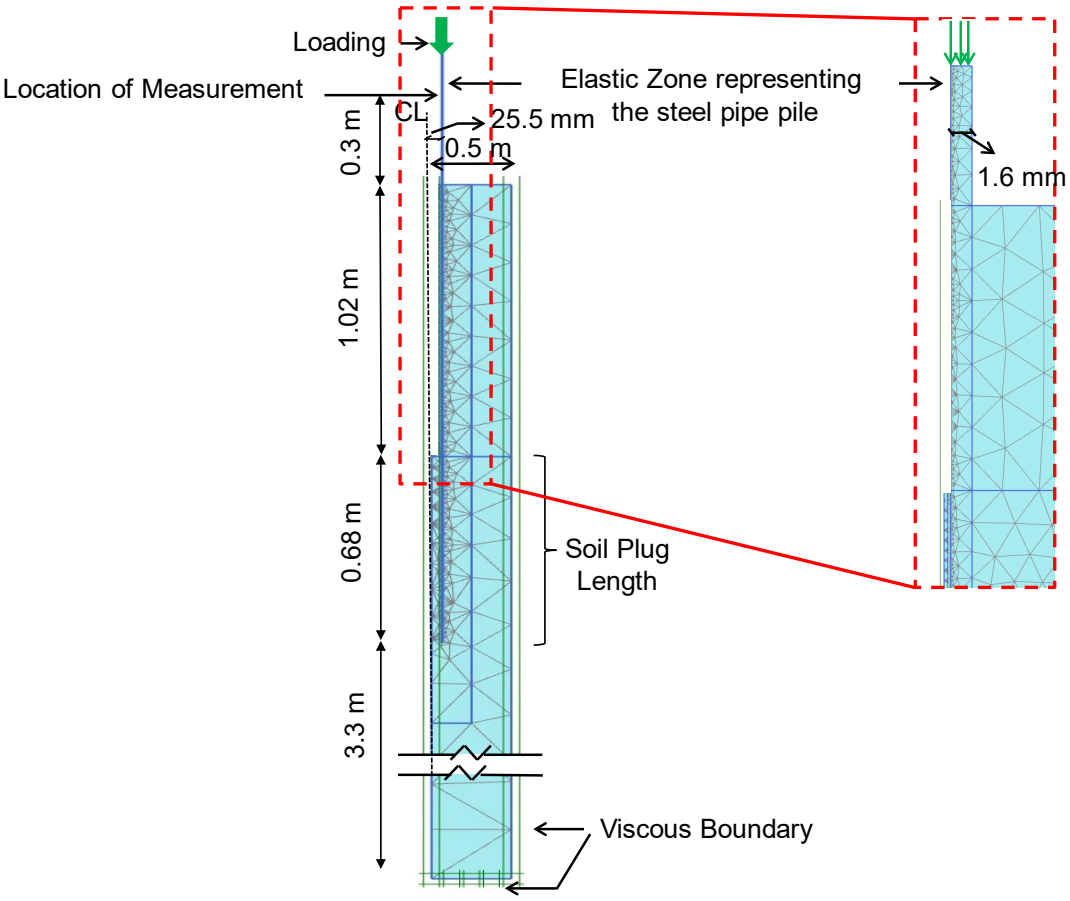

Figure 5.14 Finite element model of the pile and the adjacent ground with the corresponding generated mesh

$$C_{int} = R_{int} \times C_{soil} \tag{5.3}$$

$$\tan(\varphi_{int}) = R_{int} \times \tan(\varphi_{soil}) \leq \tan(\varphi_{soil}) \tag{5.4}$$

$$G_{int} = R_{int}^2 \times G_{soil} \tag{5.5}$$

In the parametric study, the interface and the associated Rayleigh damping parameters were changed (as shown in Figure 5.15a). The Rayleigh damping factor has a numerical specification, in which the damping matrix, C, consists of two parts, including the mass matrix, M and the stiffness matrix, K, according to Equation (5.6):

$$C = \alpha M + \beta K \tag{5.6}$$

The parameters α and β are the Rayleigh coefficients. The sensitivity analysis indicated that mainly the Rayleigh damping parameter β (the influence of stiffness in the damping) could affect the results notably. Results of the current study indicate that an interface reduction factor (R_{int}) of 0.8 and $\beta = 10^{-4}$ resulted in the most reasonable match, as shown in Figures 5.15a-b. According to Figure 5.15, it can be seen that at time t_1 (the first peak of force and velocity trace) the computed and measured Zv values correlate very well. Figure 5.16 represents the calculated displacement of pile head under the hammer impact. As can be observed, permanent displacement of pile head after allowing the effect of the blow on the system to subside is obtained 2 mm, while the maximum displacement (DMX) recorded is around 2.8 mm. The difference between the maximum displacement (the temporary displacement) and the permanent displacement is known as the elastic displacement. Variations of the maximum compressive stress and maximum tensile stress in the pile with depth are illustrated in Figures 5.17a-b, respectively. According to the sign convention, the compressive stress is regarded positive, while the tensile stress is negative. After simulating the dynamic load testing, in order to find the bearing capacity of the pile, the simulation of static load test was carried out using the parameters obtained from the best match (i.e. $R_{int} = 0.8$). In the experimental study, static load test was performed by steadily jacking the pile into the ground and recording load and displacement data points. The field measurement and numerical predictions of displacement of the pile head under static load testing are compared in Figure 5.18. As observed, the numerical predictions are in a reasonable agreement with the field measurements in the range of loads, reported in Figure 5.18.

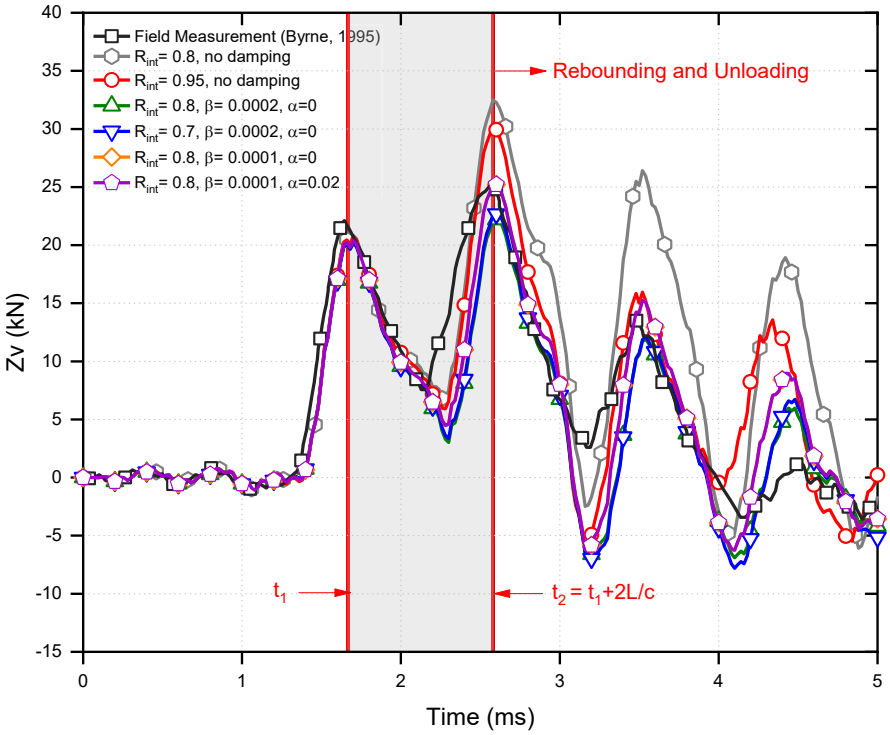

(a)

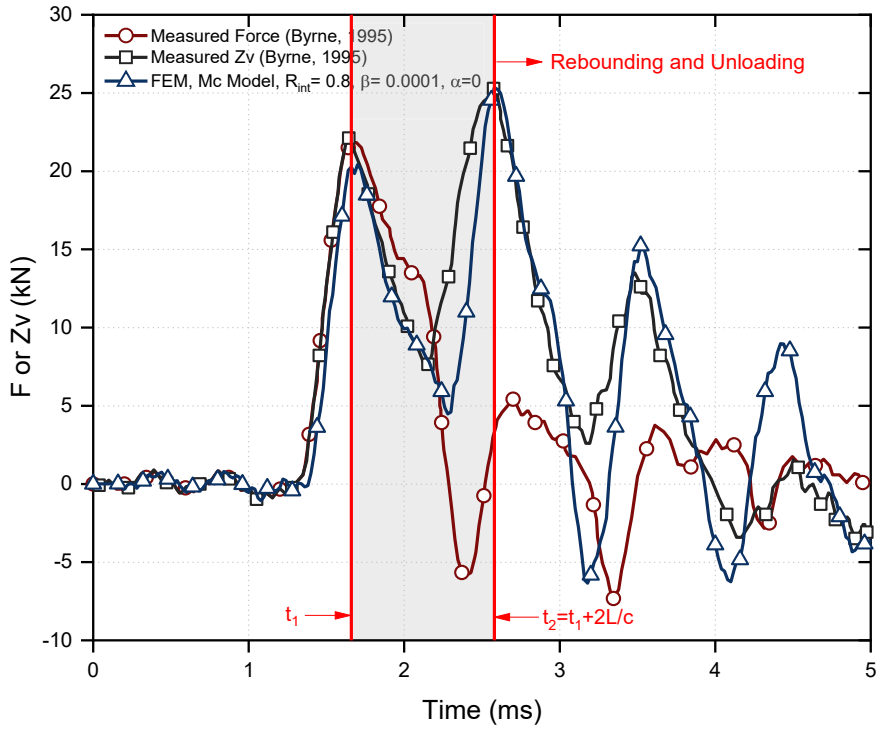

(b)

Figure 5.15 Measured force with time and numerical predictions, (a) the effect of different parameters on signal matching and (b) the best match obtained

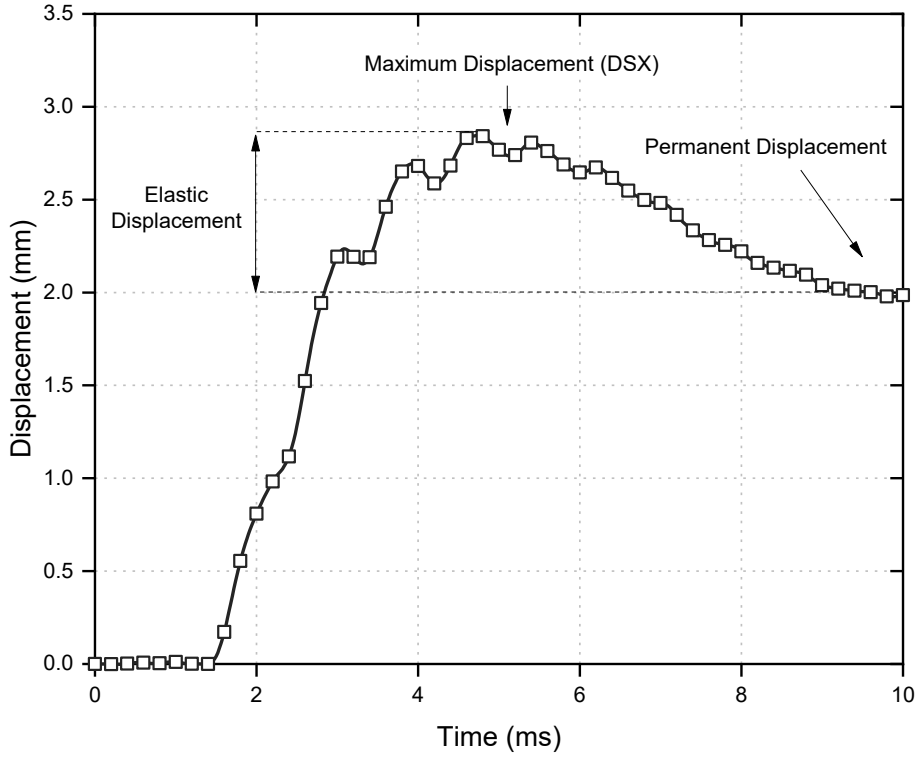

Figure 5.16 Computed displacement at the pile head

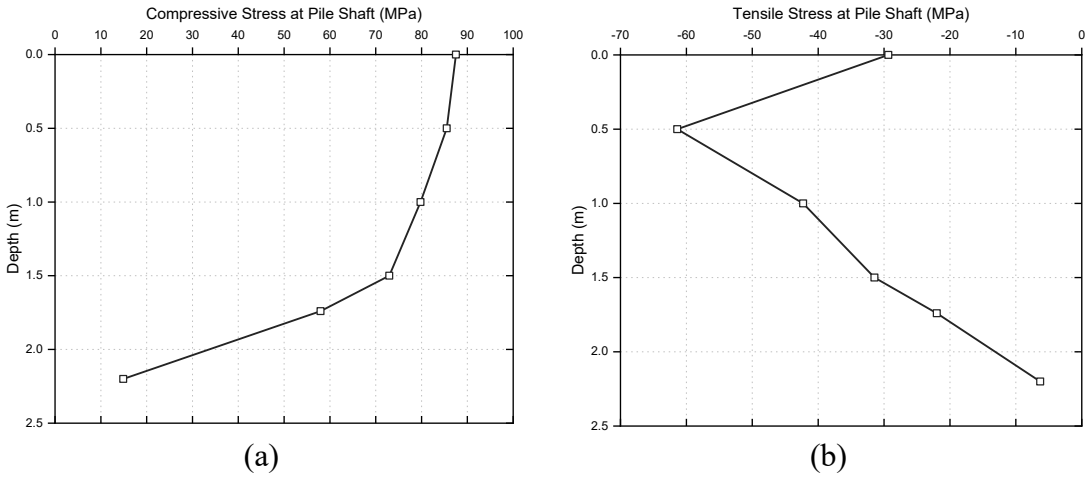

Figure 5.17 Maximum compressive (a) and tensile stresses (b) distribution along the pile shaft

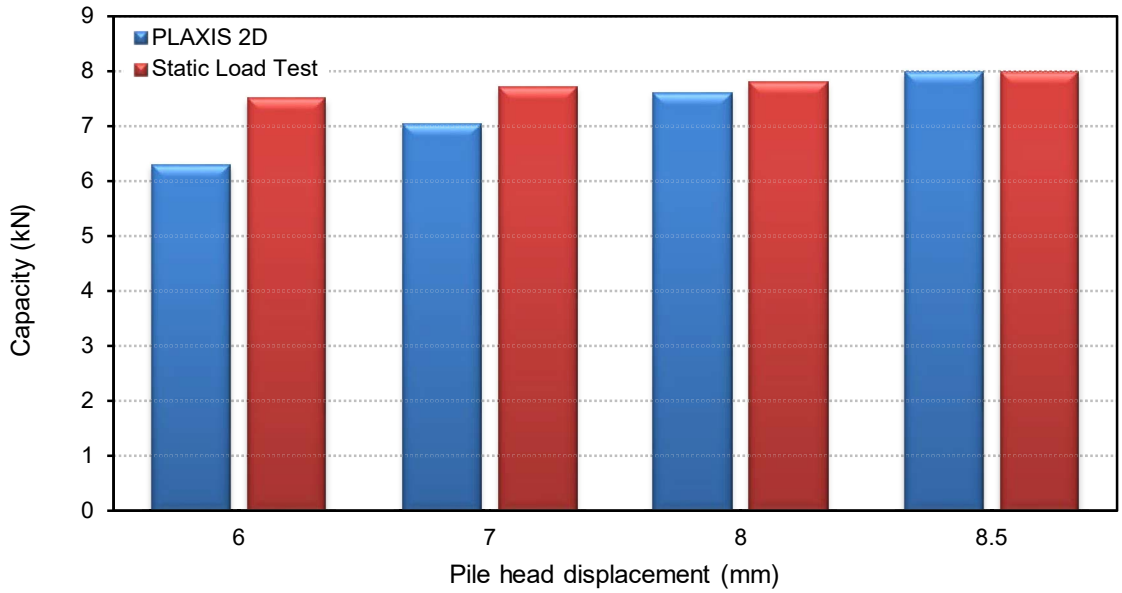

Figure 5.18 Comparison of measured and predicted pile load-displacement variation during static load testing

5.7 Open-Ended Steel Pipe Pile Driven in Multilayer Soil

5.7.1 Overview

In this section, a condition of dynamic load testing on a steel pipe pile at the end of driving (EOD) is simulated using hardening soil with small stiffness (HS-Small) in finite element software. Whilst small strain stiffness is well established for analysing small strain dynamics, a large strain modulus should be used while carrying out static and large strain analyses. Therefore, the aim of this section is to establish a continuum numerical model to obtain a reasonable match between measured and predicted results during static and dynamic loading conditions by utilising measured soil properties (not simply implementing the back calculated parameters). The field measurements are then compared with the numerical predictions and the verification exercise is followed; and thus settlements at the head and toe of a pile under a static load, applied on the top of the pile, is investigated numerically.

In fact when the behaviour of soil is simulated accurately, suitable constitutive models will capture the small strain (e.g. hysteretic damping) and large strain (e.g. irrecoverable deformations) responses, and when appropriate soil-pile interface elements and boundary conditions are utilised, continuum based numerical predictions (e.g. finite element methods) can be used to confirm the ground profile and verify the developed numerical model. Thus, the new verified numerical model can utilise meaningful soil-pile system properties that can then be used to assess the behaviour of piles under various structural loads or predict the total and differential settlements of foundations. In particular, the verified numerical model can also facilitate to assess the inner and outer shaft resistance of tubular steel piles as well as the plugging mechanism.

Obviously, when a simplified constitutive model is utilised to simulate the behaviour of soil during dynamic load testing, their parameters may need to be adjusted or back calculated (e.g. sometimes unreasonable adjustments would be required) so that the numerical predictions and field measurements of force-displacement traces will match. Indeed, any signal matching (e.g. CAPWAP) through back calculating/changing the model parameters may result in minimum disparities between predictions and measurements, however the reliability of adopted parameters due to simplicity of the model could be questionable, particularly if they are used to assess foundations under complex design loading. It can be noted that the signal matching technique (e.g. CAPWAP program) may not result in a unique set of back calculated soil-pile system parameters, and this could potentially lead to different pile load-displacements and predicted capacities.

An ideal model of a long pile passing through soil and founding on rock means that the extent to which the shaft contributes to its load carrying capacity depends on its relative

movement, which is a function of the relative stiffness of the shaft to the base (Coyle & Sulaiman 1970). Referring to Xu et al. (2011) and Gentile & Canceri (2011), steel pipe piles have been widely used in infrastructure projects in Australia. According to Grand (1970), among the different types of driven piles, steel pipe piles are preferred, because they can be driven through blockages to bedrock with minimum efforts and minimum displacement of soil. However, steel box piles are generally used when the foundation materials consist of cohesive soil underlain by a granular layer because the greatest possible skin friction area will develop along the pile and the point bearing area at the pile toe. As Han (1999) explains, steel pile foundations are used for many high-rise buildings, bridges, and offshore petroleum production platforms, as well as waterfront structures because unlike piles of other materials, steel piles are sturdy, light to handle, and can carry large compressive loads when driven into a stiff layer. In fact, they can be driven deep enough to reach a stiff layer or to mobilise a high shaft resistance, and they can be designed as small displacement piles. They are very resilient and offer high resistance to bending and buckling forces, and the pile head, which may buckle during driving, can be cut down for further driving. Steel pipe piles are also suitable for offshore structures because they can be manufactured in large diameters and driven in deep enough to resist the axial and lateral forces inherent in deep water structures (Spagnoli & Weixler 2013).

It is worth mentioning that the form of the driving shoe can influence the skin friction and toe resistance of the tubular piles. When the shoe has an extra thickness towards the inside of the pile, the internal friction of the pile would reduce as a result of shoe displacing the soil during the driving process. Therefore, presence of the shoe can influence the plugging mechanism of the tubular pile considerably. Indeed, the reduced internal skin friction induced by the driving shoe, may result in an increased driving length of the tubular pile

to achieve a fully plugged condition. Thus, practicing engineers need to be vigilant about effects of driving shoe when interpreting the results obtained from dynamic load testing and pile driving monitoring. Furthermore, similar to dynamic soil-structure interaction, it is recommended to consider variations of shear modulus and damping of the soil with shear strain during pile driving analysis.

This section utilises the as-constructed details and the results of dynamic load tests of steel pipe piles employed as a bridge foundation in a highway upgrade project in New South Wales, Australia. The respected pile has been chosen since the stratigraphy at that location is a reasonable representation of the ground conditions for most bridge piers in the project. In addition, at the location of the selected pile, a significant difference is observed between the design and as-constructed pile toe levels, while the driven length of the pile is quite short, which could make the foundation susceptible to differential settlement under structural loads.

Pile 11B, used in this study, is 28.10 m long steel pipe with an embedded length of 20 m, a diameter of 750 mm, and a wall thickness of 16 mm. A 1-m long by 25 mm thick driving shoe is used at the toe of the pile, and unplugged soil behaviour occurred during driving. The constraint modulus obtained by cone penetration test (CPT), and the seismic dilatometer (SDMT) and piezecone (CPTu) tests and shear modulus obtained by seismic dilatometer tests at the location of this pier are shown in Figures 5.19a and 5.20, respectively.

All the piers for this bridge consist of northbound piles (A and B) and southbound piles (C and D). The driving records show conclusively that they were all driven in to a nominal refusal that is defined as a maximum set of 13 mm/10 blows under a driving energy of 164 kJ. Dynamic pile testing has been carried out in accordance with Standards Australia

(1995). The force and velocity at the top of the pile were measured by four strain transducers and two piezoresistive accelerometers, and two piezoelectric accelerometers. The signals were processed by a Pile Driving Analyser (PDA) model PAX. Data were displayed on an LCD screen and digitally recorded on a computer disk for permanent storage, while the selected blows were digitised for more detailed analysis.

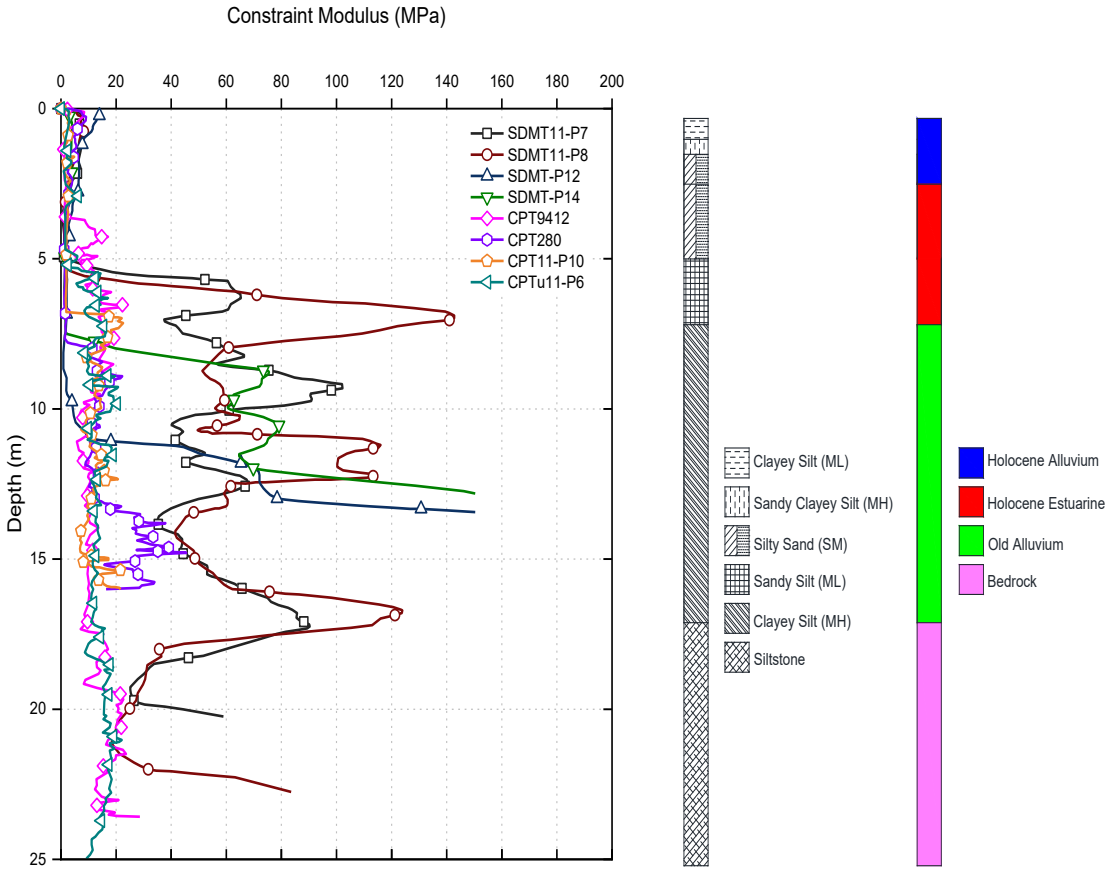

Figure 5.19 (a) Constrained modulus obtained through CPT, CPTu and SDMT tests (b) Soil stratigraphy at the location of pile 11B in terms of soil type, and (c) Soil stratigraphy at the location of pile 11B in terms of soil origin

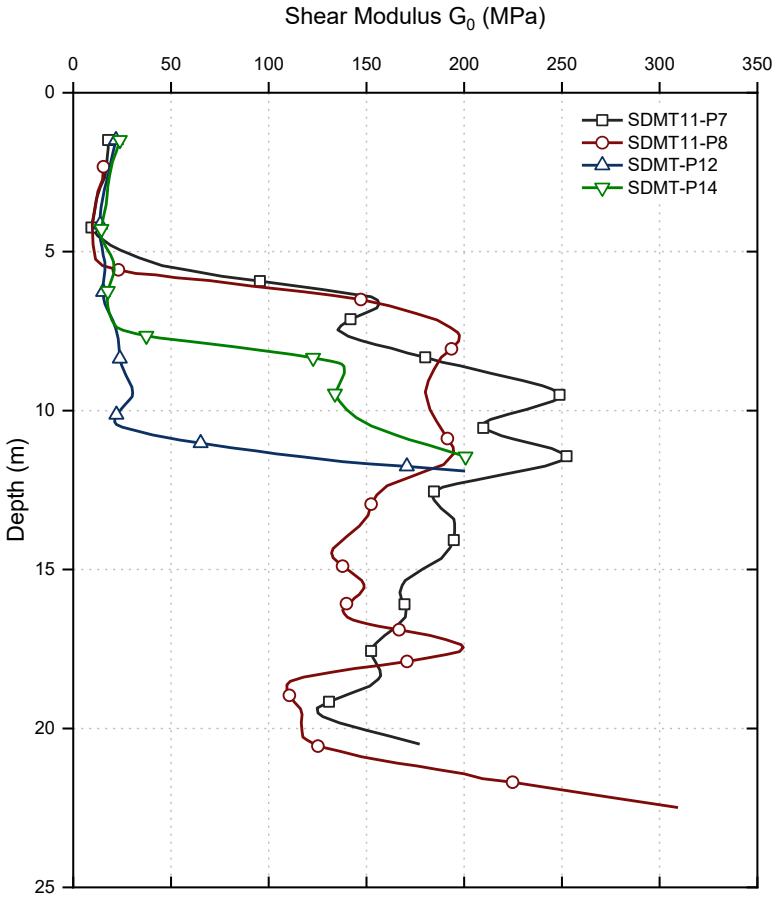

Figure 5.20 Shear modulus obtained from SDMT tests

The stratigraphy of soil at Pile 11B consists of different layers of soil that are classified as Holocene alluvium, Holocene estuarine, old alluvium, and weathered rock and bed rock, as shown in Figure 5.19c. In terms of the type of soil, the Holocene alluvium layer contains clayey silt, sandy clayey silt and silty sand; the Holocene estuarine layer contains silty sand and sandy silt; the old alluvium layer consists of clayey silt, and the weathered siltstone is located at the bottom layer, as shown in Figure 5.19b.

Since there were non-cohesive layers of soil (i.e. deposits of silty sand soil) around the shaft and weathered rocks near the toe, the possible excess pore pressure generated during pile driving would probably dissipate quickly. Accordingly, drained conditions and effective soil parameters were utilised in the numerical analyses. In this study the Mohr-Coulomb failure envelope parameters that include cohesion (c), the friction angle (φ), as

well as Poisson's ratio (υ) and the unit weight (γ) were deduced from the results of triaxial tests carried out at different depths; the selected results are reported in Figure 5.21. The Seismic Dilatometer Test (SDMT) and the Cone Penetration Test (CPT) results, reported in Figure 5.19, were utilised to obtain a secant stiffness modulus (E_{50}), correlated to the constraint modulus, as proposed by Cox & Mayne (2015) using Equation (5.7):

$$E_{50} \approx \text{MDMT} \tag{5.7}$$

where MDMT is the constrained modulus obtained from the seismic dilatometer test (SDMT). The stiffness degradation curves for various layers of soil along the length of the pile are reported in Figure 5.22. A summary of the soil properties for the HS Small constitutive model, extracted directly from the laboratory and field tests and implemented in the numerical modelling, are presented in Table 5.3.

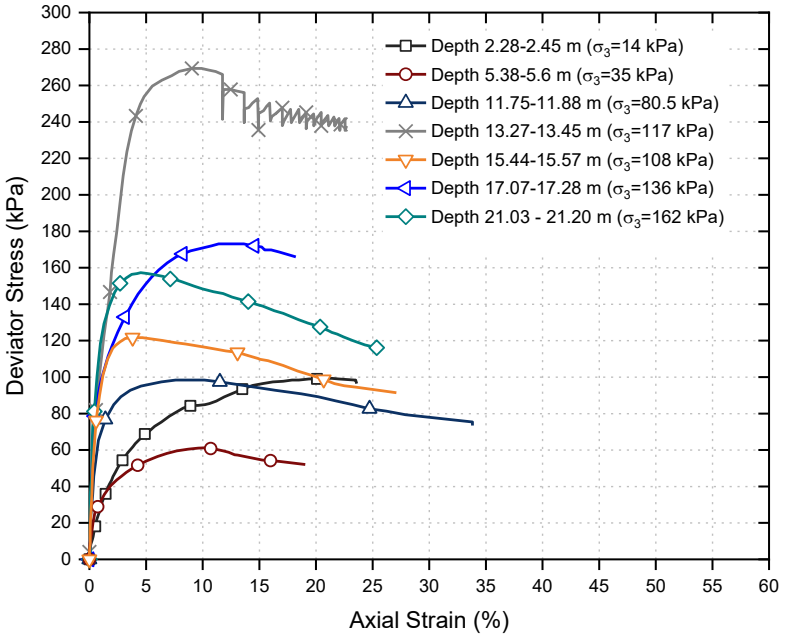

Figure 5.21 Stress-strain graphs obtained from triaxial tests conducted on samples taken from different depths

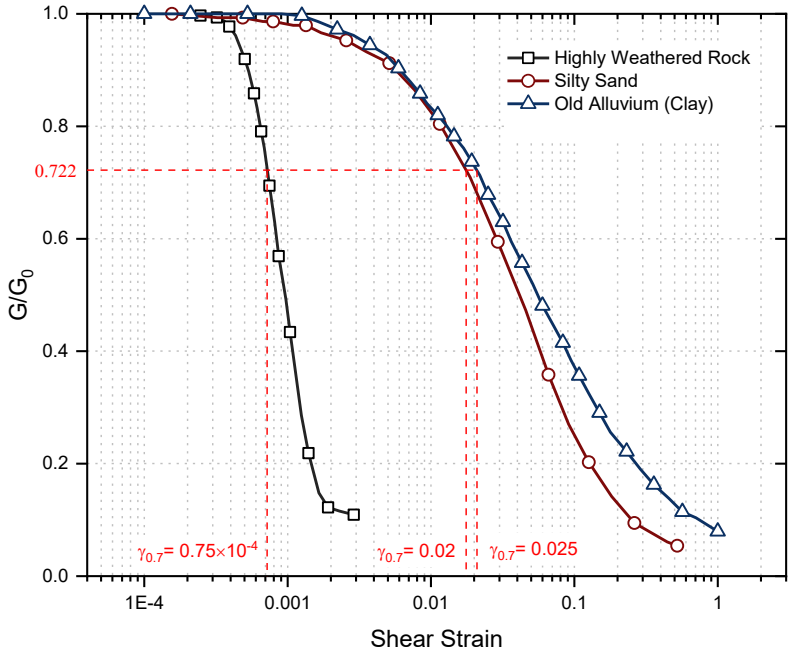

Figure 5.22 Stiffness degradation curve obtained for different soil layers

Hardening soil model with small strain stiffness (HS-Small) was utilised as the soil constitutive model and the driving shoe was simulated at the pile toe. Schematic diagram of the simulated model is shown in Figure 5.23. An axisymmetric finite element model of the pile(s) and adjacent ground is shown in Figure 5.24. In order to apply the driving load to the head of the pile, the force trace recorded at the gauge location (refer to Figure 5.25), known as "the force function", has been applied near the gauge, while for the sake of simulation, the section of pile above the gauge location was not simulated (Figure 5.26).

5.7.2 Results and Discussion

As Figure 5.25 shows, t = 2 ms corresponding to the time at which the induced compressive wave due to impact by the hammer is reflected back up to the gauge as a

result of resistance by the soil. Figure 5.26 shows that the distance between the accelerometer /strain gauge and soil surface (i.e. 4.9 m), the force trace (force function) minus velocity×impedance curve ($F(t) - Zv(t)$) remains at zero, which indicates there is no shaft friction, as expected.

Table 5.3 Hardening Soil with Small Strain Stiffness model soil properties

	Holocene Alluvium	Holocene Estuarine	Old Alluvium	Weathered Rock
E_{50} (MPa)	-	-	-	-
γ (kN/m^3)	17	17	19	22
υ	-	-	-	-
c (kPa)	5	5	6	649
ϕ (degree)	30	32	30	23
E_{50}^{ref} (MPa)	8	5	55	2500
E_{oed}^{ref} (MPa)	8	5	55	2500
E_{ur}^{ref} (MPa)	24	15	165	7500
G_0^{ref} (MPa)	40	20	225	15000
$\gamma_{0.7}$	2.5×10^{-2}	2×10^{-2}	2.5×10^{-2}	7.5×10^{-4}
m	0.5	0.5	0.5	0.5
ν_{ur}	0.2	0.2	0.2	0.2
p_{ref} (kPa)	100	100	100	100
k_0^{nc}	0.5	0.47	0.5	0.61
R_f	0.9	0.9	0.9	0.9

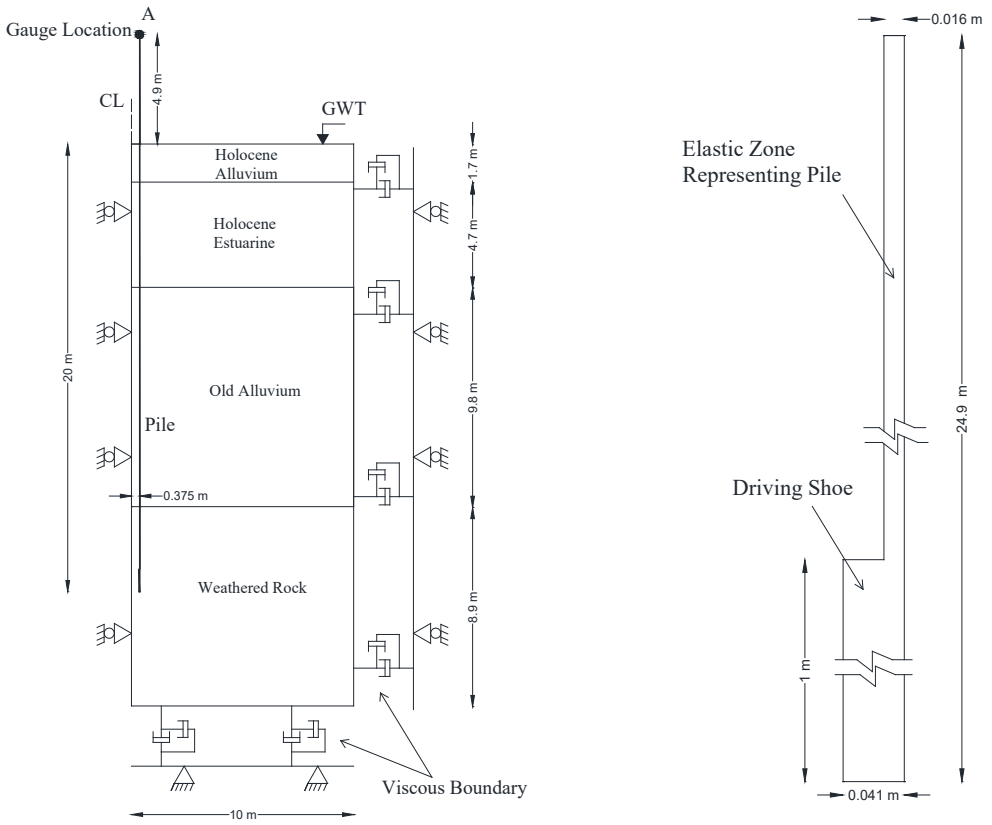

Figure 5.23 (a) Schematic diagram of the simulated model, and (b) geometry of the pile alone

To compare the measurement data and the numerical predictions, a force trace was applied over the head of the pile as an input and the velocity versus time trace was plotted as the output. After simulating the pile and applying the predicted load velocities and displacement traces at the gauge location were assessed, as illustrated in Figures 5.27 and 5.28, respectively.

Figure 5.27 shows that the finite element predictions of trace velocity agree with the one dimensional wave propagation along the pile explained by Lowery et al. (1969). They expressed that if the ground is hard or very firm (e.g. rock) at the toe, the induced downward compressive stress wave can be reflected back up the pile as a compressive

stress wave. In this case, at time $t_2 = t_1 + {}^{2L}/_{c}$ the force trace (force function) minus velocity×impedance curve ($F(t) - Zv(t)$) should be positive. Figure 5.27 shows the velocities predicted by finite element program using the HS-Small soil model, considering the hysteretic behaviour of soils, have a reasonable match with the site measurements in the loading and unloading stages.

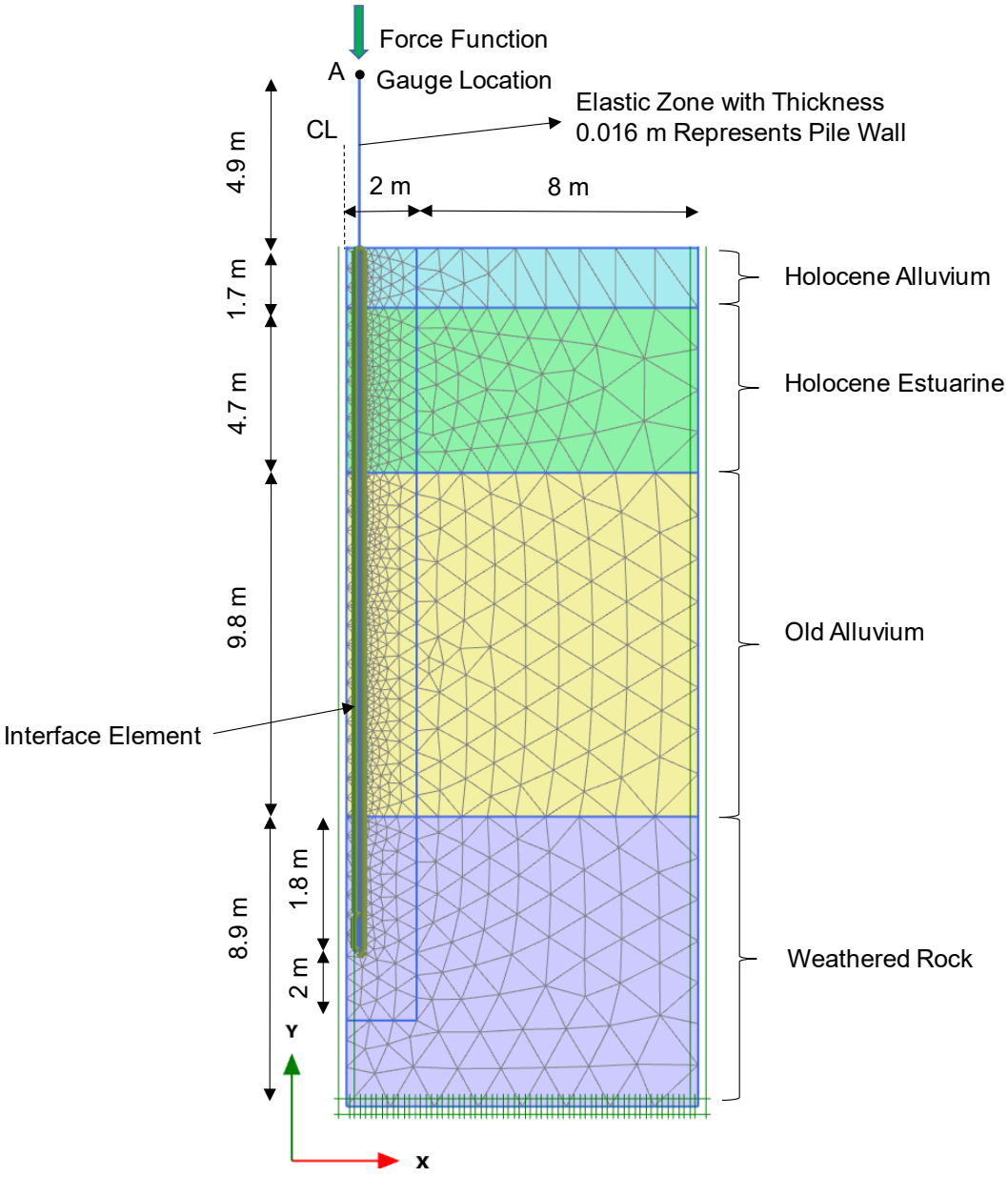

Figure 5.24 An axisymmetric finite element model of the pile and adjacent ground with the corresponding generated mesh

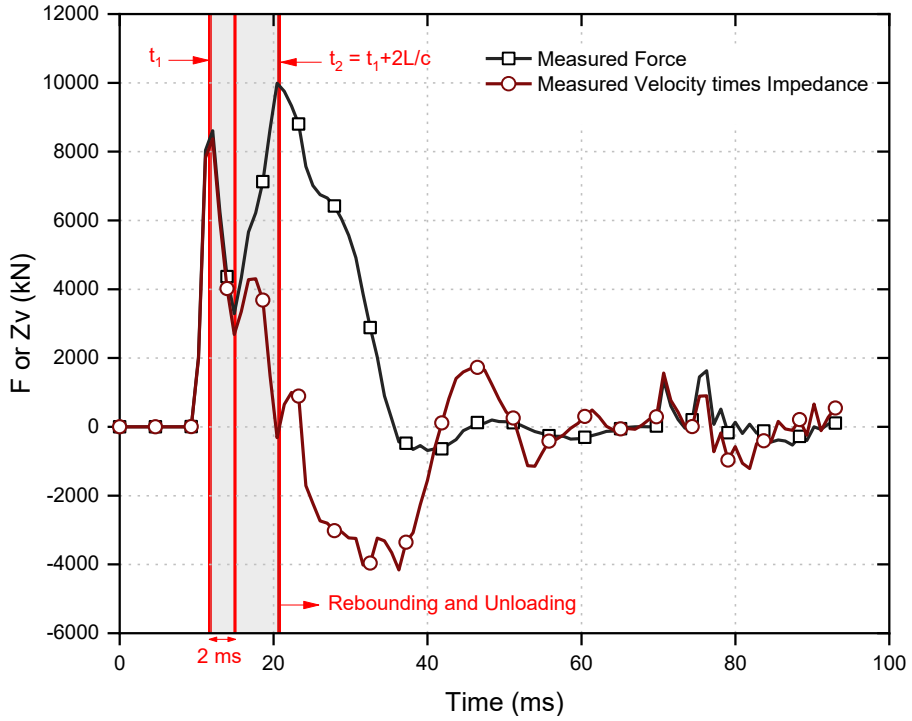

Figure 5.25 Force (F) and velocity times impedance (Zv) traces measured by PDA

Figure 5.28 also shows that the displacement of the pile head at time t_2 (the time corresponding to end of loading stage) reaches a maximum quantity before decreasing to permanent displacement (SET). The difference between the maximum and the permanent displacement is referred to as temporary compression (TC), and is attributed to elastic deformation of the pile and toe quake. Figures 5.27 and 5.28 indicate that the predictions based on the established continuum numerical model resulted in a reasonable agreement with the field measurements.

Using a code developed by the author using MATLAB software (as explained in Chapter 4) the total and static soil resistance traces against time as the main outputs of CASE method, were determined as shown in Figure 5.29. This figure also shows that the maximum total resistance (RTL) and the maximum static resistance (RMX) are mobilised when the first velocity peak is observed (i.e. when the soil resistance is fully mobilised). However, Rausche, Goble & Likins (1985) explain that in some cases of soil with a large

quake, the soil resistance may not fully be mobilised when the first peak velocity is observed (i.e. t_1).

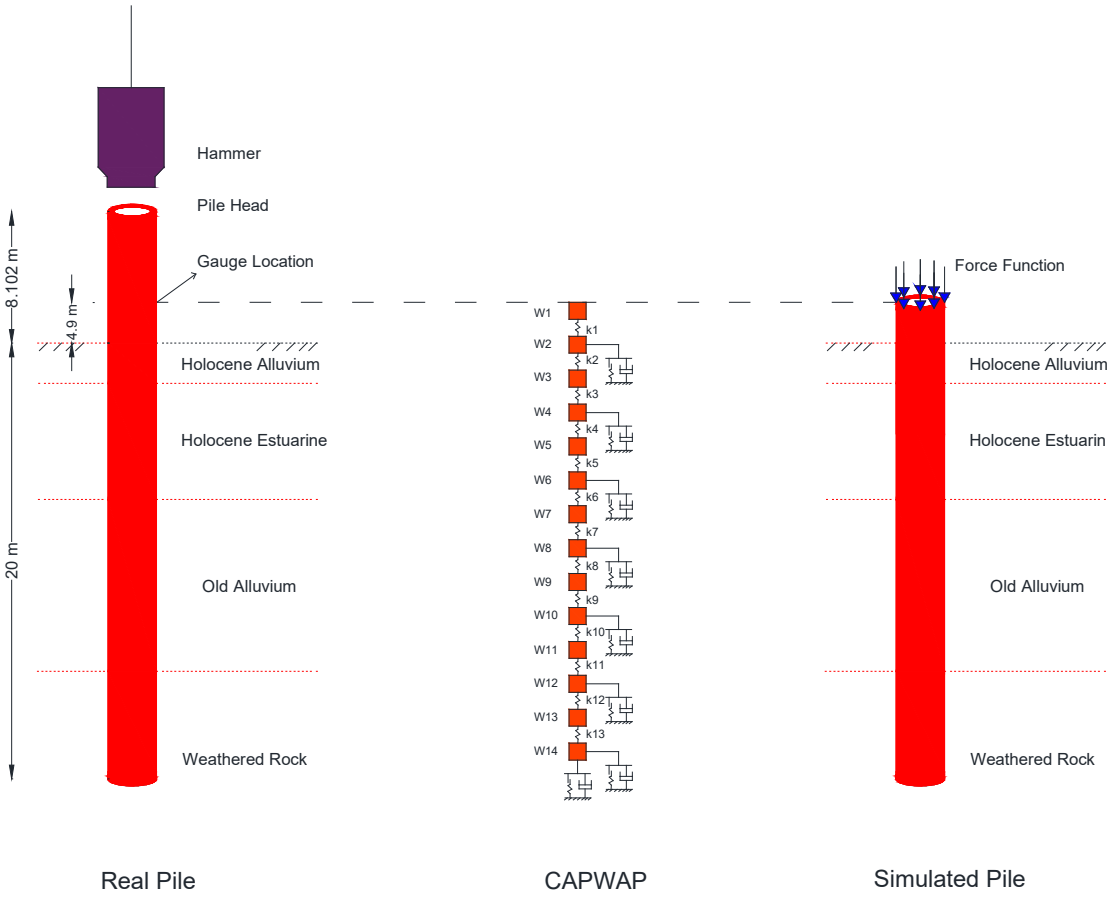

Figure 5.26 Comparison of (a) real pile, (b) CAPWAP, and (c) simulated pile in numerical modelling

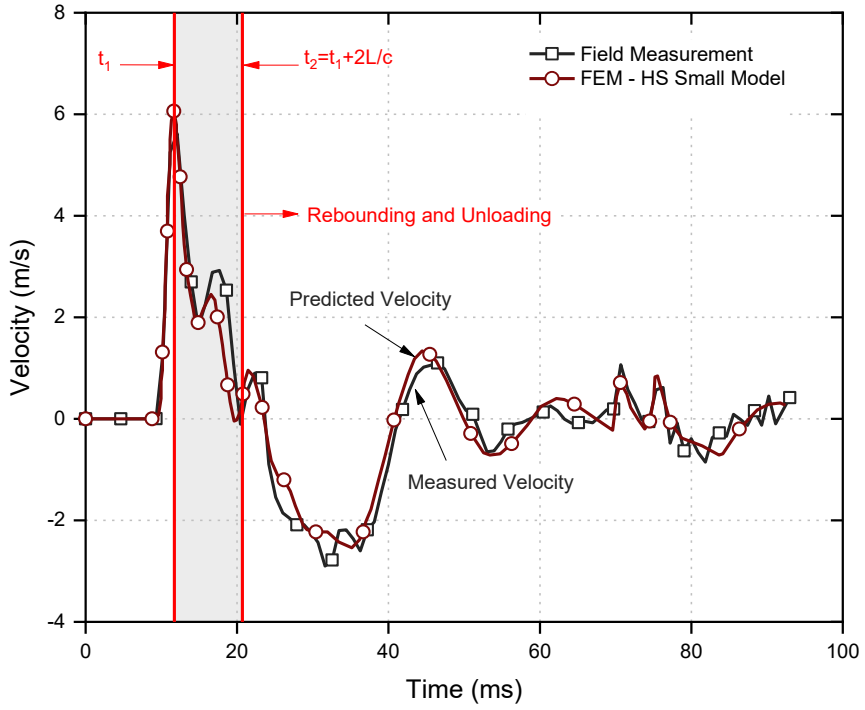

Figure 5.27 Comparison of measured and predicted velocities

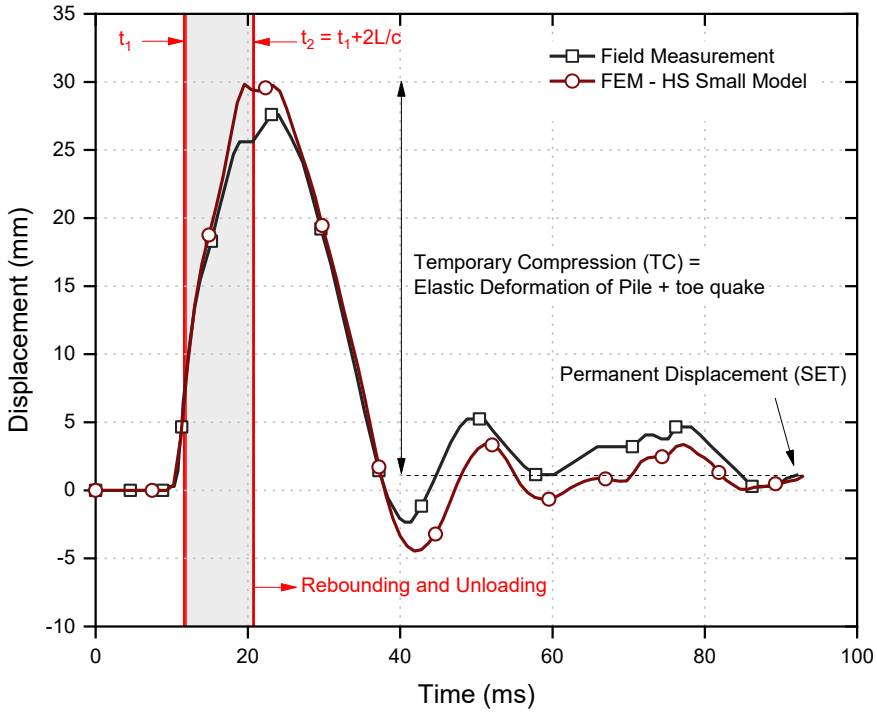

Figure 5.28 Comparison of measured and predicted displacements

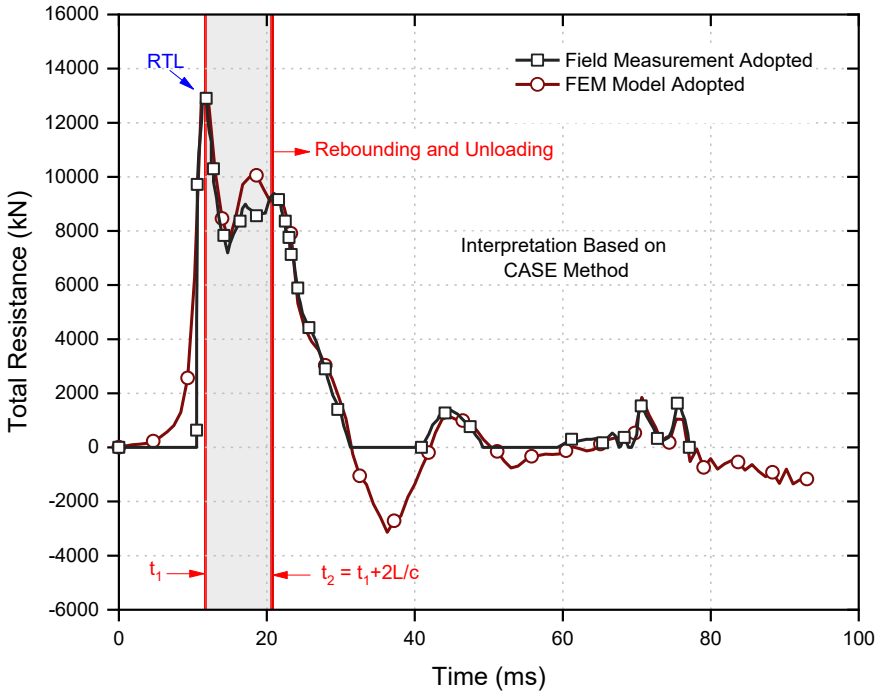

(a)

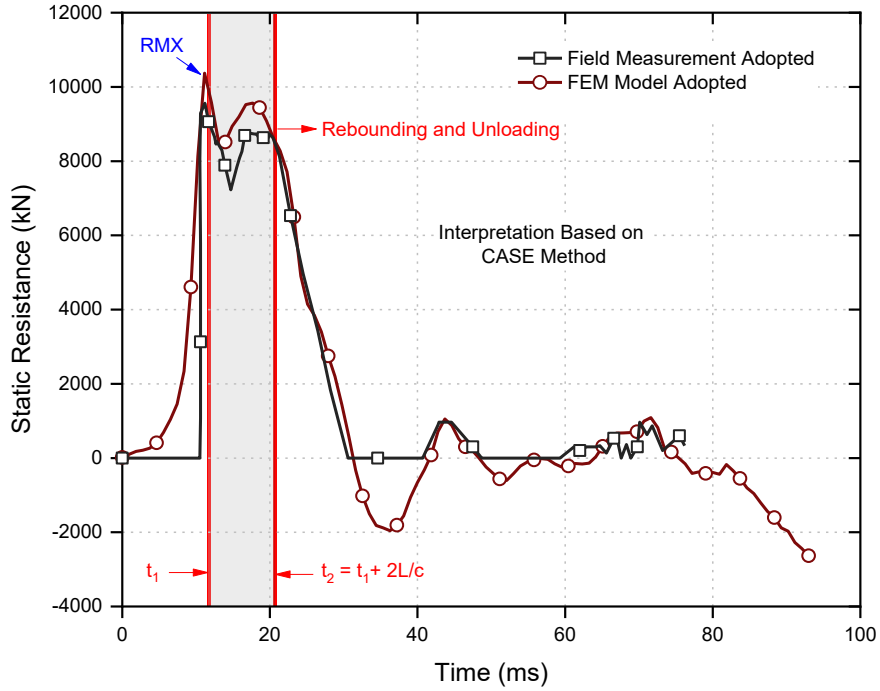

(b)

Figure 5.29 Pile resistance traces: (a) total resistance, and (b) static resistance

In addition, the variations of downward and upward propagating waves versus time have been determined and plotted using a MATLAB subroutine, while the predictions made using the authors' code have been compared to the corresponding values obtained directly from PDA, as depicted in Figure 5.30. Referring to Figure 5.30, a reasonable agreement can be perceived between the wave up and the wave down forces, determined from the numerical predictions and field measurements. It can be noted that due to the hammer impact at time t_1 the gauge only records the downward wave (Wave Down), while Figure 5.30b shows that at the same time, there is no wave travelling upwards. However, Figure 5.30b shows that at time $t_2 = t_1 + {}^{2L}/_{c}$, the maximum upward wave (Wave Up) can be seen in the wave up trace, which correlates well with the concept of one dimensional wave mechanics and the traces measured during the test.

The predicted Wave Up curve (W_U) is also used in this study to assess the soil resistance alongside an embedded pile (as explained in Chapter 4). Table 5.4 compares the shaft resistance obtained from different methods, adopted in this study. In Table 5.4, the predicted static shaft resistance (SFR) obtained from the finite element simulation are compared to the predictions from CAPWAP. In addition, shaft friction, obtained using MATLAB code based on CASE method, has been compared with PDA output, indicating the proposed method for estimating shaft friction based on upward travelling wave provides a reasonable result. However, there is a significant difference between the predictions from CASE method and the finite element predictions.

Table 5.4 Comparison of shaft resistance between different methods

CAPWAP (kN)	FEM (HS Small Model) (kN)	CASE Method (kN)	
		PDA	Current Study
9860	9963	5365	6520

Figure 5.31 indicates the transferred energy to the pile from hammer. As Figure 5.31 shows, the maximum energy is reached at time $2L/c$ after which the energy decreases until it approaches a constant value at about 40 ms; it remains constant after that because the force and velocity are very low. This subsidence of energy from peak to a constant value is mainly due to the elastic rebound of the toe and shaft of a pile, known as "soil quake". There is a reasonable correlation between the measured and the predicted curves.

In addition, the behaviour of piles under static loading conditions are evaluated by applying a vertical displacement of 33 mm at the head. As shown in Figure 5.32 and Table 5.5, the load-settlement curve, the toe resistance (R_b), the shaft resistance (R_s) and the total resistance (R_t) have been determined and compared with the load-settlement curve obtained from CAPWAP.

Table 5.5 Comparison of pile resistance obtained by CAPWAP and PLAXIS

	R_b (kN)	R_s (kN)	R_u (kN)
CAPWAP	1200	9860	11060
FEM- HS Small Model	1096	9963	11059

Figure 5.32 and Table 5.5 indicate that the shaft resistance of the pile (9963 kN) is much higher than the toe resistance (1096 kN), which correlates very well with the open-ended and unplugged behaviour of piles. The dynamic behaviour of piles, including their final displacement due to impact by the hammer (SET) versus their static behaviour, including the total resistance (R_t) obtained from CAPWAP and the finite element model, are also compared in Table 5.6.

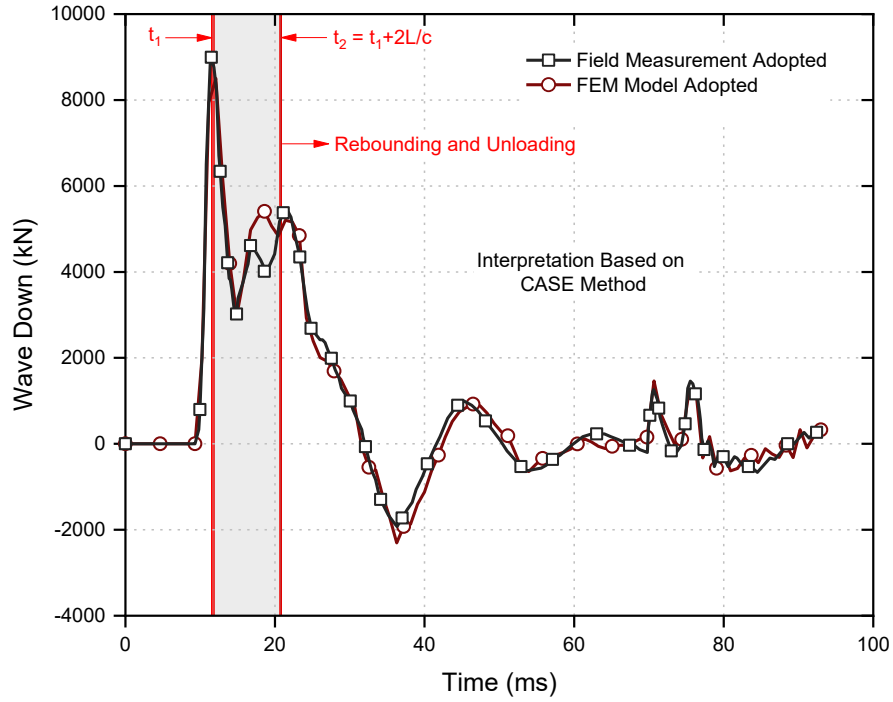

(a)

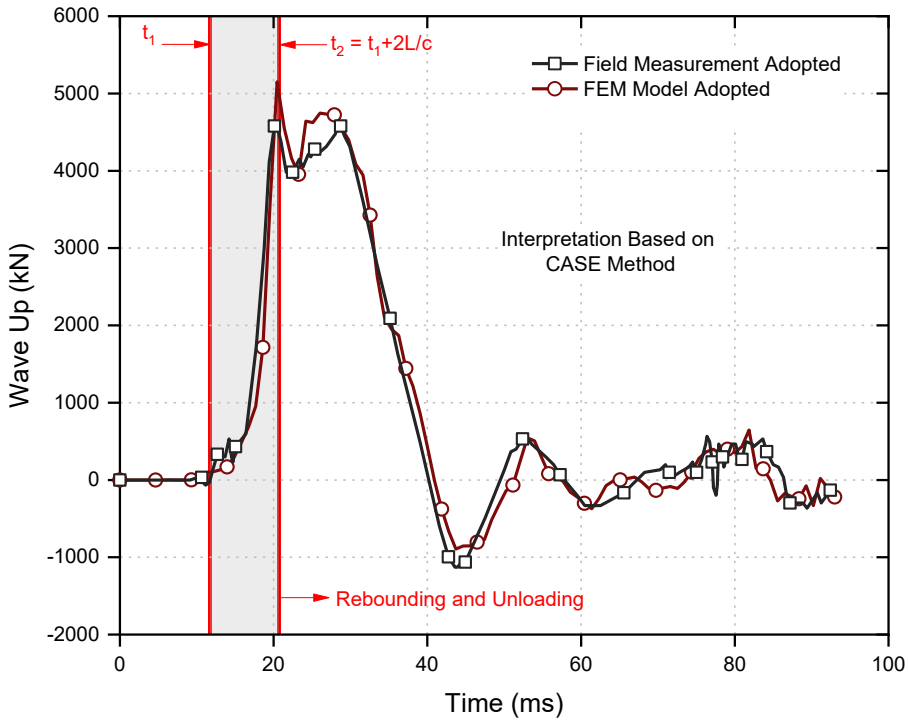

(b)

Figure 5.30 Correlation of predicted and measured data (a) downward, and (b) upward travelling waves

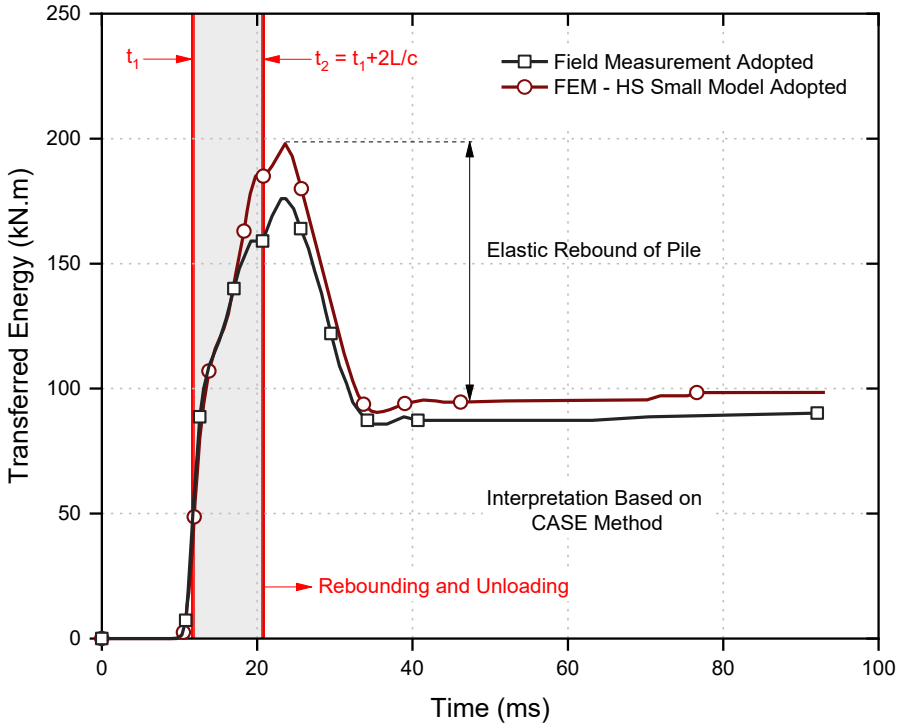

Figure 5.31 Predicted and measured applied energies versus time

Indeed, it can be inferred from Table 5.6 that the HS Small model, which considers variations of soil stiffness with the shear strain, resulted in reasonable predictions of pile behaviour subjected to static loading. It can be stated that CAPWAP predictions are based on signal matching and therefore the soil parameters are altered until the best match is found. Despite this fact, Table 5.6 shows that the model predictions using finite element method based on the original soil parameters, obtained from field and laboratory tests, as well as the HS Small constitutive model, can result in reliable predictions.

Table 5.6 Capability of correlation of dynamic and static behaviour of pile in the numerical model

	Dynamic Loading	Static Loading
	Final Displacement (mm)	Total Resistance (kN)
CAPWAP	1	11060
HS Small	1.07	11059

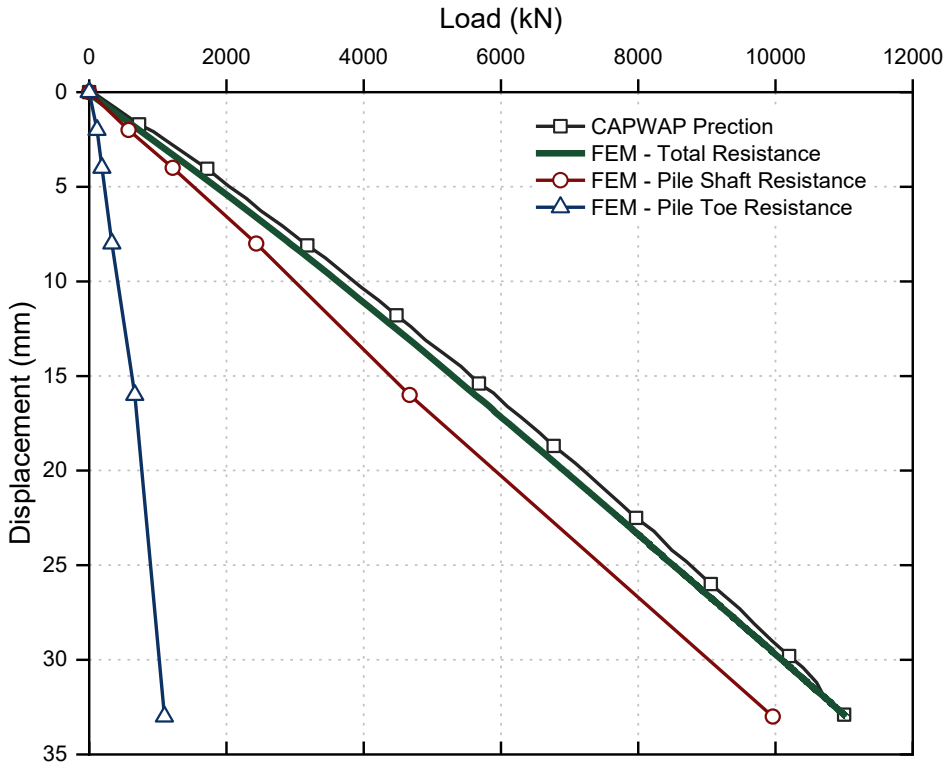

Figure 5.32 Comparison of load-settlement curve obtained by CAPWAP and the finite element program

The HS Small model can reproduce soil deformation that has been subjected to static (mainly addressing large strain cases) and dynamic loads (mainly addressing small strain behaviour) quite realistically due to the non-linear strain-strain relationships and by considering hysteretic damping in small strain and natural damping due to soil plasticity in large strain. Moreover, since formulating the HS Small model incorporates the shear and volumetric hardening processes that then make it suitable for modelling granular, over-consolidated cohesive soils, as well as soft soils. Further investigations have also been carried out to assess the performance of tubular steel piles subjected to static loading. Since the pile simulated in this section is a driven pile under a bridge pier, assessing deflections of the head and toe under the applied structural loads is important. Therefore, further investigations have taken place to evaluate its settlement and deflections of the head and toe under an unbalanced load in the bridge structure, as represented by the heavy

load platform (HLP400), plus a dead load equal to 5140 kN. As summarised in Table 5.7, the toe experienced a minor settlement of 0.02 mm, which corresponds to a resistance of 210 kN, but most of the load is taken by shaft friction (i.e. shaft friction was predicted to be 4930 kN). The relative displacement of the head (i.e. 14 mm) with respect to the toe (i.e. 0.02) is related to an elastic shortening of the pile (13.98 mm) regarding the effect of shaft resistance, whereas by neglecting the soil around the pile, the elastic deformation is 19.5 mm, which indicates the effect of shaft resistance along the length.

Table 5.7 Displacement of pile head and toe due to the SLS loading

Embedded Pile Length (m)	Dead-load + HLP400 = 5140 kN		
	Deflection at pile head (mm)	Deflection at pile toe (mm)	Elastic deformation of pile = QL/AE (mm)
20	14 mm	0.02	19.5

5.7.3 Impact of Interface and Stiffness Degradation Parameters

In this section the influence of the pile-soil interface reduction factor (R_{int}) and the reference threshold shear strain ($\gamma_{0.7}$), defined in HS-Small model on the recorded velocity and displacement traces is investigated, while simulating dynamic load testing. As mentioned earlier, to obtain the best correlation between the measured and recorded traces strength and deformation properties of the pile-soil interface were assumed to be equal to the original soil properties without any reduction. As Figure 5.33 shows, by changing the interface reduction factor (R_{int}) from 0.2 to 1 (for all layers of soil) the velocity recorded at the gauge location changes such that the head of the pile in the lower reduction factors indicates more velocity. In order to assess how the interface reduction factor affects the static resistance of pile, the velocity traces shown in Figure 5.33 were

implemented into the code written by author in MATLAB software, so different maximum static resistances (RMX) correspond to different interface reduction factors, as shown in Figure 5.34. This figure also shows that increasing the interface reduction factor (R_{int}) from 0.2 to 1 increases the maximum static resistance (RMX) from 2750 to 10370 kN; this corresponds to a 73.5% increase in pile resistance. This finding correlates very well with the continuum numerical model concept where the static resistance of a pile is defined using real soil properties, c, φ and E. In fact, the main difference between the finite element numerical models versus the lumped models used in CAPWAP is the type of parameters that changed in the analysis. In the lumped models, static resistance of the shaft and toe are introduced by placing a spring along the length and at the toe, which can be changed directly while in continuum models. Thus, the soil and pile–soil interface strength and deformation parameters can resemble the static resistance of the pile.

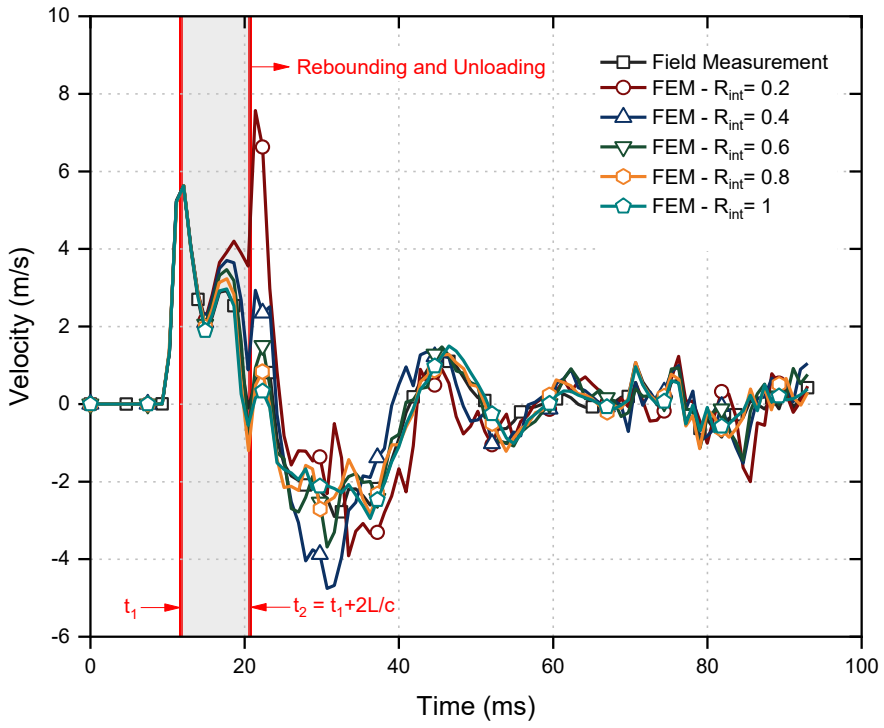

Figure 5.33 Influence of the pile-soil strength and deformation properties on the pile head velocity

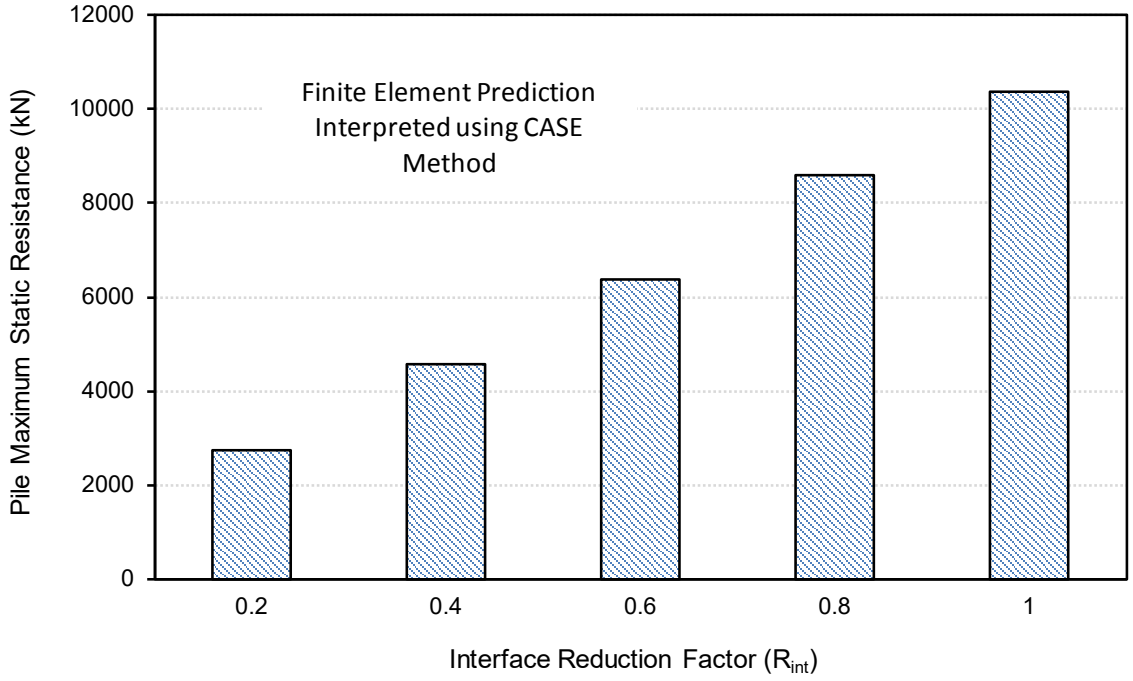

Figure 5.34 Influence of the pile-soil strength and deformation properties on the maximum static pile resistance (RMX)

To evaluate the effect that HS-Small model parameters have on the recorded displacement at the gauge location, the reference threshold shear strain ($\gamma_{0.7}$) was changed to 10^{-4} for all layers of soil. The curves of the stiffness degradation for silty sand layer for both cases are shown in Figure 5.35, including the reference shear strain equal to 0.02 and 10^{-4}. The displacement obtained for the head of the pile in the continuum numerical model by assigning a reference shear strain of 10^{-4} to all the layers of soil and the model adopting real soil parameters (benchmark model) are compared with field measurement in Figure 5.36. This figure shows that by reducing the reference shear strain in all layers of soil, the permanent displacement of pile head (SET) due to the hammer impact is 2.88 mm; when compared to the field measurements it is overestimated because according to Figure 5.35, by decreasing the reference shear strain results in more significant stiffness degradation particularly in the small strain range and consequently more reduction in soil stiffness. Hence, the head of pile indicates more permanent displacement, which does not correlate with reality.

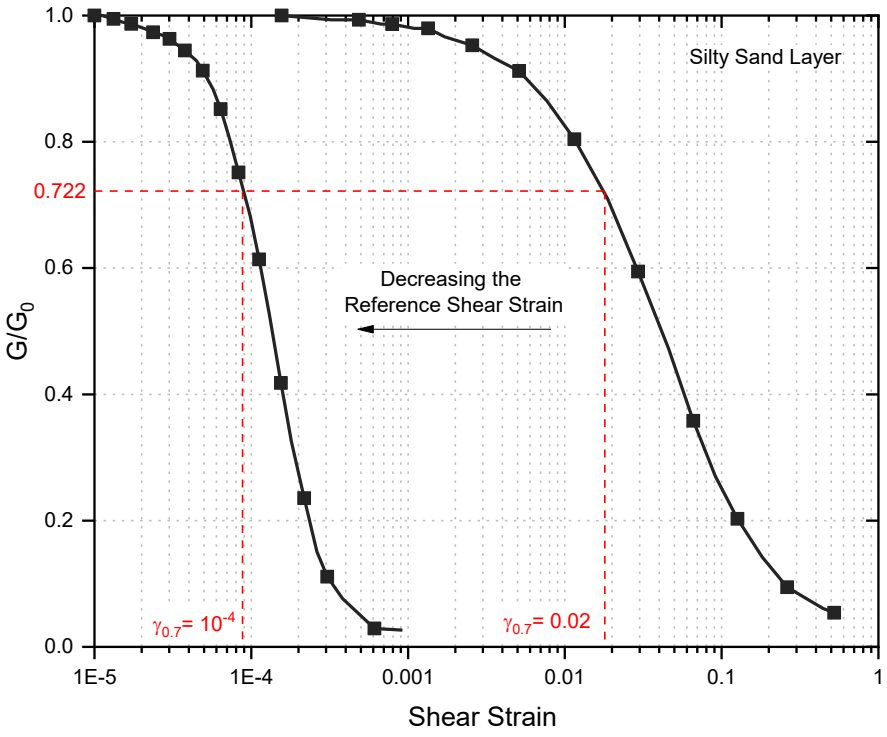

Figure 5.35 New stiffness degradation curve for silty sand layer by changing the reference shear strain

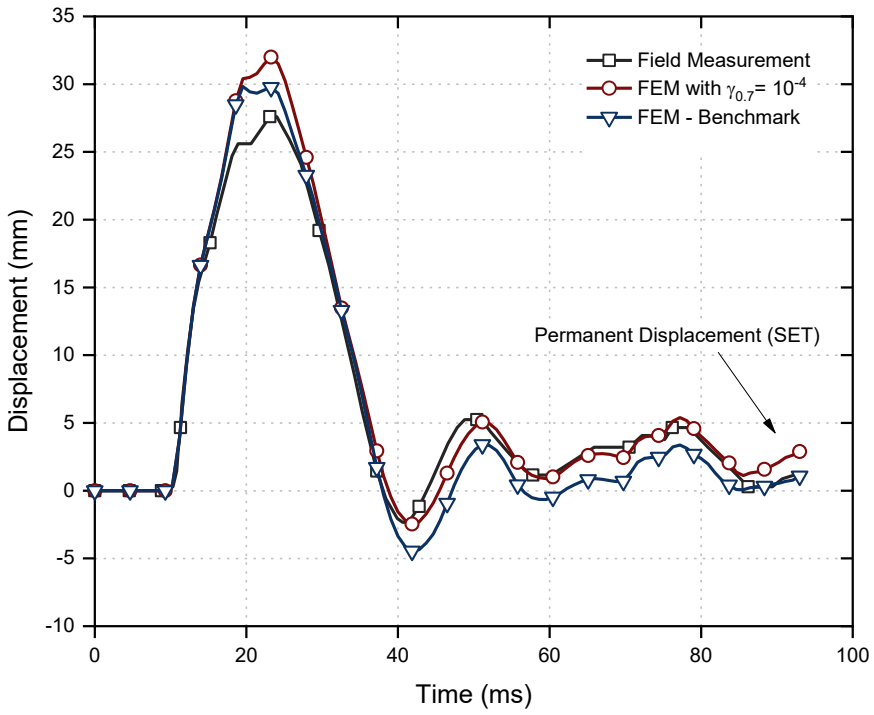

Figure 5.36 Comparison of measured and predicted displacements between CAPWAP and the continuum numerical model by assigning the reference shear strain equal to 10^{-4} to all soil layers

5.8 Ground Vibration Induced by Dynamic Pile Load Testing

5.8.1 Overview

As explained by Achuhan, Subashi & De Silva (2016), pile driving in populated areas can disturb dwellers and damage adjacent buildings and infrastructure. These vibrations make people feel uncomfortable therefore they tend to respond negatively to construction with piles in their neighbourhood. According to Massarsch & Fellenius (2008) pile driving is a source of negative environmental issues due to noise and air pollution, but they can easily be alleviated, unlike vibration from the impact of driven piles, which are difficult to determine beforehand and costly to mitigate (Massarsch and Fellenius 2008). Hence, there is an objective need to predict the level of vibration due to pile driving and dynamic load testing using proper numerical modelling.

Andersson Olivecrona (2016) conducted a numerical analysis on wave propagation and vibration generated by pile driving with the finite element software COMSOL Multi-physics. The peak particle velocity (PPV) obtained from numerical modelling, were compared to field measurements where vertical vibrations were recorded by vibration sensors (geophones) mounted 10, 20 and 40 m away from a concrete pile. In numerical simulation the impact load of the hammer was estimated by a rectangular function where a load was applied over the pile head for 0.1 seconds and then unloaded. The particle velocities were acquired by assigning linear-elastic, Mohr-Coulomb, and Drucker Prager soil models to the soil mass. Setiawan & Fad (2012) predicted the ground vibrations (peak particle velocities) due to driving a concrete pile at different distances from a pile using the finite element method. In that study the numerical simulation Mohr-Coulomb model was assigned to the soil, and the hammer load was approximated by a half sine harmonic load.

The ground vibrations induced by dynamic load testing, reported in Section 5.7 in terms of peak particle velocities (PPV) were evaluated using PLAXIS 3D software version 2017. This section aims to obtain the ground vibrations induced by dynamic pile load testing and then compare them to the recommendations of Australian and the British standards to identify the minimum distance needed to avoid the adverse effects of ground vibrations on adjacent buildings or occupants.

When planning a project where driven piles and dynamic pile loading tests are to be used, potentially vulnerable structures and installations close to the project site and proposing limiting values of ground vibrations must be identified by the design engineer. The risk of damage due to vibration and vibration-susceptible installation or environmental aspects that will affect the occupants must be evaluated. As explained by Achuhan, Subashi & De Silva (2016), after the hammer impact vibration is induced at the pile-soil interface due to the interaction of pile and adjacent soil and is transferred through the ground and interacts with above ground and underground structures. The vibration enters the structure where it may annoy occupants and cause damage. The level of ground vibration is highly dependent on the source of energy, the distance from the source of vibration, and the soil characteristics and characteristics of wave propagation.

According to Massarsch & Fellenius (2008) and Gutowski & Dym (1976) three types of ground waves should be considered when analysing pile driving, including the spherical waves (pressure waves or P-waves) emitted from the pile toe, cylindrical waves (shear waves or S-waves) propagating laterally from the pile shaft, and the surface waves (Rayleigh waves or R-waves) generated by wave refraction at a critical distance from the pile at the ground surface. These three wave types depend on the dynamic resistance (velocity-dependent soil resistance) at the pile-soil interface. In fact, the dynamic soil

resistance defines the maximum vibration velocity which can be transmitted at the pile-soil interface, hence when a pile is pushed into the ground at very slow speeds (e.g. static load testing), the total soil resistance consists of the static shaft and toe resistances, and since no dynamic forces are involved, no ground vibrations will be transmitted to the surrounding soil. When a pile being driven into the ground by an impact load (e.g. dynamic load testing), a dynamic velocity depending on soil resistance will be developed which increase the total driving resistance and causes ground vibrations. The propagation of different waves while driving of piles with an impact hammer is shown in Figure 5.37 which shows that a shear wave is generated along the pile shaft and the pressure wave at the pile toe is in a spherical shaped pattern.

The blasting seismograph vibration monitor (Figure 5.38) is the most commonly used tool for measuring vibration and determining compliance with ground vibration standards and is used in blasting and construction settings. The monitor (the data recording system) translates observations into a number of different measures of ground vibration, of which the most common one in the site is the peak particle velocity (PPV) as an indicator potential damage. The PPV is defined as the maximum instantaneous velocity of a ground particle at a point during a specified time interval. In fact, ground particles oscillate with different particle velocity when the disturbance caused by pile driving propagates away from that source with a specified wave velocity.

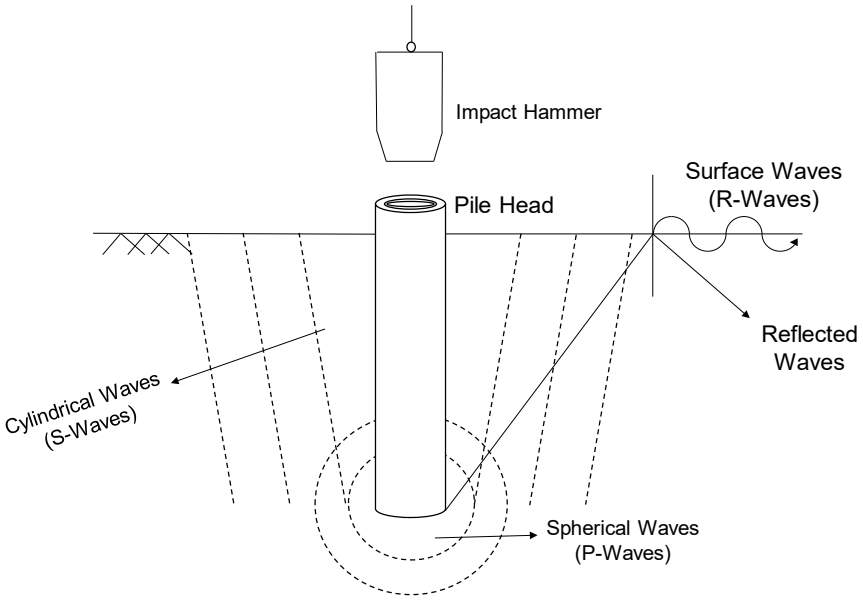

Figure 5.37 Waves generated from pile driving and dynamic load testing operations (after Dungca et al. 2016)

The motion at a particular location along the propagation path is typically specified as vertical, transverse and longitudinal or radial (mutually perpendicular) components. The PPV is a vector quantity with a value and a related direction. The peak vector sum (PVS) is typically expressed because it can be determined as the square root of the sum of the squares of the PPV values (measured by the seismograph) in all three vector directions. Virtually, all ground vibration standards are quoted in PPV values although their acceptable values vary based on different standards the frequency of the vibration components.

In this part, the dynamic pile load testing discussed in Section 5.7 was modelled in a three-dimensional finite element model and the steel pipe pile (P11) was modelled as a plate element with elastic material properties such as an elastic modulus of 200 GPa, a Poisson's ratio of 0.3 and a solid unit weight of 78.5 kN/m^3.

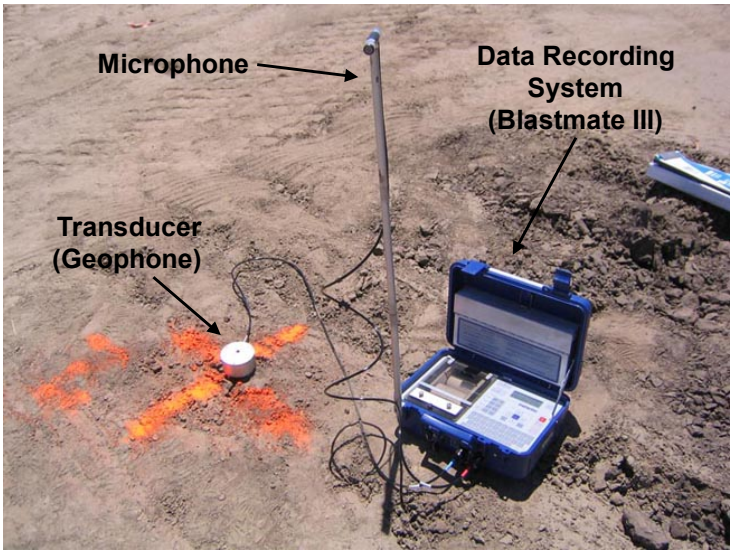

Figure 5.38 Measuring ground vibration using seismograph

(after Achuhan, Subashi & De Silva 2016)

The soil properties defined in Table 5.3 were assigned to the soil layers. Since a hardening soil model with small strain stiffness (HS-Small) was utilised as the soil constitutive model (for all soil layers), no Rayleigh damping parameters were defined into the model to simulate damping behaviour. 10-node tetrahedral elements were assigned to the model to simulate the soil, and viscous boundaries were used in the numerical model to simulate geometric damping and far-field boundaries. During simulation the interaction between pile and soil inside and outside of the pile, interface elements for both outer and inner pile surfaces were defined.

The horizontal dimensions of the simulated model were chosen large enough (100×100 m) to evaluate vibration on the soil surface at different distances from the vibration source when a pile is under a hammer impact during the dynamic pile load testing. Due to the relatively large dimensions of the simulated model, a finite element mesh with a medium size was generated in order to have a reasonable analysis time. Using the borehole option described in program three different boreholes were defined at three different locations in the numerical model, but since the defined model is not uniform the vibrations were

studied at three different radial directions (A, B and C directions), as shown in Figure 5.39c. The locations of the studied points at the surface are located 5, 10, 20, 30 and 40 m away from the pile. A schematic diagram of the defined boreholes and the dimensions of simulated model are shown in Figure 5.39.

5.8.2 Allowable Ground Vibration

Ground-borne vibrations from blasting, piling, machinery, road and rail traffic can cause concern for adjacent buildings occupants and that can lead to assessing the effect of the vibration imposed on the building structure to determine whether damage could occur. There is a major difference between the levels of vibration which damage a structure and the sensitivity of people in feeling vibration. The vibration level at which negative comment from people is possible, are below those which damage buildings; this is why standards attempt to separate those vibration intensities (the peak particle velocities) and frequencies, which potentially damage structures from those that people are concerned with.

The level of damage to buildings depends on the type and age of a structure and the geological conditions on which the structure is built. However, human response to vibration depends on vibration levels, location and time of day and different legal requirements which may apply in different jurisdictions (Achuhan et al. 2016). As mentioned earlier, ground vibrations caused by pile driving are complex radial, transverse and vertical components at the adjacent ground surface.

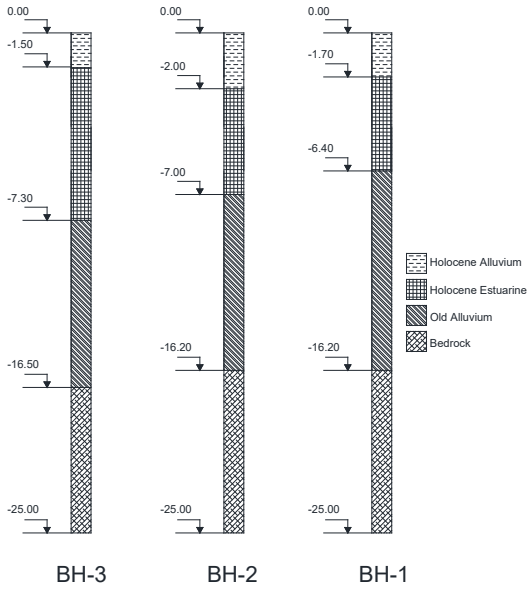

(a)

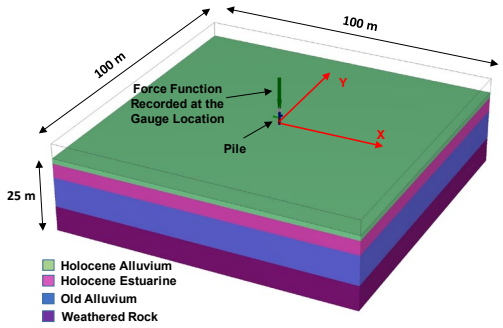

(b)

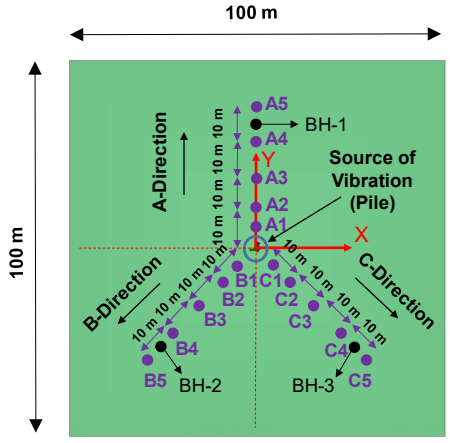

(c)

Figure 5.39 Ground vibrations induced by dynamic load testing, (a) three different boreholes defined in the model, (b) three-dimensional simulated model, and (c) plan view and the locations of vibration measurement

Vibration standards typically do not distinguish between damage potential of different vibration components and they easily specify the same limits for all three axes of measurement. There are different standards and guidelines to specify threshold values of vibrations (allowable ground vibrations) in terms of building damage and human comfort:

5.8.2.1 Building Damage

There is no specific Australian Standard for assessing building damage caused by vibrational energy, however the most pertinent accessible topics are described in different standards such as British Standards (1990 & 1993), and German Standard (1999).

According to British Standard (1990) most buildings damage from man-made sources such as construction, blasting and traffic occurs from 1 Hz to 150 Hz, while natural sources such as earthquakes typically have frequencies from 0.1 Hz to 30 Hz. The duration of applying dynamic force is an important parameter because the structural response of a building can be affected by the duration of the vibration to which it is exposed. This response can be expressed as transient or continuous based on the relationship between the time constants (Equation 5.8) related to the structural response and the forcing function:

$$t_r = \frac{1}{2\pi\xi_r f_r} \tag{5.8}$$

where,
t_r = time constant of a resonance response for resonance in seconds
ξ_r= represents the influence of the damping
f_r = resonance frequency

If the forcing function exists for less than $5t_r$ then the response is regarded as transient, otherwise the vibration is considered to be continuous. The limit above which damage may cause for a continuous nature vibration may need to be less than the reciprocal limit

for transient vibration. The time characteristic of different vibration forcing functions such as blasting, pile driving, human activities, earthquake and wind are considered to be transient. The response of a building due to pile driving is given in Table 5.8.

Table 5.8 Typical range of structural responses to the pile driving (after British Standard 1990)

Vibration forcing function	Frequency range (Hz)	Particle velocity range (mm/s)	Particle acceleration range (m/s^2)	Measurement quantities
Pile Driving	1 to 100	0.2 to 50	0.02 to 2	Pvth*

*Pvth = particle velocity time history

As explained by British Standard (1993), the probability of building damage by ground vibration is nearly zero at 12.5 mm/s peak component particle velocity. Cosmetic damage due to transient vibration takes place above the limits tabulated in in Table 5.9. This standard states that vibration magnitudes which are greater than twofold tabulated in Table 5.9 can cause minor damages while at values greater than four times the tabulated values major damages to buildings may occur. The German Standard (1999) recommends maximum levels of vibration that decrease the probability of building damage caused by vibration (Table 5.10). No damage due to vibration up to these levels has been observed for the specific class of building even minor non-structural effects such as the enlargement of cracks already present.

Table 5.9 Transient vibrations guide values for cosmetic damage (after British Standard 1993)

Type of Building	Peak component particle velocity in frequency range of predominant pulse	
	4 to 15 Hz	15 Hz and above
Reinforced or framed structures, Industrial and heavy commercial buildings	50 mm/s	
Unreinforced or light framed structures, Residential or light commercial type buildings	15 mm/s at 4 Hz increasing to 20 mm/s at 15 Hz	20 mm/s at 15 Hz increasing to 50 mm/s at 40 Hz and above

Table 5.10 Guidelines values for transient vibration on structures (after German Standard 1999)

Type of Structure	Peak particle velocity (mm/s)		
	1 to 10 Hz	10 to 50 Hz	50 to 100 Hz
Building used for commercial purposes, industrial buildings, and buildings of similar design	20	20 to 40	40 to 50
Dwellings and buildings of similar design	5	5 to 15	15 to 20
Structures that because of their particular sensitivity to vibration, do not correspond to those listed in Lines 1 or 2 and have intrinsic value (e.g. buildings that are under a preservation order)	3	3 to 8	8 to 10

5.8.2.2 Human Comfort

General guidance on human response to building vibrations is given in a number of standards such as Standards Australia (1990), International Standard (2014), and British Standards (2008 a, b & 2009).

According to British Standard (2009) threshold of perception for human beings is typically in the PPV range of 0.14 to 0.3 mm/s, and as vibrations increase above these values they can annoy or interfere with work activities. Initial awareness can be as low as 0.3 mm/s, while annoyance occurs above 1 mm/s.

5.8.3 Results and Discussion

In this section, ground vibrations induced by dynamic load testing were measured at 5m, 10m, 20m, 30m and 40m distances from the vibration source (pile) in three different directions A, B and C (as shown in Figure 5.39c). For each point, a corresponding particle velocity graph is presented. The preferred method of measuring peak particle velocity (PPV) is to record simultaneously unfiltered time histories of the three orthogonal components (vertical, transverse and longitudinal) of particle velocity. Since the majority of data and standards recommendations are expressed in terms of the peak component particle velocity, for the assessment, the maximum of the three orthogonal components should be used. For achieving this aim, vibrations in all three orthogonal components are evaluated in direction A, while only vertical vibrations are assessed in three directions A, B and C. The calculated particle velocity results are presented in Figures 5.40 and 5.41. All graphs reveal that the extracted values of particle velocity during a time interval of 1 second. This interval is corresponding to the time for a single hammer impact with an additional time for the wave to propagate. In fact, the time duration of the recorded time history depends on the character of the excitation, but herein it has been chosen such that the maximum response is recorded with appropriate accuracy.

As can be seen in Figures 5.40a-e, the vertical peak particle velocity from nearly 14 mm/s at a distance of 5 m reduces to 0.5 mm/s at 40 m distance (i.e. more than 96% reduction in ground vibration). It is clear that the magnitude of vibrations reduces with the distance,

proving the capability of the HS-Small soil model in modelling the damping behaviour of soils. In addition, the recorded vertical particle velocity in each distance (e.g. 5m, 10m, 20m, …) in all three radial directions (A,B and C) indicate approximately the same behaviour. In other words, it presented that soil particles had the same vibrational behaviour in the same distances, although in C-direction more fluctuations were observed. By comparing the particle velocities in three orthogonal directions (vertical, transverse and longitudinal directions) in A-Direction, as shown in Figures 5.41a-e, it can be inferred that all components indicate almost a same trend in the same distance. However, the vertical component seems to be a dominant component. Hence, the vertical peak particle velocity can be used as a benchmark to determine the allowable distance from vibration source to prevent human discomfort and building damage according to different building standards. The variations of vertical PPV in different distances are shown in Figure 5.42.

According to Figure 5.42 it is clear that in distances less than 10 m from pile the peak particle velocity (PPV) is more than 5 mm/s. Based on German Standard (1999) (Table 5.10) in low frequencies this PPV causes damage to dwellings and buildings with similar design. Whereas, as explained by the British standard British Standard (1993) (Table 5.9) this PPV is totally safe for all frequency ranges even for cosmetic damage. In terms of human comfort, according to the British Standard (2009) and the Standards Australia (1990) in quite close distances to the vibration source (less than 5m), which PPV is more than 10 mm/s, is likely to be unbearable.

While in the distances ranging from 10 to 30 m PPV is more than 1 mm/s, which just annoyance can occur and cause complaints. Distances around 35m, which PPV drops to less than 0.5 mm /s, is recognised as the threshold of perception by inhabitants and more

than this distance is known to be safe. A diagram of recommendations based on different standards, considered in this section, is shown in Figure 5.43.

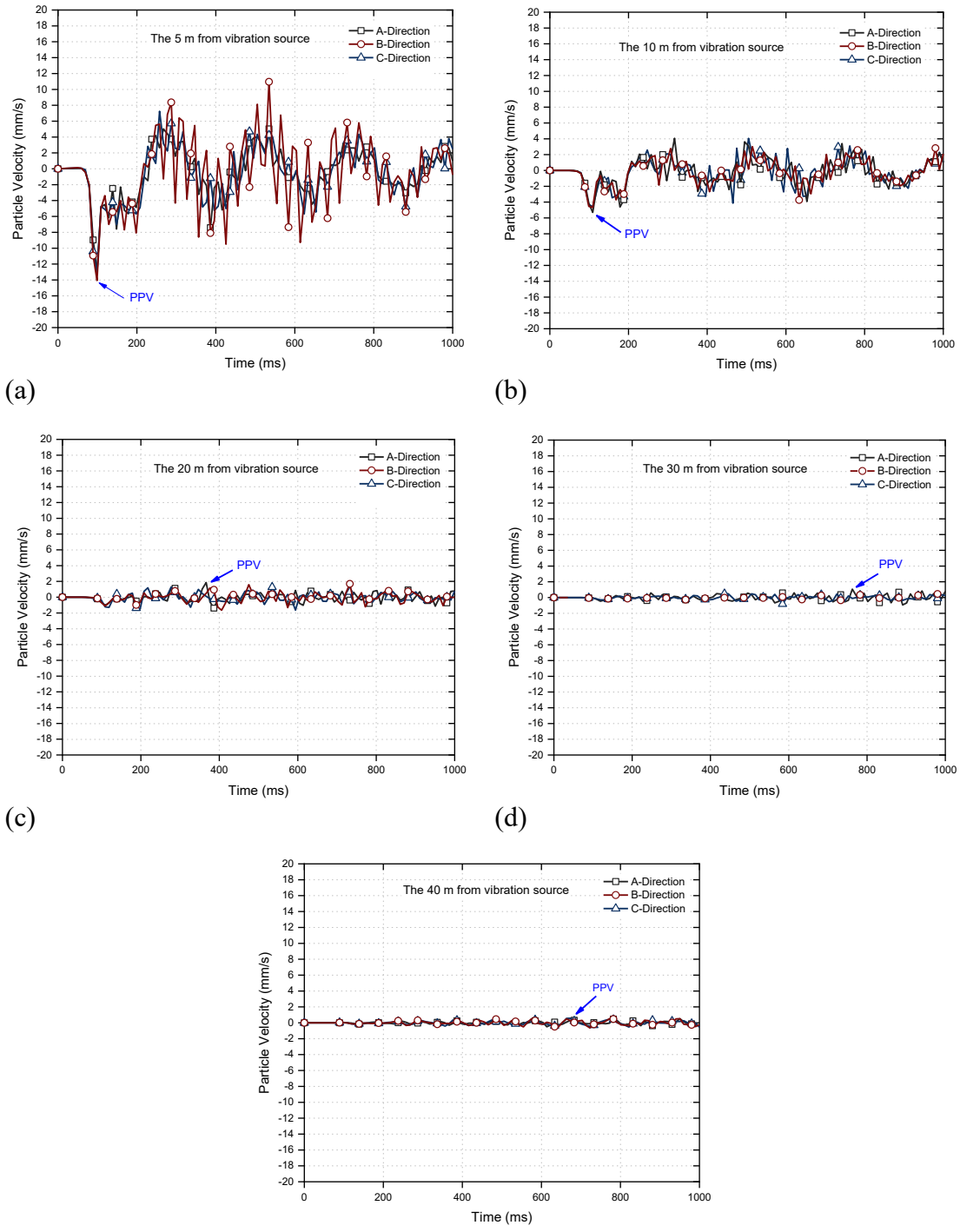

Figure 5.40 The variations of vertical particle velocities in different distances from source of vibration

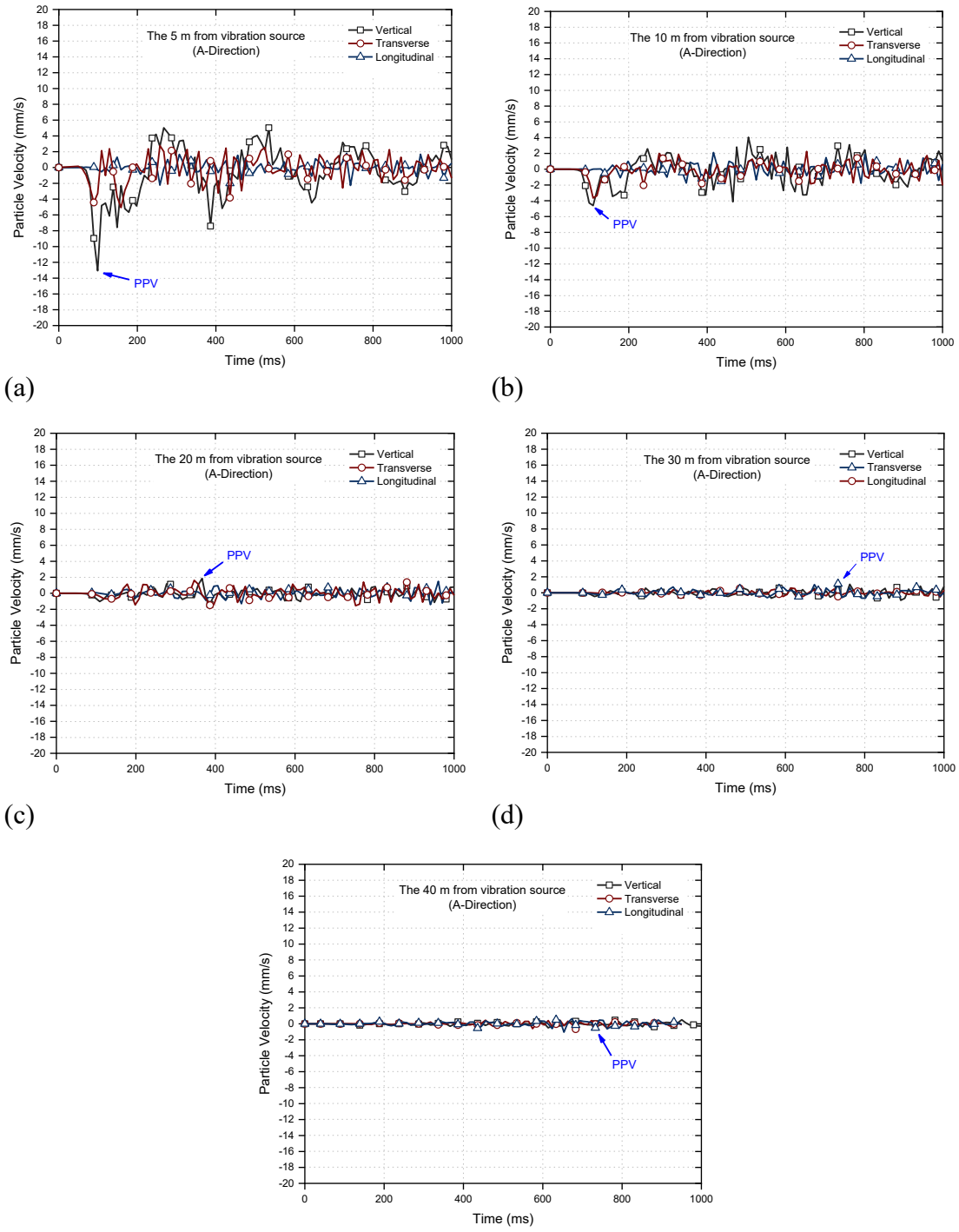

Figure 5.41 The variations of particle velocities in different distances in three different orthogonal direction, (a) 5m, (b) 10 m, (c) 20 m, (d) 30 m and (e) 40 m

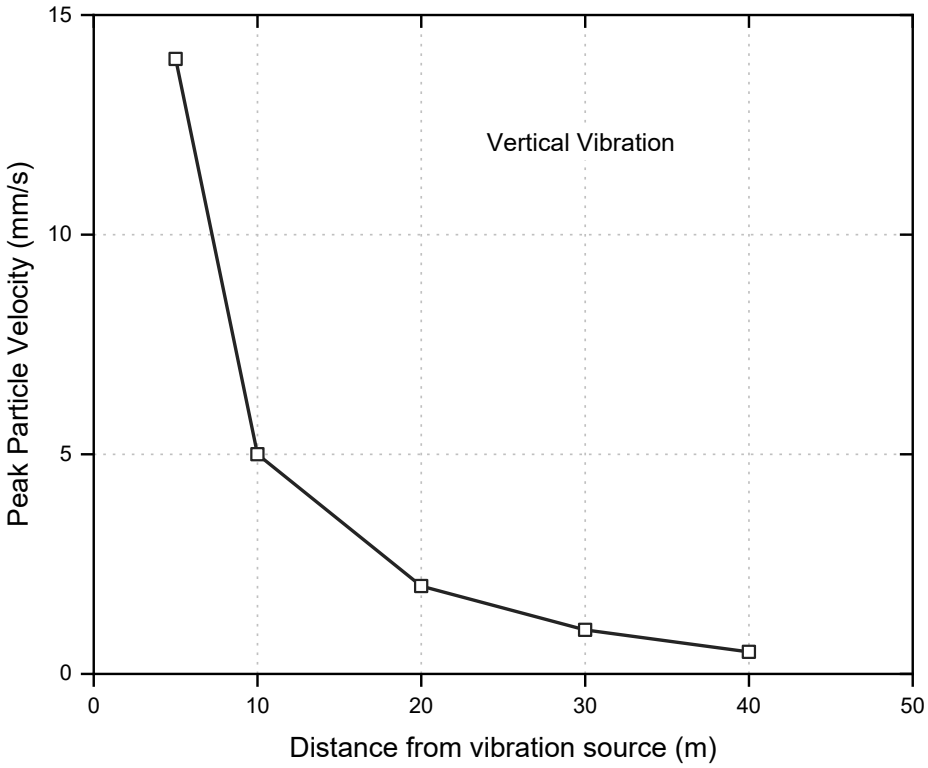

Figure 5.42 The variations of peak vertical particle velocities in different distances from the source of vibration

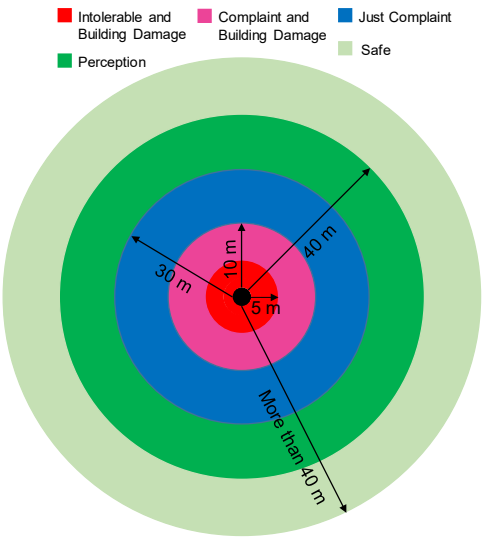

Figure 5.43 Response of the building and inhabitants in a vicinity of pile driving site

5.9 Summary

The principals of continuum based numerical modelling of dynamic pile load testing have been explained in this chapter, as a technique for interpretation of the PDA test results and evaluation of dynamic and static pile resistance as the main outputs obtained from force and velocity signals measured at the gauge location. Dynamic pile load testing simulation in finite element program provides more realistic condition compared to one-dimensional wave equation based programs such as CAPWAP as well as it retains the continuity of different stages of modelling from simulating pile driving, quality control, and investigating settlement, while all these analyses are carried out using one software. However, developing a numerical model to properly capture both large strain, small stiffness and small strain, large stiffness behaviours, observed during static and dynamic load testing, respectively, is vital. On this basis, more rigorous models that can simulate the cyclic behaviour of soil from small to large strains and wave propagation should be embraced. In this chapter, a real large-scale dynamic load test of steel pipe pile driven into the weathered rock employed as a bridge foundation in a highway upgrade project in New South Wales, Australia, was numerically simulated adopting advanced soil model Hardening Soil with Small Strain Stiffness (HS-Small model). The obtained results show a reasonable correlation between the predicted and the measured curves obtained during the dynamic load testing including the velocities and the displacements recorded in the site. In order to evaluate the performance of established numerical model more precisely, the outputs of the CASE method (displayed on the PDA screen) were assessed using a code developed in MATLAB program.

In addition, ground vibrations induced by dynamic load testing of respected pile in terms of peak particle velocities (PPV) were evaluated using three-dimensional numerical

modelling. It was aimed to obtain the ground vibrations induced by dynamic pile load testing in different distances from the pile and to compare the results with the recommendations of different standards, including the Australian and the British standards to identify the minimum distance in order to avoid the adverse effects of ground vibrations on adjacent buildings or occupants.

CHAPTER 6 Conclusions and Recommendations for Future Research

This final chapter has three parts. Section 6.1 provides a summary of the contents of this thesis, Section 6.2 summarises the main conclusions of this research work, and Section 6.3 proposes a number of potential studies for future research.

6.1 Summary

The literature review indicates that static and dynamic pile load testing are the most reliable methods for determining the bearing capacity of piles. The review also reveals that full-scale load tests are costly and time consuming. In addition, there are some limitations in the interpretation of test results using one-dimensional wave equation-based techniques and further assessment of piles performance are required near the existing piles and structures during the test. Therefore, there is an objective need for prediction of a single pile and a pile group response under pile load tests using proper numerical modelling. Accordingly, the first part of this research study set out to investigate how an established numerical model, adopting different soil models, could predict the response of piles during static load testing. Three cases were considered, the performance of a single pile, the influence of a reaction pile on a test pile, and the behaviour of group of piles during static load testing. In the first case, the performance of a concrete pile under the prescribed displacements was evaluated using the advanced soil model hypoplastic, and with and without the intergranular strain concept. A parametric study was conducted

on the parameters of the hypoplastic model that would affect the load-displacement curve as the main output of pile load testing. A numerical approach was verified with a real test by applying the Mohr-Coulomb and hardening soil models, and then the established numerical model was used to assess the interaction between the test pile and the reaction piles. The numerical modelling predictions provided further evidence for the suitability of ASTM International (2013) recommendations for the minimum distance between the reaction piles and the test pile to avoid the interaction effects. The behaviour of two real cases of pile groups under static load testing were evaluated via a linear, non-linear, and a combination of linear and non-linear analyses.

The second component of this research study focused on dynamic pile load testing. In this part, the principals behind the CASE method, as a numerical technique used in the pile driving analyser (PDA) were evaluated and the one-dimensional wave propagation concepts were investigated, from which a code in MATLAB software was developed. With this code, a real case project from the literature was assessed in terms of parameters such as the maximum static soil resistance (RMX) and the sensitivity of the results to the selection of CASE damping factor for clay deposit. The dynamic response of a driven steel pipe pile monitored as part of a highway bridge construction project in New South Wales, Australia was numerically analysed using the finite element method. In fact a continuum numerical model was established to simulate the dynamic load testing of an open-ended steel pipe pile with unplugged behaviour where adopting the measured soil properties resulted in a reasonable match between the measured and predicted results. Ground vibration induced by dynamic pile load testing was predicted by the numerical simulation and compared to the recommendations and databases of several standards to introduce the minimum allowable distance in which ground vibrations do not cause damage to adjacent structures or discomfort to nearby inhabitants.

6.2 Conclusions

This study revealed some salient aspects of pile behaviour under static and dynamic pile load testing. They can be summarised as follows:

6.2.1 Static Pile Load Testing: Numerical Simulation of Single Pile and Piles Group Behaviour

- Soil models such as the Mohr-Coulomb model, the hardening soil model, and the hypoplastic model incorporating the intergranular strain parameters were evaluated to capture the non-linearity behaviour of soil observed during static pile load testing. In the case of using interface element between soil and pile, all the models showed less sensitivity to the mesh size than when the interface element was removed. However, in case of using the interface element, both the Mohr-Coulomb and hardening soil models were less sensitive to element size than the hypoplastic model.
- By activating the intergranular strain (IGS) concept of the hypoplastic model the load-displacement curves from the saturated dense and loose sand deposits were overestimated much more than other soil models. Because the hypoplastic soil model can predict successfully the soil behaviour in the range of medium to large strain, while the intergranular strain concept can predict soil behaviour appropriately in the high quasi-elastic soil stiffness observed in the small strain range under cyclic loading. intergranular strain tensor indicated that during the static load testing, soil is in the hypoplastic state in the vicinity of the pile and further from the pile, the soil remains elastic. This finding correlates very well with the large strain behaviour of soil surrounding a pile during the static load testing.
- Both elastic-perfectly-plastic Mohr-Coulomb and hardening soil constitutive soil models agreed reasonably well with the Davisson criteria based on the simulation of

a real static load test conducted in stiff overconsolidated clay. However, the hardening soil model predicted the capacity corresponding to the maximum displacement of a pile more accurately than the Mohr-Coulomb soil model because it can consider the stress path and its effect on soil stiffness, and capture the actual non-linear behaviour of soils.

- When the spacing between reaction piles during static load testing increases, it has less effect on test pile settlement however, results of this study correlate reasonably well with ASTM International (2013), which recommends that reaction piles should be at least 6D centre-to-centre spacing (5D clear distance, where D is the pile diameter). Moreover, increasing the number of reaction piles has almost no effect on the settlement of a test pile, where the correction factor (F_c) is almost 1.08 for 6D spacing. As the reaction piles move farther away from the test pile, the settlement of the test pile for a given load increases, corresponding to the reduced interaction between piles.
- A combined nonlinear and linear analysis (NL-LE), where the soil adjacent to the pile shaft was modelled using the HS model and the soil in the remaining area was modelled as linear elastic model, could account for the variations for the stiffness between piles inside a group and indicated far better predictions for the settlement of group piles. Furthermore, during a numerical simulation it was proved that due to lower stiffness of the central pile, this pile can support a lower load portion tan the corner piles. Using the traditional definition of the ultimate load capacity, defined as the load causing a settlement of 10% of the pile diameter, the bearing capacity of one of the corner piles was estimated to be 17% higher than the central pile.

6.2.2 CASE Method: Theory, Concept and Application in a Real Case Project

- A sensitivity analysis of the CASE damping factor in the code developed by MATLAB software shows that the maximum static soil resistance increased by almost 45% when this factor changed in a reasonable range for clay and silty clay soil (from 0.7 to 1). However, as time progressed and dissipation of pore water pressures occurred, the sensitivity of predictions to damping decreased. In other words, immediately after driving and in unconsolidated soil conditions, the sensitivity analysis revealed that the damping factor would have more influence than the corresponding values for consolidated conditions.

6.2.3 Dynamic Pile Load Testing: Numerical Simulation, Interpretation of the Results, and Assessment of Ground Vibration Induced by Dynamic Testing

- In this study, the simulated pile driving process introducing the intergranular strain (IGS) concept resulted in more reasonable predictions than the basic hypoplastic model in terms of the pile head displacement and the velocity recorded at the gauge location since IGS extension can accumulate far less strains. In addition, the results showed that by increasing the hammer impact time (decreasing the frequency of loading) the length of the induced stress wave increases, and therefore the induced and reflected waves overlapped considerably. This finding correlates well with the fact that in short piles (i.e. the length of the pile is considerably smaller than the stress wave length), the downward and upward travelling waves can overlap before the peak force or the velocity at the gauge location is reached. Furthermore, normalised intergranular tensors showed that introducing the IGS into the model the soil close to a pile would indicate the small strain behaviour during the unloading stage observed during pile driving.

- Despite using a simple soil constitutive model (Mohr-Coulomb) when simulating the dynamic load testing of a small-scale steel pipe pile, the soil-pile interface properties influences the dynamic response of the pile significantly. It was indicated that the effects of damping parameter β (related to soil stiffness) was more influential than damping parameter α (related to soil mass). The results showed that, using unified soil parameters and by adopting proper interaction and damping parameters, a reasonable match between numerical predictions and field measurements can be achieved. Therefore, the continuum numerical modelling can be used for interpretation of pile load testing, while the soil properties obtained from site investigations can directly be applied.
- Continuum-based numerical simulation adopting an advanced constitutive soil model hardening soil with small strain stiffness indicated a reasonable correlation between the measured and predicted results for a real and large-scale dynamic pile load testing by utilising the soil properties, obtained from different tests such as CPT, SDMT and triaxial tests, without any need for an iterative signal matching process. Further numerical assessment of head and toe deformations subjected to static loads using the hardening soil model with small strain stiffness, confirmed the suitability of this soil model for both static and dynamic load tests.
- This study shows that establishing a numerical model that utilises meaningful soil parameters to capture the static and dynamic behaviour of piles will enable design engineers to utilise a unified modelling framework for the design and quality control of piling projects. This study also showed that advanced soil constitutive models can result in good predictions without having to alter the soil parameters for the sake of signal matching. Moreover, the technique introduced to analyse dynamic pile load

testing can be exploited to evaluate different stages of simulation from pile driving to quality control with only one software package.

- The ground vibrations analysis indicated that particle velocity induced by the real and large-scale dynamic pile load testing further away decreases, thus proving that material damping into soil can be simulated correctly in the finite element program using the advanced HS-Small soil model. For instance, the vertical component of vibration was recorded in three different radial directions and it was observed that the peak particle velocity (PPV) from close distances (less than 10 m) reduces more than 96% in distances of more than 40m.
- After comparing the Ground vibrations indicated by PPV with the recommendations given by British, German and Australian standards, it was proved that distances of less than 10 m are intolerable and buildings may be damaged, but by increasing the distance up to 30 m reduces the risk of building damage, albeit complaints from inhabitants will occur. At quite long distances (more than 30 m) only the perception of vibration exists and it can be tolerated by most people, but because ground vibration at close distances is high, people feel discomfort and buildings may be damaged due to the impact piling. Therefore, impact piling and dynamic pile load testing is not recommended for urban and densely populated areas.

6.3 Recommendations for Future Research

This research can be expanded through the following studies:

- To assess the interaction between reaction piles and test piles under static load testing, further analyses is needed to better understand of the behaviour of piles during a static test. Future research may concentrate on the drained versus undrained conditions, by controlling the axial capacity of piles during static load testing. In addition, the

influence of other anchorage systems such as cable anchors on the test pile can be investigated and compared to the reaction piles system to evaluate the influence zone in each system. Furthermore, it is valuable to numerically perform more rigorous deformation analysis, adopting more advanced soil models such as hypoplastic soil model, and compare the results with those obtained by the hardening soil model.

- Part of this research focused on the assessment of the concrete bored piles group behaviour under axial static load testing. Future research may employ open-ended steel pipe piles with unplugged behaviour in a group in two different conditions including rigid cap resting on the ground and free-standing cap. Then the bearing capacity efficiency factor and settlement ratio of the pile group in different layouts can be evaluated.
- Part of this research concentrated on the continuum-based numerical simulation of dynamic pile load testing adopting basic and advanced soil models such as Mohr-Coulomb and hardening soil with small strain stiffness models to capture a reasonable correlation between measured and predicted traces during dynamic tests. This simulation can be performed using hypoplastic soil model with intergranular strain concept in which both large strain and small strain behaviours of soil during loading and unloading stages can be predicted appropriately. In addition, since in the hypoplastic soil model the interface shear strength has been directly defined in strength parameters instead of using a reduction factor (R_{int}), defined by the Mohr-Coulomb and hardening soil models, means that a more reasonable match between measured and predicted force and velocity traces can be expected.
- In this study, dynamic pile load testing was simulated numerically using finite element software and the obtained results correlated with the previously published field measurements to indicate the capability the continuum-based numerical

simulation. Further research could focus on an experimental study where steel pipe piles, steel H-piles and concrete piles in different soil layers are tested under different hammer energies to measure the force and velocity traces at the gauge location. The focus of the experimental study will especially be on the situations in which one-dimensional wave equation-based programs such as CAPWAP exhibit some limitations and the obtained static pile resistance does not correlate very well with static load testing. For instance, conducting dynamic pile load testing of open-ended steel pipe piles in dense sand deposits, due to the formation of soil plug inside the pile, can disturb the assumption of one-dimensional wave equation solution, and over-predicts the static soil resistance. In these situations, continuum-based numerical simulations providing more realistic and precise solution can be introduced as an alternative solution.

- Ground vibration induced by dynamic pile load testing can be further investigated and its influence on adjacent buildings can be assessed. The effects of dynamic pile load testing of solid concrete and open-ended steel pipe piles based on peak particle velocity and recorded at different distances from the source of vibration can be evaluated and compared.
- Future research should consider densification effects during pile penetration in sandy soils. This needs advanced soil models where change in void ratio due to densification can be quantified and subsequent effects on the mechanical properties can be automatically adjusted during the numerical analysis.
- Pile driving in clayey soils pile setup is an important issue. When penetrating below the water table, pore pressures will generate and sophisticated numerical models which can simulate cyclic loading related stiffness and strength degradation as well as excess pore pressure generation needs to be the aim of future research.

References

Achuhan, R., Subashi, G. & De Silva, S. 2016, 'Comparison between ground vibrations induced by impact piling and bored piling', paper presented to the *7th International Conference on Sustainable Built Environment*, Kandy, Sri Lanka.

Alielahi, H. & Adampira, M. 2016, 'Comparison between empirical and experimental ultimate bearing capacity of bored piles—a case study', *Arabian Journal of Geosciences*, vol. 9, no. 1, p. 78.

Andersson Olivecrona, S. 2016, 'Numerical analysis of vibrations due to impact pile driving', MSc Thesis, Lund University.

Applelianlian 2013, *Pile driving analyzer*, viewed 13 June 2016, <https://applelianlian.wordpress.com/2013/08/06/pile-driving-analyzer-pda-test/>.

ASTM International 2010, *Standard test method for high-strain dynamic testing of piles*, ASTM D4945, ASTM International, Philadelphia.

ASTM International 2013, *Standard test methods for deep foundations under static axial compressive load*, ASTM D1143, ASTM International, West Conshohocken.

Authier, J. & Fellenius, B.H. 1980, 'Quake values determined from dynamic measurements', paper presented to the *First International Conference on Application of Stress-Wave Theory to Piles* Stockholm, Sweden.

Bai, X., He, W., Jia, J. & Han, Y. 2006, 'Experimental Study on the Interaction Mechanism of Cap—Pile Group—Soil', *Marine Georesources and Geotechnology*, vol. 24, no. 3, pp. 173-82.

Benamar, A. 2000, 'Dynamic pile response using two pile-driving techniques', *Soil Dynamics and Earthquake Engineering*, vol. 20, no. 1-4, pp. 243-7.

Benz, T. 2007, *Small-strain stiffness of soils and its numerical consequences*, Institute of Geotechnique, University of Stuttgart, Germany.

Bhowmik, D., Baidya, D. & Dasgupta, S. 2016, 'A numerical and experimental study of hollow steel pile in layered soil subjected to vertical dynamic loading', *Soil Dynamics and Earthquake Engineering*, vol. 85, pp. 161-5.

Bowles, J.E. 1996, *Foundation analysis and design*, McGraw-Hill, New York, USA.

Brinkgreve, R., Kumarswamy, S. & Swolfs, W.M. 2017, *PLAXIS 2D Reference Manual*, Delft, Netherlands.

British Standard 1990, *Evaluation measurement for vibration in buildings- part 1: Guide for measurement of vibrations and evaluation of their effects on buildings*, BS 7385.1, British Standard, London.

British Standard 1993, *Evaluation and measurement for vibration in buildings-part 2: Guide to damage levels from ground-water vibration*, BS 7385.2, British Standrad, London.

British Standard 2008a, *Guide to evaluation of human exposure to vibration in buildings: Blast-induced vibration*, BS 6472.2, British Standard, London.

British Standard 2008b, *Guide to evaluation of human exposure to vibration in buildings: Vibration sources other than blasting*, BS 6472.1, British Standard, London.

British Standard 2009, *Code of practice for noise and vibration control on construction and open sites – Part 2: Vibration*, BS 5228.2, British Standard, London.

Brucy, F., Meunier, J. & Nauroy, J. 1991, 'Behavior of pile plug in sandy soils during and after driving', paper presented to the *Offshore Technology Conference*, Houston, Texas.

Bruno, D. & Randolph, M. 1999, 'Dynamic and static load testing of model piles driven into dense sand', *Geotech Geoenv Eng.*, vol. 125, no. 11, pp. 988-98.

Byrne, B. 1995, 'Driven pipe piles in dense sand', *Australian Geomechanics Journal*, no. 27, pp. 72-80.

Byrne, B. & Randolph, M. 2003, 'Seasonal variations in the performance of driven piles in sand', paper presented to the *Australian Geomechanics Society Symposium* Sydney, Australia.

Cao, W., Chen, Y. & Wolfe, W. 2014, 'New load transfer hyperbolic model for pile-soil interface and negative skin friction on single piles embedded in soft soils', *Int. J. Geomech*, vol. 14, no. 1, pp. 10.1061/(ASCE)GM.943-5622.0000289.

Chapman, G. 1993, 'The specification of static pile testing', *Australian Geomechanics Journal*, no. 24.

Chiesura, G. 1998, 'Some dynamic parameters of drilled piles under low and high-energy tests.“', paper presented to the *Seventh International Conference and Exhibition on Piling and Deep Foundations*, Vienna, Austria.

Christophe, J. 2014, 'Calculation of dynamic pile bearing capacity based on the displacement during driving', MSC Thesis, Faculty of Civil Engineering and Geosciences, Delft University of Technology.

Coduto, D. 2001, *Foundation Analysis and Design*, Prentice Hall, New Jersey.

Comodromos, E.M., Anagnostopoulos, C.T. & Georgiadis, M.K. 2003, 'Numerical assessment of axial pile group response based on load test', *Computers and Geotechnics*, vol. 30, no. 6, pp. 505-15.

Cox, C. & Mayne, P. 2015, 'Soil stiffness constitutive model parameters for geotechnical problems: A dilatometer testing approach', paper presented to the *Third International Conference on Flat Dilatometer*, Rome, Italy.

Coyle, H.M., Bartoskewitz, R.E. & Berger, W.J. 1973, *Bearing Capacity Prediction by Wave Equation Analysis*, Research report 125-BF, Texas Transportation Institute, Texas Highway Department, USA.

Coyle, H.M. & Sulaiman, I.H. 1970, 'Bearing capacity of foundation piles: state of the art', paper presented to the *49th Annual Conference of the Highway Research Board*, Washington, USA.

Crowther, C.L. 1988, *Load testing of deep foundations. The planning, design and conduct of pile load tests*, Wiley (John) & Sons, Limited, UK.

Dai, G., Salgado, R., Gong, W. & Zhang, Y. 2012, 'Load tests on full-scale bored pile groups', *Canadian Geotechnical Journal*, vol. 49, no. 11, pp. 1293-308.

Das, B.M. 2004, *Fundamentals of Geotechnical Engineering*, Cengage Learning, Inc, CA, United States.

Davisson, M. 1972, *Innovations in Foundation Construction*, Department of Civil Engineering, Illinois Institute of Technology, USA.

Dung, P.H. 2009, 'Modelling of installation effect of driven piles by hypoplasticity', MSC Thesis, Faculty of Civil Engineering & Geosciences, Delft University of Technology.

Dungca, J., Acosta, D., Juego, M., Sanchez, H. & Sanchez, I. 2016, 'The propagation behaviour of pile-driving-induced vibration done on soil at varying distances and its effects on existing structures', *International Journal of Geomate*, vol. 10, no. 21, pp. 1877-83.

Dutch International 2017, *Method statement for compressive load testing*, viewed 18 August 2018, <http://www.uaedic.com/?page_id=83>.

Elmi Anaraki, K. 2008, 'Hypoplasticity investigated', MSC Thesis, Delft University of Technology, Faculty of Civil Engineering & Geosciences.

ESC Group 2018, *Pile Fabrication and Welding*, viewed 25 September 2018, <https://www.escpiling.com/fabrication-and-welding>.

Fakharian, K., Masouleh, S.F. & Mohammadlou, A.S. 2014, 'Comparison of end-of-drive and restrike signal matching analysis for a real case using continuum numerical modelling', *Soils and Found*, vol. 54, no. 2, pp. 155-67.

Fakharian, K., Meskar, M. & Mohammadlou, A. 2013, 'Effect of surcharge pressure on pile static axial load test results', *International Journal of Geomechanics*, vol. 14, no. 6, p. 04014024.

Fang, H.Y., Winterkorn, H.F. & Van Nostrand, R. 1975, *Foundation Engineering Handbook*, New York.

Fattah, M.Y. & Al-Soudani, W.H. 2016, 'Bearing capacity of open-ended pipe piles with restricted soil plug', *Ships and Offshore Structures*, vol. 11, no. 5, pp. 501-16.

Fawaz, A., Hagechehade, F. & Farah, E. 2014, 'A study of the pressuremeter modulus and its comparison to the elastic modulus of soil', *Study of Civil Engineering and Architecture*, vol. 3, pp. 7-15.

Fellenius, B.H. 1975, 'Test loading of piles and new proof testing procedure', *Geotechnical and Geoenvironmental Engineering*, vol. 101, pp. 855-69.

Fellenius, B.H. 1980, 'The analysis of results from routine pile loading tests. ', *Ground Engineering Journal*, vol. 13, no. 6, pp. 19-31.

Fellenius, B.H. 1990, *Guidelines for the interpretation and analysis of the static loading test: a continuing education short course text*, A continuing education short course text, Deep Foundations Institute, USA.

Fellenius, B.H. & Altaee, A. 2002, 'Pile dynamics in geotechnical practice-six case histories', paper presented to the *International Deep foundations Congress, An International Perspective on Theory, Design, Construction, and Performance*, Orlando, USA.

Fleming, K., Weltman, A., Randolph, M. & Elson, K. 2008, *Piling engineering*, Taylor and Francis, Abingdon, England.

Fuller, F.M. & Hoy, H.E. 1970, *Pile load tests including quick-load test method, conventional methods, and interpretations*, Highway Research Record, 49th Annual Meeting, USA.

Garnier, J. 2001, 'Wave propagation in one-dimensional random media', *Panoramas et Synth'eses*, vol. 12, pp. 101-38.

Gary Puntman 2018, *Foundation, Concrete and Earthquake Engineering, weblog*, viewed 12 October 2018, <https://www.civil-engg-world.blogspot.com/2013/01/What-Working-Stress-of-Concrete-Designing-Pile-Foundation.html>.

Gentile, G. & Canceri, J. 2011, 'Design and construction planning of the Macleay River and Floodplain Bridge ', paper presented to the *8th of Austroads Bridge Conference, Sydney, Australia*.

German Standard 1999, *Vibration in buildings-Part 3: effects on structures provides recommended maximum levels of vibration that reduce the likelihood of building damage caused by vibration*, DIN 4150.3, German Standard, Berlin.

Goble, G. & Rausche, F. 1980, 'Pile drivability predictions by CAPWAP', paper presented to the *Numerical methods in offshore piling Conference*, London, UK.

Goble, G.G., Likins, G. & Rausche, F. 1975, *Bearing capacity of piles from dynamic measurements*, Technical Report, Department of Solid Mechanics, Structures and Mechanical Design, Case Western Reserve University, Cleveland, USA.

Goble, G.G. & Rausche, F. 1976, *Wave equation analysis of pile driving: WEAP program*, WEAP Program Manual, US Department of Transportation, Federal Highway Administration, Offices of Research and Development.

Gowthaman, S. & Nasvi, M. 2018, 'Three-dimensional numerical simulation and validation of load-settlement behaviour of a pile group under compressive loading', *Engineer*, vol. 51, no. 01, pp. 9-21.

Grand, B.A. 1970, 'Types of piles: their characteristics and general use', paper presented to the *49th Annual Conference of the Highway Research Board*, Washington, USA.

Gravare, C., Goble, G., Rausche, F. & Likins, G. 1980, 'Pile driving construction control by the Case method', *Ground Engineering Journal: United Kingdom, March issue*, pp. 20-5.

Green, T. & Kightley, M. 2005, 'CAPWAP testing-theory and application', paper presented to the *16th International Conference on Soil Mechanics and Geotechnical Engineering*, Osaka, Japan.

Gudehus, G. 1996, 'A comprehensive constitutive equation for granular materials', *Soils and Foundations*, vol. 36, no. 1, pp. 1-12.

Gunaratne, M. 2013, *The foundation engineering handbook*, CRC Press, USA.

Hajduk, E.L., Wright, W.B., Casey, T.J. & Dullanty, R.E. 2004, 'Steel Pipe Pile Design, Installation, and Dynamic Testing for a New Pier in Georgetown, SC', paper presented to the *Fifth International Conference on Case Histories in Geotechnical Engineering*, New York, USA.

Han, G.-x., Gong, Q.-m. & Zhou, S.-h. 2015, 'Soil arching in a piled embankment under dynamic load', *Int. J. Geomech*, vol. 15, no. 6, pp. 10.1061/(ASCE)GM.943-5622.0000443, 04014094.

Han, Y. 1999, 'Axial load tests and analysis for open-ended steel tubular piles driven into weathered rock', MSC Thesis, Department of Civil Engineering, University of Ottawa, Cananda.

Handley, B., Ball, J., Bell, A. & Suckling, T. 2006, *Handbook on Pile Load Testing*, Federation of Piling Specialists, Beckenham, Australia.

Hannigan, P.J., Goble, G.G., Thendean, G., Likins, G.E. & Rausche, F. 1998, *Design and construction of driven pile foundations-volume II. Design and Construction of Driven Pile Foundations*

U.S. Department of Transportation, Federal Highway Administration, Washington, USA.

Haque, M.N., Abu-Farsakh, M.Y. & Tsai, C. 2016, 'Field investigation to evaluate the effects of pile installation sequence on pile setup behavior for instrumented test piles', *Geotech. Test. J.*, vol. 39, no. 5, pp. 769-85.

Heritier, B., Paquet, J. & Stain, R. 1991, 'The accuracy and limitations of full scale dynamic shaft testing', paper presented to the *Transportation Research Board, 70th Annual Meeting*, USA.

Hertlein, B. & Davis, A. 2007, *Nondestructive testing of deep foundations*, John Wiley & Sons, USA.

Hoľko, M. & Stacho, J. 2014, 'Comparison of Numerical Analyses with a Static Load Test of a Continuous Flight Auger Pile', *Slovak Journal of Civil Engineering*, vol. 22, no. 4, pp. 1-10.

Huang, J., Kelly, R., Li, D., Zhou, C. & Sloan, S. 2016, 'Updating reliability of single piles and pile groups by load tests', *Computers and Geotechnics*, vol. 73, pp. 221-30.

Hussein, M.H. & Goble, G.G. 2004, 'A brief history of the application of stress-wave theory to piles', paper presented to the *Current Practices and Future Trends in Deep Foundations*, Geotechnical Special Publication, USA.

International Standard 2014, *Mechanical vibration and shock - evaluation of human exposure to whole body vibration Part 2: Vibration in buildings (1 Hz to 80 Hz)*, ISO 2631.2, International Organisation for Standardisation

Ismael, N.F. 2001, 'Axial load tests on bored piles and pile groups in cemented sands', *Geotechnical and Geoenvironmental Engineering*, vol. 127, no. 9, pp. 766-73.

Issacs, D. 1931, 'Reinforced concrete pile formulas', *Institution of Engineers Australia*, vol. 3, no. 9, pp. 305-23.

Ju, J. 2015, 'Prediction of the settlement for the vertically loaded pile group using 3D finite element analyses', *Marine Georesources & Geotechnology*, vol. 33, no. 3, pp. 264-71.

Karlowskis, V. 2014, 'Soil Plugging of Open-Ended Piles During Impact Driving in Cohesion-less Soil', MSC Thesis, School of Architecture and the Built Environment, Civil and Architectural Engineering, Soil and Rock Mechanics, KTH Royal Institute of Technology, Sweden.

Kasali, G., Lemke, J., Jabakhanji, R. & Mabsout, M. 2006, 'Finite element model of dynamic pile test using embedded transducers', paper presented to the *GeoCongress Conference: Geotechnical Engineering in the Information Technology Age*, Atlanta, USA.

Kim, D., Bica, A.V., Salgado, R., Prezzi, M. & Lee, W. 2009, 'Load testing of a closed-ended pipe pile driven in multilayered soil', *Geotech. Geoenv. Eng.* , vol. 135, no. 4, pp. 463-73.

Klain, D. 1993, 'Static and dynamic performance of piles', PhD Thesis, Department of Civil Engineeing, University of Wetern Australia, Australia.

Klos, J. & Tejchman, A. 1981, 'Bearing capacity calculation for pipe piles', paper presented to the *10th International Conference on Soil Mechanics and Foundation Engineering* Stockholm, Sweden.

Kolymbas, D. 1985, 'A generalised hypoelastic constitutive law', paper presented to the *11th International Conference of Soil Mechanics and Foundation Engineering*, San Francisco, USA.

Lee, J., Salgado, R. & Paik, K. 2003, 'Estimation of load capacity of pipe piles in sand based on cone penetration test results', *Geotechnical and Geoenvironmental Engineering*, vol. 129, no. 5, pp. 391-403.

Lee, S., Chow, Y., Karunaratne, G. & Wong, K. 1988, 'Rational wave equation model for pile-driving analysis', *Geotechnical Engineering*, vol. 114, no. 3, pp. 306-25.

Likins, G. 2015, 'Pile Testing – State of the Art ', paper presented to the *8th Seminar on Special Foundations Engineering and Geotechnics*, Sao Paulo, Brazil.

Likins, G.E. & Rausche, F. 2004, 'Correlation of CAPWAP with static load tests', paper presented to the *Seventh International Conference on the Application of Stresswave Theory to Piles*, Kuala Lumpur, Malaysia.

Likitlersuang, S., Teachavorasinskun, S., Surarak, C., Oh, E. & Balasubramaniam, A. 2013, 'Small strain stiffness and stiffness degradation curve of Bangkok clays', *Soils and Foundations*, vol. 53, no. 4, pp. 498-509.

Lowery, L.L., Hirsch, T., Edwards, T.C., Coyle, H.M. & Samson, C. 1969, *Pile driving analysis: State of the art*, Texas Transportation Institute, Texas A & M University, Texas.

Lysmer, J. & Kuhlemeyer, R.L. 1969, 'Finite dynamic model for infinite media', *Engineering Mechanics* vol. 95, no. 4, pp. 859-78.

Makredes, H. & Likins, G. 1982, 'Bearing capacity of piles from dynamic measurements', paper presented to the *Seventh Southeast Asian Geotechnical Conference*, Hong Kong.

Manna, B. & Baidya, D. 2009, 'Vertical vibration of full-scale pile—analytical and experimental study', *Geotechnical and Geoenvironmental Engineering*, vol. 135, no. 10, pp. 1452-61.

Mašın, D. 2010, *PLAXIS implementation of Hypoplasticity*, Delft, Netherlands.

Mašín, D. 2015, *Hypoplasticity for practical applications*, PhD course on hypoplasticity, Zhejiang University, China.

Masouleh, S.F. & Fakharian, K. 2008, 'Application of a continuum numerical model for pile driving analysis and comparison with a real case', *Comput. Geotech*, vol. 35, no. 3, pp. 406-18.

Massarsch, K.R. & Fellenius, B.H. 2008, 'Ground vibrations induced by impact pile driving', paper presented to the *Sixth International Conference on Case Histories in Geotechnical Engineering*, Arlington, USA.

Mhaiskar, S., Khare, M. & Vaidya, R. 2010, 'High strain dynamic pile testing and static load test–a correlation study', paper presented to the *Indian Geotechnical Conference* Bombay, India.

Mijena, E.H. 2012, 'A comparison of friction piles bearing capacity based on theoretical and empirical mathematical models', MSC Thesis, Department of Civil and Transport Engineering, Norwegian University of Science and Technology.

Morgano, C., White, B. & Allin, R. 2008, 'Dynamic testing in sensitive and difficult soil conditions', paper presented to the *8th International Conference on the Application of Stress-Wave Theory to Piles*, Lisbon, Portugal.

Nath, B. 1990, 'A continuum method of pile driving analysis: Comparison with the wave equation method', *Computers and Geotechnics*, vol. 10, no. 4, pp. 265-85.

Naturalzemin 2019, *CFA Piles*, viewed 12 December 2018, <http://www.naturalzemin.com/en/services/cfa-pile/>.

Ng, K.W. 2011, 'Pile setup, dynamic construction control, and load and resistance factor design of vertically-loaded steel H-Piles', PhD Thesis, Department of Civil, Construction, and Environmental Engineering, Iowa State University, United States.

Ng, K.W. & Sritharan, S. 2013, 'Improving dynamic soil parameters and advancing the pile signal matching technique', *Comput. Geotech*, vol. 54, pp. 166-74.

Ng, K.W., Suleiman, M.T., Roling, M., AbdelSalam, S.S. & Sritharan, S. 2011, *Development of LRFD Design Procedures for Bridge Piles in Iowa Field Testing of Steel H-Piles in Clay, Sand, and Mixed Soils and Data Analysis (Volume II)*, Departmental Report, TR-583, Department of Transportation, Iowa, USA.

Niemunis, A. & Herle, I. 1997, 'Hypoplastic model for cohesionless soils with elastic strain range', *Mechanics of Cohesive-frictional Materials*, vol. 2, no. 4, pp. 279-99.

Obrzud, R.F. 2010, 'On the use of the Hardening Soil Small Strain model in geotechnical practice', paper presented to the *Numerics in Geotechnics and Structures Conference*, Lausanne, Switzerland.

Paikowsky, S. & Chernauskaus, L. 2008, 'Dynamic analysis of open ended pipe piles', paper presented to the *8th international conference on the application of the stress wave theory to piles*, Lisbon, Portugal.

Paikowsky, S.G. 2006, *Innovative load testing systems*, Prepared for Transportation Research Board of the National Academies, USA.

Pile Buck 2018, *Pile Types and Guidelines for Selection*, viewed 28 September 2018, <http://www.pilebuck.com/pile-driving-by-pile-buck/chapter-2-pile-types-guidelines-selection/>.

Pinto, P., Grazina, J. & Lourenco, J. 2008, 'Evaluation of 1D and 2D numerical modelling techniques of dynamic pile testing', paper presented to the *8th International Conference on the Application of Stress Wave Theory to Piles*.

Poulos, H.G. & Davis, E.H. 1980, *Pile foundation analysis and design*, Wiley, New York.

Prakash, S. & Sharma, H.D. 1990, *Pile foundations in engineering practice*, John Wiley & Sons.

Rajapakse, R.A. 2016, *Pile design and construction rules of thumb*, Butterworth-Heinemann, New York, USA.

Randolph, M. 2003, 'Science and empiricism in pile foundation design', *Geotechnique*, vol. 53, no. 10, pp. 847-76.

Rausche, F. 1970, 'Soil response from dynamic analysis and measurements on piles', PhD Thesis, Department of Solid Mechanics, Structures, and Mechanical Design, Case western reserve university.

Rausche, F. 1990, *Reasons for CAPWAP underprediction and overprediction*, PDA Users Day, Cleveland, USA.

Rausche, F., Goble, G.G. & Likins, G.E. 1985, 'Dynamic determination of pile capacity', *Geotechnical Engineering*, vol. 111, no. 3, pp. 367-83.

Rausche, F., Robinson, B. & Liang, L. 2000, 'Automatic signal matching with CAPWAP', paper presented to the *Sixth International Conference on the Application of Stress-Wave Theory to Piles*, London, UK.

Rezazadeh, S. & Eslami, A. 2017, 'Empirical methods for determining shaft bearing capacity of semi-deep foundations socketed in rocks', *Rock Mechanics and Geotechnical Engineering*, vol. 9, no. 6, pp. 1140-51.

Robinson, B. & Rausche, F. 2000, *Dynamic Pile Load Test and Crosshole Sonic Logging Results*, Reports submitted by GRL to the FHWA, USA.

Salgado, R. 2008, *The engineering of foundations*, McGraw-Hill New York.

Schanz, T., Desrues, J. & Vermeer, P. 1997, 'Comparison of sand data on different plane strain devices', paper presented to the *Deformation and Progressive Failure in Geomechanics Symposium, IS-Nagoya 97*, Nagoya, Japan.

Setiawan, B. & Fad, Z.G. 2012, 'Prediction of Ground Vibrations During Pile Driving Through Finite Element Method Simulations', paper presented to the *16th Indonesian Society of Geotechnical Engineering Conference*, Jakarta, Indonesia.

Shooshpasha, I., Mola-Abasia, H. & Amiri, I. 2013, 'Evaluation of static and dynamic methods for determining the bearing capacity of the driven pipe piles', *Int. J. Eng.* , vol. 27, no. 2, pp. 307-14.

Sitharam, T. 2013, *Advanced Foundation Engineering*, PRODUCTIVITY PRESS, Indian Institute of Science, Bangalore.

Smith, E.A. 1960, 'Pile driving analysis by the wave equation', *Soil Mechanics and Foundation Division*, vol. 127, no. 1, pp. 1145-70.

Smith, I., To, P. & Wilson, S. 1986, 'Plugging of pipe piles', paper presented to the *3rd International Conference on Numerical Methods in Offshore Piling*, Paris, France.

Smoltczyk, U. 2003, *Geotechnical Engineering Handbook, Procedures*, vol. 2, John Wiley & Sons.

Spagnoli, G. & Weixler, L. 2013, 'Drilling technologies for offshore foundation engineering', paper presented to the *32nd international conference on ocean, offshore and arctic engineering*, Nantes, France.

Standards Australia 1990, *Evaluation of human exposure to whole-body vibration Part 2: Continuous and shock- induced vibration in buildings (1 to 80 Hz)*, AS 2670.2, Standards Australia, Sydney.

Standards Australia 1995, *Piling design and installation*, AS 2159, Standards Australia, Sydney.

Stuckmeyer, M.G. 2014, 'Two driven pile load tests for use in Missouri LRFD guidelines', MSC Thesis, Missouri University of Science and Technology, USA.

Surjadinata, J. 2007, *Analysis and design of pile foundations: pile testing*, Lecture Notes, Department of Civil Engineering, The University of Sydney

Svinkin, M. & Woods, R. 2009, 'Dynamic loads for high-strain dynamic pile testing', paper presented to the *17th International Conference on Soil Mechanics and Geotechnical Engineering*, Seoul, South Korea.

Swan, C.C. 2013, *Changes in soil during pile driving*, Supplemental Note of Foundation Engineering, The University of Iowa, USA.

Szechy, C. 1961, 'The effect of vibration and driving upon the voids in granular soil surrounding a pile', paper presented to the *5th International Conference on Soil Mechanics and Foundation Engineering*, Paris, France.

Tomlinson, M. & Woodward, J. 2014, *Pile design and construction practice*, CRC Press Inc, UK.

Von Wolffersdorff, P.A. 1996, 'A hypoplastic relation for granular materials with a predefined limit state surface', *Mechanics of Cohesive-frictional Materials*, vol. 1, no. 3, pp. 251-71.

Weech, C.N. 2002, 'Installation and load testing of helical piles in a sensitive fine-grained soil', MSC Thesis, Department of Civil Engineering, University of British Columbia.

Wehnert, M. & Vermeer, P. 2004, 'Numerical analyses of load tests on bored piles', paper presented to the *9th Numerical methods in geomechanics*, Ottawa, Canada.

Wong, M.-k. 2006, 'A study of capacity predictions for driven piles by dynamic pile testing', PhD Thesis, Department of Civil Engineering, The University of Hong Kong.

Xu, B., Bull, G., Tomic, D. & Clover, A. 2011, 'Steel pipe pile wall for the northern abutment of Go Between Bridge in Brisbane, Australia', paper presented to the *8th Austroads Bridge Conference*, Sydney, Australia.

Yang, J. 2006, 'Influence zone for end bearing of piles in sand', *Geotechnical and Geoenvironmental Engineering*, vol. 132, no. 9, pp. 1229-37.

Yetginer, A., White, D. & Bolton, M. 2006, 'Field measurements of the stiffness of jacked piles and pile groups', *Géotechnique*, vol. 56, no. 5, pp. 349-54.

Yi, L. 2004, 'Finite element study on static pile load testing', MSC Thesis, Department of Civil Engineering, National University of Singapore, Singapore.

Yu, F. & Yang, J. 2011, 'Base capacity of open-ended steel pipe piles in sand', *Journal of Geotechnical and Geoenvironmental Engineering*, vol. 138, no. 9, pp. 1116-28.

Yu, F. & Yang, J. 2012, 'Base capacity of open-ended steel pipe piles in sand', *Geotechnical and Geoenvironmental Engineering*, vol. 138, no. 9, pp. 1116-28.

Zhou, J., Zhang, L., Zhang, X., Jiang, H. & Oh, E. 2019, 'Behaviour of Displacement Concrete Pile under Ccompressive Loads', *International Journal of Geomate*, vol. 16, no. 54, pp. 200-8.

Appendices

Boreholes Information at the location of Pier 11 of Bypass Bridge

&

Measured Data during the Dynamic Pile Load Testing

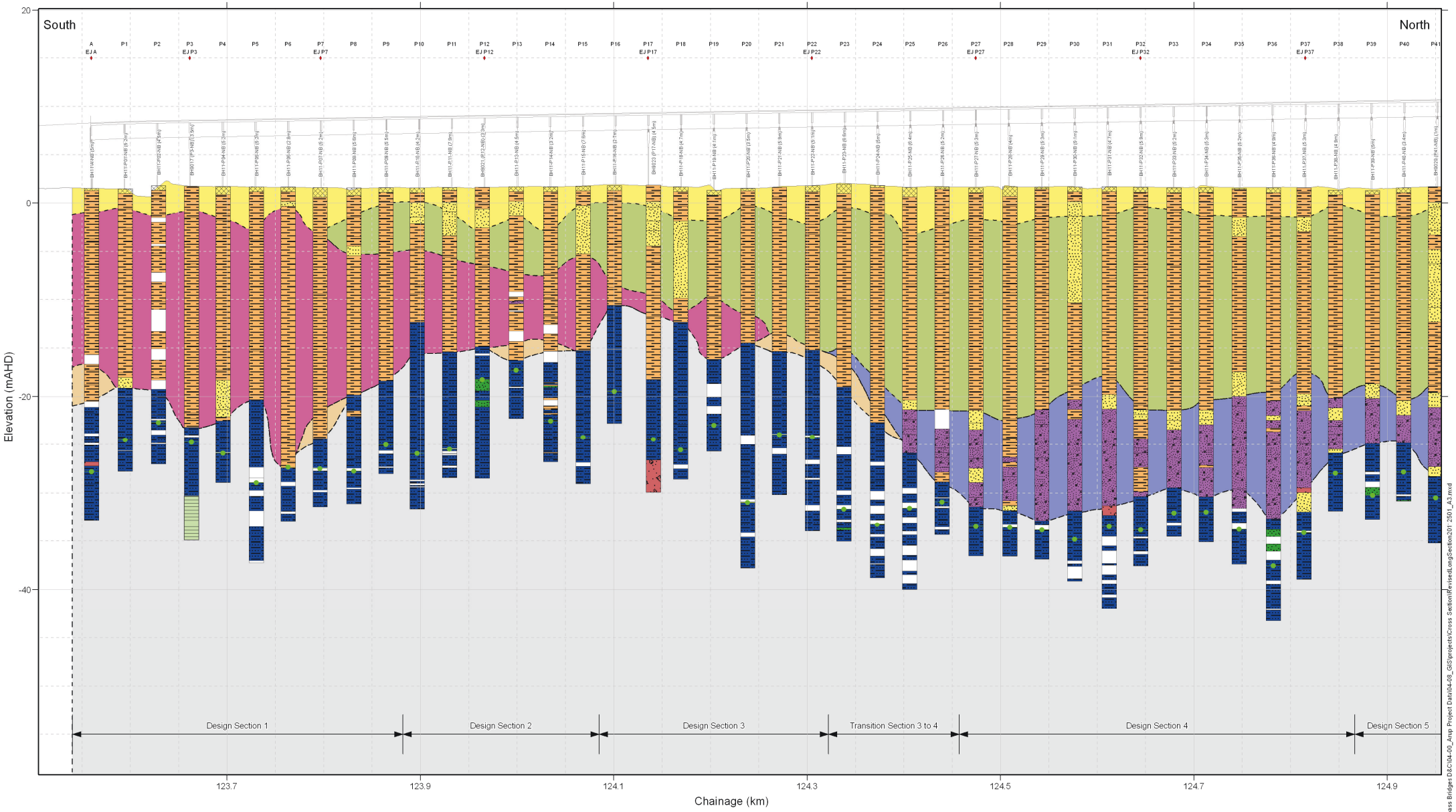

Borehole Material (Main Component)

- Fill
- Clays and Silts
- Sands
- Gravels
- Cobbles and Boulders
- Core Loss
- Siltstone/ Mudstone
- Laminite
- Sandstone
- Fault Breccia
- Conglomerate

Geological Unit

- Holocene Alluvium
- Holocene Estuarine
- Old Alluvium (Weathered)
- Old Alluvium (Channel Deposits)
- Residual Soil
- Rock
- Proposed Toe Level

BH1-P11-NB (-3m) - BH ID (Offset, +ve West)
EJ - Expansion Joint
A/ B - Abutment
P2 - Pier Number

Abigroup
Constructing Australia's Future

benaim

Client: Abigroup

Job Title: MRFB

Drawing Title: Geological Long Section: Northbound 1 of 2

10 x Vertical Exaggeration

Issue	Date	By	Chkd	Appd
P3	2011-09-12	ID	KN	TM

ARUP
Level 10, 201 Kent Street
Sydney, NSW 2001
Tel +61 (2)9320 9320 Fax +61 (2)9320 9321
www.arup.com

Scale at A3	Drawing Status
NTS	Final

Coordinate System: GDA94, MGA94 - Zone 56

Job No	Figure No
221203-00	Appendix B-1

\\global.arup.com\australasia\SYD\Projects\221203 - Kempsey Bypass Bridges D&C\04-00_Arup Project Data\04-08_GIS\projects\Cross Section\RevisedLongSection\201 2501_A3.mxd

DISTANCE ALONG BASELINE (m)

REDUCED LEVEL (m .)

BH11-P09-NB
BH11-P10-NB
BH11-P11-NB
BH9021 (P12-NB)
BH11-P13-NB
BH11-P14-NB
BH11-P15-NB

Minimum check (C) = 0% Unchecked (U) = 86% of holes

Source data status: of holes
Database check status: Full check (A) = 0% Partial/selective check (B) = 0%

SCALE 1:222V 1:611H @ A3L

LEGEND

Hole offset is +ve to the RIGHT of the baseline

HoleID
(Offset)

PLAN

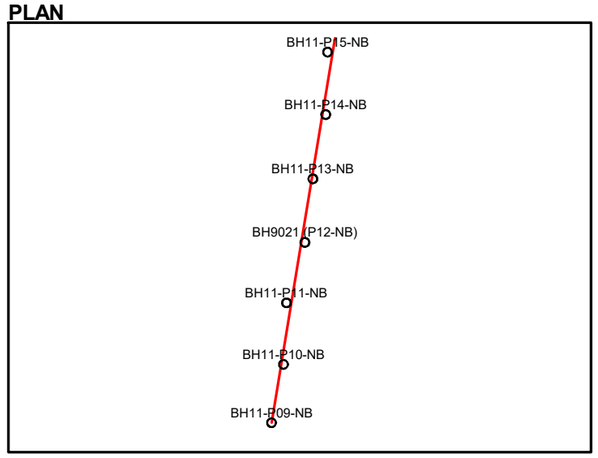

- Fill [Fill]
- Topsoil [Topsoil]
- Holocene Alluvium [Holocene Alluvium]
- Holocene Estuarine [Holocene Estuarine]
- Old Alluvium (Channel deposits) [Old Alluvium (Channel deposits)]
- Old Alluvium (Weathered) [Old Alluvium (Weathered)]
- Residual Soil [Residual Soil]
- Bedrock [Bedrock]

- TOPSOIL
- CL CLAY
- ML CLAY
- CH CLAY
- SILTSTONE
- CORE LOSS
- MH SILT
- SM SAND
- SC SAND
- GC GRAVEL
- MUDSTONE
- SANDSTONE

- SP SAND
- SILTSTONE
- CORE LOSS
- SANDSTONE

MRFB
GEOLOGICAL CROSS SECTION
Design Section 2 Northbound

221203

FIGURE B.4

<<DrawingFileSpec>>

DISTANCE ALONG BASELINE (m)

REDUCED LEVEL (m .)

BH11-P09-SB (1.0)
S M
VS W
F W
XW EL
VL
DW L
SW M
H

BH11-P10-SB (-1.6)
VST-H M
S-F M
VS-S M
S-F M
VS-S M
VST-H M
S-F M
VST-H M
XW
VST-H D
DW L
SW L-M
SW L-M
SW L-M
SW L-M

BH11-P11-SB (0.2)
S W
S-F W
S W
VL-L W
VL W
S W
F-S W
ST W
VST W
RS VL
XW L
DW M
M-H
EL
L
XW/RS EL
DW L
EL
VL
L-M
XW/RS EL
XW/RS VL
EL
EL
VL
VL-L

BH11-P12-SB (1.9)
S M
VS W
S W
F W
XW VL
XW EL-VL
DW VL
RS EL
DW VL
VL-L
SW L
M-H
H
FR H-VH

BH11-P13-SB (-0.9)
S D
F-S M
F M-W
VS-S W
F M-W
F-S M
VST M
ST-VST M
VST-H M
ST-VST M
VST-H M
H M
H D-M
H D-M
XW EL
DW L
L-M

BH11-P14-SB (-1.0)
S M
S-F M
L-MD M
S M
F-S M
ST M
DW L
DW L
SW L-M

BH11-P15-SB (0.4)
S D-M
M M
S M
S M
S-F M
ST-VST M
XW EL
SW M-H
DW/EW EL-VL
SW M
DW/EW EL-VL
SW M

Source data status: of holes
Database check status: Full check (A) = 0% Partial/selective check (B) = 0% Minimum check (C) = 0% Unchecked (U) = 100% of holes

SCALE 1:222V 1:611H @ A3L

LEGEND

Hole offset is +ve to the RIGHT of the baseline

HoleID (Offset)

PLAN

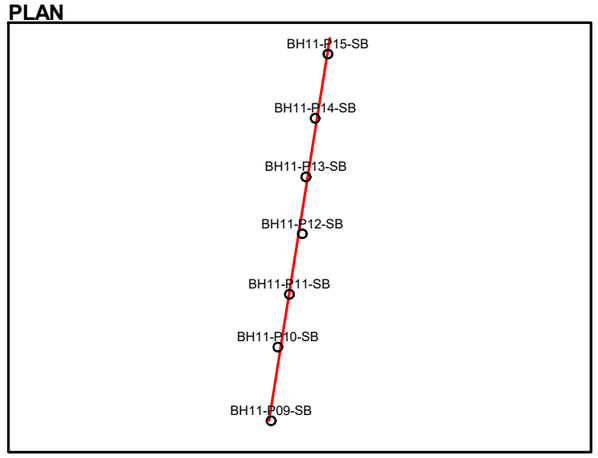

- Fill [Fill]
- Topsoil [Topsoil]
- Holocene Alluvium [Holocene Alluvium]
- Holocene Estuarine [Holocene Estuarine]
- Old Alluvium (Channel deposits) [Old Alluvium (Channel deposits)]
- Old Alluvium (Weathered) [Old Alluvium (Weathered)]
- Residual Soil [Residual Soil]
- Bedrock [Bedrock]

- TOPSOIL
- CH CLAY
- CL CLAY
- ML CLAY
- CORE LOSS
- SILTSTONE
- MH SILT
- SM SAND
- OL ORGANIC SILT

MRFB
GEOLOGICAL CROSS SECTION
Design Section 2 Southbound

221203

FIGURE B.16

<<DrawingFileSpec>>

ARUP — BOREHOLE RECORD

BH11-P11-NB (HOLE) | SHEET 1 OF 4

CLIENT	Abigroup	LOGGED BY	JY/RS
PROJECT	MRFB	CHECKED BY	JD
		DRILLED DATE	10-May-11 to 01-Jun-11
CONTRACTOR	Boart Longyear	ANGLE	Vertical
DRILL MODEL	T600/CME	BEARING	-
DRILLER	Denzil Roberts/Paul Wilson	HOLE DIAMETER	(*See Notes)
		GROUND LEVEL	~RL 1.60m
		LOCATION	489225 E 6563825 N
		ELEVATION DATUM	Australian Height Datum
		COORDINATE SYSTEM	Map Grid of Australia (MGA)

DRILLING	STRATA				MATERIAL DESCRIPTION	CONDITION		OBSERVATION
SAMPLE, TEST, BIT, SUPPORT, ETC.	R.L. (m.)	DEPTH (m)	GROUP SYMBOL	LEGEND	SOIL TYPE Plasticity / Grain Size, Colour, Minor Components	WATER / MOISTURE	CONSISTENCY: COHESIVE (VS, S, F, ST, VST, H) / NON COHESIVE (VL, L, MD, D, VD)	SOIL ORIGIN, STRUCTURE, ETC.
	1.30	0.30	ML		Clayey SILT (ML) low to medium plasticity, dark brown, trace rootlets.	M		**Topsoil**
			ML		Clayey SILT (ML) low to medium plasticity, dark brown, trace rootlets.	M		**Holocene Alluvium**
	0.60	1.00	MH		Sandy Clayey SILT (MH) medium plasticity, grey, sand, fine grained.	M		**Holocene Alluvium**
pH = 5.5 @ 1m pH = 6 @ 3m	0.10	1.50	SM		Silty SAND (SM) fine grained, grey, trace rootlets, iron stained.	M		**Holocene Alluvium**
	-0.90	2.50	SM		Silty SAND, (SM) fine grained, grey, trace shells and shell fragments.	M		**Holocene Estuarine**
						M		
					.... 4.00m increase in silt content			
B Bulk	-3.40	5.00	ML		Sandy SILT (ML) low plasticity, grey, sand, fine grained, trace shells and shell fragments.	M		**Holocene Estuarine**
	-5.60	7.20	MH		Clayey SILT (MH) medium plasticity, green-grey, iron stained.			**Old Alluvium (Weathered)**
B Bulk						M		
						M		

NOTES *Hole Diameter 150mm to 27.00m depth. (Sonic then 76mm to 30.00m depth NQ)
Soil consistency assessed on recovered disturbed sample.

JOB 221203

ARUP

BOREHOLE RECORD

BH11-P11-NB
HOLE

SHEET 2
OF 4

CLIENT	Abigroup	LOGGED BY	JY/RS
PROJECT	MRFB	CHECKED BY	JD
		DRILLED DATE	10-May-11 to 01-Jun-11
CONTRACTOR	Boart Longyear	ANGLE	Vertical
DRILL MODEL	T600/CME	BEARING	-
DRILLER	Denzil Roberts/Paul Wilson	HOLE DIAMETER	(*See Notes)
		GROUND LEVEL	~RL 1.60m
		LOCATION	489225 E 6563825 N
		ELEVATION DATUM	Australian Height Datum
		COORDINATE SYSTEM	Map Grid of Australia (MGA)

DRILLING	STRATA				MATERIAL DESCRIPTION	CONDITION			OBSERVATION
SAMPLE, TEST, BIT, SUPPORT, ETC.	R.L. (m.)	DEPTH (m)	GROUP SYMBOL	LEGEND	SOIL TYPE Plasticity / Grain Size, Colour, Minor Components	WATER / MOISTURE	CONSISTENCY: COHESIVE (VS, S, F, ST, VST, H)	CONSISTENCY: NON COHESIVE (VL, L, MD, D, VD)	SOIL ORIGIN, STRUCTURE, ETC.
			MH		Clayey SILT (MH) medium plasticity, green-grey, iron stained. *(continued)*				**Old Alluvium (Weathered)**
		11			.... 11.00m becoming pale grey, apparent structure				
		12			.... 12.00m - 17.00m increased iron stained portion				
		13							
		14							
		15							
		16							
	-15.40	17 17.00			SILTSTONE grey, iron stained, extremely weathered, very low strength.	D			**Bedrock**
B Bulk		18							
		19							

NOTES *Hole Diameter 150mm to 27.00m depth. (Sonic then 76mm to 30.00m depth NQ)
Soil consistency assessed on recovered disturbed sample.

JOB 221203

BOREHOLE RECORD

ARUP

BH11-P11-NB
HOLE

SHEET 3
OF 4

CLIENT	Abigroup	LOGGED BY	JY/RS
PROJECT	MRFB	CHECKED BY	JD
		DRILLED DATE	10-May-11 to 01-Jun-11
CONTRACTOR	Boart Longyear	ANGLE	Vertical
DRILL MODEL	T600/CME	BEARING	-
DRILLER	Denzil Roberts/Paul Wilson	HOLE DIAMETER	(*See Notes)
		GROUND LEVEL	~RL 1.60m
		LOCATION	489225 E 6563825 N
		ELEVATION DATUM	Australian Height Datum
		COORDINATE SYSTEM	Map Grid of Australia (MGA)

DRILLING	STRATA				MATERIAL DESCRIPTION	CONDITION										OBSERVATION
SAMPLE, TEST, BIT, SUPPORT, ETC.	R.L.	DEPTH	GROUP SYMBOL	LEGEND	SOIL TYPE Plasticity / Grain Size, Colour, Minor Components	WATER / MOISTURE	CONSISTENCY									SOIL ORIGIN, STRUCTURE, ETC.
							COHESIVE					NON COHESIVE				
	m.	m					VS	S	F	ST	VST	H	VL	L	MD	D	VD	
					SILTSTONE grey, iron stained, extremely weathered, very low strength. *(continued)*													**Bedrock**
		21																
		22			.... 22.00m increased iron stained portion													
		23			.... 23.00m becoming grey-brown													
		24			.... 24.25m becoming dark grey													
		25																
	-23.65	25.25			SILTSTONE grey, slightly weathered, medium strength.													**Bedrock**
		26																
		27			Borehole continued as a Cored Drillhole													
		28																
		29																

NOTES *Hole Diameter 150mm to 27.00m depth. (Sonic then 76mm to 30.00m depth NQ)
Soil consistency assessed on recovered disturbed sample.

JOB 221203

ARUP

CORED BOREHOLE RECORD

BH11-P11-NB
HOLE

SHEET 4
OF 4

CLIENT	Abigroup	LOGGED BY	JY/RS
PROJECT	MRFB	CHECKED BY	JD
		DRILLED DATE	10-May-11 to 01-Jun-11
CONTRACTOR	Boart Longyear	ANGLE	Vertical
DRILL MODEL	T600/CME	BEARING	-
DRILLER	Denzil Roberts/Paul Wilson	HOLE DIAMETER	(*See Notes)
		GROUND LEVEL	~RL 1.60m
		LOCATION	489225 E 6563825 N
		ELEVATION DATUM	Australian Height Datum
		COORDINATE SYSTEM	Map Grid of Australia (MGA)

DRILLING				STRATA			MATERIAL DESCRIPTION	DISCONTINUITIES					
TCR % (Drill rate)	SCR / (RQD)	FLUSH RETURN % (TYPE)	SAMPLES ($CaCO_3$, SPT, UCS, etc)	R.L. m.	DEPTH m	GRAPHIC LOG	ROCK TYPE Grain Size, Texture/Fabric, Colour, Minor Components	WEATHERING	ESTIMATED ROCK STRENGTH (EL VL L M H VH EH)	Is 50 (MPa)	FREQUENCY (per m) (30 10 3 1)	SPECIFIC TYPE	SPECIFIC ANGLE	SPECIFIC THICKNESS (mm)	GENERAL DESCRIPTION: Planarity, Roughness, Coating, Infill
					21										
					22										
					23										
					24										
					25										
					26										
				-25.40	27 27.00		Continued from Borehole								
				-25.50	27.10		CORE LOSS.								
				-25.70	27.30		SILTSTONE fine grained, thinly laminated, dark grey, iron stained.	DW		D0.84					
				-25.95	27.55		CORE LOSS.								
				-25.98	27.58		SILTSTONE fine grained, thinly laminated, dark grey, iron stained.	DW							
				-26.13	27.73		CORE LOSS.	DW							
					28		SILTSTONE fine grained, thinly laminated, dark grey, iron stained.					Sh			IR Ro4 FE
												Sh			IR Ro4 FE
										D0.81		Sh			IR Ro3 CL
				-27.20	28.80		CORE LOSS.	SW							
				-27.40	29 29.00		SILTSTONE fine grained, thinly laminated, dark grey, iron stained.	SW				Sh			IR Ro4 CL
												Sh			IR Ro4 CL
												Sh			IR Ro4 CL
67()	13/(0)	80 %													
87()	11/(9)	80 %		-28.40	30.00		End of Borehole at 30.00m								

NOTES

*Hole Diameter 150mm to 27.00m depth. (Sonic then 76mm to 30.00m depth NQ)
Soil consistency assessed on recovered disturbed sample.

See explanatory notes for details of abbreviations and basis of descriptions

JOB 221203

ARUP

BOREHOLE RECORD

BH11-P11-SB
HOLE

SHEET 1
OF 4

CLIENT	Abigroup	LOGGED BY	JQ
PROJECT	MRFB	CHECKED BY	KN
		DRILLED DATE	21-Mar-11 to 23-Mar-11
CONTRACTOR	Terratest	ANGLE	Vertical
DRILL MODEL	EDSON 3000	BEARING	-
DRILLER	James Hodder	HOLE DIAMETER	(*See Notes)
		GROUND LEVEL	~RL 1.60m
		LOCATION	489242 E 6563828 N
		ELEVATION DATUM	Australian Height Datum
		COORDINATE SYSTEM	Map Grid of Australia (MGA)

DRILLING	STRATA				MATERIAL DESCRIPTION	CONDITION		OBSERVATION
SAMPLE, TEST, BIT, SUPPORT, ETC.	R.L. (m.)	DEPTH (m)	GROUP SYMBOL	LEGEND	SOIL TYPE Plasticity / Grain Size, Colour, Minor Components	WATER / MOISTURE	CONSISTENCY: COHESIVE (VS, S, F, ST, VST, H) / NON COHESIVE (VL, L, MD, D, VD)	SOIL ORIGIN, STRUCTURE, ETC.
B 1	1.10	0.50	CH		Silty CLAY (CH) high plasticity, brown, trace grass roots, organic smell.	W		**Topsoil**
			CH		Clayey SILT (CH) high plasticity, grey-brown, trace sand.	W		**Holocene Alluvium**
B		1			.... 0.80m becoming grey mottled brown			
B						W		
	0.00	1.60	SM		Silty SAND (SM) fine grained, grey-brown, with clay, high plasticity, brown.	W		**Holocene Alluvium**
B		2				W		
B					.... 2.20m becoming grey-brown mottled yellow			
	-1.40	3 3.00	MH		Clayey SILT (MH) dark grey,.	W		**Holocene Estuarine**
		4						
		5						
		6						
		7						
	-6.40	8 8.00	CH		Silty CLAY (CH) high plasticity, pale grey.	W		**Old Alluvium (Weathered)**
		9			.... 9.00m becoming brown-grey mottled brown			

NOTES *Hole Diameter 75.7mm to 23.20m depth. (NMLC)
Auger to 2.50m, washbored to 15.32m then NMLC to 23.20m. Hole ended at 23.20m due to loss of equipment. Properties of soil inferred from mud flushings and drill respone during washboring

JOB 221203

BOREHOLE RECORD

ARUP

BH11-P11-SB
HOLE

SHEET 2
OF 4

CLIENT	Abigroup
PROJECT	MRFB
CONTRACTOR	Terratest
DRILL MODEL	EDSON 3000
DRILLER	James Hodder
ANGLE	Vertical
BEARING	-
HOLE DIAMETER	(*See Notes)
LOGGED BY	JQ
CHECKED BY	KN
DRILLED DATE	21-Mar-11 to 23-Mar-11
GROUND LEVEL	~RL 1.60m
LOCATION	489242 E 6563828 N
ELEVATION DATUM	Australian Height Datum
COORDINATE SYSTEM	Map Grid of Australia (MGA)

DRILLING	STRATA				MATERIAL DESCRIPTION	CONDITION			OBSERVATION
SAMPLE, TEST, BIT, SUPPORT, ETC.	R.L. (m.)	DEPTH (m)	GROUP SYMBOL	LEGEND	SOIL TYPE Plasticity / Grain Size, Colour, Minor Components	WATER / MOISTURE	CONSISTENCY: COHESIVE (VS, S, F, ST, VST, H)	CONSISTENCY: NON COHESIVE (VL, L, MD, D, VD)	SOIL ORIGIN, STRUCTURE, ETC.
		11	CH		Silty CLAY (CH) high plasticity, pale grey. *(continued)*				**Old Alluvium (Weathered)**
					.... 10.40m trace sand				
		12							
		13							
		14							
					.... 14.30m becoming stiffer	W			
		15			.... 15.05m becoming very stiff	W			
					Borehole continued as a Cored Drillhole				
		16							
		17							
		18							
		19							

NOTES

*Hole Diameter 75.7mm to 23.20m depth. (NMLC)
Auger to 2.50m, washbored to 15.32m then NMLC to 23.20m. Hole ended at 23.20m due to loss of equipment. Properties of soil inferred from mud flushings and drill respone during washboring

JOB 221203

ARUP

CORED BOREHOLE RECORD

BH11-P11-SB
HOLE

SHEET 3
OF 4

CLIENT	Abigroup	LOGGED BY	JQ
PROJECT	MRFB	CHECKED BY	KN
		DRILLED DATE	21-Mar-11 to 23-Mar-11
CONTRACTOR	Terratest	ANGLE	Vertical
DRILL MODEL	EDSON 3000	BEARING	-
DRILLER	James Hodder	HOLE DIAMETER	(*See Notes)
		GROUND LEVEL	~RL 1.60m
		LOCATION	489242 E 6563828 N
		ELEVATION DATUM	Australian Height Datum
		COORDINATE SYSTEM	Map Grid of Australia (MGA)

DRILLING				STRATA			MATERIAL DESCRIPTION				DISCONTINUITIES			
TCR % (Drill rate)	SCR / (RQD)	FLUSH RETURN % (TYPE)	SAMPLES ($CaCO_3$, SPT, UCS, etc)	R.L. m.	DEPTH m	GRAPHIC LOG	ROCK TYPE Grain Size, Texture/Fabric, Colour, Minor Components	WEATHERING	ESTIMATED ROCK STRENGTH EL VL L M H VH EH	Is 50 (MPa)	FREQUENCY (per m) 30 10 3 1	SPECIFIC TYPE	SPECIFIC ANGLE	SPECIFIC THICKNESS (mm)	GENERAL DESCRIPTION Planarity, Roughness, Coating, Infill
					11										
					12										
					13										
					14										
					15										
				-13.72	15.32		Continued from Borehole								
							Clayey SILT (MH) medium to high plasticity, brown mottled grey, with weathered siltstone fragments.	RS							
				-14.17	15.77		SILTSTONE fine grained, red-brown.	XW							
			UCS		16							Jo	5	10	PL Ro3 gS
	98()		UCS												
	85/(64)				17										
							.... 17.50m becoming pale grey mottled brown			D0.12					
					18			DW				Be	1	20	PL Ro2 C
												Be	40	2	PL Ro2 CL
												Be	40	2	PL Ro2 FE CL
	100()											Jo	20	50	PL Ro3 CL
										D0.18 A0.08		Be	15	5	PL Ro2 C
												Be	30	2	PL Ro2 C
	72/(42)				19							Fo	0	45	PL Ro4 CL
												Fo	15	3	PL Ro4 CL
												Be	10	2	PL Ro2 FE
100()	100()			-18.08	19.68			XW/RS				We	10	180	PL Ro3 C, G
	0/(0)		UCS=1MPa				SILTSTONE fine grained, red-brown. .... 19.68m becoming dark grey mottled brown, iron	DW				Be	0	16	PL Ro3 C
			UCS												

NOTES

*Hole Diameter 75.7mm to 23.20m depth. (NMLC)
Auger to 2.50m, washbored to 15.32m then NMLC to 23.20m. Hole ended at 23.20m due to loss of equipment. Properties of soil inferred from mud flushings and drill respone during washboring.

See explanatory notes for details of abbreviations and basis of descriptions

JOB 221203

ARUP

CORED BOREHOLE RECORD

BH11-P11-SB
HOLE

SHEET 4
OF 4

CLIENT	Abigroup
PROJECT	MRFB
CONTRACTOR	Terratest
DRILL MODEL	EDSON 3000
DRILLER	James Hodder
ANGLE	Vertical
BEARING	-
HOLE DIAMETER	(*See Notes)
LOGGED BY	JQ
CHECKED BY	KN
DRILLED DATE	21-Mar-11 to 23-Mar-11
GROUND LEVEL	~RL 1.60m
LOCATION	489242 E 6563828 N
ELEVATION DATUM	Australian Height Datum
COORDINATE SYSTEM	Map Grid of Australia (MGA)

DRILLING | STRATA | MATERIAL DESCRIPTION | DISCONTINUITIES

TCR % (Drill rate)	SCR / (RQD)	FLUSH RETURN % (TYPE)	SAMPLES ($CaCO_3$, SPT, UCS, etc)	R.L. (m.)	DEPTH (m)	GRAPHIC LOG	ROCK TYPE Grain Size, Texture/Fabric, Colour, Minor Components	WEATHERING	ESTIMATED ROCK STRENGTH (EL VL L M H VH EH)	Is 50 (MPa)	FREQUENCY (per m) (30 10 3 1)	SPECIFIC: TYPE	SPECIFIC: ANGLE	SPECIFIC: THICKNESS (mm)	GENERAL DESCRIPTION: Planarity, Roughness, Coating, Infill
100()	90/(69)				21		stained SILTSTONE fine grained, red-brown. *(continued)*	DW		D0.12		Be	76	1	PL Ro2 C
												Be	75	2	PL Ro3 C
												We	2	60	PL Ro3 C
			UCS							D0.35					
							.... 21.60m becoming yellow brown			D0.23					
				-20.27	21.87		.... 21.80m becoming dark grey			D0.24					
70()	55/(43)				22		CORE LOSS.								
				-20.68	22.28		SILTSTONE fine grained, abundant clay seam in-between, grey-brown.	XW/RS				Be	0	105	PL Ro3 C
												Be	0	30	PL Ro3 C
												Be	0	40	PL Ro3 C
				-21.10	22.70							Be	0	62	PL Ro3 C
							CORE LOSS.								
				-21.43	23.03										
				-21.60	23.20		SILTSTONE fine grained, grey-brown.	XW/RS				Be	0		PL Ro3 C
							End of Borehole at 23.20m								
					24										
					25										
					26										
					27										
					28										
					29										

NOTES

*Hole Diameter 75.7mm to 23.20m depth. (NMLC)
Auger to 2.50m, washbored to 15.32m then NMLC to 23.20m. Hole ended at 23.20m due to loss of equipment. Properties of soil inferred from mud flushings and drill respone during washboring.

See explanatory notes for details of abbreviations and basis of descriptions

JOB 221203

ARUP Macleay River and Floodplain Bridge	**Client:**	Abigroup	**Date:**	1/06/2011
	Project:	MRFB	**Title:**	Core Photographs
	Borehole ID:	BH11-P11-NB	**Page:**	1 of 1

ARUP Macleay River and Floodplain Bridge	**Client:**	Abigroup	**Date:**	23/03/2011
	Project:	MRFB	**Title:**	Core Photographs
	Borehole ID:	BH11-P11-SB	**Page:**	1 of 1

Client Ref To be advised

Abigroup

Kempsey Bypass

FSG Project No. 1152

Dynamic Pile Testing Report

Pile P11B

FSG Report 1152-REP-016.0-P11B-EOD-110829

Foundation Specialists Group Pty Ltd
PDA Testing Services
29 August 2011

Introduction

This is a factual report on the following PDA Testing and CAPWAP Analysis :

Project :	Kempsey Bypass
Client :	Abigroup
Date of Testing :	26-8-11
Piles Tested and Reported :	P11B
Applicable Standards :	AS2159-1995 Australian Standard : Piling – Design and Installation ASTM 4945-00 American Society for Testing and Materials Standard Test Method for High-Strain Dynamic Testing of Piles

Testing Method :

Dynamic pile testing was performed in accordance with AS 2159-1995. Pile-top force and velocity were measured using 4 No. strain transducers, 2 No. piezoresistive accelerometers, and 2 No. piezoelectric accelerometers. The signals were processed by a Pile Driving Analyzer® model PAX. Data was simultaneously displayed on an LCD screen and digitally recorded on computer disk for permanent storage. Selected blows were digitised for more detailed analysis.

Pile Details:

Installation details provided by the Contractor Abigroup for the pile tested are summarised in Table 1, the pile installation record and related graphs are included in Appendix C.

Table 1 - Pile Detail Summary

Pile No.	P11B
Type	Steel
Pile Shape	Steel Tube
Pile Dimensions	750mm diameter x 16mm wall
End Condition	Open
Special Details	Pile Shoe 1m x 25mm
Yield Strength (Mpa)	350
Total Length (m)	28.102
Installation Date	26/08/2011
Toe Level (m AHD)	-19.29
Pile Penetration (m)	20.089
Rake	Vertical
Driving Hammer	Junttan HHK14s
Driving Stroke (mm)	1500
Driving Set (mm/blow)	1.25
Driving TC (mm)	26.75

Field Results :

The Pile Driving Analyzer® results are summarized in Tables 2, 3. Appendix A also contains PDA field plots of selected data.

Table 2 - Physical Summary of Testing Sequence

Test Date	26-8-11
Test Type	Drive
Toe Level (m)	-19.29
Pile Penetration (m)	20.089
Setup duration (days) :	0
Strength at Test Date (MPa)	350
Testing Hammer :	Junttan HHK14s
Ram Weight (t)	14
Hammer Cushion	Blue Nylon
Pile Cushion	NA
Blow No(s)	last 10
Stroke (mm)	1500
Set (mm) *	10
T.C. (mm) *	26.75

* Set and Temporary Compression (T.C.) are for individual or average values per blow

Field Results contd :

Table 3 - Key PDA Parameters for Selected Blow

Selected Representative Blow		139	
LBG	Length below gauges	24.9	(m)
FMX	Maximum Force	9744	(kN)
DMX	Max Displacement	28	(mm)
EMX	Maximum Energy Transfer	175.7	(kJ)
ETR	Hammer Efficiency	85.3	(%)
BPM	Hammer Blow Rate	1.9	(blows/minute)
VMX	Max Pile Top Velocity	6.13	(m/s)
JC	Correlated Case Damping Factor	0.8	(-)
RMX	PDA Capacity Estimate	9035	(kN)
SFR	Case Shaft Friction Estimate	5365	(kN)
QUS	Simplified Hiley Formula	12180	(kN)
BTA	PDA Integrity Factor	100	(%)
LTD	Length to BTA	NA	(m)
CSX	Peak Avg Stress at Pile Top	264.1	(MPa)
CSI	Max Local Stress at Pile Top	305.3	(MPa)
CSB	Peak Avg Stress at Pile Toe	5.7	(MPa)
TSX	Max Case Tension Stress	85	(MPa)
WS	Pile Top Wavespeed	5123	(m/s)
WC	Overall Wavespeed	5123	(m/s)

Field Results contd :

Table 4 - PDA Field Data Indicators and Assessment

Data Quality Measures

No of Sets of Gauges	4
No. Strain Used for Analysis	4
No. Accel. Used for Analysis	4
Pile Top Bending	Medium
Data Noise Level	Low

Data was of a high standard. 4 accelerometers and 4 strain transducers were used and the data was considered representative and of acceptable standard after minor adjustment.

Pile Stresses

Max Compression Stress (MPa)	**Max**	264.1	**Allowable**	315.0	**OK?**	Yes
Max Tension Stress (MPa)	**Max**	85	**Allowable**	315.0	**OK?**	Yes

Compressive stresses do not exceed allowable limits and are acceptable throughout the pile.

Pile Integrity

The CAPWAP analysis also indicates no loss of impedance in the section, and hence no indication of any damage.

CAPWAP® Analysis:

Pile P11B was subjected to further analysis using the CAse Pile Wave Analysis Program, CAPWAP®. The results of these analyses are included in Appendix B; a guide to the report is given in Appendix C. The results of the analyses are summarised in Table 3.

Table 5 - CAPWAP® Analysis

Test ID		1152-P11B-#3D-SL140-BN139-LP20000	
SL	Data File Storage Location	140	
BN	Blow Number	139	
Rskin	Shaft Resistance	9860	(kN)
Rtoe	Toe Resistance	1200	(kN)
Rtotal	Total Mobilized Resistance	11060	(kN)
WL	Working Load	TBA	(kN)
S*	Ultimate Structural Load	8007	(kN)
øg	Geotechnical Reduction Factor	0.78	(-)
Rug	Min Ultimate Geotechnical Capacity	10266	(kN)
dWL	Deflection at Working Load	TBA	(mm)

The analysis was implemented using conventional model parameters.

Correlation with Hiley Formula (QUS):

Table 6 provides the basis for control of untested piles which are represented by this pile test.

Table 6 - Derivation of Dynamic Reduction Factor for untested piles

R	Ram Weight	137.34	(kN)
h	Ram Stroke	1500	(mm)
e	Efficiency	85.3	(%)
E	Energy	175.73	(kNm)
s	Set	1.25	(mm)
TC	Temporary Compression	26.75	(mm)
Hiley	Hiley Capacity	12015	(kN)
Capwap	Capwap Total Capacity	11060	(kN)
DRF Set	Dynamic Reduction Factor Set Multiplier	0.05	(-)
DRF Base	Dynamic Reduction Factor Base	1.02	(-)

The Hiley correlation factors are extremely important for the evaluation of untested piles represented by the piles which are tested. The factors here are particular for this test, and FSG will provide recommendations based on further tests as they occur. It is very important that these be applied based on the actual delivered hammer energy.

Other Results and Supporting Information

Other results and supporting information can be found in the following Appendices:

Appendix A :	Case Method analysis results
Appendix B :	Capwap analysis Summaries
Appendix C :	Important Information About Your Dynamic Pile Testing Report

Pearse Casey B.A., B.A.I.

PDA Testing Services

1152 KEMPSEY BYPASS

PDA OP: NP

PILE DRIVING ANALYZER ®
Version 2011.105

1152-P11-B-#3D-LP20000-1_1
750MM X 16MM X 28.102M1

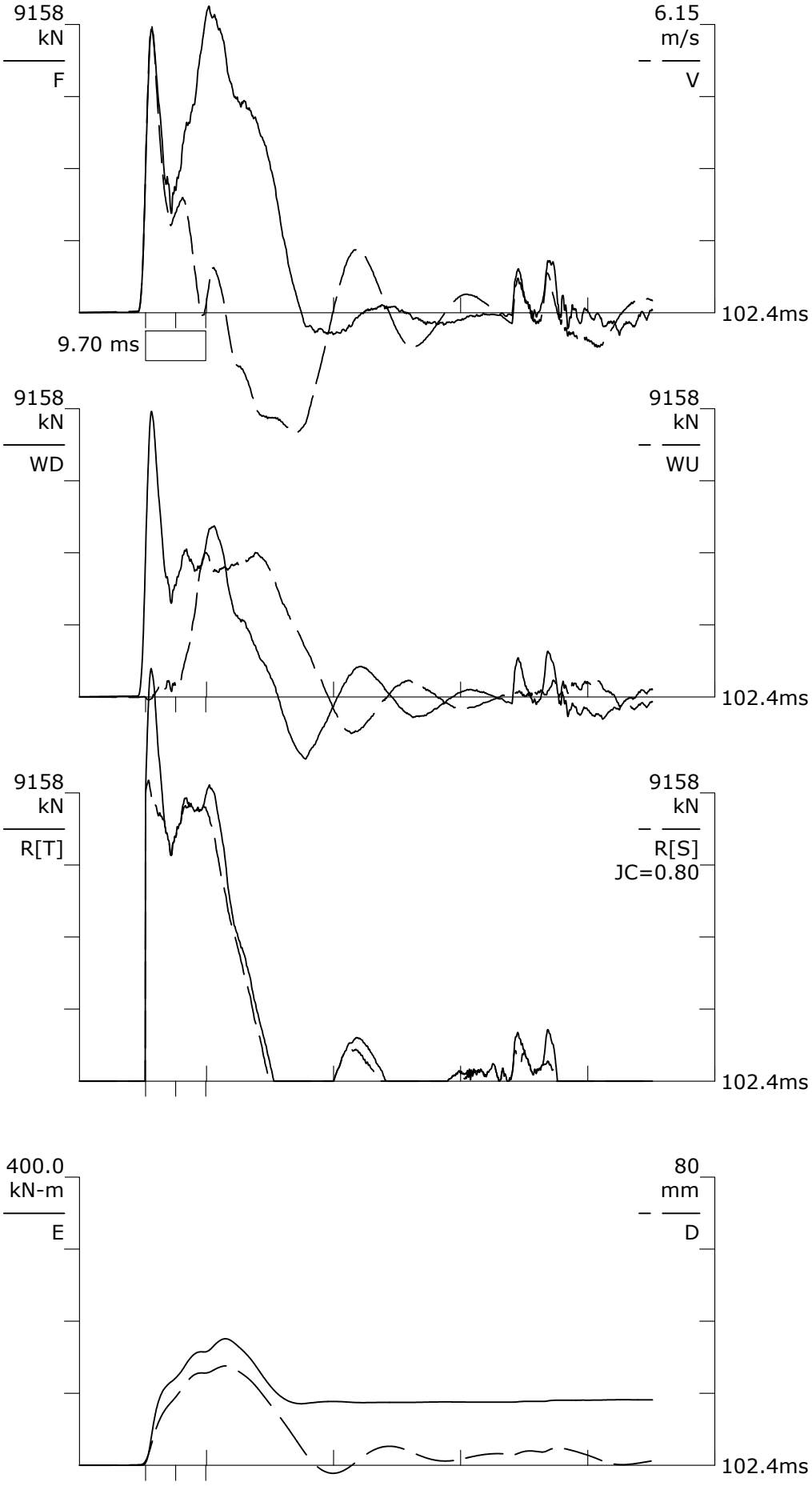

BN 138/139
26/08/2011 2:40:55 PM

FMX	9744	kN
EMX	175.7	kN-m
VMX	6.13	m/s
RMX	9035	kN
DMX	28	mm
CSB	5.7	MPa
CSI	305.3	MPa
SET	1	mm
QUS	12180	kN
LE	24.9	m
AR	368.95	cm^2
EM	206843	MPa
SP	77.3	kN/m3
WS	5123.0	m/s
EA/C	1490	kN-s/m
LP	20.0	m

F134 A1234

F1: [C483] 92 (1.02)
F3: [G603] 95.2 (1.02)
F4: [G613] 94.4 (1.02)
A1: [36357] 1160 g's/v (0.98)
A2: [15191] 1000 g's/v (0.98)
A3: [K2957] 335 mv/5000g's (0.98)
A4: [K2958] 330 mv/5000g's (0.98)

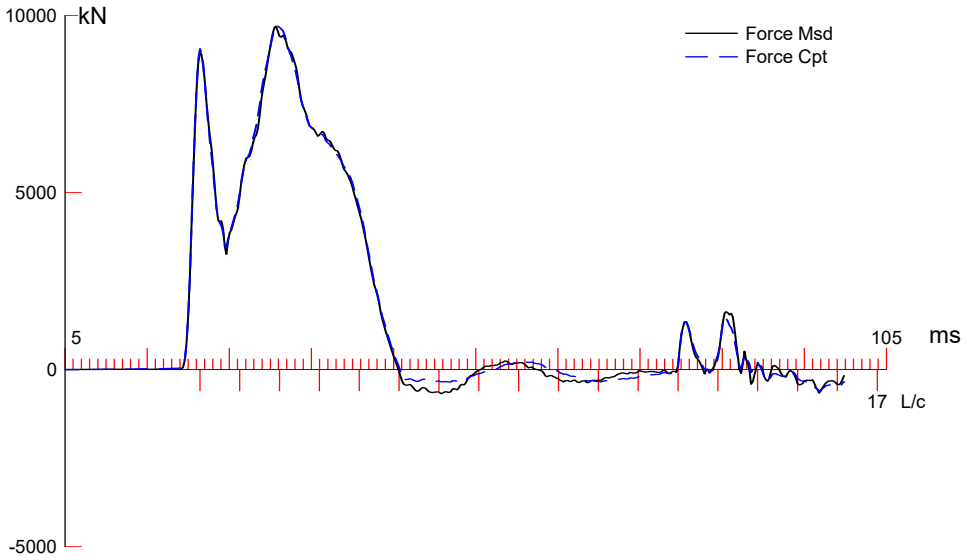

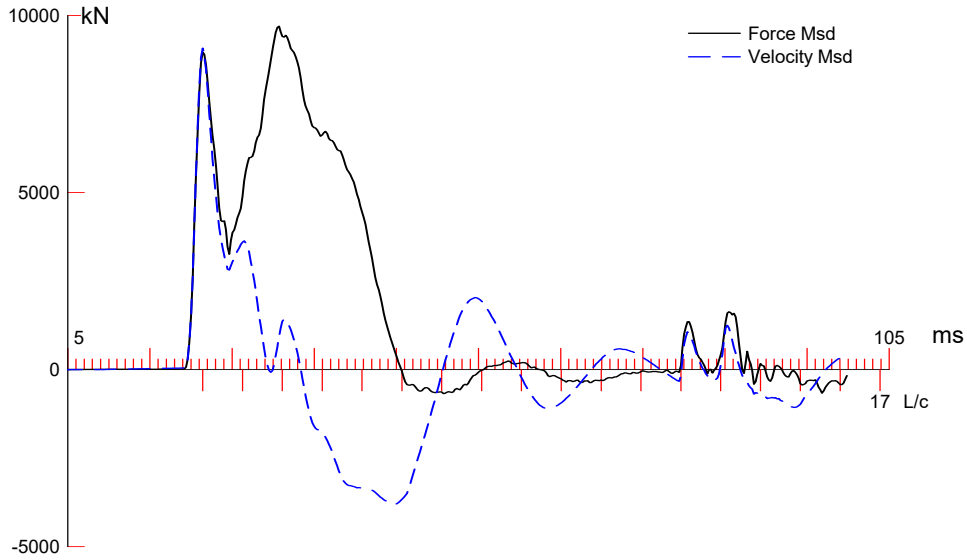

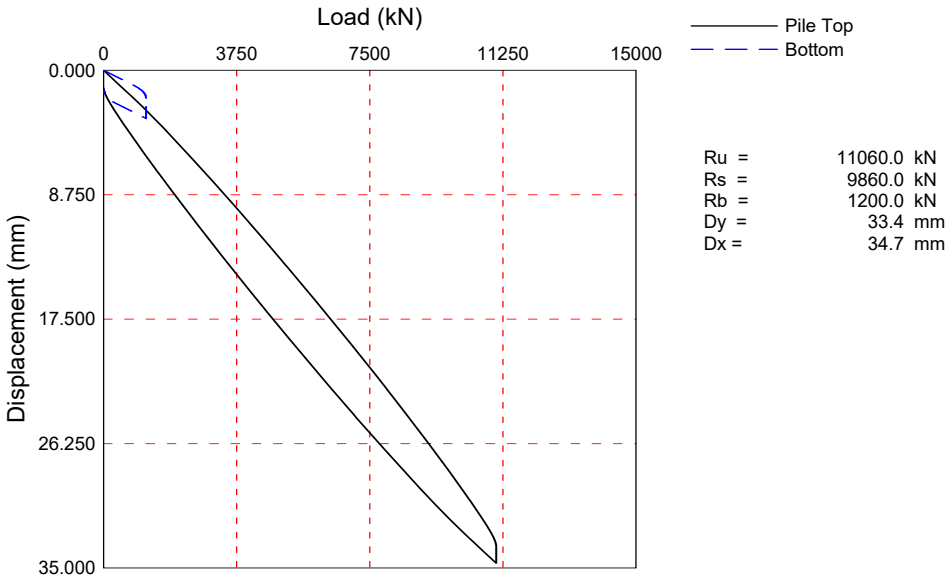

Ru = 11060.0 kN
Rs = 9860.0 kN
Rb = 1200.0 kN
Dy = 33.4 mm
Dx = 34.7 mm

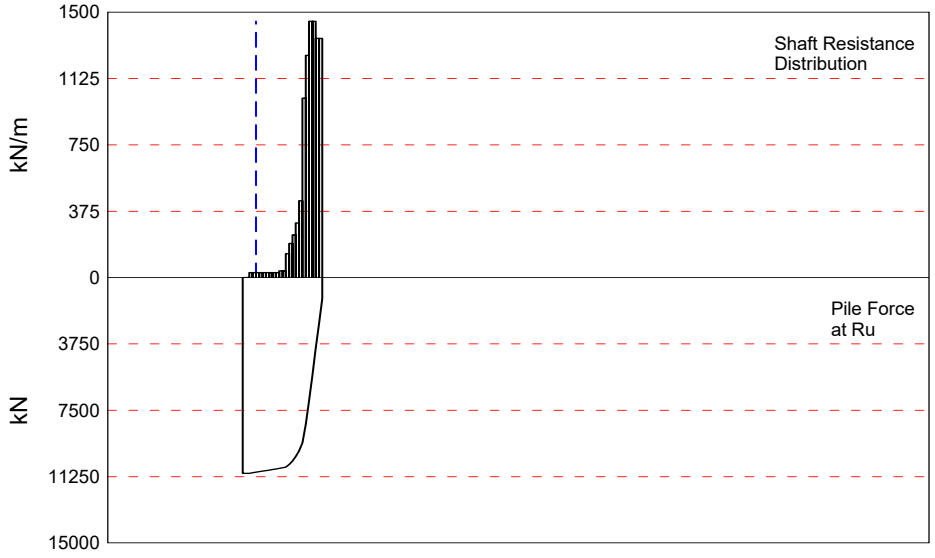

CAPWAP SUMMARY RESULTS

Total CAPWAP Capacity: 11060.0; along Shaft 9860.0; at Toe 1200.0 kN

Soil Sgmnt No.	Dist. Below Gages m	Depth Below Grade m	Ru kN	Force in Pile kN	Sum of Ru kN	Unit Resist. (Depth) kN/m	Unit Resist. (Area) kPa	Smith Damping Factor s/m	Quake mm
				11060.0					
1	1.0	-3.8	0.0	11060.0	0.0	0.00*	0.00*	0.000	2.000
2	2.1	-2.8	0.0	11060.0	0.0	0.00*	0.00*	0.000	2.000
3	3.1	-1.7	30.0	11030.0	30.0	28.97*	12.30*	0.500	2.000
4	4.1	-0.7	30.0	11000.0	60.0	28.97*	12.30*	0.500	2.000
5	5.2	0.3	30.0	10970.0	90.0	92.17	39.12	0.500	2.000
6	6.2	1.4	30.0	10940.0	120.0	28.97	12.30	0.500	2.000
7	7.2	2.4	30.0	10910.0	150.0	28.97	12.30	0.500	2.000
8	8.3	3.4	30.0	10880.0	180.0	28.97	12.30	0.500	2.000
9	9.3	4.5	30.0	10850.0	210.0	28.97	12.30	0.500	2.000
10	10.4	5.5	30.0	10820.0	240.0	28.97	12.30	0.500	2.000
11	11.4	6.5	30.0	10790.0	270.0	28.97	12.30	0.500	2.000
12	12.4	7.6	40.0	10750.0	310.0	38.63	16.39	0.500	2.000
13	13.5	8.6	40.0	10710.0	350.0	38.63	16.39	0.500	2.000
14	14.5	9.6	140.0	10570.0	490.0	135.20	57.38	0.500	2.000
15	15.5	10.7	200.0	10370.0	690.0	193.14	81.97	0.500	2.000
16	16.6	11.7	250.0	10120.0	940.0	241.43	102.47	0.500	2.000
17	17.6	12.8	320.0	9800.0	1260.0	309.03	131.16	0.500	2.000
18	18.6	13.8	450.0	9350.0	1710.0	434.57	184.44	0.500	2.000
19	19.7	14.8	1050.0	8300.0	2760.0	1014.00	430.36	0.500	2.000
20	20.7	15.9	1300.0	7000.0	4060.0	1255.43	532.82	0.500	2.000
21	21.7	16.9	1500.0	5500.0	5560.0	1448.58	614.79	0.500	2.000
22	22.8	17.9	1500.0	4000.0	7060.0	1448.58	614.79	0.500	2.000
23	23.8	19.0	1400.0	2600.0	8460.0	1352.00	573.81	0.500	2.000
24	24.9	20.0	1400.0	1200.0	9860.0	1352.00	573.81	0.500	1.500
Avg. Shaft			410.8			493.00	173.34	0.500	1.929
Toe			1200.0				2716.24	0.500	1.500

*Guide friction or other non-soil resistance.

Soil Model Parameters/Extensions		Shaft	Toe
Case Damping Factor		3.310	0.403
Unloading Quake	(% of loading quake)	150	100
Reloading Level	(% of Ru)	100	100

CAPWAP match quality = 2.47 (Wave Up Match) ; RSA = 0
Observed: final set = 1.250 mm; blow count = 800 b/m
Computed: final set = 0.100 mm; blow count = 9999 b/m
Replay Factor: F1:1.020; F3:1.020; F4:1.020;
V1:0.980; V2:0.980; V3:0.980; V4:0.980;

max. Top Comp. Stress = 259.8 MPa (T= 31.1 ms, max= 1.032 x Top)
max. Comp. Stress = 268.2 MPa (Z= 18.6 m, T= 25.7 ms)
max. Tens. Stress = -57.40 MPa (Z= 14.5 m, T= 50.7 ms)
max. Energy (EMX) = 169.05 kJ; max. Measured Top Displ. (DMX)=27.60 mm

EXTREMA TABLE

Pile Sgmnt No.	Dist. Below Gages m	max. Force kN	min. Force kN	max. Comp. Stress MPa	max. Tens. Stress MPa	max. Trnsfd. Energy kJ	max. Veloc. m/s	max. Displ. mm
1	1.0	9584.3	-657.4	259.8	-17.82	169.05	6.0	26.109
2	2.1	9453.9	-705.7	256.2	-19.13	164.44	6.0	24.992
4	4.1	9331.0	-1015.8	252.9	-27.53	153.03	5.9	22.707
6	6.2	9370.5	-1268.4	254.0	-34.38	139.83	5.8	20.404
7	7.2	9409.7	-1384.0	255.0	-37.51	133.37	5.8	19.255
8	8.3	9425.5	-1497.6	255.5	-40.59	127.00	5.7	18.105
9	9.3	9417.8	-1606.9	255.3	-43.55	120.66	5.7	16.955
10	10.4	9395.5	-1733.5	254.7	-46.99	114.30	5.6	15.793
11	11.4	9365.9	-1853.0	253.9	-50.22	107.92	5.5	14.615
12	12.4	9346.3	-1963.0	253.3	-53.21	101.49	5.4	13.419
13	13.5	9340.3	-2046.7	253.2	-55.47	94.62	5.2	12.210
14	14.5	9394.1	-2117.8	254.6	-57.40	87.80	4.9	10.981
15	15.5	9490.6	-2066.9	257.2	-56.02	78.22	4.6	9.756
16	16.6	9653.8	-1935.7	261.7	-52.47	67.93	4.2	8.538
17	17.6	9829.4	-1751.8	266.4	-47.48	57.72	3.7	7.345
18	18.6	9893.4	-1499.1	268.2	-40.63	47.85	3.1	6.188
19	19.7	9602.8	-1101.7	260.3	-29.86	38.30	2.5	5.090
20	20.7	8261.5	-444.3	223.9	-12.04	26.73	1.9	4.117
21	21.7	6715.5	-0.0	182.0	-0.00	17.49	1.5	3.288
22	22.8	5179.8	-0.0	140.4	-0.00	10.73	1.3	2.621
23	23.8	3889.5	-0.0	105.4	-0.00	6.36	1.0	2.116
24	24.9	2854.5	-0.0	77.4	-0.00	1.89	0.9	1.760
Absolute	18.6			268.2			(T =	25.7 ms)
	14.5				-57.40		(T =	50.7 ms)

CASE METHOD

J =	0.0	0.1	0.2	0.3	0.4	0.5	0.6	0.7	0.8	0.9
RP	9097.0	9104.7	9112.5	9120.2	9128.0	9135.8	9143.5	9151.3	9159.1	9166.8
RX	13085.5	12579.2	12072.9	11566.6	11060.3	10554.0	10047.8	9541.5	9035.2	8834.7
RU	13575.0	13117.7	12660.4	12203.0	11745.7	11288.4	10831.1	10373.8	9916.4	9459.1

RAU = 8239.2 (kN); RA2 = 8938.2 (kN)

Current CAPWAP Ru = 11060.0 (kN); Corresponding J(RP)= 0.00; J(RX) = 0.40

VMX	TVP	VT1*Z	FT1	FMX	DMX	DFN	SET	EMX	QUS
m/s	ms	kN	kN	kN	mm	mm	mm	kJ	kN
6.13	21.63	4519.6	4499.8	9743.9	27.601	1.257	1.250	175.7	12179.9

PILE PROFILE AND PILE MODEL

Depth	Area	E-Modulus	Spec. Weight	Perim.
m	cm^2	MPa	kN/m^3	m
0.00	368.95	206842.7	77.287	2.356
24.85	368.95	206842.7	77.287	2.356

Toe Area 0.442 m^2

Top Segment Length 1.04 m, Top Impedance 1489.63 kN/m/s

Pile Damping 1.0 %, Time Incr 0.202 ms, Wave Speed 5123.0 m/s, 2L/c 9.7 ms

STATIC ANALYSIS

Monotonic D-Toe, E-P R-Toe

Step No.	Top Load	Top Disp.	Toe Load	Toe Disp.
	kN	mm	kN	mm
0	0.0	0.000	0.0	0.000
2	310.6	0.723	13.6	0.017
4	621.3	1.445	27.3	0.034
6	931.6	2.168	40.9	0.051
8	1230.4	2.884	54.6	0.068
10	1507.1	3.585	68.2	0.085
13	1898.0	4.611	88.6	0.111
16	2273.0	5.613	109.1	0.136
19	2634.7	6.594	129.6	0.162
22	2982.3	7.547	150.0	0.188
25	3313.3	8.467	170.5	0.213
28	3630.2	9.358	190.9	0.239
31	3930.4	10.214	211.4	0.264
34	4222.0	11.050	231.8	0.290
37	4499.5	11.855	252.3	0.315
41	4857.8	12.901	279.6	0.349
45	5200.8	13.910	306.8	0.384
49	5527.6	14.880	334.1	0.418
53	5841.4	15.817	361.4	0.452

STATIC ANALYSIS

Monotonic D-Toe, E-P R-Toe

Step No.	Top Load kN	Top Disp. mm	Toe Load kN	Toe Disp. mm
57	6140.2	16.716	388.7	0.486
61	6424.8	17.580	415.9	0.520
66	6763.2	18.613	450.0	0.563
71	7082.3	19.596	484.1	0.605
76	7379.0	20.520	518.2	0.648
81	7654.0	21.387	552.3	0.690
87	7967.6	22.382	593.2	0.742
93	8262.6	23.325	634.1	0.793
99	8539.2	24.218	675.1	0.844
106	8832.0	25.177	722.8	0.903
113	9104.2	26.077	770.5	0.963
121	9396.1	27.051	825.1	1.031
129	9664.4	27.955	878.4	1.100
138	9928.8	28.859	933.5	1.176
149	10189.9	29.777	993.7	1.270
162	10447.3	30.702	1054.8	1.381
177	10680.3	31.569	1111.7	1.509
199	10903.1	32.465	1169.0	1.696
218	11003.0	32.946	1193.2	1.858
232	11041.3	33.187	1200.0	1.977
242	11052.8	33.308	1200.0	2.063
247	11057.0	33.364	1200.0	2.105
250	11059.0	33.396	1200.0	2.131
251	11059.6	33.406	1200.0	2.139
252	11060.0	33.416	1200.0	2.148
325	11060.0	34.038	1200.0	2.770
362	11060.0	34.354	1200.0	3.086
381	11060.0	34.516	1200.0	3.247
390	11060.0	34.592	1200.0	3.324
395	11060.0	34.635	1200.0	3.367
397	11060.0	34.652	1200.0	3.384
398	11060.0	34.660	1200.0	3.392
402	10749.4	33.938	1186.4	3.375
403	10594.0	33.576	1179.5	3.367
404	10438.7	33.215	1172.7	3.358
406	10128.4	32.492	1159.1	3.341
408	9829.6	31.776	1145.4	3.324
410	9552.9	31.075	1131.8	3.307
413	9162.0	30.050	1111.4	3.282
416	8787.0	29.047	1090.9	3.256
419	8425.3	28.067	1070.4	3.230
422	8077.7	27.114	1050.0	3.205
425	7746.7	26.193	1029.5	3.179
428	7429.8	25.302	1009.1	3.154

STATIC ANALYSIS

Monotonic D-Toe, E-P R-Toe

Step No.	Top Load kN	Top Disp. mm	Toe Load kN	Toe Disp. mm
431	7129.6	24.446	988.6	3.128
434	6838.0	23.610	968.2	3.103
437	6560.5	22.805	947.7	3.077
441	6202.2	21.760	920.4	3.043
445	5859.2	20.750	893.2	3.009
449	5532.4	19.780	865.9	2.975
453	5218.6	18.843	838.6	2.941
457	4919.8	17.944	811.3	2.907
461	4635.2	17.081	784.1	2.872
466	4296.8	16.047	750.0	2.830
471	3977.7	15.064	715.9	2.787
476	3681.0	14.140	681.8	2.745
481	3406.0	13.274	647.7	2.702
487	3092.4	12.279	606.8	2.651
493	2797.4	11.335	565.9	2.600
499	2520.8	10.443	524.9	2.549
506	2228.0	9.484	477.2	2.489
513	1955.8	8.584	429.5	2.429
521	1663.9	7.610	374.9	2.361
529	1395.6	6.706	321.6	2.293
538	1131.2	5.802	266.5	2.216
549	870.1	4.883	206.3	2.122
562	612.7	3.958	145.2	2.012
577	379.7	3.092	88.3	1.884
599	156.9	2.195	31.0	1.696
645	4.5	1.318	3.4	1.449